TABLE OF CONTENTS

ABSTRACT

With the increased availability of computers of various sizes, it is becoming more common to predict the responses of geotechnical structures using numerical analyses which incorporate more realistic models of soil behaviour. The main objective of this research is to develop and evaluate a series of unified critical state models. These models are then used to solve some typical boundary value problems in geotechnical engineering.

The new models are based on a critical state model called CASM which was formulated based on both the state parameter concept and a non associated flow rule. The main feature of CASM is that a single set of yield and plastic potential functions is used to model the behaviour of clay and sand under both drained and undrained loading conditions.

These models are developed by incorporating a new non-linear elasticity rule, the combined hardening concept and the bounding surface plasticity theory. A new non-linear elasticity rule for clay materials is introduced into CASM, this gives a better prediction on the behaviour of soil. The new combined volumetric-deviatoric hardening model is named CASM-d and provides a better prediction of the behaviour of lightly overconsolidated clays and loose sands. The new bounding surface model is named CASM-b and provides a more realistic prediction of soil behaviour inside the state boundary surface. The new cyclic bounding surface model is named CASM-c and provides a good prediction of soil behaviour under cyclic loading conditions.

To evaluate their adequacy, CASM and its extensions are implemented into a finite element package called CRISP. This program was specifically developed to incorporate the critical state type of constitutive models.

The analyses of a variety of typical geotechnical engineering problems are carried out to further check the validity of the new constitutive models. The models prove themselves to be very robust and useful tools for solving a wide range of practical geotechnical problems under different loading conditions.

ACKNOWLEDGEMENTS

The research described in this thesis was carried out at The University of Nottingham during the period of March 2001 to February 2004. The generous financial support from both The University of Nottingham and Universities U.K. (*ORS* Award) are gratefully acknowledged.

I would like to thank my supervisor, Professor Hai-Sui Yu, first for helping me during my undergraduate study and then giving me the opportunity to do my PhD. Without his excellent guidance, patient supervision and provision of financial assistance, this thesis would not have been possible.

I wish to thank Dr. Amir Rahim from the CRISP consortium for his technical support with the finite element program CRISP.

My thanks must be given to Dr. Glenn McDowell for many useful discussions on basic soil mechanics.

My thanks are extended to James Walker and Steve Hau for their valuable time spent proof reading this thesis.

I thank Steve Hau for sharing with me many useful discussions on our common research interests.

I appreciate the help and friendship of all colleagues from the Nottingham Centre for Geomechanics, in particular Wee Loon Lim, Steve Hau and Jun Wang.

Thanks also go to my Vietnamese friends at The University of Nottingham, their friendship made my research an enjoyable experience.

Finally, I owe my greatest thanks to my parents and sister for their love, belief, support and encouragement throughout the period of my studies.

LIST OF TABLES

LIST OF FIGURES

NOMENCLATURE

Chapter 2

$\delta\varepsilon_q^e$	Triaxial elastic deviatoric strain increment
$\delta\varepsilon_p^e$	Triaxial elastic volumetric strain increment
$\delta\varepsilon_q^p$	Triaxial plastic deviatoric strain increment
$\delta\varepsilon_p^p$	Triaxial plastic volumetric strain increment
ν	Specific volume
Γ	Intersection of *CSL* with p'=1 kPa in (ν,lnp') space
μ	Poisson's ratio
λ	Slope of the critical state line in (ν,lnp') space
κ	Slope of the unloading, line in (ν,lnp') space
$\boldsymbol{\beta}$	State parameter vector in plastic potential
η	Stress ratio
$\boldsymbol{\sigma}$	Stress vector
$\Delta\boldsymbol{\varepsilon}$	Strain increment vector
$\Delta\boldsymbol{\sigma}$	Stress increment vector
$\delta\varepsilon_a$	Vertical (axial) strain increment
$\delta\varepsilon_p$	Triaxial volumetric strain increment
$\delta\varepsilon_q$	Triaxial deviatoric strain increment
$\delta\varepsilon_r$	Radial strain increment
σ'_a	Vertical (axial) effective stress
ε_a	Vertical (axial) strain
σ_a	Vertical (axial) total stress
ε_p	Triaxial volumetric strain
$\delta p'$	Volumetric effective stress increment
δq	Deviatoric stress increment
ε_q	Triaxial deviatoric strain
σ'_r	Radial effective stress
ε_r	Radial strain
σ_r	Radial total stress

$\boldsymbol{D}$	Stress constitutive matrix
e	Voids ratio
E	Young's modulus
$F(\boldsymbol{\sigma},\boldsymbol{k})$	Yield surface
G	Shear modulus
$G(\boldsymbol{\sigma},\boldsymbol{\beta})$	Plastic potential
H	Hardening modulus
v_κ	Intersection of unloading-reloading line with p'=1 kPa in (v,lnp') space
K	Bulk modulus
K_o	Coefficient of lateral earth pressure at rest
$K_{o,nc}$	Coefficient of the earth pressure at rest for 1D normal compression
$\boldsymbol{k}$	Hardening/Softening parameter
M	Slope of critical state line in (p',q) space
N	Specific volume of isotropically normally consolidated soil when p'=1 kPa
p'	Mean effective stress
p'_o	Preconsolidation pressure
q	Deviatoric stress
u	Pore water pressure

Chapter 3

Λ	Constant used in the derivation of the hardening modulus
Γ	Intersection of *CSL* with p'=1 kPa line in (v,lnp') space
μ	Poisson's ratio hardening modulus
λ	Slope of the critical state line in (v,lnp') space
κ	Slope of the unloading, reloading line in (v,lnp') space
ξ	State parameter
$\boldsymbol{\beta}$	State parameter vector in plastic potential
η	Stress ratio
ξ_R	Reference state parameter
$F(\boldsymbol{\sigma},\boldsymbol{k})$	Yield surface
G	Shear modulus

$G(\boldsymbol{\sigma},\boldsymbol{\beta})$	Plastic potential
H	Hardening modulus
v_κ	Intersection of unloading-reloading line with p'=1 kPa line in (v,lnp') space
K	Bulk modulus
M	Slope of critical state line in (p',q) space
n	Stress-state coefficient
N	Specific volume of isotropically normally consolidated soil when p'=1 kPa
p'_o	Preconsolidation pressure
p'_x	Mean effective stress at critical state which has the same preconsolidation pressure with the current stress (see Figure 3.1)
r	Spacing ratio

Chapter 4

ϕ'	Angle of shearing resistance
θ	Lode angle
λ	Slope of the critical state line in (v,lnp') space
κ	Slope of the unloading, reloading line in (v,lnp') space
$\Delta\boldsymbol{\varepsilon}$	Strain increment vector
$\Delta\boldsymbol{\sigma}$	Stress increment vector
A, l, m	Parameters for non-linear elastic rule used by Atkinson (2000)
D^e	Elastic stress constitutive matrix
D^{ep}	Elastic-plastic stress constitutive matrix
e_o	Initial void ratio
$F(\boldsymbol{\sigma},\boldsymbol{k})$	Yield surface
$G(\boldsymbol{\sigma},\boldsymbol{\beta})$	Plastic potential
G	Shear modulus
H	Hardening modulus
K	Bulk modulus
M	Slope of critical state line in (p',q) space
$M_{\max}$	Slope of the *CSL* under triaxial compression (θ=-30°) in (p',q) space
n	Stress-state coefficient

OCR	Overconsolidation ratio defined in terms of mean effective stresses
p'	Mean effective stress
p'_o	Preconsolidation pressure
q	Deviatoric stress
r	Spacing ratio
t	Parameter for the new non-linear elastic rule used for clays by CASM and its extensions, equals 0.5 for simplicity
v	Specific volume

Chapter 5

$\delta\varepsilon_q^p$	Triaxial plastic deviatoric strain increment
$\delta\varepsilon_p^p$	Triaxial plastic volumetric strain increment
Γ	Intersection of *CSL* with p'=1 kPa line in (v,lnp') space
α	New parameter introduced in CASM-d
μ	Poisson's ratio hardening modulus
λ	Slope of the critical state line in (v,lnp') space
κ	Slope of the unloading, reloading line in (v,lnp') space
η	Stress ratio
$\delta p'_o$	Preconsolidation pressure increment
D	Non-dimensional parameter used by Nova and Wood (1979) and Krenk (2000) in their constitutive models
F	Yield surface
G	1. Plastic potential 2. Shear modulus
H	Hardening modulus
K	Bulk modulus
M	Slope of the *CSL* under triaxial compression (θ=-30°) in (p',q) space
n	Stress-state coefficient
OCR	Overconsolidation ratio defined in terms of mean effective stresses
p'_o	Preconsolidation pressure
r	Spacing ratio
v	Specific volume

Chapter 6

$\delta\varepsilon_p^p$	Triaxial plastic volumetric strain increment
Γ	Intersection of *CSL* with p'=1 kPa line in (v,lnp') space
μ	Poisson's ratio hardening modulus
γ	Ratio between current stress and image stress
λ	Slope of the critical state line in (v,lnp') space
κ	Slope of the unloading, reloading line in (v,lnp') space
F	Yield surface
G	1. Plastic potential
	2. Shear modulus
h	New parameter introduced in CASM-b
H	Hardening modulus at current stress point
H_j	Hardening modulus at image stress point
K	Bulk modulus
m	New parameter introduced in CASM-b
M	Slope of the *CSL* under triaxial compression (θ=-30°) in (p',q) space
n	Stress-state coefficient
OCR	Overconsolidation ratio defined in terms of mean effective stresses
p'_j	Image mean effective stress
p'_{oj}	Preconsolidation pressure of the bounding surface
q_j	Image deviatoric stress
r	Spacing ratio

Chapter 7

Γ	Intersection of *CSL* with p'=1 kPa line in (v,lnp') space
μ	Poisson's ratio hardening modulus
γ	Ratio between current stress and image stress
λ	Slope of the critical state line in (v,lnp') space
κ	Slope of the unloading, reloading line in (v,lnp') space
F	Yield surface
G	1. Plastic potential
	2. Shear modulus

h	New parameter introduced in CASM-b
H	Hardening modulus at current stress point
H_j	Hardening modulus at image stress point
H_R	New hardening modulus parameter for reloading
H_U	New hardening modulus parameter for unloading
k	New parameter to control shakedown behaviour
K	Bulk modulus
m	New parameter introduced in CASM-b
M	Slope of the *CSL* under triaxial compression (θ=-30°) in (p',q) space
n	Stress-state coefficient
OCR	Overconsolidation ratio defined in terms of mean effective stresses
r	Spacing ratio

Chapter 8

$S_{um}^{L/D}$	Undrained shear strength derived for finite length to diameter pressuremeters
S_{um}^{∞}	Undrained shear strength derived for infinite long pressuremeters
$S_{um}^{\infty} / S_{um}^{L/D}$	Correction factor for prediction of undrained shear strength using pressuremeters
ε	Cavity strain
$(\varepsilon)_{\max}$	Maximum cavity strain
Γ	Intersection of *CSL* with p'=1 kPa line in (v,lnp') space
μ	Poisson's ratio hardening modulus
ψ	Pressuremeter pressure
λ	Slope of the critical state line in (v,lnp') space
κ	Slope of the unloading, reloading line in (v,lnp') space
$\psi_{\lim}$	Pressuremeter limit pressure
ξ_o	Initial state parameter
σ_o	Isotropic initial stress
ΔV	Volume change per unit length in a pressuremeter test
A	Area of a strip or circular footing
a	Radius of a cylindrical cavity at any time

$a_{external}$	Outer radius of a cylindrical cavity
a_o	Initial radius of a cylindrical cavity
B	Width of a strip footing or anchor
D	Diameter of pressuremeter
h	New parameter introduced in CASM-b
H	Depth of embedment for an anchor
K	Bulk modulus
L	Length of pressuremeter
m	New parameter introduced in CASM-b
M	Slope of the *CSL* under triaxial compression (θ=-30°) in (p',q) space
n	Stress-state coefficient
N_c	1. Bearing capacity factor for footings
	2. Breakout factor for anchors
N_c^{mob}	Mobilised bearing capacity factor for footings
OCR	Overconsolidation ratio defined in terms of mean effective stresses
p'_i	Initial mean effective stress
p'_o	Preconsolidation pressure
p'_f	Mean effective stress at critical state
q_f	Deviatoric stress at critical state
q_u	Ultimate vertical average applied pressure
Q_u	Ultimate vertical load applied to footings and anchors
q_v	Vertical average applied pressure
r	Spacing ratio
S_G	Pressuremeter undrained shear strength derived by using
	Gibson and Anderson's method
S_H	Pressuremeter undrained shear strength derived by using
	Houlsby and Withers's method
S_u	Theoretical triaxial undrained shear strength
v	Specific volume of a soil sample
v_o	Initial specific volume of a soil sample
V	Inner volume per unit length in a pressuremeter test

Chapter 9

$\delta\varepsilon_q^p$	Triaxial plastic deviatoric strain increment
$\delta\varepsilon_p^p$	Triaxial plastic volumetric strain increment
α	New parameter introduced in CASM-d
η	Stress ratio, $=q/p'$
c	New parameter introduced in the new flow rules proposed by Yu (2003)
G	Plastic potential
h	New parameter introduced in CASM-b
H	Hardening modulus at current stress point
H_j	Hardening modulus at image stress point
H_R	New hardening modulus parameter for reloading
H_U	New hardening modulus parameter for unloading
k	New parameter to control shakedown behaviour
m	New parameter introduced in CASM-b
M	Slope of the *CSL* under triaxial compression (θ=-30°) in (p',q) space
n	Stress-state coefficient
p'	Mean effective stress
p'_o	Preconsolidation pressure

CHAPTER 1

INTRODUCTION

1.1. BACKGROUND AND RESEARCH OBJECTIVES

When a soil engineer was faced with a design situation involving the prediction of movement of soil masses, the traditional approach was to treat it as either a stability or a deformation problem and to proceed to seek solutions assuming either rigid plasticity or linear elasticity for the soil behaviour. This was due to the fact that the use of more realistic soil models would involve very complicated field equations for the stresses and deformations.

However, in the last two decades, due to the availability of large digital computers and advances in computational analysis techniques, it has become feasible to perform the stress analysis of geotechnical structures involving complex geometries and material behaviour. A key element in such an analysis is the development of proper and realistic constitutive modelling of the behaviour of soils.

The classical soil mechanics theory is based on simple elastic-perfectly plastic models. The Tresca and Von Mises models are expressed in terms of total stresses and applied to the undrained soil behaviour of soils. Using the well known Coulomb failure criterion, the Mohr-Coulomb and Drucker-Prager models were developed: these are expressed in terms of effective stresses to describe the general behaviour of soils. However, these models are restricted in their ability to reproduce real soil behaviour.

The development of critical state constitutive models has provided a major advance in the use of plasticity theory in geomechanics. Although the popular Cam-clay models prove to be successful in modelling normally consolidated clays, it is well known that they cannot predict many important features of the behaviour of sands and overconsolidated clays. Modifications to the standard Cam-clay models have been proposed over the last three decades, however, one common problem still exists which is the ability of any single model to predict the behaviour of both clay and sand materials.

The motivation for a unified description for sands and clays comes not only from the qualitative similarity in their macroscopic response, as well as from the recognition that there is no clearly defined threshold when a sandy clay switches from behaving like a clay to a sand as the particle size distribution changes, but also from the numerical advantage of dealing with a single algorithm for problems involving several soil types.

Furthermore, the standard critical state models all belong to the volumetric hardening group of models which means that the hardening parameter is purely a function of the volumetric strain, but not the deviatoric strain. However, there is no valid argument to support this assumption (Nova and Wood, 1979; Collins and Kelly, 2002; Krenk, 2000).

Another drawback is that many important features with respect to the cyclic response of soil cannot be adequately described by the standard critical state models. The principal reason is because the classical concept of a yield surface provides little flexibility in describing the change of the plastic modulus with loading direction and implies a purely elastic stress range within the yield surface.

The three main objectives of the research reported in this thesis are:

1. *To incorporate a unified critical state model (CASM) into a finite element code.*
2. *To extend CASM by incorporating a new non-linear elasticity rule, the combined hardening concept and the bounding surface plasticity theory.*
3. *To evaluate and apply CASM and its extensions to analyse a variety of typical boundary value problems in geotechnical engineering.*

The unified critical state model CASM (Clay And Sand Model) is derived based on the critical state theory and formulated in terms of the state parameter concept (Yu, 1995, 1998). The main feature of CASM is that a single set of yield and plastic potential functions is used to model the behaviour of clay and sand under both drained and undrained loading conditions. This strain hardening model requires only seven material parameters (two more than the traditional Cam-clay models), all of which have clear physical meanings and are relatively simple to determine in routine laboratory or field tests.

To evaluate their adequacy, CASM and its extensions are implemented into a finite element package called CRISP. This program was developed at Cambridge University and was introduced mainly to incorporate the critical state type of constitutive models.

The ability of the models to predict the behaviour of clay and sand under both drained and undrained loading conditions is demonstrated by comparing of the finite element results with the laboratory data. Analyses of a variety of typical geotechnical engineering problems are carried out to further check the validity of the new constitutive models.

1.2. STRUCTURE OF PRESENTATION

Following this introductory chapter, this thesis is divided into eight further distinct chapters. The chapters essentially reflect the order in which the research was carried out. A brief outline of the contents of each chapter is shown below.

Chapter 2 reviews the appropriate literature in the field of constitutive modelling of soil. This chapter is divided into three parts. The first part describes a brief review of constitutive models used to predict soil behaviour. This is followed by a summary of the critical state soil mechanics theory. Chapter 2 finishes with a discussion of the methods of analysis in geotechnical engineering. A description of the finite element program CRISP is also presented in this section.

In Chapter 3, the critical state model CASM is thoroughly reviewed. An outline of the original work carried out in this thesis is also described in Chapter 3.

A new non-linear elasticity rule adopted for CASM, which is only applicable to clays, is presented in Chapter 4. Succeeding this is a discussion on the incorporation of CASM into the finite element code CRISP. This includes formulations of the model in the three-dimensional stress space and computer implementation. To conclude the chapter, the validation of CASM is presented.

In Chapter 5, CASM is extended into a new model called CASM-d. This uses the combined hardening plasticity concept. After describing the incorporation of CASM-d into CRISP, the performance of the new model is investigated and it is finally validated with experimental data.

In Chapter 6, another new model, called CASM-b, is developed from CASM by applying the bounding surface plasticity theory. The process of incorporating CASM-b into CRISP is illustrated in the second part of Chapter 6. Some simulations of the triaxial test using CASM-b concludes this chapter.

The bounding surface in Chapter 6 is extended further in Chapter 7 to produce CASM-c. This model can predict the behaviour of soil under cyclic loading conditions. Chapter 7 also describes how CASM-c is incorporated into CRISP. It ends with the validation of CASM-c.

Chapter 8 deals with the analyses of typical boundary value problems in geotechnical engineering. The models detailed in Chapters 3, 4, 6 and 7 are used. This involves the analysis of the pressuremeter tests, surface rigid strip and circular footings, horizontal strip anchors and unpaved pavements.

The conclusions drawn from the research project and suggestions for future work are outlined in Chapter 9.

In addition to this, the appendices that contain some data and numerical derivations are found at the end of the thesis.

CHAPTER 2

LITERATURE REVIEW

2.1. SOIL MODELS IN GEOTECHNICAL ENGINEERING

2.1.1. Introduction

Scientific understanding proceeds by way of constructing and analysing models of the segments or aspects of reality under study. The purpose of these models is not to give a mirror image of reality, but rather to single out and make available for intensive investigation those decisive elements. Hence, good models provide the key to understanding reality (Wood, 1990).

The simplest type of model is elastic. The behaviour of an elastic material can be described by generalisations of the Hooke's law: '*there is an one-to-one relationship between stress and strain'*. However, for many materials the overall stress-strain response cannot be condensed into such a unique relationship because many states of strain can correspond to one state of stress and vice versa. Hence, it is necessary to have more sophisticated models to be able to predict real soil behaviour. This has lead to the introduction of elastic-perfectly plastic models (e.g. Tresca and Mohr-Coulomb models) and then to elastic-plastic critical state models (e.g. Cam-clay models).

There are three basic sets of equations that most of the numerical techniques must satisfy for the solution of load deformation problems of soil masses. They are:

- *Equilibrium* equations: all the forces (body, surface, inertia and stress) must be in equilibrium
- *Compatibility* equations: relations between strains and displacements
- *Constitutive* equations: stress-strain relations of materials

The first two sets of equations (i.e. *Equilibrium* and *Compatibility*) are independent of the material. It is the *Constitutive* equations that express the influence of material on the behaviour of the soil.

There are two trends on the philosophy of constitutive modelling. The first employs very simple models with relatively few parameters (often with physical meaning), each for a specific application and for specific types of soils such as rocks, sands, normally and lightly overconsolidated clays and heavily overconsolidated clays. The second tends to use all-embracing models with a relatively large number of parameters (some may have no physical meaning). It is the user's task to choose the type of model that is suitable for the problem at hand.

This section presents a brief review of the constitutive models commonly used in geotechnical engineering. Based on the fundamental theories, all the models can be classified into the following groups:

- Elastic models
- Elastic-plastic models
- Elastic-viscoplastic models

2.1.2. Elastic models

These are the simplest of all and yet are still used very widely for traditional geotechnical engineering calculations.

The behaviour of an elastic material can be described by generalisations of the Hooke's law: the stresses are uniquely determined by the strains. Elastic constitutive models can take many forms: some assume the soil to be isotropic, others assume that it is anisotropic, some assume the soil to be linear, others that it is non-linear with

parameters dependent on the stress and/or strain level. One essential feature shared by all of these models is that all the deformations are recoverable once the load is removed.

The elastic moduli (Young's modulus E and Poisson's ratio μ) can be either linear or non-linear functions of the stresses. For soils, it is more fundamental to use a different pair of elastic constants: bulk modulus K and shear modulus G which divide the elastic deformation into a volumetric part and a distortional part respectively. The constitutive equation which relates increments of stress to increments of strain for elastic models takes the following form:

$$\Delta\boldsymbol{\sigma} = \boldsymbol{D}\Delta\boldsymbol{\varepsilon} \tag{2.1}$$

where:

$$\Delta\boldsymbol{\sigma} = \left|\Delta\sigma_x \quad \Delta\sigma_y \quad \Delta\sigma_z \quad \Delta\tau_{xy} \quad \Delta\tau_{yz} \quad \Delta\tau_{zx}\right|$$

$$\Delta\boldsymbol{\varepsilon} = \left|\Delta\varepsilon_x \quad \Delta\varepsilon_y \quad \Delta\varepsilon_z \quad \Delta\gamma_{xy} \quad \Delta\gamma_{yz} \quad \Delta\gamma_{zx}\right|$$

$\boldsymbol{D}$ is the elastic stress constitutive matrix

$\boldsymbol{D}$ is a function of the elastic moduli. For example, in the case of linear isotropic elasticity, $\boldsymbol{D}$ can be expressed as the following:

$$D = \begin{vmatrix} K+\frac{4}{3}G & K-\frac{2}{3}G & K-\frac{2}{3}G & 0 & 0 & 0 \\ & K+\frac{4}{3}G & K-\frac{2}{3}G & 0 & 0 & 0 \\ & & K+\frac{4}{3}G & 0 & 0 & 0 \\ & \text{Symmetric} & & G & 0 & 0 \\ & & & & G & 0 \\ & & & & & G \end{vmatrix}$$

In the case of fully anisotropic elasticity, the matrix $\boldsymbol{D}$ will become fully populated with 36 parameters. However, thermodynamic strain considerations (Love, 1927) imply that the matrix $\boldsymbol{D}$ is symmetrical, the total number of independent anisotropic parameters therefore reduces to 21.

In non-linear elasticity, it is often assumed that the material parameters depend on the stress and/or strain level. Most of the non-linear elastic models that are currently in use assume isotropic behaviour.

Even though elastic models are very simple and easy to use, they do not accurately predict the behaviour of real soils. Another problem which was pointed out by Sathialingam (1991) is that the elastic formulations are not conservative since energy may, under certain circumstances, be continuously extracted from the soil sample by subjecting it to a simple stress cycle.

2.1.3. Elastic-plastic models

In these models, soil behaviour is characterised by the existence of reversible and irreversible deformations called elastic and plastic deformations respectively. It is observed that for soils there exists a yield surface where the response of the soil changes from stiff to less stiff. For stress changes inside a chosen yield surface, the response is elastic. As soon as a stress change engages the yield surface, a combination of elastic and plastic responses occurs. These models, however, do not include the effects of time.

There are four basic requirements for an elastic-plastic model to be fully characterised, these are:

- Elastic properties
- Yield surface
- Plastic potential
- Hardening rule

Each of the requirements listed will be described briefly below:

<u>Elastic properties:</u>

The way in which elastic, recoverable deformations of the soil are to be described.

Yield surface:

$$F(\boldsymbol{\sigma},\boldsymbol{k}) = 0 \tag{2.2}$$

The boundary in a general stress space of a region within which it is reasonable to describe the deformations as elastic and recoverable. This function separates purely elastic from elastic-plastic behaviour.

The yield surface is a function of the stress state $\boldsymbol{\sigma}$ and state parameter $\boldsymbol{k}$ which controls its size. $\boldsymbol{k}$ is also called the hardening/softening parameter. For perfect plasticity $\boldsymbol{k}$ is constant. Hence, the yield surface is of a constant size. For hardening or softening plasticity, $\boldsymbol{k}$ varies with plastic straining to represent how the magnitude of the stress state at yield changes.

If the hardening or softening is related to the magnitude of the plastic strains, the model is known as *strain hardening/softening*. Alternatively, if it is related to the magnitude of plastic work, the model is known as *work hardening/softening*.

The value of the yield function F is used to identify the material behaviour. Purely elastic behaviour occurs if $F(\boldsymbol{\sigma},\boldsymbol{k})<0$, and elastic-plastic behaviour occurs if $F(\boldsymbol{\sigma},\boldsymbol{k})=0$. $F(\boldsymbol{\sigma},\boldsymbol{k})>0$ signifies an impossible situation.

Plastic potential:

$$G(\boldsymbol{\sigma},\boldsymbol{\beta}) = 0 \tag{2.3}$$

The mode of plastic deformation that occurs when the soil is yielding. A plastic potential is needed to specify the relative magnitudes of various components of plastic deformation. The plastic potentials also form a family of curves in the stress space like the yield surface.

The plastic potential is a function of stress state $\boldsymbol{\sigma}$ and $\boldsymbol{\beta}$ which is a vector of state parameters. This vector is immaterial and depends on the stress state.

The plastic potential provides an indication of the relative sizes of the strain components. The plastic incremental strain vector at a particular stress state will

be normal to the plastic potential surface passing through that point of stress state.

In some cases, for simplicity it is assumed that the plastic potential surface and the yield surface are identical, then the material is said to obey the postulate of normality or follow a law of associated flow (i.e. the nature of plastic deformation, or flow, is associated with the yield surface of the material). If the plastic potential surface is different from the yield surface, then the material is said to follow a non-associated flow rule.

Hardening rule:

A hardening rule describes the way in which the absolute magnitude of the plastic deformation is linked with the changing size of the yield surface. This rule prescribes how the state parameter $\boldsymbol{k}$ varies with plastic straining. This together with the plastic potential gives the magnitudes of the plastic deformations.

In some models, there are also other requirements needed, such as a requirement about the condition under which failure occurs, namely a condition beyond which the stress state cannot pass.

In general, there are two types of elastic-plastic models which will be mentioned in the following sections:

- Elastic-perfectly plastic models
- Elastic-plastic models

2.1.3.1. Elastic-perfectly plastic models

Examples of models in this category are: Tresca, Von Mises, Mohr-Coulomb and Drucker-Prager models.

Elastic-perfect plasticity or Rigid plasticity implies that the yield surface is fixed in the stress space. There is no expansion or contraction of the yield surface; hence the yield function only depends upon the stresses and the hardening parameter is a constant.

2.1.3.2. Elastic-plastic models

They are models in which soil behaviour is characterised by the existence of reversible (or elastic) and irreversible (or plastic) deformations. The mathematical theory of elastic-plasticity is well established and has been the foundation for the development of soil models. Various permutations and combinations of the yield functions, plastic potentials and hardening rules give rise to different models.

One of the major developments of constitutive models in the last 30 years is the introduction of models based on the critical state soil mechanics theory. This was started by Roscoe and his co-workers at the University of Cambridge in the late 50's (Roscoe, Schofield and Wroth, 1958, 1959; Poorooshasb and Roscoe, 1961; Roscoe and Poorooshasb, 1963; Roscoe, Schofield and Thurairajah, 1963; Roscoe and Schofield, 1963; Schofield and Wroth, 1968; Roscoe and Burland, 1968). A full review on critical state soil mechanics is presented in section 2.2.

Other examples of elastic-plastic models are those by Pender (1978), Prevost (1978) and Mroz and Pietruszczak (1983).

2.1.4. Elastic-viscoplastic models

Elastic-viscoplastic models are the most realistic and logical models for soil mechanics problems because time effects on soil behaviour are taken into account rather than those due to consolidation. However, the penalty for this is that the models are much more complicated and when implemented through computer programs, they are very costly in terms of both time and computer memory.

Most of the elastic-viscoplastic models in the literature could be classified to the following three criteria (Kutter and Sathialingam, 1992):

- The elastic response of the material is either:
  - Rate dependent
  - Rate independent

- Time is incorporated into the constitutive relations either:
  - Explicitly
  - Indirectly through evolution of internal variables
- Plastic strains either:
  - Occur at all states
  - Are zeros in a so-called 'static' region of stress space

Various models of this type have been developed. Some of them will be listed here: Adachi and Okano (1974); Adachi and Oka (1982); Dafalias (1982); Zienkiewick et. al. (1975) and Zienkiewick and Humpheson (1977); Nova (1982); Sekiguchi (1984); Katona and Mulert (1984); Katona (1984); Sathialingam (1991).

2.1.5. Other modern approaches

Apart from the traditional elastic-plastic theory introduced above, there are two other approaches which are worth mentioning here. They are the theories of hyperplasticity and hypoplasticity.

Hyperplasticity is an approach to plasticity based on thermomechanical principles and was originally suggested by Ziegler (1977, 1983) and later advocated by Houlsby (1981), Collins and Houlsby (1997), Houlsby and Purzin (2000) and Purzin and Houlsby (2001). The advantage of this approach is that it allows a compact development of plasticity theories which are guaranteed to obey thermodynamics principles. An important feature of this framework is that it has close links to conventional plasticity. Within hyperplasticity, the constitutive behaviour of a dissipative material can be completely defined by two potential functions. The first function is either the Gibbs free energy or the Helmholtz free energy. The second potential is the dissipation function. The interpretation of this framework in terms of conventional plasticity theory demonstrates that the classical yield surface, flow and hardening rules are all hidden within these two scalar potential functions.

Hypoplasticity constitutive models, as described by Wu and Kolymbas (1990), Kolymbas (1991) and Kolymbas and Wu (1993), originate from a formalism alternative to elastoplasticity. Hypoplasticity is a new approach to constitutive modelling of

granular media in terms of rational continuum mechanics. It aims to describe the inelastic phenomena of granular materials (like cohensionless soils) without using the additional notions introduced by elastoplasticity (such as yield surface, plastic potential etc.). Hypoplasticity recognises that inelastic deformations may occur from the very beginning of the loading process. It does not a priori distinguish between elastic and plastic deformations. The outstanding feature of hypoplasticity is its simplicity: not only does it avoid the aforementioned additional notions but it also uses a unique equation which holds equally for loading and unloading. The distinction between loading and unloading is automatically accomplished by the equation itself.

2.2. CRITICAL STATE THEORY

2.2.1. Introduction

The theory of soil behaviour known as 'critical state soil mechanics' was developed from the application of the theory of plasticity to soil mechanics. The first critical state models were the series of Cam-clay formulations developed at the University of Cambridge by Roscoe and his co-workers. The formulation of the original Cam-clay model as an elastic-plastic constitutive law was presented by Roscoe and Schofield (1963) and Schofield and Wroth (1968). Afterwards, Roscoe and Burland (1968) proposed the modified Cam-clay model.

The theory of critical state soil mechanics has been used widely since then and has resulted in the development of many models. The purpose of all of these models is to achieve a better agreement between predicted and observed soil behaviour. In this section, a brief description of the critical state soil mechanics theory is presented.

2.2.2. The critical state concept

Most of the formulations in critical state models have been carried out in the conventional triaxial stress space in order to confine attention to the conventional

laboratory consolidation and triaxial test conditions. This would also enable a preliminary verification of the models. After the verification and validation processes, the models are generalised to the three-dimensional stress space.

The state of a soil sample in the triaxial stress space is fully described by three parameters, namely p', q and ν defined as:

$$p' = \frac{\sigma'_a + 2\sigma'_r}{3} = \frac{\sigma_a + 2\sigma_r}{3} - u \qquad \text{: mean normal effective stress}$$

$$q = \sigma'_a - \sigma'_r = \sigma_a - \sigma_r \qquad \text{: deviatoric stress}$$

ν: specific volume, i.e. the volume of soil containing unit volume of solid material, $\nu = 1 + e$

where

σ'_a: vertical (axial) effective stress

σ_a: vertical (axial) total stress

σ'_r: radial effective stress

σ_r: radial total stress

e: voids ratio

u: pore water pressure

These three parameters (p', q and ν) will vary during a triaxial test. The progress of a soil sample during a test can be represented by a series of points describing a path in a three-dimensional space with axes p', q and ν. Different types of test (drained, undrained, compression or extension) will lead to different test paths in this (p', q, ν) space. Critical state soil mechanics gives us the set of rules for calculating test paths in the (p', q, ν) space: usually two parameters are determined by the type of test and there is a simple procedure for determining the third.

There are also parameters which are soil constants. For example in the cases of original Cam-clay and modified Cam-clay, there are five constant parameters, namely M, Γ, κ, λ and μ (or G) (where M is the slope of the critical state line in the (p', q) space; Γ, κ, and λ are defined in Figure 2.1b; μ is the Poisson's ratio and G is the shear modulus). In other

models, there may be more. These constant parameters describe the fundamental properties of a particular soil with a given mineralogy.

Corresponding to the stress parameters p' and q are the strain parameters ε_p (volumetric strain) and ε_q (deviatoric strain):

$$\varepsilon_p = \varepsilon_a + 2\varepsilon_r \tag{2.4}$$

$$\varepsilon_q = \frac{2}{3}\left(\varepsilon_a - \varepsilon_r\right) \tag{2.5}$$

where

ε_a: vertical (axial) strain

ε_r: radial strain

ε_p and ε_q describe the strains from the start of the test. Strain increments are denoted $\delta\varepsilon_p$ and $\delta\varepsilon_q$:

$$\delta\varepsilon_p = \delta\varepsilon_a + 2\delta\varepsilon_r \tag{2.6}$$

$$\delta\varepsilon_q = \frac{2}{3}\left(\delta\varepsilon_a - \delta\varepsilon_r\right) \tag{2.7}$$

The reason the factor '2/3' appears in the definition of shear strain ε_q is so that the work done by a small increment of straining is equal to both $\sigma'_a\delta\varepsilon_a+2\sigma'_r\delta\varepsilon_r$ and $p'\delta\varepsilon_p+q\delta\varepsilon_p$. Thus the stress strain parameters correspond to one another in that multiplication leads to the correct evaluation of work done in deformation.

If a soil sample is allowed to change its volume during a shearing test, it will either dilate or contract depending on its initial state of density (i.e. initial values of p', q and ν). The volumetric yielding process will continue until the soil sample reaches a critical void ratio (or specific volume), after which the volume of the soil will remain constant during subsequent deformations. *This constant volume state is known to as the Critical State*. Hence, at critical state we have:

$$\frac{\delta\varepsilon_p}{\delta\varepsilon_q} = 0 \qquad \frac{\delta q}{\delta\varepsilon_q} = 0 \qquad \frac{\delta p'}{\delta\varepsilon_q} = 0$$

A soil deforming with a void ratio lower than the critical value at a given stress level tends to increase its volume, whereas a soil at a void ratio higher than the critical state tends to decrease its volume.

Critical states for a given soil form a unique line in the (p',q,v) space which is referred to as the critical state line (*CSL*) and has the following equations:

$$q = Mp' \tag{2.8}$$

$$v = \Gamma - \lambda \ln p' \tag{2.9}$$

where M, Γ, and λ are soil constants.

For isotropic stress conditions (i.e. q=0), the plastic compression of a normally consolidated soil can be represented by a unique line called the isotropic normal compression line (*NCL*) or reference consolidation line. This can be expressed as:

$$v = N - \lambda \ln p' \tag{2.10}$$

where N is the specific volume when p'=1kPa or 1MPa, depending on the chosen units.

If the soil is unloaded and reloaded, the path in (v,lnp') is quasi-elastic (i.e. hysteretic), as shown in Figure 2.1a. However, the behaviour is idealised as perfectly elastic (as shown in Figure 2.1b) so that equation of a typical unload-reload line is:

$$v = v_\kappa - \kappa \ln p' \tag{2.11}$$

where κ is soil constant and v_κ is dependent on the stress history of the soil. For this reason, unload-reload lines are known as 'κ-lines' and are used in critical state soil models such as Cam-clay.

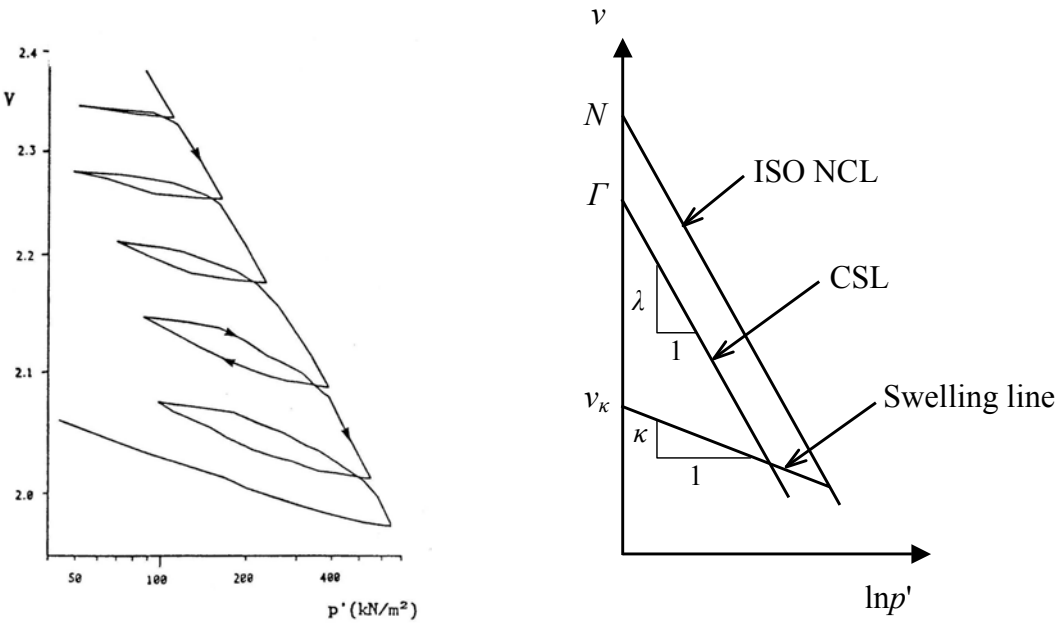

(a) (b)

Figure 2.1. (a) True unload-reload behaviour and (b) idealised unload-reload behaviour of Speswhite kaolin in the (v,ln$p$') space (Al-Tabbaa, 1987)

2.2.3. The original Cam-clay model

The Cam-clay models (original and modified) are essentially based on the following assumptions:

- For convenience, it is assumed that changes in size of the current yield surface are related to changes in volume. This permits the compression and shearing of clays to be simply brought into a single picture and leads to a class of what can be called volumetric hardening models.
- All the assumptions stated in section 2.1.3 for an elastic-plastic model are retained in the original and modified Cam-clay models.

The original Cam-clay model was developed by Roscoe and Schofield (1963). It is assumed that recoverable changes in volume accompany any changes in the mean effective stresses p' according to the expression:

$$\delta\varepsilon_p^e = \kappa \frac{\delta p'}{v p'} \tag{2.12}$$

This implies a linear relationship between specific volume and the logarithm of mean effective stress p' for elastic unloading-reloading. Therefore, the bulk modulus is:

$$K = \frac{\delta p'}{\delta\varepsilon_p^e} = \frac{v p'}{\kappa} \tag{2.13}$$

Recoverable changes in shear strain are given by:

$$\delta\varepsilon_q^e = \frac{\delta q}{3G} \tag{2.14}$$

and G is either assumed to be constant (so μ varies) or determined from K and a constant effective Poisson's ratio (μ).

The original Cam-clay yield surface is derived from the work equation as follows:

$$p'\delta\varepsilon_p^p + q\delta\varepsilon_q^p = Mp'\delta\varepsilon_q^p \tag{2.15}$$

In equation 2.15, the terms in the left hand side are the energy available for dissipation and the terms in the right side follow Taylor's (1948) analysis of the shear box which assumes that this dissipated energy is entirely due to friction. Since the direction of the strain increment vector $\left(\delta\varepsilon_p^p, \delta\varepsilon_q^p\right)$ is assumed to be normal to the yield locus (i.e. the yield locus and plastic potential coincide) then:

$$\frac{\delta\varepsilon_p^p}{\delta\varepsilon_q^p} = -\frac{\delta q}{\delta p'} \tag{2.16}$$

The corresponding plastic potential in the (q,p') space is given as the following expression:

$$\frac{q}{p'} = \eta = M \ln \frac{p'_o}{p'} \tag{2.17}$$

where p'_o is the preconsolidation pressure which is the value of p' when η=0. The curve is plotted in Figure 2.2.

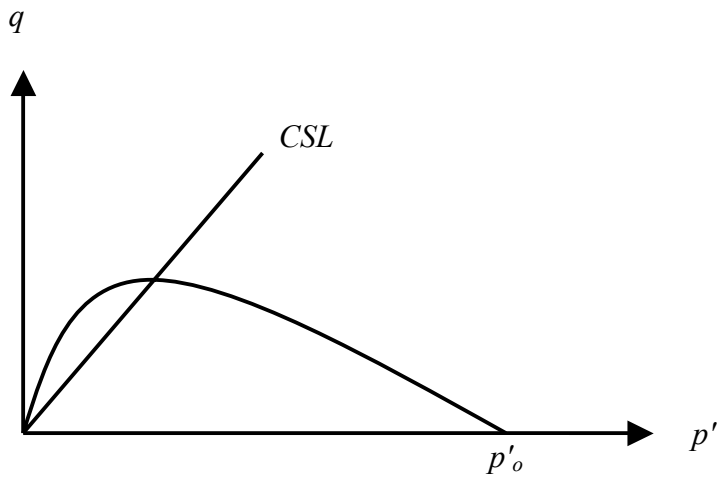

Figure 2.2. The original Cam-clay model yield surface

In original Cam-clay, it is assumed that the plastic flow obeys the principle of normality or has an associated flow rule: that is the plastic potential and the yield surface coincide. This is convenient when implementing the model in finite element calculations because the constitutive matrix (D^{ep}) is symmetric if the plastic potential (G) is equal to the yield surface (F). The yield surface is therefore:

$$q = Mp' \ln \frac{p'_o}{p'} \tag{2.18}$$

The yield surface is assumed to expand with a constant shape, and the size of the yield surface is assumed to be related to the changes in volume only, according to the following equation:

$$\delta\varepsilon_p^p = \frac{(\lambda - \kappa)}{v} \frac{\delta p'_o}{p'_o} \tag{2.19}$$

The plastic stress-strain relationship for elastic-plastic models is defined as:

$$\begin{bmatrix} \delta\varepsilon_p^p \\ \delta\varepsilon_q^p \end{bmatrix} = \frac{1}{H} \begin{bmatrix} \dfrac{\partial F}{\partial p'}\dfrac{\partial G}{\partial p'} & \dfrac{\partial F}{\partial q}\dfrac{\partial G}{\partial p'} \\ \dfrac{\partial F}{\partial p'}\dfrac{\partial G}{\partial q} & \dfrac{\partial F}{\partial q}\dfrac{\partial G}{\partial q} \end{bmatrix} \begin{bmatrix} \delta p' \\ \delta q \end{bmatrix} \tag{2.20}$$

After substituting the expressions for the yield and plastic potential surfaces into equation 2.20, the elastic and plastic stress-strain responses for the original Cam-clay model can be summarised in matrix form as:

$$\begin{bmatrix} \delta\varepsilon_p^e \\ \delta\varepsilon_q^e \end{bmatrix} = \begin{bmatrix} \dfrac{1}{K} & 0 \\ 0 & \dfrac{1}{3G} \end{bmatrix} \begin{bmatrix} \delta p' \\ \delta q \end{bmatrix} \tag{2.21}$$

$$\begin{bmatrix} \delta\varepsilon_p^p \\ \delta\varepsilon_q^p \end{bmatrix} = \frac{(\lambda-\kappa)}{vMp'(M-\eta)} \begin{bmatrix} (M-\eta)^2 & (M-\eta) \\ (M-\eta) & 1 \end{bmatrix} \begin{bmatrix} \delta p' \\ \delta q \end{bmatrix} \tag{2.22}$$

2.2.4. The modified Cam-clay model

The modified Cam-clay model was developed by Roscoe and Burland (1968) as a modification of the original Cam-clay model. This model successfully reproduces the major deformation characteristics of soft clay and is more widely used for numerical predictions than the original Cam-clay model. It has been used effectively in several applications, a summary of these applications can be found in Wroth and Houlsby (1985).

One of the main improvements of the modified Cam-clay model from the original Cam-clay model is the prediction of the coefficient of the earth pressure at rest ($K_{o,nc}$) for one-dimensional normal compression. For one-dimensional normal compression, original Cam-clay predicts a zero value for $\eta_{o,nc}$, so it cannot distinguish between isotropic and one-dimensional normal compression. Furthermore, the discontinuity of the original Cam-clay yield surface at q=0 causes difficulties because the associated flow rule will predict an infinite number of possible strain increment vectors for isotropic

compression. This causes difficulty in finite element formulation. The modified Cam-clay model overcomes these problems by adopting an elliptical-shaped yield surface (shown in Figure 2.3) which has the following expression:

$$q^2 = M^2\left(p'\,p'_o - p'^2\right) \tag{2.23}$$

or $$\frac{p'}{p'_o} = \frac{M^2}{M^2 + \eta^2} \tag{2.24}$$

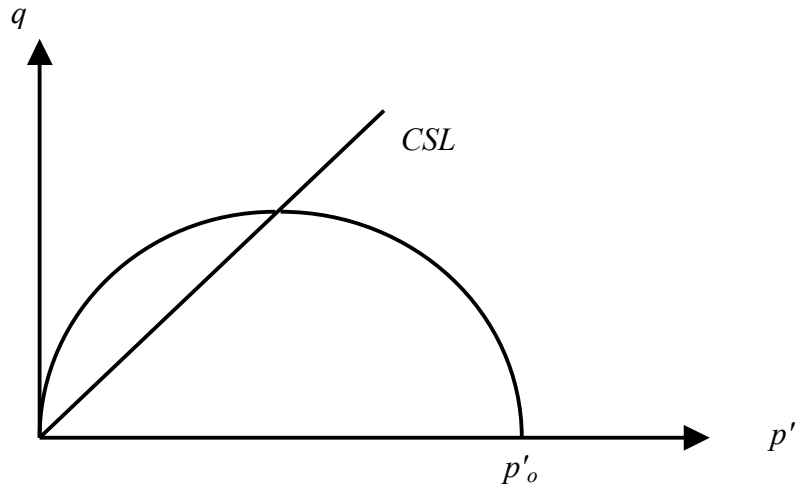

Figure 2.3. The modified Cam-clay model yield surface

When the stress states are within the current yield surface, the elastic properties of modified Cam-clay are the same as those in the original Cam-clay model (see section 2.2.3).

Because of the assumption that the soil obeys the normality condition, the plastic potential (G) is the same as the yield surface (F):

$$G = F = q^2 - M^2\left[p'\left(p'_o - p'\right)\right] = 0 \tag{2.25}$$

The flow rule for modified Cam-clay is then calculated by application of the normality condition:

$$\frac{\delta\varepsilon_p^p}{\delta\varepsilon_q^p} = \frac{\partial G / \partial p'}{\partial G / \partial q} = \frac{M^2 - \eta^2}{2\eta} \tag{2.26}$$

The yield surface is assumed to expand with a constant shape and its size is controlled by the preconsolidation pressure (p'_o). The hardening relationship for modified Cam-clay is the same as that for original Cam-clay:

$$\delta\varepsilon_p^p = \frac{(\lambda-\kappa)}{v}\frac{\delta p'_o}{p'_o} \tag{2.27}$$

The elastic and plastic stress-strain responses can be written in matrix form as:

$$\begin{bmatrix}\delta\varepsilon_p^e \\ \delta\varepsilon_q^e\end{bmatrix} = \begin{bmatrix}\frac{1}{K} & 0 \\ 0 & \frac{1}{3G}\end{bmatrix}\begin{bmatrix}\delta p' \\ \delta q\end{bmatrix} \tag{2.28}$$

$$\begin{bmatrix}\delta\varepsilon_p^p \\ \delta\varepsilon_q^p\end{bmatrix} = \frac{(\lambda-\kappa)}{vp'(M^2+\eta^2)}\begin{bmatrix}(M^2-\eta^2) & 2\eta \\ 2\eta & \frac{4\eta^2}{(M^2-\eta^2)}\end{bmatrix}\begin{bmatrix}\delta p' \\ \delta q\end{bmatrix} \tag{2.29}$$

2.2.5. Shortcomings of the original and modified Cam-clay models

The original and modified Cam-clay models are known to be able to predict the behaviour of normally and lightly overconsolidated clay reasonably well. However, there are several shortcomings which will be discussed briefly in this section.

1. The original Cam-clay model cannot distinguish between isotropic and one-dimensional compression (Bolton, 1991). Furthermore, the discontinuity of the original Cam-clay yield surface at q=0 causes difficulties because the associated flow rule will predict an infinite number of possible strain increment vectors for isotropic compression. This causes difficulty in the finite element formulation. However, this problem is eliminated with the modified Cam-clay model.
2. The original and modified Cam-clay models were developed based on the assumption that soils are isotropic. It is well known that natural soils are anisotropic due to the mode of deposition. Many soils have been deposited over areas of large lateral extent and the deformations they have experienced during and after deposition have been essentially one-dimensional.

3. The original and modified Cam-clay models do not take into account the time effect on soil deformation known as creep.
4. The original and modified Cam-clay models overestimate the failure stresses on the 'dry' side (i.e. states to the left of the critical state line). These models predict a peak strength in undrained heavily overconsolidated clay which is not usually observed in experiments. This is due to the yield surfaces adopted in these models.
5. Another main problem with the original and modified Cam-clay models is their poor prediction of shear strains within the yield surface (Wroth and Houlsby, 1985). This is because either the shear modulus or the Poisson's ratio is assumed to be constant.
6. The original and modified Cam-clay models cannot successfully model the behaviour of sand. The main problems lie in the fact that sand does not closely obey the principle of normality, and experimental data shows that the critical state point does not lie at the top of the yield locus but lies to the left of the peak. This implies that undrained tests on normally consolidated sands can exhibit a peak value of q before the critical state is approached which cannot be predicted by these models.
7. The modelling of soils under cyclic loading is another deficiency in these elastic-plastic models. The essential features of the Cam-clay models are that on primary loading large plastic strains occur but on subsequent unload-reload cycles within the yield surface only purely elastic strains are produced. This is not suitable for modelling the behaviour of soil under cyclic loading because in reality, all unload-reload cycles result in the gradual accumulation of permanent strain and/or pore pressure and hysteretic behaviour occurs.

2.2.6. Other critical state models

In order to achieve better agreement between the predicted and observed soil behaviour, a large number of modifications have been proposed to the standard Cam-clay models. A brief review on some of the most important modifications may be found in Gens and Potts (1988). Zienkiewicz and Naylor (1973) proposed a yield surface for heavily overconsolidated clays. Nova and Wood (1978) and Pastor et. al. (1985) developed

critical state models for sands. Ohta and Wroth (1976) and Whittle (1993) have models for one-dimensionally consolidated soils with an anisotropic yield surface. Three-dimensional critical state models were proposed in Roscoe and Burland (1968) as well as in Zienkiewicz and Pande (1977).

2.2.7. Kinematic hardening critical state models

The development of critical state soil mechanics was a major advance in the use of plasticity theory in geomechanics. Still, however, some very important aspects of soil behaviour, mainly in relation to the cyclic response, cannot be adequately described. The principal reason is that the classical concept of a yield surface provides little flexibility in describing the change of the plastic modulus with loading direction and implies a purely elastic stress range within the yield surface. Therefore, the need for new concepts in plasticity theory became a necessity.

There have been two major developments in this field over the last 35 years, namely the concept of multi surface, kinematic hardening plasticity theory introduced by Mroz (1967) and Iwan (1967) and the bounding surface plasticity theory introduced by Dafalias and Popov (1975) and Dafalias (1975).

In isotropic hardening models such as Cam-clays, the yield surface expands with the plastic deformation so that the size of the elastic region becomes very large. However, experimental observations show that truly recoverable elastic behaviour occurs only for a very small range of strain, typically 0.001% (Jardin et al., 1984), and high stiffness only occurs immediately after a major change in the direction of an effective stress or strain path.

Kinematic hardening models allow this response to be reproduced by including a small inner true yield surface which bounds a small truly elastic region. This inner yield surface is carried around by the current stress state following a translation rule. Moreover, a kinematic hardening model together with the bounding surface model described below are the two types of models that are capable of producing some of the essential features of soil experiencing cyclic loading.

The concept of kinematic hardening or multi surface plasticity was first introduced by both Mroz (1967) and Iwan (1967). Mroz uses a single yield surface together with a set of hypersurfaces to define the variation of the plastic modulus whereas Iwan uses a set of yield surfaces. Essentially their models serve the same purposes.

This theory was originally applied to metal plasticity and subsequently to soils by Prevost (1978) and Mroz, Norris and Zienkiewicz (1978, 1979). More recently, some similar soil models have been formulated by Al Tabbaa (1987) (with two surfaces called 'Bubble' model) and Stallebrass (1990) and Stallebrass and Taylor (1997) (with three surfaces called 3SKH model, see Figure 2.4). McDowell and Hau (2003) extended Stallebrass and Taylor's work by introducing a new plastic potential to get better predictions of the $K_{o,nc}$ value and shear strain.

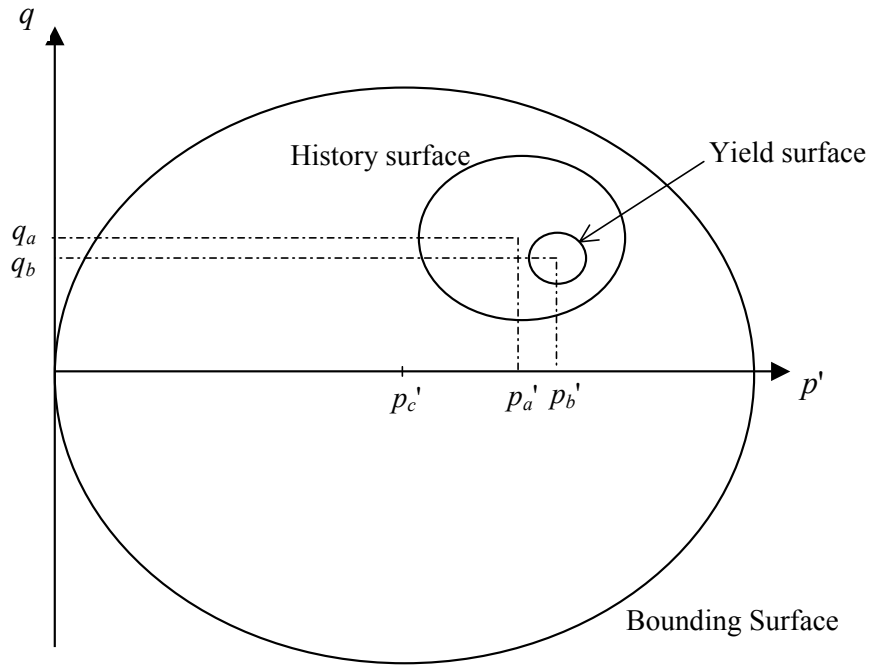

Figure 2.4. Sketch of the 3-SKH model in the triaxial stress space (Stallebrass, 1990)

2.2.8. Bounding surface critical state models

Since the time of its introduction, the concept of the bounding surface in the stress space has been used by many authors in a variety of plasticity constitutive models (e.g. Dafalias and Herrmann, 1980; Aboim and Roth, 1982; McVay and Taesiri, 1985; Bardet, 1986). The salient features of a bounding surface formulation are that plastic deformation may occur for stress states within the yield surface and it is possible to have a very flexible variation in the plastic modulus during a loading path.

The theory can be succinctly summarised as follows: for any given stress state within or on the bounding surface, a proper mapping rule associates a corresponding 'image' stress point on the surface: a measure of the distance between the actual and image stress points is used to specify the plastic modulus at the actual stress state in terms of a bounding plastic modulus at the 'image' stress state (Dafalias and Herrmann, 1987a and 1987b). In other words, the bounding surface plasticity theory assumes that plastic deformation is allowed within the state boundary surface. The sketch of a typical bounding surface model in the triaxial stress space is shown in Figure 2.5.

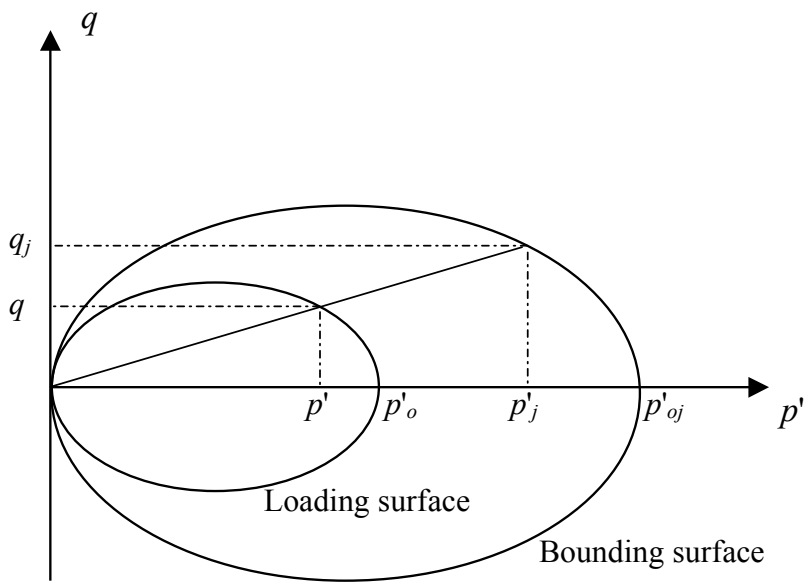

Figure 2.5. Sketch of a typical bounding surface model in the triaxial stress space

2.3. METHODS OF ANALYSIS IN GEOTECHNICAL ENGINEERING

2.3.1. Introduction

Three common methods of analysis in geotechnical engineering are presented in this section. The most widely used numerical method is described, namely the finite element method. Finally, the finite element program CRISP is introduced.

2.3.2. Methods of analysis in geotechnical engineering

As pointed out in the previous sections, fundamental considerations assert that for an exact theoretical solution the requirements of equilibrium, compatibility and constitutive relations together with the boundary conditions must all be satisfied. Current methods of analysis in geotechnical engineering categories (according to Potts and Zdravkovic, 1999) can be grouped into the following types of analysis:

- Closed form analysis
- Simple analysis
- Numerical analysis

2.3.2.1. Closed form analysis

If for a particular geotechnical structure, it is possible to establish a realistic constitutive model for material behaviour, identify the boundary conditions and combine these with the equations of equilibrium and compatibility, an exact theoretical solution can be obtained. This solution is called a closed form solution. The solution is only exact for the idealised problem but it is still approximate for the real problem because assumptions have been made in idealising the real physical problem into an equivalent mathematical form.

A closed form solution is the ultimate method of analysis. In this approach, all solution requirements are satisfied and the theories of mathematics are used to obtain complete analytical expressions defining the full behaviour of the problem. However, as soil is a

very complex material which behaves non-linearly when loaded, complete analytical solutions are often impossible in real problems. In fact, solutions can only be obtained for two very simple classes of problems:

- Firstly, there are solutions in which the soil is assumed to behave in an isotropic linear elastic manner. While these can be useful for providing a first estimate of the results, they are of little use for investigating stability. Comparison with observed behaviour indicates poor agreement.
- Secondly, there are solutions for problems which contain sufficient geometric symmetries so that the problem reduces to being essentially one-dimensional in the sense that one variable is of interest and is a function of only one co-ordinate. Expansion of spherical and infinitely long cylindrical cavities in an infinite elastic-plastic continuum are examples.

2.3.2.2. Simple analysis

In order to get solutions for the more realistic problems, approximations must be introduced. One way of doing this is to relax some of the constraints imposed on the basic solution requirements. However, mathematics is still used to obtain an approximate analytical solution.

Limit Equilibrium, *Stress Field* and *Limit Analysis* (upper bound (or unsafe) and lower bound (or safe) methods) fall into the category of simple methods. All methods essentially assume the soil is at failure but differ in the manner in which they arrive at a solution.

None of the simple methods satisfy all the basic requirements and therefore do not necessarily produce an exact theoretical solution. When applied to geotechnical problems, they do not distinguish between different methods of construction, nor account for the in-situ stress conditions. The information provided from simple methods is on local stability only and separate calculations are required to investigate the overall stability. However, because of their simplicity and ease of use, simple methods form the main stay of most design approaches and it is likely that they will always play an

important role in the design of geotechnical structures. In particular, they are appropriate at the early stages of the design process to obtain first estimate of both the stability and structural forces.

2.3.2.3. Numerical analysis

Another way to obtain more realistic solutions for geotechnical engineering problems is to introduce numerical approximations. In this approach, all requirements of a theoretical solution are considered but may only be satisfied in an approximate manner. Because of the complexities involved and the non-linearlities in soil behaviour, all methods are numerical in nature.

Their ability to accurately reflect real behaviour of the soil and structure essentially depends on:

- The ability of the constitutive model to represent real soil behaviour
- The correctness of the boundary conditions imposed

The most commonly used technique in geotechnical problems is the *Finite Element Method*. This method essentially involves a computer simulation of the history of the boundary value problem from the beginning, through construction and in the long term. According to Desai (1979), formulation and application of the finite element method are considered to consist of the following eight basic steps:

(i) Discretise and Select Element Configuration
(ii) Select Approximation Models or Functions
(iii) Define Strain - Displacement and Stress-Strain (Constitutive) Relations
(iv) Derive Element Equations
(v) Assemble Element Equations to Obtain Global Equations and Introduce Boundary Conditions
(vi) Solve for the Primary Unknowns
(vii) Solve for Derived or Secondary Quantities
(viii) Interpret the Results

2.3.3. SAGE CRISP

CRISP (CRItical State soil mechanics Program) is a geotechnical finite element program incorporating the critical state soil mechanics theory (Britto and Gunn, 1987). It was developed by research workers at Cambridge University Engineering Department from 1975 onwards and was first released publicly in 1982. SAGE Engineering Ltd has added a Microsoft Windows graphical user interface and technical enhancements to the latest version to create SAGE CRISP.

SAGE CRISP operates in either two-dimensional plane strain or axis-symmetry. The effective stress principal is an integral part of the finite element analysis engine. Thus, SAGE CRISP can perform drained, undrained and fully coupled (Biot) consolidation analyses.

The adequacy of a finite element solution is largely dependent upon the constitutive models used. SAGE CRISP incorporates over twenty soil models and three structural models. These models have been developed over the course of the past 20 years, during which time they have achieved widespread recognition and respect. The soil models include linear elastic, elastic-perfectly plastic and critical state soil models.

The accuracy of a finite element solution is directly related to the type of finite element used. SAGE CRISP provides sufficient element types to give accurate solutions to most geotechnical problems. One, two and three-dimensional elements are available along with an interface element for soil structure interaction analysis. New element types can also be added into SAGE CRISP with relatively little effort.

The small-displacement, small-strain approach is used throughout SAGE CRISP to avoid the extra complexity of using the strain and stress tensors which are appropriate to large deformations and strains. The program does however, contain the option of updating the co-ordinates of nodal points as the analysis proceeds. This is equivalent to a first approximation to an updated Lagrangian formulation. Large-strain approach can also be used in SAGE CRISP but this solution scheme has yet to be verified.

SAGE CRISP has three solution schemes to analyse non-linear problems. In the incremental or Tangent Stiffness Technique, the user divides the total load acting into a

number of small increments and the program applies each of these incremental loads in turn. During each increment, the stiffness properties appropriate for the current stress levels are used in the calculations. This approach is very easy to implement and is numerically stable (compared to other approaches). However, it needs a large number of increments to obtain accurate results for complicated problems. The Modified Newton Raphson (MNR) Displacement Method and the Modified Tangent Stiffness Method (by means of applying an out of balance load in the next increment) use fewer increments for the same level of accuracy but take longer to analyse.

SAGE CRISP is frequently used as a test bed for new constitutive models which can be bolted onto the existing finite element code. This is the reason why SAGE CRISP is used in this study.

CHAPTER 3

CASM: A UNIFIED MODEL FOR CLAY AND SAND

3.1. DESCRIPTION OF THE MODEL

3.1.1. Introduction

CASM (Clay And Sand Model) was developed by Yu (1995, 1998). This is a simple, unified critical state constitutive model for both clay and sand. The main feature of CASM is that a single set of yield and plastic potential functions is used to model the behaviour of clay and sand under both drained and undrained loading conditions.

This model uses the state parameter concept and a non-associated flow rule. Yu stated that because the state parameter may be determined easily for both clay and sand, it might be regarded as a better quantity than the overconsolidation ratio (*OCR*) for describing soil response under various loading conditions. The state parameter (ξ) is a function of other basic parameters:

$$\xi = \nu + \lambda \ln p' - \Gamma \tag{3.1}$$

It is noted that ξ is zero at the critical state, positive on the 'wet' side and negative on the 'dry' side. All the definitions of the state parameter, the reference state parameter and the critical state constants can be found in Figure 3.1.

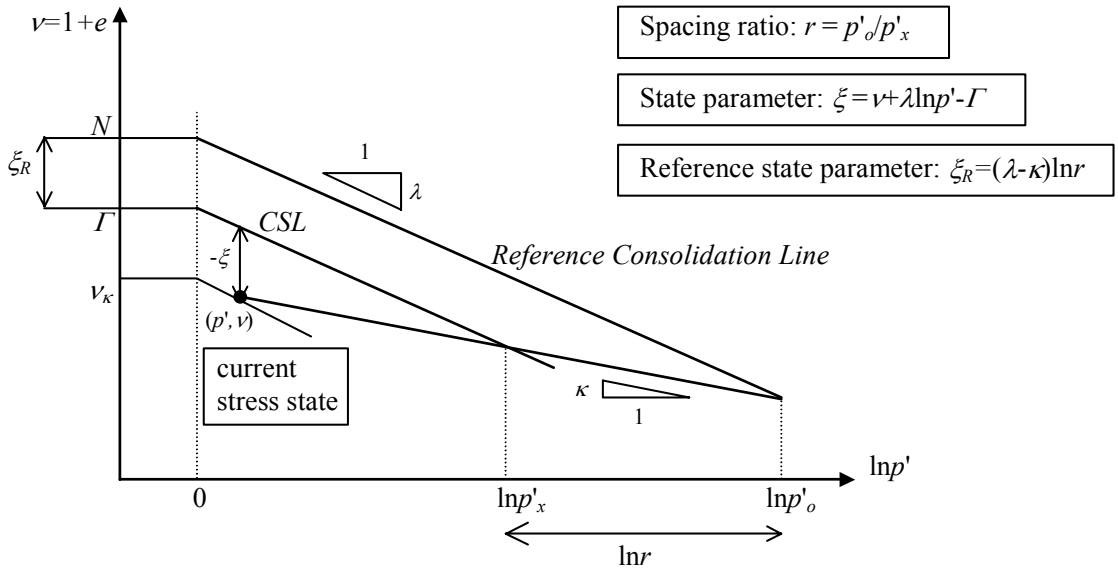

Figure 3.1. State parameter, reference state parameter and critical state constants

3.1.2. Yield surface

The yield surface function for CASM can be expressed in terms of the conventional triaxial parameters as follows:

$$F(\sigma,k)=\left(\frac{q}{Mp'}\right)^{n}+\frac{\ln\left(\frac{p'}{p'_{o}}\right)}{\ln r} \tag{3.2}$$

In equation 3.2, n and r are the two new parameters introduced in CASM. The stress-state coefficient (n) is a parameter used to specify the shape of the yield surface and r is the spacing ratio used to control the intersection point of the critical state line and the yield surface. The reference state parameter (ξ_R) denotes the vertical distance between the *CSL* and the reference consolidation line.

The shapes of the CASM yield surface with r=3 and different values of n are plotted in Figure 3.2 below:

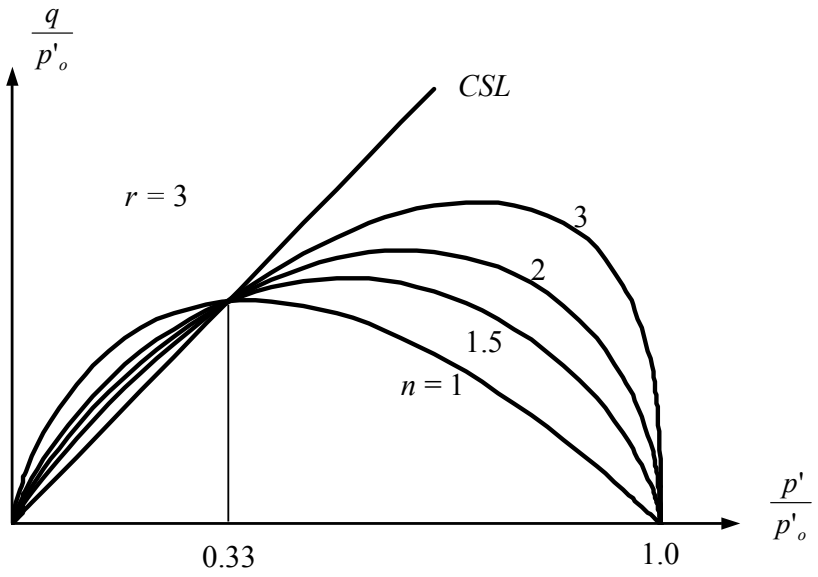

Figure 3.2. CASM's yield surface shape

It is interesting to note that the original Cam-clay model can be recovered exactly from CASM by choosing n=1 and r=2.7183. In addition, the 'wet' side of the modified Cam-clay model can also be matched accurately using CASM by choosing r=2 in conjunction with a suitable n value (typically around 1.5-2, dependent on material).

It should also be noted that the intersection point between the critical state line and the yield surface in this model does not necessarily occur at the maximum deviatoric stress (as in the original and modified Cam-clay models). This reproduces an important feature of the observed yield surface for sand which is the deviatoric stress often reaches a local peak before approaching the critical state.

3.1.3. Plastic potential

The plastic potential in CASM follows the stress-dilatancy relation of Rowe (1962). This flow rule, which was originally developed from minimum energy considerations of particle sliding, has met with greatest success in describing the deformation of sands and other granular materials. Rowe's stress-dilatancy relation is very similar to the original Cam-clay model (see Figure 3.3). Hence, it may also be used to describe the experimental stress-dilatancy data for clays. The flow rule can be expressed, for triaxial compression, as follow:

$$\frac{\delta\varepsilon_p^p}{\delta\varepsilon_q^p} = \frac{\partial G/\partial p'}{\partial G/\partial q} = \frac{9(M-\eta)}{9+3M-2M\eta} \tag{3.3}$$

Therefore by integration, the equation of the plastic potential takes the form:

$$G(\sigma,\beta) = 3M(\ln p' - \ln\beta) + (3+2M)\ln\left(\frac{2q+3p'}{p'}\right) - (3-M)\ln\left(\frac{3p'-q}{p'}\right) = 0 \tag{3.4}$$

where the size parameter β can be determined easily for any given stress state (p',q) by solving the above equation. The plastic flow rule adopted in CASM is non-associated because the plastic potential function is not identical to the yield surface.

The three different flow rules adopted in the original Cam-clay model , the modified Cam-clay model and CASM are shown in Figure 3.3. This figure shows the shapes of the plastic potentials of the three models which pass through one common stress point (p'_1,q_1). The shape of CASM's plastic potential is very similar to that of the original Cam-clay model and like original Cam-clay, CASM's plastic potential has a vertex and the flow rule has a discontinuity for η=0.

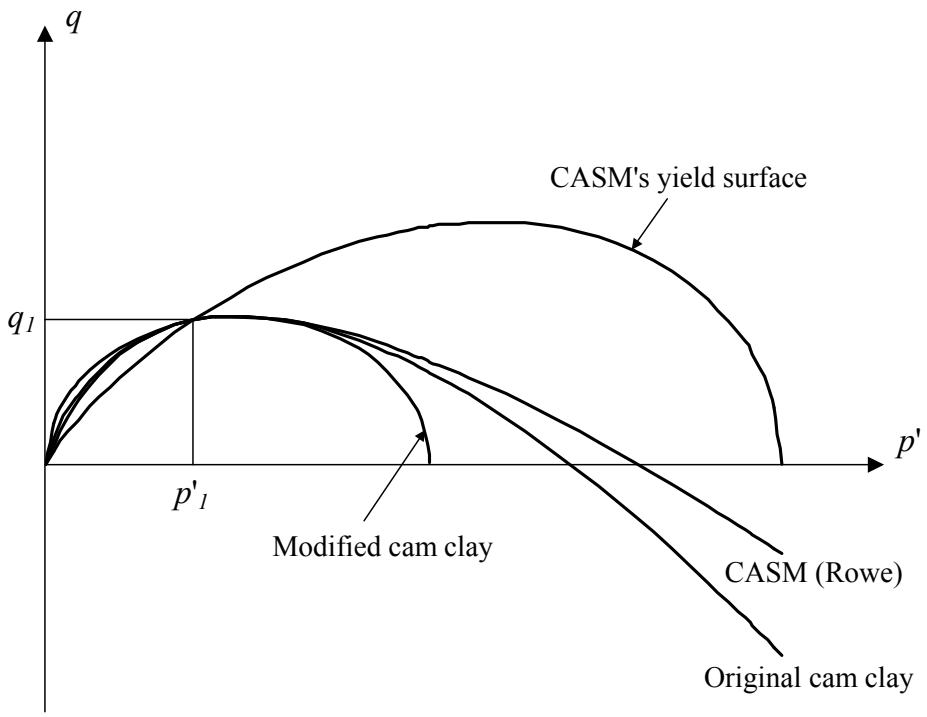

Figure 3.3. Shapes of different plastic potential surfaces

Figure 3.4 graphically presents the directions of the plastic strain increments obtained from CASM's flow rule in the (p',q) plane once yielding has occurred. The volumetric $\left(\delta\varepsilon_p^p\right)$ and deviatoric $\left(\delta\varepsilon_q^p\right)$ components of a plastic strain increment are also shown in this figure. It clearly shows that CASM is a non associated model since the plastic strain increments are not perpendicular to the yield surface at the point of yielding.

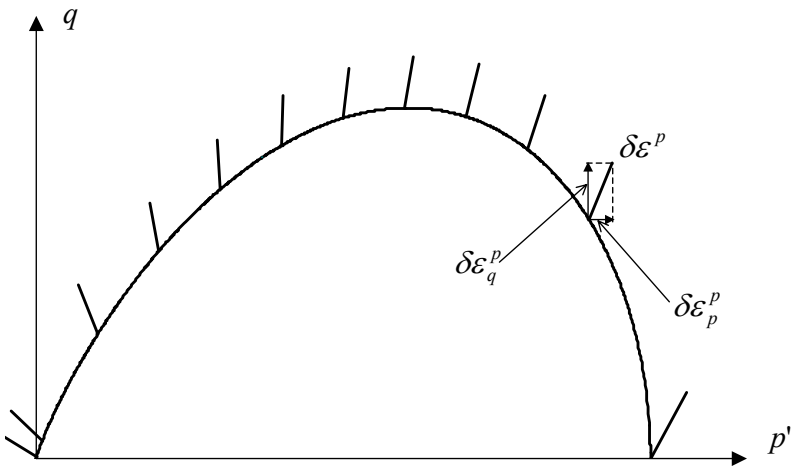

Figure 3.4. Plastic strain increments for CASM

3.1.4. Elastic behaviour

The elastic behaviour of this critical state model is the same as in the Cam-clay models with the tangent modulus (K) and shear modulus (G) being defined by the following expressions (a constant Poisson's ratio (μ) is assumed):

$$K = \frac{\partial p'}{\partial \varepsilon_p^e} = \frac{(1+e)}{\kappa} p' = \frac{\nu p'}{\kappa} \tag{3.5}$$

$$G = \frac{3(1-2\mu)K}{2(1+\mu)} = \frac{3(1-2\mu)}{2(1+\mu)} \frac{\nu p'}{\kappa} \tag{3.6}$$

3.1.5. Hardening rule and plastic behaviour

The yield surface size, which is governed by the preconsolidation pressure (p'_o), is taken as the hardening parameter and is related to the plastic volumetric strain $\left(\varepsilon_p^p\right)$ by the equation:

$$\delta p'_o = \frac{v p'_o}{(\lambda - \kappa)} \delta \varepsilon_p^p \tag{3.7}$$

The plastic hardening modulus (H), which is needed for the calculation of the elastic-plastic stiffness matrix (D^{ep}), can be derived for CASM as follows (the derivation of H is described in details in Chapter 4):

$$H = -\frac{1}{\Lambda}\frac{\partial F}{\partial k} dk = -\frac{1}{\Lambda}\frac{\partial F}{\partial p'_o} dp'_o = \frac{3v}{(\lambda - \kappa)\ln r}\left(\frac{3+2M}{2q+3p'} - \frac{3-M}{3p'-q}\right) \tag{3.8}$$

The elastic and plastic stress-strain responses can be written in matrix form as:

$$\begin{bmatrix} \delta \varepsilon_p^e \\ \delta \varepsilon_q^e \end{bmatrix} = \begin{bmatrix} \frac{1}{K} & 0 \\ 0 & \frac{1}{3G} \end{bmatrix} \begin{bmatrix} \delta p' \\ \delta q \end{bmatrix} \tag{3.9}$$

$$\begin{bmatrix} \delta \varepsilon_p^p \\ \delta \varepsilon_q^p \end{bmatrix} = \frac{(\lambda - \kappa)\ln r}{3v\left(\frac{3+2M}{2q+3p'} - \frac{3-M}{3p'-q}\right)} \begin{bmatrix} \left(\frac{1}{p'\ln r} - \frac{nq^n}{M^n p'^{n+1}}\right) \times \left(\frac{9+6M}{2q+3p'} - \frac{9-3M}{3p'-q}\right) & \left(\frac{nq^{n-1}}{M^n p'^n}\right) \times \left(\frac{9+6M}{2q+3p'} - \frac{9-3M}{3p'-q}\right) \\ \left(\frac{1}{p'\ln r} - \frac{nq^n}{M^n p'^{n+1}}\right) \times \left(\frac{2(3+2M)}{2q+3p'} + \frac{3-M}{3p'-q}\right) & \left(\frac{nq^{n-1}}{M^n p'^n}\right) \times \left(\frac{2(3+2M)}{2q+3p'} + \frac{3-M}{3p'-q}\right) \end{bmatrix} \begin{bmatrix} \delta p' \\ \delta q \end{bmatrix} \tag{3.10}$$

3.1.6. Model constants and their identification

It can be seen that there are a total of 7 model constants required in CASM, all of which can be determined in the laboratory. They are μ, κ, λ, Γ, M, r (or ξ_R) and n.

- The elastic behaviour is modelled by the Poisson's ratio (μ) and the slope of the swell line (κ). Poisson's ratio is typically in the range of 0.15-0.35 for clays and sands. A typical value of κ for sands is 0.005 and its value is generally much larger for clays ranging between 0.01 and 0.06.
- The critical state line for a soil is fully defined by the constants λ, Γ, and M. Measurement of these critical state constants is straightforward for clays. However, for sands these measurement prove to be much more difficult and special care needs to be exercised when determining them using triaxial testing (Been et. al., 1991).
- The spacing ratio (r) is used to estimate the reference state parameter (ξ_R) which corresponds to the loosest state a soil is likely to reach in practice. For the sake of simplicity, the standard Cam-clay models assume a single constant spacing ratio for all soil types. In the original and modified Cam-clay models, r is fixed at 2.718 and 2.0 respectively. Although reasonable for clays, this simplification is found to be less successful for sands. In CASM, the assumption of a variable r is adopted. Experimental data indicates that for clays, r typically lies in the range of 1.5-3 and for sands the value of r is generally much larger (Coop and Lee, 1993; Crouch et. al., 1994). For most applications, it is satisfactory to treat the *NCL* as the reference consolidation line and therefore the measurement of r for clays does not impose any difficulty because the *NCL* can be easily located. In contrast, locating the *NCL* for sands is much more difficult because a test device able to supply very high pressure is required. However, if the *NCL* for a given sand cannot be measured, it is acceptable to choose a positive state parameter (typically ranging between 0.05 and 0.2) that is unlikely to be encountered in practice as the reference state parameter (ξ_R).
- The value of the stress-state coefficient (n) is typically between 1.0 and 5.0. To determine n for a given soil, it is necessary to plot the stress paths

from a few triaxial tests (both drained and undrained) on soils of different initial conditions in terms of stress ratio (η) against the state parameter (ξ). Using the general stress strain relation adopted in CASM, experimental state boundary surfaces should be regarded as a straight line in the plot of $\ln[1-(\xi/\xi_R)]$ against $\ln(\eta/M)$. The stress-state coefficient (n) is the slope of the state boundary surface in this particular log-log plot. Details for the derivation of n can be found in Yu (1998).

3.2. EXTENSIONS OF CASM

By using the state parameter concept and a non-associated flow rule, a simple unified critical state model has been developed. It can be said that for simple monotonic loading conditions, CASM has struck the right balance between simplicity and practicality. It will be shown in the coming chapters that CASM can capture the overall behaviour of clay and sand observed under both drained and undrained loading conditions. In particular, the behaviour of heavily overconsolidated clays and dense sands can be satisfactorily modelled. This represents a very useful extension of the Cam-clay models which is known to be only valid for normally consolidated clays.

However, some very important aspects of soil behaviour mainly in relation to the cyclic response cannot be adequately described by CASM. The principal reason is that the classical concept of a yield surface provides little flexibility in describing the change of the plastic modulus with loading direction and implies a purely elastic stress range within the yield surface. The need for extending CASM therefore becomes a necessity.

In the next five chapters, the main original contributions of this research will be presented. They are summarised below:

In Chapter 4, a new non-linear elasticity rule, which is only applicable to clays, is introduced into CASM so that a better prediction of soil behaviour is achieved. The processes of generalising CASM into the three-dimensional stress space, implementing CASM into CRISP and validating CASM are also presented.

Chapter 5 presents CASM-d which is an extension of CASM using the combined hardening theory. It is argued that this model is more realistic than the traditional volumetric hardening models because deviatoric stresses are also assumed to give an additional contribution to hardening.

CASM-b, an extension of CASM using the bounding surface plasticity theory, is introduced in Chapter 6. The salient features of a bounding surface formulation are that plastic deformation may occur for stress states within the yield surface and the possibility to have a very flexible variation of the plastic modulus during a loading path. This model is more realistic than CASM in terms of predicting behaviour of overconsolidated clays and sands.

CASM-b is extended further in Chapter 7 to give CASM-c, a bounding surface critical state model with cyclic loading prediction capability. In this model, by assuming different expressions of the hardening modulus for three loading cases (virgin loading, unloading and reloading), the cyclic behaviours of soils can be predicted.

Applications of CASM, CASM-b and CASM-c to some typical boundary value problems in geotechnical engineering are presented in Chapter 8. The performances of these models are assessed and some useful results are obtained.

CHAPTER 4

FINITE ELEMENT IMPLEMENTATION OF CASM

4.1. NON-LINEAR ELASTICITY

The traditional critical state family of models often assumes a non-linear (pressure dependent) bulk modulus (K) and either a constant shear modulus (G) or a constant Poisson's ratio (μ).

Typical experimental evidence (e.g. Al-Tabbaa (1987), see Figure 2.1) provides strong support for the assumption that the elastic bulk modulus varies linearly with the mean effective pressure ($K=vp'/\kappa$).

The question is how the shear behaviour of the soil is to be described in the elastic region. In the Cam-clay models and current version of CASM, if a constant value of Poisson's ratio is chosen, then the deduced shear modulus will be proportional to p'. However, as pointed out by Zytynski et. al. (1978), for highly overconsolidated soils this assumption leads to a far too low value of the shear modulus. As a result, the elastic strains will be overpredicted and, on failure when strain-softening occurs, the recovery in elastic strain due to stress relief will swamp the plastic strains. The alternative of assuming a constant shear modulus and allowing the Poisson's ratio to vary will sometimes lead to negative values of μ, which is physically unreasonable, and it is also generally not in accord with experimental observations.

Therefore, it is felt that a new expression for the shear modulus should be adopted for CASM in order to predict better the behaviour of soil.

Atkinson (2000) summarised the work of a number of researchers and stated that for very small strain deformation, the shear modulus could be taken in a general form as:

$$G = A[f(v)](p')^{l} OCR^{m} \tag{4.1}$$

where

$f(v)$:	some function of the specific volume
OCR:	the overconsolidation ratio defined as p'_o/p' where p'_o is the preconsolidation pressure
A, l, m:	material parameters

It should be noted that OCR is defined in terms of the mean effectives stresses. This is not the conventional definition which defines the overconsolidation ratio as the maximum previous vertical effective stress divided by the current vertical effective stress $\left(OCR_{conventional} = {(\sigma'_v)_{\max}}/{\sigma'_v} \right)$. Only the former definition is used in this thesis.

If the overconsolidation ratio (OCR) is defined with respect to a normal compression line, the state can be defined by only two of v, p' and OCR and the above equation can be written as:

$$\frac{G}{p'_a} = A\left(\frac{p'}{p'_a}\right)^{l} OCR^{m} \tag{4.2}$$

where p'_a is the reference pressure and makes the equation dimensionally consistent. (p'_a influences the value of A and is normally taken as 1 kPa or as atmospheric pressure).

In this study, the following function proposed by Houlsby and Wroth (1991) for the variation of the shear modulus with the stresses is adopted:

$$G = \left[\frac{G}{p'}\right]_{nc} p' OCR^{t} = \left[\frac{G}{p'}\right]_{nc} p'^{(1-t)} (p'_o)^{t} \tag{4.3}$$

where

$\left[\frac{G}{p'}\right]_{nc}$: value of $\left[\frac{G}{p'}\right]$ when the soil is normally consolidated

t: lies between 0 and 1

OCR: overconsolidation ratio defined as above

i.e. G is dependent on $p'^{(1-t)}$ and $(p'_o)^t$. In this study, a value of t equal to 0.5 will be used for simplicity.

Houlsby and Wroth (1991) showed that this non-linear rule has the advantage that it incorporates the concept of normalisation of clay properties with respect to pressure, whilst allowing a realistic variation of the shear modulus with the overconsolidation ratio to be described. A second advantage of this formulation is that by combining with the expression of the undrained shear strength (S_u), the rigidity index (G/S_u), which plays an important role in many geotechnical engineering analyses, can be expressed as a power function of the overconsolidation ratio as follows:

$$\left[\frac{G}{S_u}\right]_{nc} = \left[\frac{G}{S_u}\right]_{nc} OCR^{(t-\Lambda)} \tag{4.4}$$

where Λ is a factor equal to $(\lambda-\kappa)/\lambda$ and λ and κ are the slopes of the isotropic normal compression line and unloading-reloading line in the v-lnp' plot respectively.

Houlsby and Wroth (1991) compared the results obtained from this method with some exiting data and they found that the trends of behaviour observed experimentally were broadly matched by their formulation.

It can be seen from equations 4.3 and 4.4 that the new expression of the shear modulus is a function of the overconsolidation ratio. As a result, this rule can only be applied to clay materials with a low OCR value. This rule does not apply for sands.

Hence, in this study, the non-linear elastic rule described above will only be used for clays when CASM and its extensions are implemented into CRISP.

4.2. IMPLEMENTATION OF CASM INTO CRISP

4.2.1. Introduction

New constitutive soil models can be implemented into CRISP by using the Material Model Interface (MMI). The MMI was originally developed by Dr Andrew Chan (Birmingham University, U.K.). The introduction of MMI has made the incorporation of new soil models easier.

There are four important stages in CRISP which call the MMI. These are:

A. Reading in the material properties (subroutine MSUB1)
B. Initialising in-situ stresses, yield surface and other initial parameters (subroutine MSINSIT)
C. Assembling the stiffness (subroutine FRONTZ for symmetric stiffness or FRONTU for unsymmetrical stiffness)
D. Evaluating the stresses and updating various parameters (subroutine UPOUT)

Stages C and D are passed through within an incremental/iterative solution, while stages A and B are called only at the start of the program run.

The MMI is represented by subroutine CRSM2D and is called through each of the above stages with a flag (ISWDP) which indicates the progress of the program. The flags are described as follows:

ISWDP=1, the program is reading properties (stage A above)
ISWDP=5, the program is initialising stresses (stage B above)
ISWDP=3 or 4, the program is assembling stiffness (stage C above)
ISWDP=2, the program is evaluating stresses (stage D above)

ISWDP=3 is for symmetric stiffness, ISWDP=4 is for unsymmetrical stiffness which would require the special FRONTAL SOLVER in CRISP.

To implement a new model into CRISP, a new code using a FE condition that utilises the switches above would need to be written. A model ID for the new model would also need to be chosen.

Basically, the developer will have to write two new SUBROUTINES for each new model implemented. These SUBROUTINES will then be linked to the main program to finish the implementation process.

4.2.2. Special considerations with CASM

It was mentioned in Chapter 3 that CASM uses a non-associated flow rule. Hence, unlike the Cam-clay models already installed in CRISP, CASM's plastic potential function is not identical to its yield surface function.

Due to the difference mentioned above, the SOLVER and STIFFNESS MATRIX GENERATOR used by CASM are also different from the SOLVER and STIFFNESS MATRIX GENERATOR used by the Cam-clay models (unsymmetrical SOLVER and STIFFNESS MATRIX GENERATOR have to be used instead of symmetric SOLVER and STIFFNESS MATRIX GENERATOR).

It can be seen from Figure 3.2, when n=1 the shape of CASM's yield surface is similar to that of the original Cam-clay model. There is a discontinuity in the yield surface at q=0. This discontinuity presents problems both theoretically and numerically. To overcome this, it is assumed that when q is very small [ABS(q)<10^{-5} kPa] CASM's yield surface shape will be the same as the yield surface shape obtained from the modified Cam-clay model (see Figure 2.3). By making this adjustment, the above problem is eliminated.

4.2.3. Generalisation of CASM in the three-dimensional stress space

Chapter 3 describes the critical state soil models entirely in relation to the standard triaxial test for soils. Thus it is possible to describe the effective stress state of a soil

sample by just two stress parameters (p' and q). To extend the models to more general two- and three-dimensional stress spaces, some additional assumptions are necessary.

We replace the previous definitions of p' and q by:

$$p' = \frac{1}{3}\left(\sigma'_1 + \sigma'_2 + \sigma'_3\right) = \frac{1}{3}\left(\sigma'_x + \sigma'_y + \sigma'_z\right) = \frac{1}{3}\left(\sigma_x + \sigma_y + \sigma_z\right) - u \tag{4.5}$$

$$q = \left[\frac{\left(\sigma_x' - \sigma'_y\right)^2 + \left(\sigma_z' - \sigma'_x\right)^2 + \left(\sigma_y' - \sigma'_z\right)^2}{2} + 3\tau_{xy}^{\ 2} + 3\tau_{zx}^{\ 2} + 3\tau_{yz}^{\ 2}\right]^{\frac{1}{2}} \tag{4.6}$$

Also, another parameter will be needed, namely the Lode angle θ which is defined as:

$$\theta = \tan^{-1}\left[\frac{1}{\sqrt{3}}\left(2\frac{\sigma'_2 - \sigma'_3}{\sigma'_1 - \sigma'_3} - 1\right)\right] = -\frac{1}{3}\sin^{-1}\left(\frac{27}{2}\frac{\det s}{q^3}\right) \tag{4.7}$$

where

$$\det s = \begin{vmatrix} \sigma'_x - p' & \tau_{xy} & \tau_{zx} \\ \tau_{xy} & \sigma'_y - p' & \tau_{yz} \\ \tau_{zx} & \tau_{yz} & \sigma'_z - p' \end{vmatrix}$$

The choice of these parameters is not arbitrary because the above quantities have geometric significance in the principal effective stress space. In Figure 4.1, $\sqrt{3}p'$ is a measure along the space diagonal ($\sigma'_1=\sigma'_2=\sigma'_3$) of the current deviatoric plane from the origin, $\sqrt{2/3}q$ is the distance from the current stress state to the space diagonal in the deviatoric plane and the magnitude of θ defines the orientation of the stress state within the deviatoric plane.

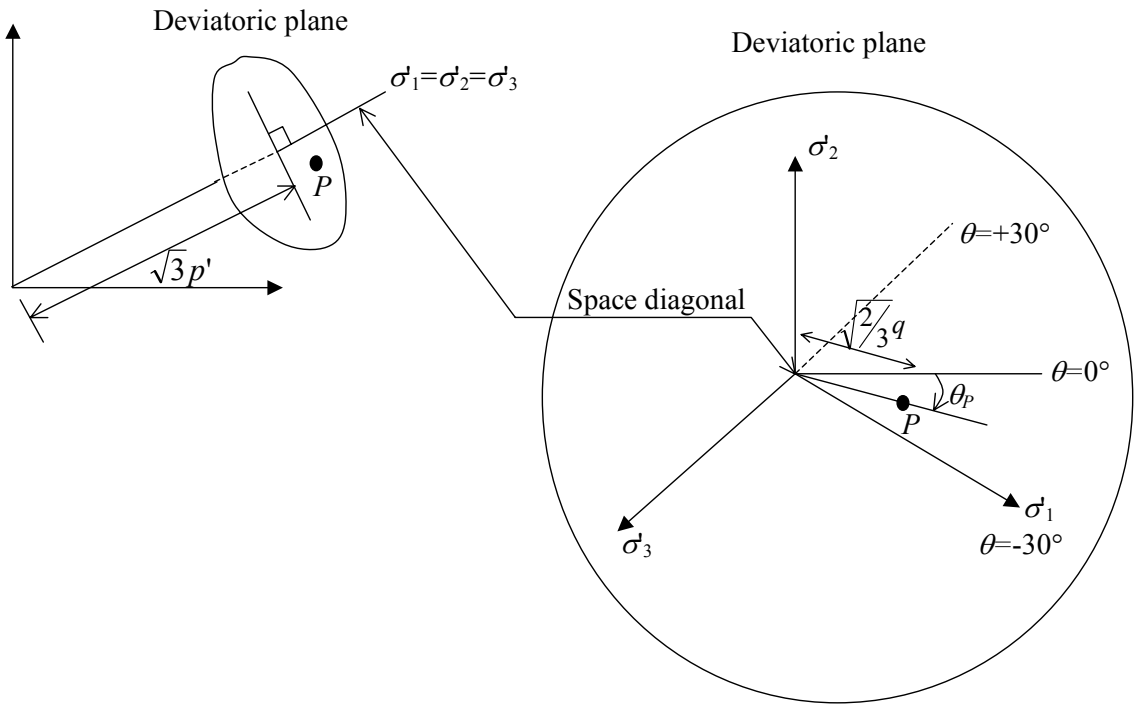

Figure 4.1. Stress parameters in principal stress space

In order to perform a non-linear finite element analysis using elastic-plastic models of soil behaviour, it is necessary to compute the modulus matrix D^{ep} relating an increment of strain to an increment of stress:

$$\Delta\sigma = D^{ep}\Delta\varepsilon \tag{4.8}$$

Starting from the yield function $F(\boldsymbol{\sigma},\boldsymbol{k})=0$ and the plastic potential $G(\boldsymbol{\sigma},\boldsymbol{\beta})=0$, there is a piece of standard manipulation to obtain a formula for D^{ep} (e.g. Potts and Zdravkovic, 1999):

$$D^{ep} = D^{e} - \frac{D^{e}\dfrac{\partial G}{\partial \sigma}\left[\dfrac{\partial F}{\partial \sigma}\right]^{T} D^{e}}{\left[\dfrac{\partial F}{\partial \sigma}\right]^{T} D^{e}\dfrac{\partial G}{\partial \sigma} + H} \tag{4.9}$$

where D^{e} is the elastic stiffness matrix (see section 2.1.2) and H is the hardening modulus.

From the expressions of the yield and plastic potential equations, the terms in the above equation are derived as follows:

$$\frac{\partial F}{\partial \sigma} = \frac{\partial F}{\partial p'}\frac{\partial p'}{\partial \sigma} + \frac{\partial F}{\partial q}\frac{\partial q}{\partial \sigma} + \frac{\partial F}{\partial M}\frac{\partial M}{\partial \theta}\frac{\partial \theta}{\partial \sigma} \tag{4.10}$$

$$\frac{\partial F}{\partial p'} = \frac{1}{p' \ln r} - \frac{n q^n}{M^n p'^{n+1}}$$

$$\frac{\partial p'}{\partial \sigma} = \frac{1}{3}\begin{bmatrix} 1 & 1 & 1 & 0 & 0 & 0 \end{bmatrix}$$

$$\frac{\partial F}{\partial q} = \frac{n q^{n-1}}{M^n p'^n}$$

$$\frac{\partial q}{\partial \sigma} = \frac{3}{2q}\begin{bmatrix} (\sigma_x - p') & (\sigma_y - p') & (\sigma_z - p') & 2\tau_{xy} & 2\tau_{zx} & 2\tau_{yz} \end{bmatrix}$$

$$\frac{\partial F}{\partial M} = \frac{-n q^n}{p'^n M^{n+1}}$$

$$M(\theta) = M_{\max}\left[\frac{2\alpha^4}{1+\alpha^4+(1-\alpha^4)\sin 3\theta}\right]^{\frac{1}{4}}$$

(It is noted that the use of the above equation will be presented in the next section)

$$\frac{\partial M}{\partial \theta} = \frac{3\sqrt[4]{2}}{4} M_{\max} \frac{\alpha(\alpha^4 - 1)\cos 3\theta}{\left[1+\alpha^4+(1-\alpha^4)\sin 3\theta\right]^{\frac{5}{4}}}$$

$$\frac{\partial \theta}{\partial \sigma} = \frac{9}{2\cos(3\theta) q^3}\left[\frac{3\det s}{q}\left\{\frac{\partial q}{\partial \sigma}\right\} - \left\{\frac{\partial \det s}{\partial \sigma}\right\}\right]$$

$$\frac{\partial \det s}{\partial \sigma_x} = 2p'^2 - \frac{2}{3}\sigma_x(\sigma_y + \sigma_z) - \frac{1}{3}\left(\sigma_y{}^2 + \sigma_z{}^2\right) + \frac{1}{3}\left(\tau_{xy}{}^2 + \tau_{zx}{}^2 - 2\tau_{yz}{}^2\right)$$

$$\frac{\partial \det s}{\partial \sigma_y} = 2p'^2 - \frac{2}{3}\sigma_y(\sigma_x + \sigma_z) - \frac{1}{3}\left(\sigma_x{}^2 + \sigma_z{}^2\right) + \frac{1}{3}\left(\tau_{xy}{}^2 + \tau_{yz}{}^2 - 2\tau_{zx}{}^2\right)$$

$$\frac{\partial \det s}{\partial \sigma_z} = 2p'^2 - \frac{2}{3}\sigma_z(\sigma_y + \sigma_x) - \frac{1}{3}\left(\sigma_y{}^2 + \sigma_x{}^2\right) + \frac{1}{3}\left(\tau_{yz}{}^2 + \tau_{zx}{}^2 - 2\tau_{xy}{}^2\right)$$

$$\frac{\partial \det s}{\partial \tau_{xy}} = -2\tau_{xy}\left(\sigma_z - p\right) + 2\tau_{zx}\tau_{yz}$$

$$\frac{\partial \det s}{\partial \tau_{zx}} = -2\tau_{zx}\left(\sigma_y - p\right) + 2\tau_{yz}\tau_{xy}$$

$$\frac{\partial \det s}{\partial \tau_{yz}} = -2\tau_{yz}\left(\sigma_x - p\right) + 2\tau_{zx}\tau_{xy}$$

Hence,

$$\frac{\partial F}{\partial \sigma_x} = \frac{1}{3p'\ln r}\left[1 - \ln\left(\frac{p'_o}{p'}\right)^n\right] + \frac{3nq^{n-2}}{2M^n p'^n}\left(\sigma_x - p'\right)$$

$$\frac{\partial F}{\partial \sigma_y} = \frac{1}{3p'\ln r}\left[1 - \ln\left(\frac{p'_o}{p'}\right)^n\right] + \frac{3nq^{n-2}}{2M^n p'^n}\left(\sigma_y - p'\right)$$

$$\frac{\partial F}{\partial \sigma_z} = \frac{1}{3p'\ln r}\left[1 - \ln\left(\frac{p'_o}{p'}\right)^n\right] + \frac{3nq^{n-2}}{2M^n p'^n}\left(\sigma_z - p'\right)$$

$$\frac{\partial F}{\partial \tau_{xy}} = \frac{3nq^{n-2}}{M^n p'^n}\tau_{xy}$$

$$\frac{\partial F}{\partial \tau_{zx}} = \frac{3nq^{n-2}}{M^n p'^n}\tau_{zx}$$

$$\frac{\partial F}{\partial \tau_{yz}} = \frac{3nq^{n-2}}{M^n p'^n}\tau_{yz}$$

$$\frac{\partial G}{\partial \sigma} = \frac{\partial G}{\partial p'}\frac{\partial p'}{\partial \sigma} + \frac{\partial G}{\partial q}\frac{\partial q}{\partial \sigma} \tag{4.11}$$

$$\frac{\partial G}{\partial p'} = 3\left(\frac{3+2M}{2q+3p'} - \frac{3-M}{3p'-q}\right)$$

$$\frac{\partial p'}{\partial \sigma} = \frac{1}{3}\begin{bmatrix}1 & 1 & 1 & 0 & 0 & 0\end{bmatrix}$$

$$\frac{\partial G}{\partial q} = \frac{2(3+2M)}{2q+3p'} + \frac{3-M}{3p'-q}$$

$$\frac{\partial q}{\partial \sigma} = \frac{3}{2q}\begin{bmatrix}(\sigma_x - p') & (\sigma_y - p') & (\sigma_z - p') & 2\tau_{xy} & 2\tau_{zx} & 2\tau_{yz}\end{bmatrix}$$

Hence,

$$\frac{\partial G}{\partial \sigma_x} = \left[\frac{3+2M}{2q+3p'} - \frac{3-M}{3p'-q}\right] + \frac{3}{2q}\left[\frac{2(3+2M)}{2q+3p'} + \frac{3-M}{3p'-q}\right](\sigma_x - p')$$

$$\frac{\partial G}{\partial \sigma_y} = \left[\frac{3+2M}{2q+3p'} - \frac{3-M}{3p'-q}\right] + \frac{3}{2q}\left[\frac{2(3+2M)}{2q+3p'} + \frac{3-M}{3p'-q}\right](\sigma_y - p')$$

$$\frac{\partial G}{\partial \sigma_z} = \left[\frac{3+2M}{2q+3p'} - \frac{3-M}{3p'-q}\right] + \frac{3}{2q}\left[\frac{2(3+2M)}{2q+3p'} + \frac{3-M}{3p'-q}\right](\sigma_z - p')$$

$$\frac{\partial G}{\partial \tau_{xy}} = \left[\frac{2(3+2M)}{2q+3p'} + \frac{3-M}{3p'-q}\right]\frac{3\tau_{xy}}{q}$$

$$\frac{\partial G}{\partial \tau_{zx}} = \left[\frac{2(3+2M)}{2q+3p'} + \frac{3-M}{3p'-q}\right]\frac{3\tau_{zx}}{q}$$

$$\frac{\partial G}{\partial \tau_{yz}} = \left[\frac{2(3+2M)}{2q+3p'} + \frac{3-M}{3p'-q}\right]\frac{3\tau_{yz}}{q}$$

$$H = -\frac{1}{\Lambda}\frac{\partial F}{\partial k}dk = -\frac{1}{\Lambda}\frac{\partial F}{\partial p'_o}dp'_o \tag{4.12}$$

$$dp'_o = p'_o\, d\varepsilon_p^p \frac{\nu}{\lambda-\kappa} = p'_o \frac{\nu}{\lambda-\kappa}\Lambda\frac{\partial G}{\partial p'}$$

$$\frac{\partial F}{\partial p'_o} = -\frac{1}{p'_o \ln r}$$

$$\frac{\partial G}{\partial p'} = 3\left(\frac{3+2M}{2q+3p'} - \frac{3-M}{3p'-q}\right)$$

$$H = -\frac{1}{\Lambda}\left(-\frac{1}{p'_o \ln r}\right)p'_o \frac{\nu}{\lambda-\kappa}\Lambda \times 3\left(\frac{3+2M}{2q+3p'} - \frac{3-M}{3p'-q}\right)$$

Hence,

$$H = \frac{3\nu}{(\lambda-\kappa)\ln r}\left(\frac{3+2M}{2q+3p'} - \frac{3-M}{3p'-q}\right) \tag{4.13}$$

4.2.4. Shapes of yield and plastic potential surfaces in the deviatoric plane

In numerical analysis, the constitutive models have to be generalised into the three-dimensional stress space by making some assumptions about the shapes of the yield and plastic potential surfaces in the deviatoric plane (surface perpendicular to the line $\sigma'_1=\sigma'_2=\sigma'_3$ in the three-dimensional stress space, see Figure 4.1). The simplest generalisation is to assume a circular shape for both surfaces (Roscoe and Burland, 1968). However, it is well known that a circle does not provide a good representation of the failure condition for soils whereas a Mohr-Coulomb type of failure criterion would be more appropriate.

With the three-dimensional definitions of p', q and the new parameter θ introduced in the above section, the yield and plastic potential equations become:

$$F(\sigma,k)=\left(\frac{q}{M(\theta)p'}\right)^{n}+\frac{\ln\left(\frac{p'}{p'_{o}}\right)}{\ln r} \tag{4.14}$$

$$G(\sigma,\beta)=3M\left(\ln p'-\ln\beta\right)+\left(3+2M\right)\ln\left(\frac{2q+3p'}{p'}\right)-\left(3-M\right)\ln\left(\frac{3p'-q}{p'}\right) \tag{4.15}$$

In equation 4.14, the slope of the critical state line (M) is expressed as a function of the Lode angle (θ) and determines the shape of the failure surface in the deviatoric plane. In this study, the relationship between M and θ which was proposed by Sheng et al. (2000) will be used:

$$M\left(\theta\right)=M_{\max}\left[\frac{2\alpha^{4}}{1+\alpha^{4}+\left(1-\alpha^{4}\right)\sin 3\theta}\right]^{\frac{1}{4}} \tag{4.16}$$

where

$$\alpha=\frac{3-\sin\phi'}{3+\sin\phi'}$$

ϕ' : friction angle of the soil at critical state

$M_{\max}$: slope of the *CSL* under triaxial compression (θ=-30°) in the (p',q) plane

The slope M of the *CSL* in the plastic potential equation 4.15 is regarded as constant when evaluating the derivatives of the plastic potential with respect to the stresses. This is to assume that the shape of the plastic potential surface in the deviatoric plane will be circular. The use of this assumption is to apply a non-associated flow rule. For a given stress state on the yield surface, the value of M in the plastic potential is also determined using equation 4.16 so that the plastic potential surface will pass through the current stress point. The shapes of the yield and plastic potential surfaces in the deviatoric plane can be seen in Figure 4.2. It is noted that the plastic potential plotted is only for the cases when the current stress states are defined as M=$M_{\max}$ (such as triaxial compressive loading conditions).

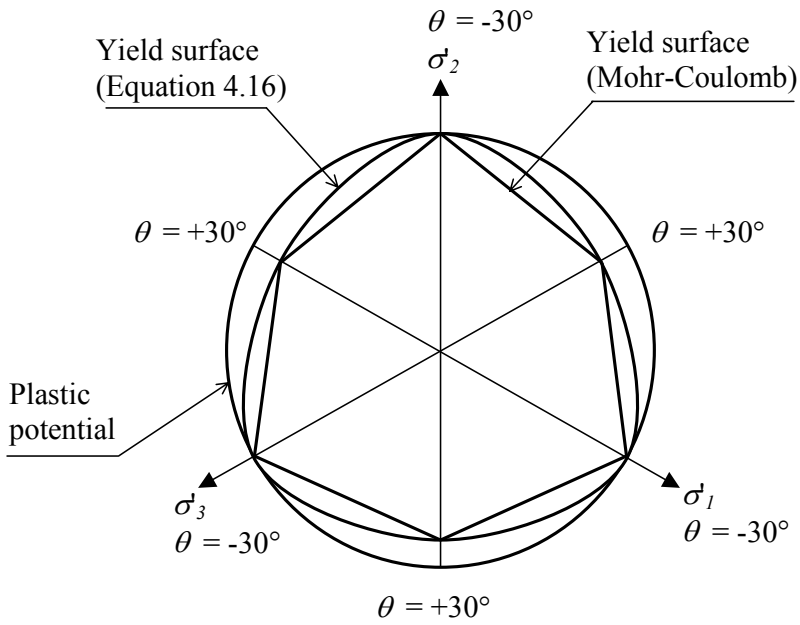

Figure 4.2. Shapes of the yield and plastic potential surfaces in the deviatoric plane

4.2.5. Justification of the yield surface and plastic potential shapes in the deviatoric plane

It is mentioned above that a circular shape of the yield surface in the deviatoric plane does not provide a good representation of the failure condition for soils where a Mohr-Coulomb type of failure criterion would be more appropriate. This statement is validated by a number of authors who did laboratory tests on both sand and clay.

Some of the experimental data is shown in Figures 4.3 and 4.4. Shibata and Karube (1965) did undrained tests on normally consolidated Osaka alluvial clay and they found that the failure surface for this clay in the deviatoric plane was curved and circumscribed the Mohr-Coulomb hexagon as shown in Figure 4.3.

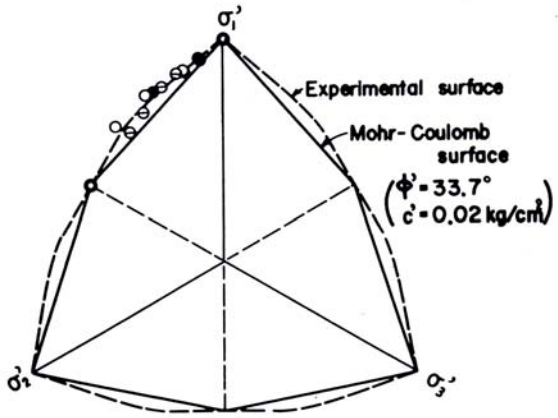

Figure 4.3. Failure surface of Osaka alluvial clay in the deviatoric plane (Shibata and Karube, 1965)

Figure 4.4 shows the results reported by Lade (1984) on experiments of dense Monterey No.0 sand (Figure 4.4a) and normally consolidated remoulded Edgar plastic kaolinite (Figure 4.4b). The results are also compared with the Mohr-Coulomb failure surface. It can be seen again that using a circular shape for the yield surface in the deviatoric plane would greatly overestimate the three-dimensional strengths of both sand and clay materials. However, a Mohr-Coulomb criterion would always underestimate the strengths. As a result, a criterion lying somewhere between these two criteria will be more appropriate.

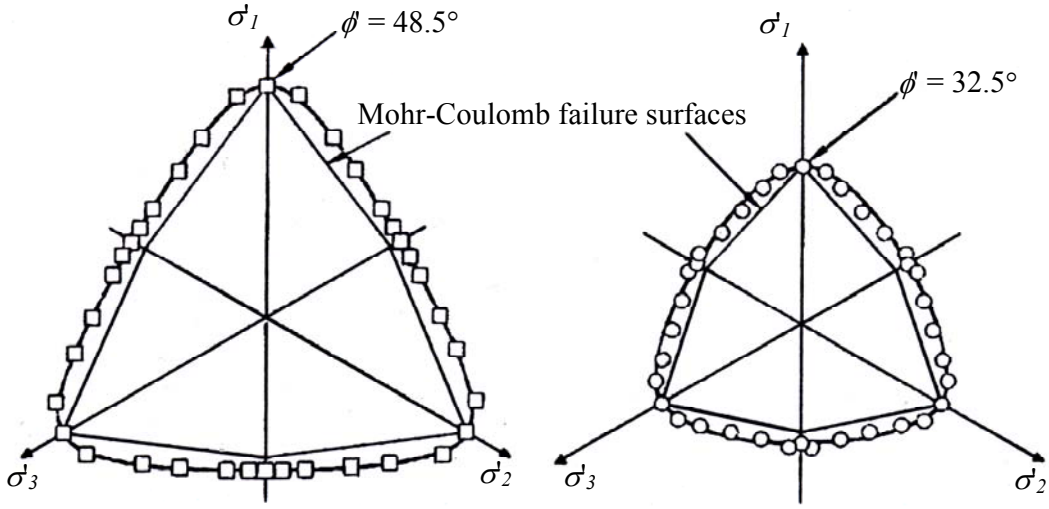

(a) Dense Monterey No. 0 sand

(b) Normally consolidated remoulded Edgar kaolinite

Figure 4.4. Failure surfaces of sand and clay in the deviatoric plane (Lade, 1984)

Therefore, it has been decided that throughout this study, a similar shape to the Mohr-Coulomb failure criterion (i.e. Sheng et al. (2000) shape in Figure 4.2) will be adopted for the yield surface in the deviatoric plane.

For the shape of the plastic potential in the deviatoric plane, however, there has been little evidence to support one assumption or another. In order to investigate the effect of the shape of the plastic potential in the deviatoric plane, undrained analyses of both circular (an axis-symmetric problem) and strip (a plane strain problem) surface rigid footings were carried out. The footings were loaded to failure. The finite element mesh used is shown in Figure 4.5. Fifteen-noded cubic strain triangle elements were used for the circular footing and six-noded linear strain triangle elements were used for the strip footing. The model parameters chosen are relevant to London clay:

M=0.888, λ=0.161, κ=0.062, μ=0.3, Γ=2.759, n=2, r=2.718

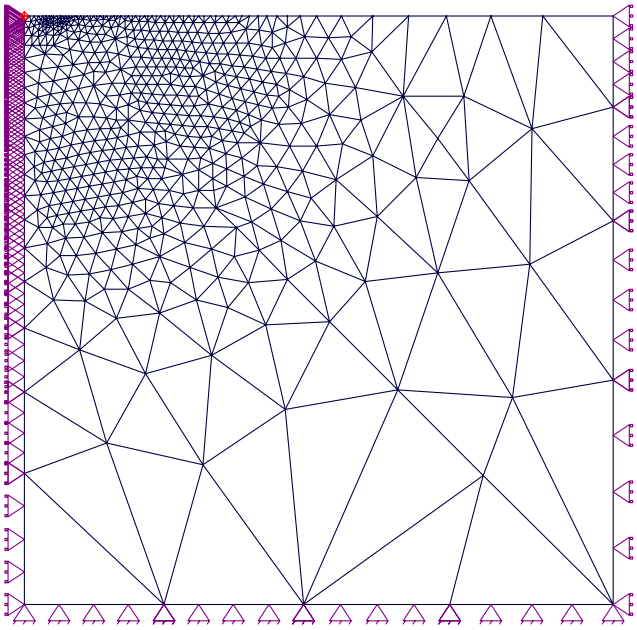

Figure 4.5. Finite element mesh for footing problems

Two versions of CASM have been implemented into CRISP for this investigation. Both versions have the Sheng et al. (2000) shape for the yield surface in the deviatoric plane. The shapes of the plastic potentials in the deviatoric plane are different as follows:

- In the first version, M varies according to equation 4.16, and $\delta M/\delta\theta$ is also allowed to vary according to equation 4.16 (i.e. the plastic potential has the Sheng et al. (2000) shape in Figure 4.2). This version is denoted as S in Figure 4.6.
- In the second version, M varies according to equation 4.16, but $\delta M/\delta\theta$ is assumed to be zero (i.e. circular plastic potential in the deviatoric plane). This version is denoted as C in Figure 4.6.

The results of this investigation are presented in Figure 4.6 where the applied vertical load is plotted against the vertical displacement. For a circular footing (axis-symmetric problem), the effect of the shape of plastic potential in the deviatoric plane is found to be insignificant, see Figure 4.6a. It is shown in Figure 4.6b however, that the shape of the plastic potential in the deviatoric plane has a more significant effect for the plane strain problem, especially near the failure state. These findings agree with the findings of Potts and Gens (1984) who showed that in plane strain problems, the shape of the plastic potential in the deviatoric plane has a dominating influence on the predicted behaviour especially for drained conditions. However, the answer remains unclear since there is no experimental data to support any of the options. Potts and Gens (1984) also indicated that it is often necessary to have different shapes of the yield and plastic potential surfaces in the deviatoric plane.

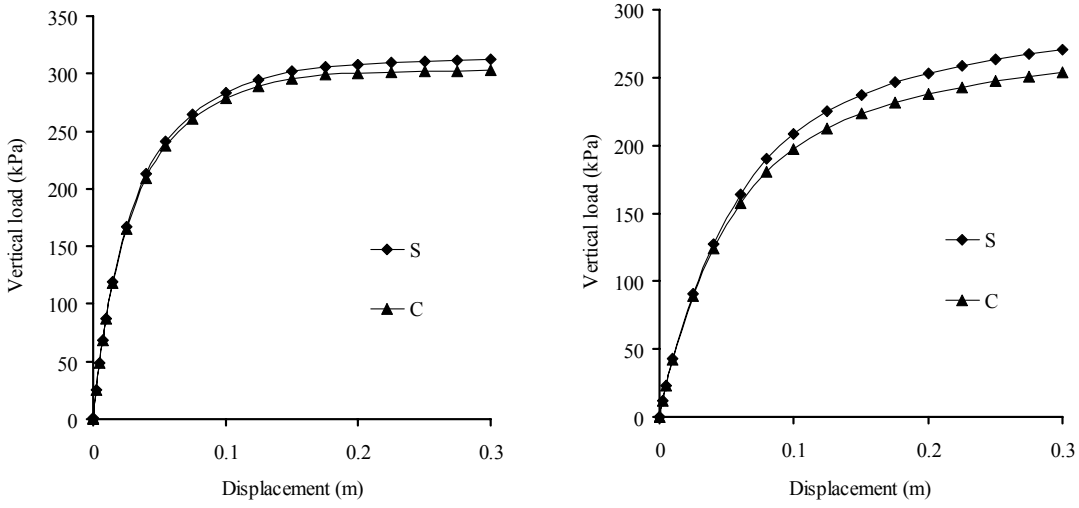

(a) Circular footing (b) Strip footing

Figure 4.6. Effect of the shape of plastic potential on the deviatoric plane

Therefore, for the sake of simplicity, a circular shape for the plastic potential in the deviatoric plane will be assumed in this study but with the value of M updated with the stresses (i.e. M varies according to equation 4.16 but $\delta M/\delta\theta=0$ or version C of CASM is adopted). Nevertheless, further work is needed to justify this assumption.

4.3. VALIDATION OF CASM

Results from triaxial tests have been used in most basic research work on shear strength and pore pressure characteristics. Many basic soil parameters can be obtained directly or indirectly from the results of triaxial tests. Furthermore, triaxial testing is increasingly being used in the solution of practical problems.

In this section, the performance of CASM will be assessed by predicting the behaviour of clay and sand in the triaxial tests. The finite element results will be compared with data from a classical series of tests as well as the finite element results obtained from the original Cam-clay model. Because the same tests will be analysed again by other models, all the triaxial tests simulated in Chapters 4, 5 and 6 are numbered for the ease of comparison. There are altogether 11 tests.

For all the triaxial tests simulated by CASM and its extensions in this research, the mesh shown in Figure 4.7 is used. Only a quarter of the soil sample is modelled due to symmetry. The mesh consists of four fifteen-noded cubic strain triangle elements. The fixity conditions and in-situ stresses are also shown in Figure 4.7.

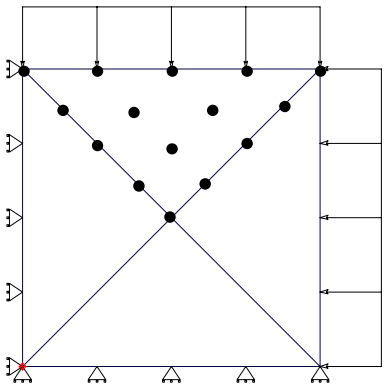

Figure 4.7. Finite element mesh for the triaxial test

It should be noted that the Tangent Stiffness Technique is used as the non-linear solution scheme throughout this study. All of the tests were stress-controlled. The number of increments for each analysis is increased until a stable result is obtained. For all the analyses of the triaxial tests, the loading and unloading (in Chapter 7 only) processes are divided into 2000 load increments, it was found that this number of increments gave stable and satisfied solutions for the problem.

Because the same model and soil parameters are used, all results of the triaxial tests in this chapter are similar to that reported in Yu (1998). The only difference is that Yu used a one-element program to get his results while the author of this thesis used the finite element program CRISP.

4.3.1. Drained and undrained behaviour of normally consolidated and overconsolidated clays (Tests 1-4)

To assess the performance of CASM for clay, test data performed on remoulded Weald clay at Imperial College, London was used (Bishop and Henkel, 1957). Out of the four tests discussed, two were drained and the other two were undrained tests. Under these conditions, both normally consolidated (OCR=1) and overconsolidated (OCR=24) samples were tested. The material constants used for CASM are as follows:

$$M=0.9,\ \lambda=0.093,\ \kappa=0.025,\ \mu=0.3,\ \Gamma=2.06,\ n=4.5,\ r=2.718$$

It should be noted that the *NCL* has been used as the reference consolidation line and therefore the reference state parameter (ξ_R) is equal to the initial state parameter of the normally consolidated sample. The critical state constants for Weald clay are from Parry (1956).

Figures 4.8-4.11 present comparisons of the model predictions and the measured behaviour for both drained and undrained compression of normally and overconsolidated Weald clays. For comparison purposes, the equivalent predictions from the original Cam-clay model have also been presented. It is found that while Cam-clay is reasonable for modelling normally consolidated clays, it is not good for modelling overconsolidated clays.

Figures 4.8-4.11 indicate that the predictions from CASM are consistently better than those from Cam-clay for normally and overconsolidated clays under both drained and undrained loading conditions. In particular, CASM is found to be able to capture the overall behaviour of the overconsolidated clay observed in the laboratory reasonably well.

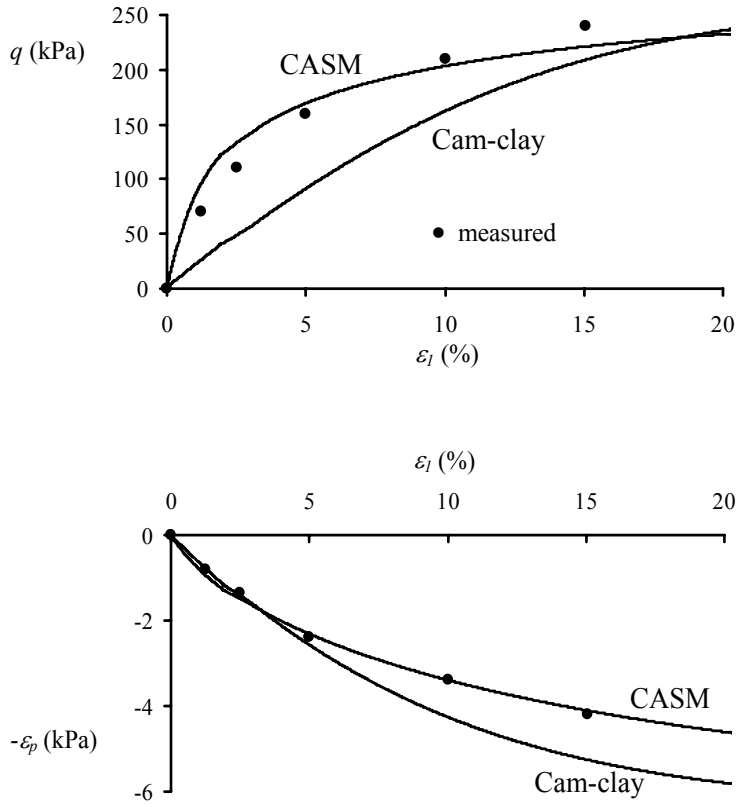

Figure 4.8. Test 1: Drained compression of a normally consolidated sample of Weald clay

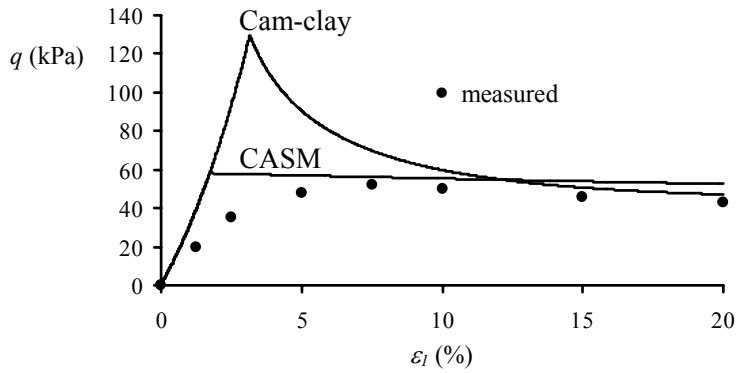

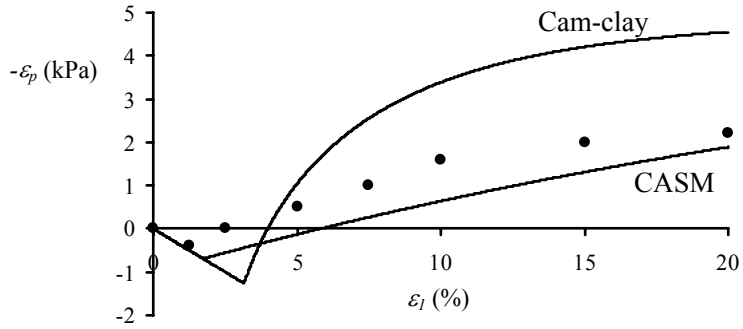

Figure 4.9. Test 2: Drained compression of a heavily overconsolidated sample of Weald clay

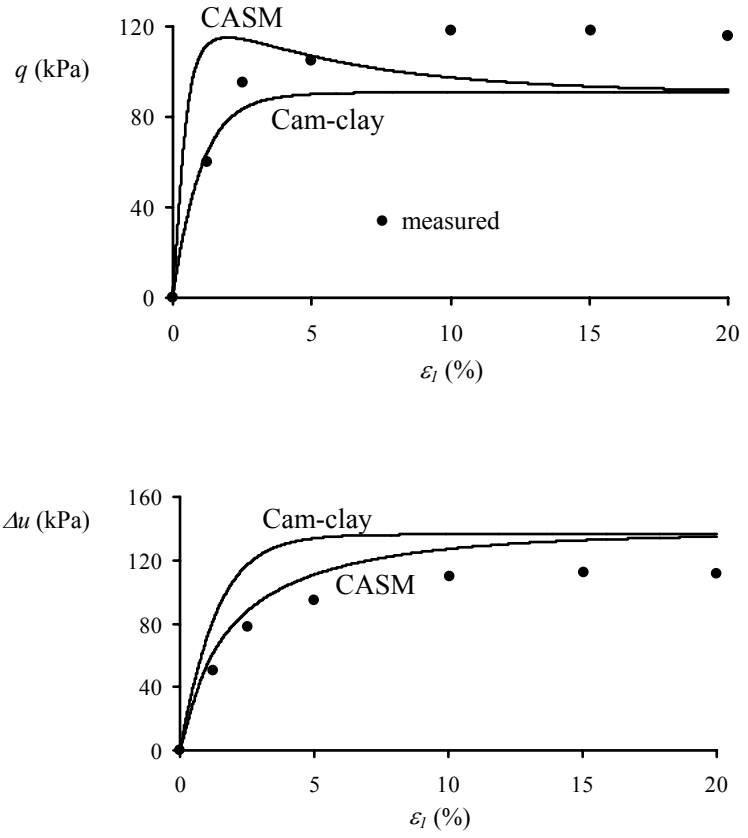

Figure 4.10. Test 3: Undrained compression of a normally consolidated sample of Weald clay

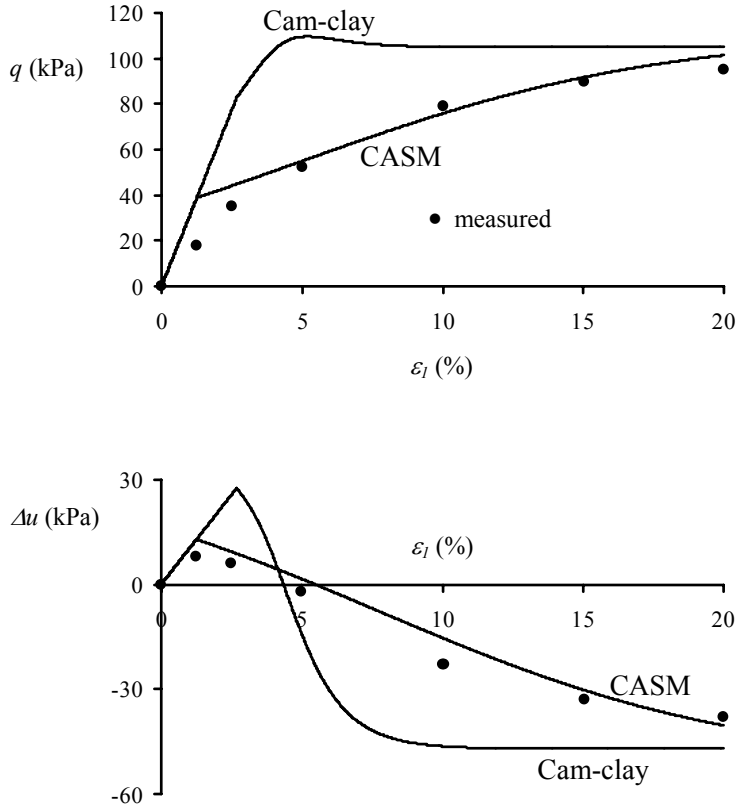

Figure 4.11. Test 4: Undrained compression of a heavily overconsolidated sample of Weald clay

It is noted that one obvious deficiency with CASM is that it tends to under-predict the shear strain at peak strength. Also the curves produced by CASM are not as smooth as the observed curves. These are due to the fact that, like Cam-clay, CASM does not allow any plastic deformation to develop within the state boundary surface.

4.3.2. Drained behaviour of loose, medium and dense sands (Tests 5-7)

To check the performance of CASM for sand, test data reported by Been *et al* (1991) and Jefferies (1993) on a predominantly quartz sand with a trace of silt known as Erksak 330/0.7 was used. Three tests were selected for comparison with CASM. These tests are on the densest sample D667 (with an initial void ratio of 0.59 at the initial cell pressure of 130 kPa), the medium dense sample D662 (with an initial void ratio of 0.677 at the initial cell pressure of 60 kPa) and the loosest sample D684 (with an initial void ratio of

0.82 at the initial cell pressure of 200 kPa). The material constants used in the CASM predictions are as follows:

$$M=1.2,\ \lambda=0.0135,\ \kappa=0.005,\ \mu=0.3,\ \Gamma=1.8167,\ n=4.0,\ r=6792.0$$

Observations show that the critical deviatoric stress for sands is much lower than the peak deviatoric stress. Therefore, the value of r in this analysis was chosen to be very big to be able to predict this behaviour ($r=p'_o/p'_x$, where p'_o and p'_x are the preconsolidation pressure and the critical mean effective stress respectively, see also Figure 3.1).

In order to allow for the prediction of sand behaviour from its loosest to its densest state, the reference state parameter (ξ_R) is assumed to be equal to the initial state parameter of the loosest sample D684. The critical state constants for Erksak sand are from Been *et al.* (1991) and Jefferies (1993) and because the accurate elastic constants are not known for Erksak sand, some typical values are used in the prediction.

Figures 4.12-4.14 present comparisons of the predictions and the measured behaviour for tests on the samples D667, D662 and D684. It is clear from these figures that overall CASM is quite satisfactory for predicting the measured behaviour of dense, medium and loose sands.

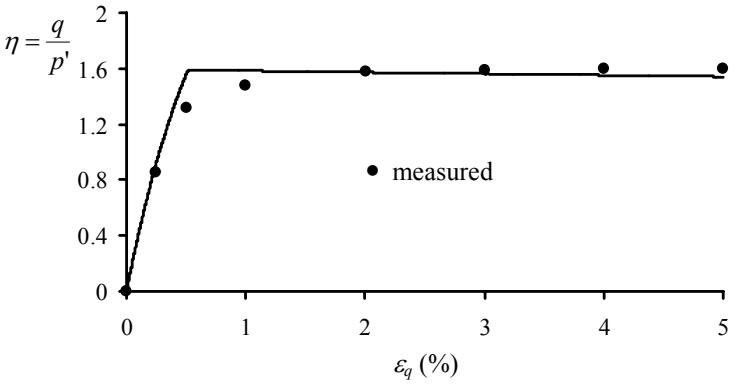

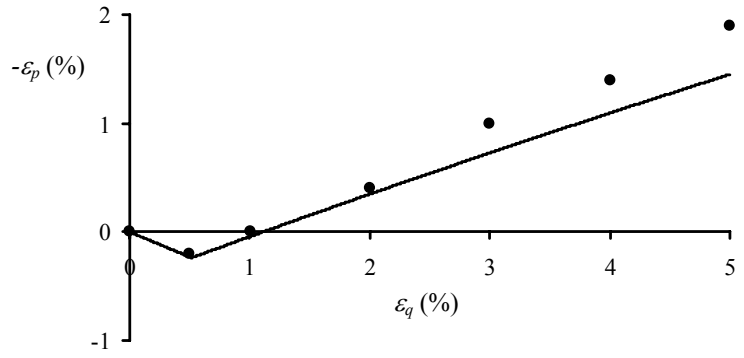

Figure 4.12. Test 5: Drained compression of a dense sample of Erksak 330/0.7 sand

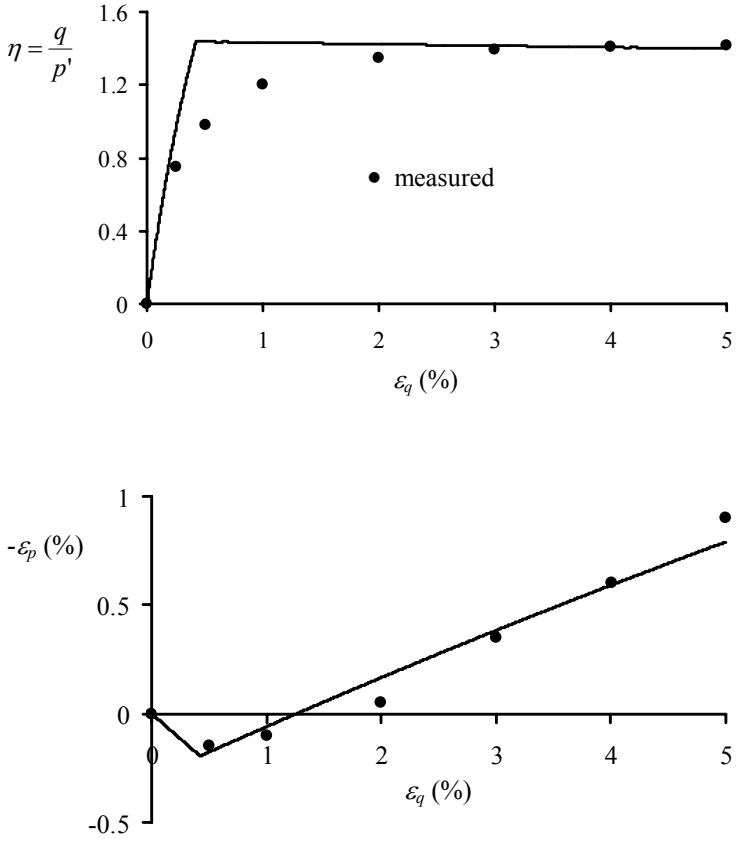

Figure 4.13. Test 6: Drained compression of a medium sample of Erksak 330/0.7 sand

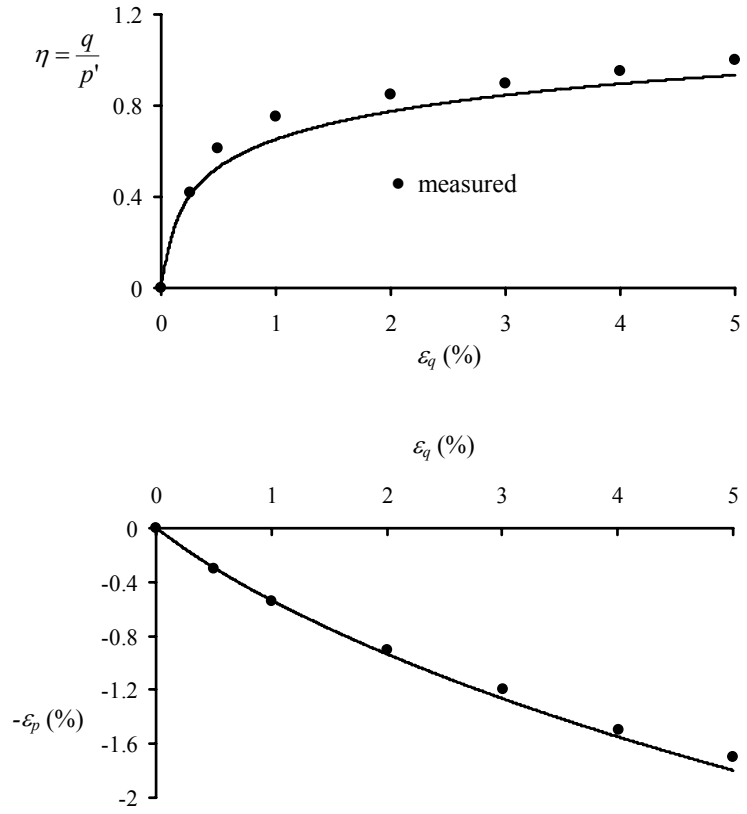

Figure 4.14. Test 7: Drained compression of a loose sample of Erksak 330/0.7 sand

4.3.3. Undrained behaviour of very loose sand (Tests 8-11)

The term 'very loose' is used here to describe sand in a state which is much looser than its critical state. It is well known that very loose sands can collapse and strain-soften during monotonic undrained loading and ultimately reach a critical state. During monotonic undrained loading loose sand reaches a peak resistance and then rapidly softens to a steady state. This is a condition necessary for liquefaction to occur. Most existing critical state models are unable to model this behaviour.

To demonstrate the ability of CASM to model undrained behaviour of very loose sand, test data obtained by Sasitharan *et. al.* (1994) on Ottawa sand was used. Four tests have been selected for comparison with CASM. These tests were on the samples with initial void ratio of 0.793 and 0.804. Different initial mean effective stresses were used. The material constants used in the CASM predictions are as follows:

$$M=1.19,\ \lambda=0.0168,\ \kappa=0.005,\ \mu=0.3,\ \Gamma=2.06,\ n=3,\ \xi_R=\xi_o$$

The critical state constants for Ottawa sand are from Sasitharan *et. al.* (1994). Again the accurate elastic constants are not known for this sand and some typical values have to be adopted. When CASM is used to model the undrained behaviour of a very loose sand, the reference state parameter (ξ_R) can be assumed to be equal to the initial state parameter (ξ_o) of each sample. It is shown below that this assumption proves to be very satisfactory for predicting undrained behaviour of very loose sands.

Figures 4.15-4.18 are comparisons of the CASM predictions and the measured behaviour for undrained tests on the four very loose samples. It is evident from these figures that CASM can be satisfactorily used to predict the measured behaviour of undrained tests on very loose sands. In particular, CASM predicts that the peak strength is developed at a very small axial strain. Afterwards the response shows a marked strain softening with increasing axial strain before approaching the critical state.

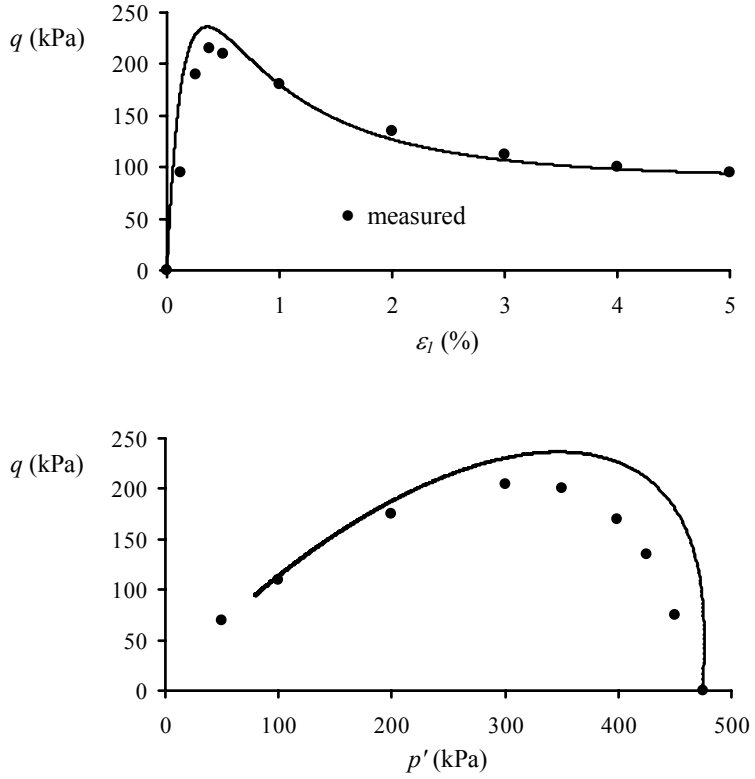

Figure 4.15. Test 8: Undrained compression of a very loose Ottawa sand (e_o=0.793, p'_o=475 kPa)

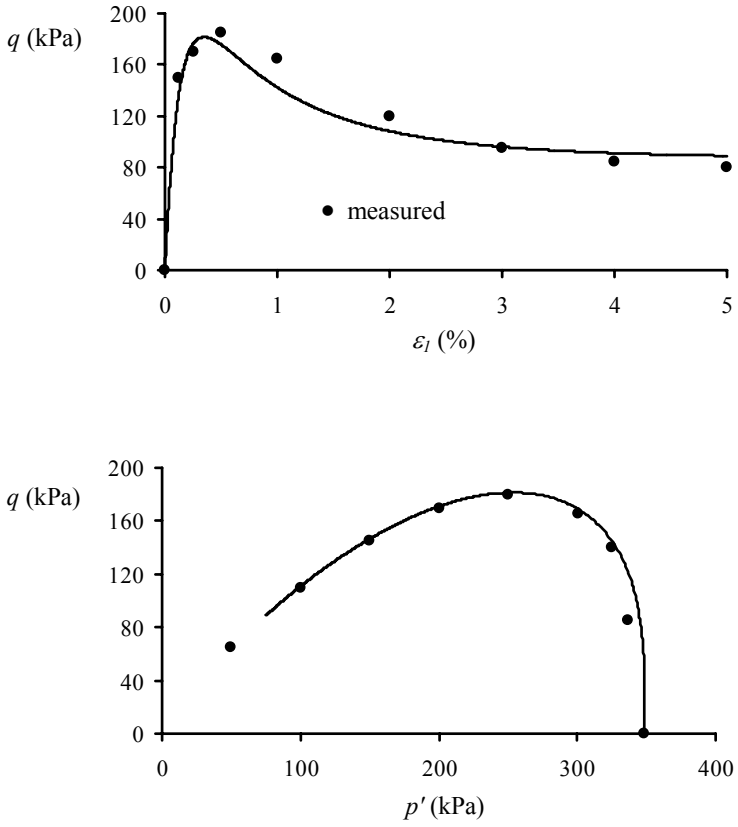

Figure 4.16. Test 9: Undrained compression of a very loose Ottawa sand (e_o=0.793, p'_o=350 kPa)

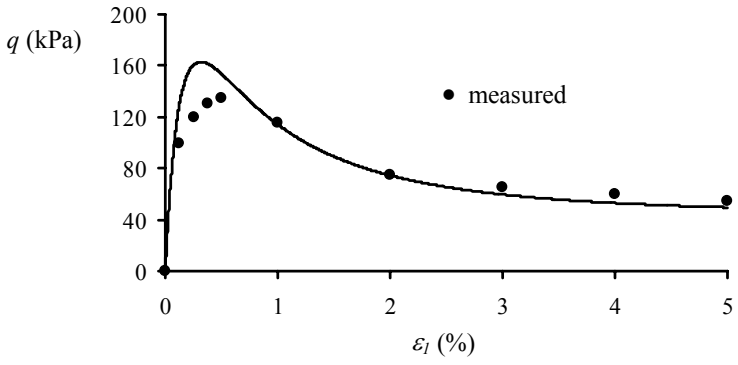

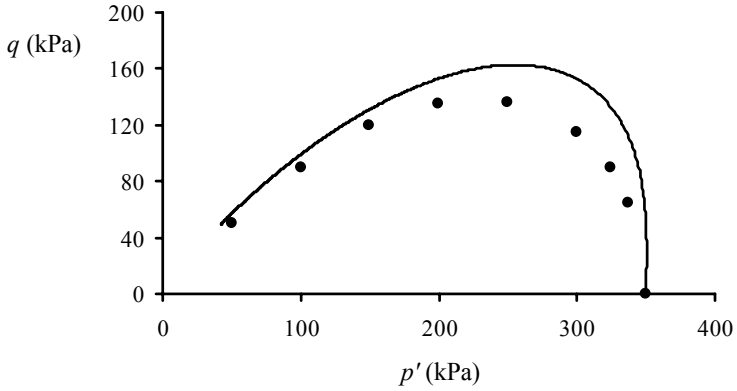

Figure 4.17. Test 10: Undrained compression of a very loose Ottawa sand (e_o=0.804, p'_o=350 kPa)

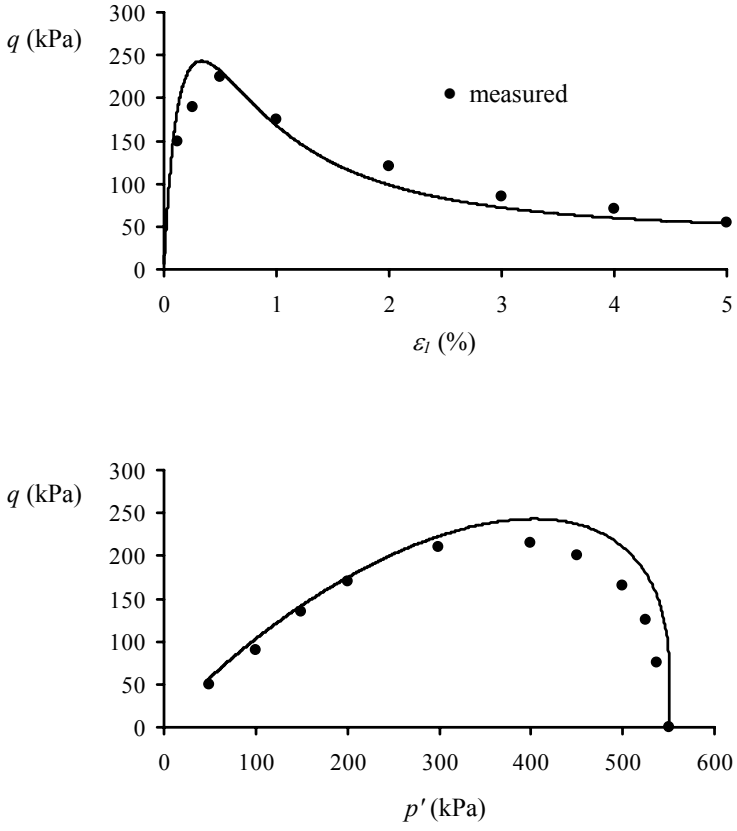

Figure 4.18. Test 11: Undrained compression of a very loose Ottawa sand (e_o=0.804, p'_o=550 kPa)

It should be noted however that the critical state soil mechanics models used here can only be applied when the principles of continuum mechanics hold; CASM therefore cannot model the formation of shear bands and the deformation within shear bands often observed in soils. Figures 4.15-4.18 only show the finite element results obtained when the tests were displacement-controlled.

4.4. SUMMARY

In this chapter, a new non-linear elastic rule proposed by Houlsby and Wroth (1991) for clays has been adopted for CASM. The processes of generalising CASM into three-dimensional stress space and implementing it into CRISP have also been presented. The shapes of the yield and plastic potential surfaces in the deviatoric plane have been chosen. Experimental data and numerical simulations have been used to justify the choices made. CASM has been validated by simulating triaxial tests for a number of materials under different loading conditions. CASM's finite element results have been compared with data from a classical series of tests as well as the finite element results obtained from the original Cam-clay model. It has been found that the predictions from CASM were consistently better than those from Cam-clay for normally and overconsolidated clays under both drained and undrained loading conditions. In particular, CASM has been found to be able to capture reasonably well the overall behaviour of the overconsolidated clay and sand observed in the laboratory. It has proven itself to be a useful extension of the Cam-clay models.

However, some deficiencies of CASM have been pointed out. CASM tends to under-predict the shear strain at peak strength. The curves produced by CASM for overconsolidated soils are not as smooth as the observed curves. This deficiency is due to the fact that, like Cam-clay, CASM does not allow any plastic deformation to develop within the state boundary surface. This drawback will be dealt with in Chapter 6.

CHAPTER 5

CASM-d: A NEW COMBINED VOLUMETRIC-DEVIATORIC HARDENING MODEL

5.1. INTRODUCTION

In the standard critical state soil mechanics theory, hardening is obtained from the volume changes alone (and hence, the name volumetric hardening). Therefore, hardening stops and unlimited plastic deformation can take place once the critical state of zero incremental dilation has been reached (Krenk, 2000). However, a more realistic model would assume that the work done by the deviatoric stresses gave an additional contribution to the hardening.

A combined deviatoric and density hardening model was first introduced by Nova and Wood (1979). They used the following expression for the relation of the incremental preconsolidation pressure ($\delta p'_o$) and the incremental strains ($\delta\varepsilon_p^p$, $\delta\varepsilon_q^p$):

$$\delta p'_o = \frac{p'_o}{(\lambda - \kappa)}\left(\delta\varepsilon_p^p + D \times \delta\varepsilon_q^p\right) \tag{5.1}$$

where D is a new non-dimensional parameter which is positive during hardening process and suddenly becomes zero at the start of softening.

More recently, by using the techniques of thermomechanics, Collins and Kelly (2002) came up with the following expression:

$$\delta p'_o = \frac{1}{(\lambda - \kappa)}\left(p' \times \delta\varepsilon_p^p + D \times q \times \delta e\right) \tag{5.2}$$

where again D is a non-dimensional weight parameter and δe is the change in void ratio.

5.2. CASM-d, DESCRIPTION OF THE MODEL

5.2.1. Yield surface, plastic potential and elastic parameters

The yield surface, plastic potential and elastic properties of the new model are exactly the same as the original CASM model. Details are described in Chapters 3 and 4.

5.2.2. Assumption on the new hardening rule

In this study, the following assumption has been made:

$$\delta p'_o = \frac{v p'_o}{(\lambda - \kappa)}\left(\delta\varepsilon_p^p + \alpha \times \delta\varepsilon_q^p\right) \tag{5.3}$$

$$\Leftrightarrow \qquad \delta p'_o = \frac{v p'_o}{(\lambda - \kappa)}\delta\varepsilon_p^p\left(1 + \alpha \times \frac{\delta\varepsilon_q^p}{\delta\varepsilon_p^p}\right) \tag{5.4}$$

In equations 5.3 and 5.4, α is the new model parameter which controls the contribution of the incremental plastic deviatoric strain $\left(\delta\varepsilon_q^p\right)$ to the rate of change of the hardening parameter (p'_o). When α is zero, CASM-d is identical to CASM.

It should be noted that this assumption does not satisfy the critical state condition. In fact, the critical state condition will never be met by this model. By the definition of the critical state, $\delta p'_o$ has to be zero. However, this cannot happen because $\delta p'_o$ is now dependent upon $\delta\varepsilon_q^p$ and this quantity is non-zero.

5.2.3. Hardening modulus

The dilatancy rule is obtained from the plastic potential as follows (Rowe, 1962):

$$\frac{\delta\varepsilon_p^p}{\delta\varepsilon_q^p} = \frac{9(M-\eta)}{9+3M-2M\eta} \tag{5.5}$$

(5.4) & (5.5):

$$\delta p'_o = \frac{vp'_o}{(\lambda-\kappa)}\delta\varepsilon_p^p\left(1+\alpha\times\frac{(9+3M-2M\eta)}{9(M-\eta)}\right) \tag{5.6}$$

Calculating the hardening modulus, H:

$$H = -\frac{1}{\Lambda}\frac{\partial F}{\partial p'_o}\delta p'_o \tag{5.7}$$

$$\delta p'_o = \frac{vp'_o}{(\lambda-\kappa)}\delta\varepsilon_p^p\left(1+\alpha\times\frac{(9+3M-2M\eta)}{9(M-\eta)}\right) \tag{5.8}$$

$$\delta\varepsilon_p^p = \Lambda\frac{\partial G}{\partial p'} \tag{5.9}$$

(5.8) & (5.9):

$$\delta p'_o = \frac{vp'_o}{(\lambda-\kappa)}\left(1+\alpha\times\frac{(9+3M-2M\eta)}{9(M-\eta)}\right)\times\Lambda\frac{\partial G}{\partial p'} \tag{5.10}$$

$$\frac{\partial G}{\partial p'} = 3\times\left(\frac{3+2M}{2q+3p'}-\frac{3-M}{3p'-q}\right) \tag{5.11}$$

(5.10) & (5.11):

$$\delta p'_o = \frac{vp'_o}{(\lambda-\kappa)}\left(1+\alpha\times\frac{(9+3M-2M\eta)}{9(M-\eta)}\right)\times\Lambda\times 3\times\left(\frac{3+2M}{2q+3p'}-\frac{3-M}{3p'-q}\right) \tag{5.12}$$

$$\frac{\partial F}{\partial p'_o} = -\frac{1}{p'_o \ln r} \tag{5.13}$$

(5.7), (5.12) & (5.13):

$$H = -\frac{1}{\Lambda}\frac{\partial F}{\partial p'_o}\delta p'_o = \left(-\frac{1}{\Lambda}\right)\times\left(-\frac{1}{p'_o \ln r}\right)\times\left(\begin{array}{l}\dfrac{\nu p'_o}{(\lambda-\kappa)}\left(1+\alpha\times\dfrac{(9+3M-2M\eta)}{9(M-\eta)}\right)\\ \times\Lambda\times 3\times\left(\dfrac{3+2M}{2q+3p'}-\dfrac{3-M}{3p'-q}\right)\end{array}\right) \tag{5.14}$$

So,

$$H = \frac{3\nu}{(\lambda-\kappa)\ln r}\left(\frac{3+2M}{2q+3p'}-\frac{3-M}{3p'-q}\right)\left(1+\alpha\times\frac{9+3M-2M\eta}{9(M-\eta)}\right) \tag{5.15}$$

Hence, the elastic and plastic stress-strain responses of CASM-d can be written in matrix form as:

$$\begin{bmatrix}\delta\varepsilon_p^e\\ \delta\varepsilon_q^e\end{bmatrix} = \begin{bmatrix}\dfrac{\kappa}{\nu p'} & 0\\ 0 & \dfrac{1}{3G}\end{bmatrix}\begin{bmatrix}\delta p'\\ \delta q\end{bmatrix} \tag{5.16}$$

$$\begin{bmatrix}\delta\varepsilon_p^p\\ \delta\varepsilon_q^p\end{bmatrix} = \frac{(\lambda-\kappa)\ln r}{3\nu\left\{\begin{array}{l}\left(\dfrac{3+2M}{2q+3p'}-\dfrac{3-M}{3p'-q}\right)\times\\ \left(1+\alpha\times\dfrac{9+3M-2M\eta}{9(M-\eta)}\right)\end{array}\right\}}\begin{bmatrix}\left(\dfrac{1}{p'\ln r}-\dfrac{nq^n}{M^n p'^{n+1}}\right)\times & \left(\dfrac{nq^{n-1}}{M^n p'^n}\right)\times\\ \left(\dfrac{9+6M}{2q+3p'}-\dfrac{9-3M}{3p'-q}\right) & \left(\dfrac{9+6M}{2q+3p'}-\dfrac{9-3M}{3p'-q}\right)\\ \left(\dfrac{1}{p'\ln r}-\dfrac{nq^n}{M^n p'^{n+1}}\right)\times & \left(\dfrac{nq^{n-1}}{M^n p'^n}\right)\times\\ \left(\dfrac{2(3+2M)}{2q+3p'}+\dfrac{3-M}{3p'-q}\right) & \left(\dfrac{2(3+2M)}{2q+3p'}+\dfrac{3-M}{3p'-q}\right)\end{bmatrix}\begin{bmatrix}\delta p'\\ \delta q\end{bmatrix} \tag{5.17}$$

5.2.4. Incorporation of CASM-d into CRISP

CASM-d has been generalised into the three-dimensional stress space and then implemented into CRISP, the procedure are similar to those described in Chapter 4. The only part of the source code which needed to be modified from the original CASM was the calculation of the hardening modulus where equation 4.13 was replaced by equation 5.15.

5.3. ANALYSIS OF TRIAXIAL TESTS USING CASM-d

Once again, the triaxial test was used to assess the performance of CASM-d. The tests described in Chapter 4 were repeated. All the test conditions and assumptions were retained. Four different values of the new parameter α were used for each test and the results are shown below. CASM can be recovered from CASM-d when α is set to zero. Hence, a direct comparison with the original model can be made.

5.3.1. Drained and undrained behaviour of normally consolidated and overconsolidated clays (Tests 1-4)

M=0.9, λ=0.093, κ=0.025, μ=0.3, Γ=2.06, n=4.5, r=2.714

Figures 5.1-5.4 present the results from CASM-d on normally consolidated and heavily overconsolidated clays in which the deviatoric stress (q) and excess pore pressure (Δu) are plotted against the axial strain (ε_1).

It can be seen that the new parameter α has a profound effect on the stress-strain prediction from the new model. CASM-d is a very flexible tool for predicting soil behaviours.

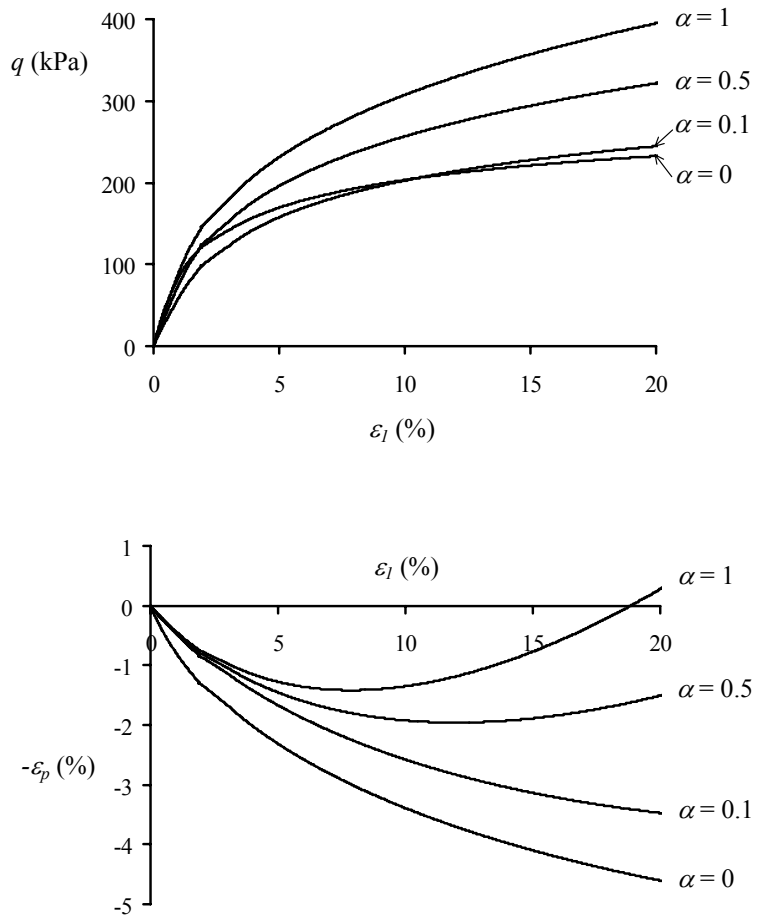

Figure 5.1. Test 1: Drained compression of a normally consolidated sample of Weald clay

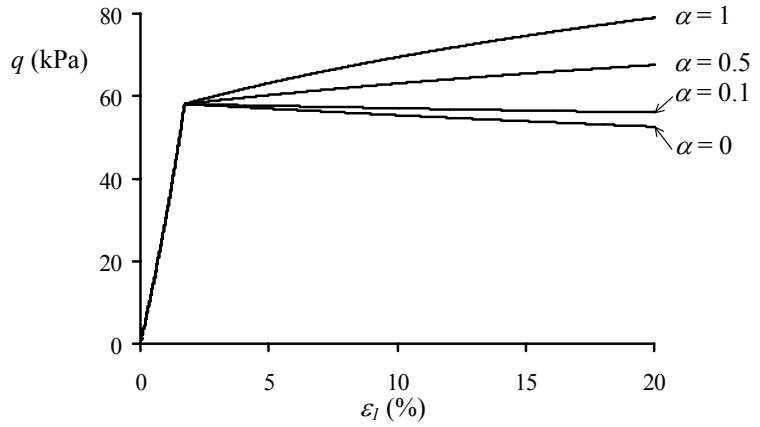

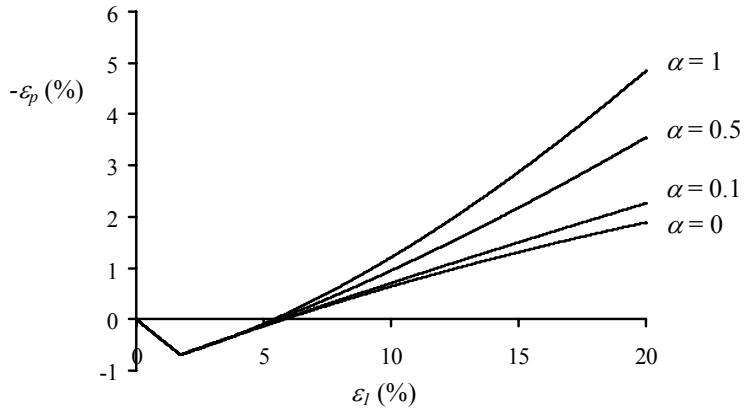

Figure 5.2. Test 2: Drained compression of a heavily overconsolidated sample of Weald clay

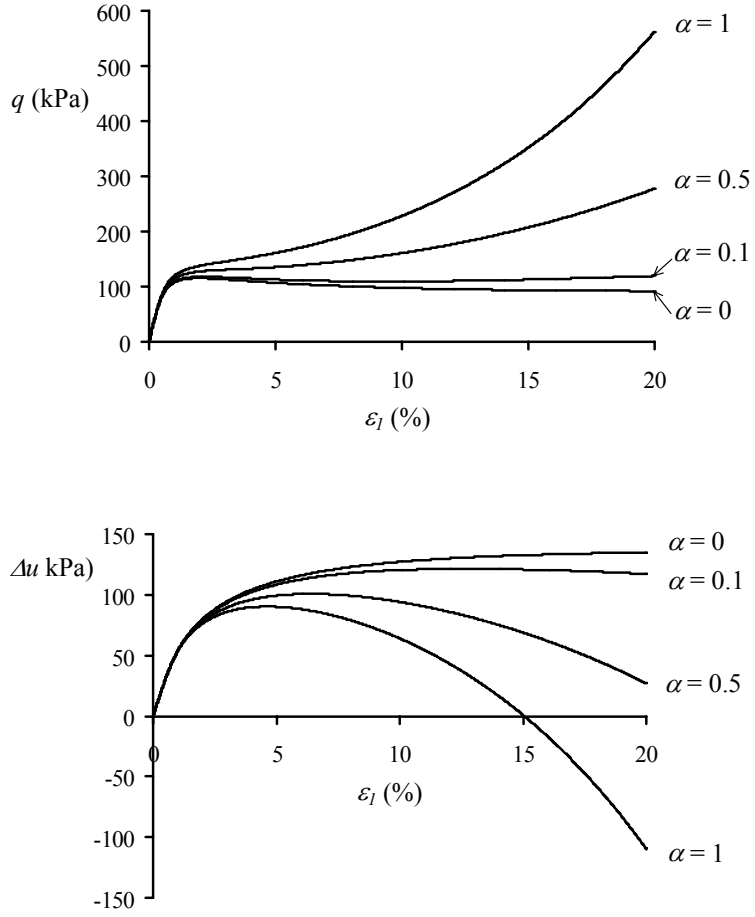

Figure 5.3. Test 3: Undrained compression of a normally consolidated sample of Weald clay

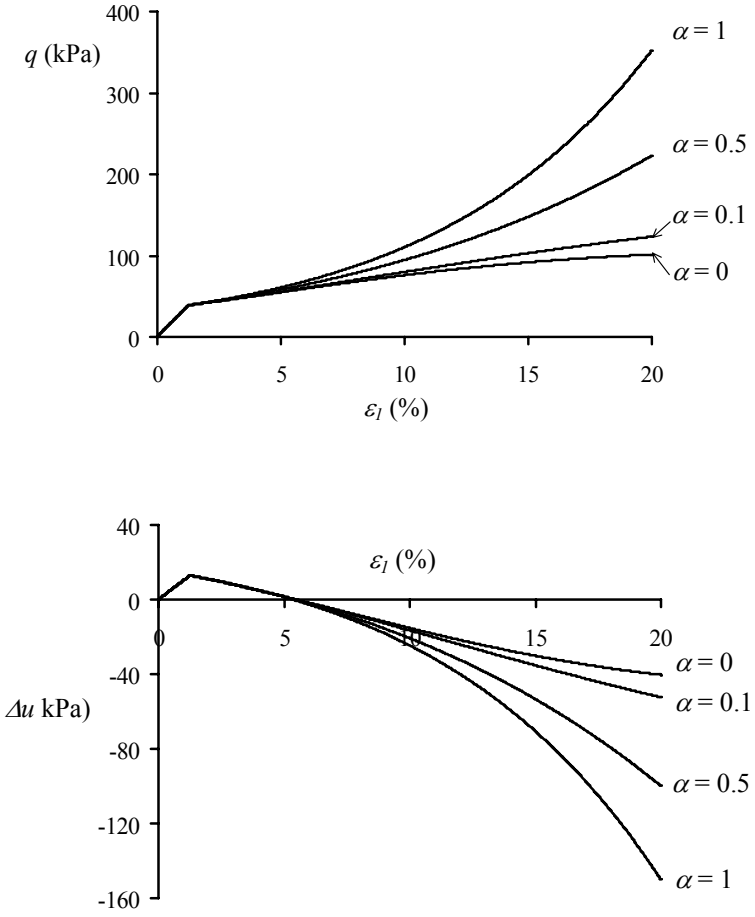

Figure 5.4. Test 4: Undrained compression of a heavily overconsolidated sample of Weald clay

However, as mentioned above, one major drawback of this type of models is that the critical states are not reached even at large strains. This is evident from Figures 5.1-5.4 where the shear stress, volumetric strain and excess pore water pressure have not reached a flat maximum after 20% axial strain, while the samples compress substantially as the tests proceed. One way of avoiding this problem is to assume that α is a function of the strain level, i.e. α decays to zero as the strain level increases.

5.3.2. Drained behaviour of loose, medium and dense sands (Tests 5-7)

M=1.2, λ=0.0135, κ=0.005, μ=0.3, Γ=1.8167, n=4.0, r=6792.0

Figures 5.5-5.7 present the analysis results of Erksak sand obtained using CASM-d. The stress ratio (η=q/p') and volumetric strain (ε_p) are plotted against the deviatoric strain (ε_q).

Figures 5.5 and 5.6 show that unlike clay, α has little impact on the prediction of drained dense sands. Combined hardening models give slightly higher values of the stress ratios (η) and volumetric strains (ε_p) in the (η,ε_q) and (ε_p,ε_q) curves respectively. For drained prediction of loose sand (see Figure 5.7), the new model predicts a higher value of stress ratio but a lower absolute value of volumetric strain as the value of α increases. For higher values of α, the volumetric strain reaches a flat maximum. This fact, which CASM fails to predict, is well supported by experimental data.

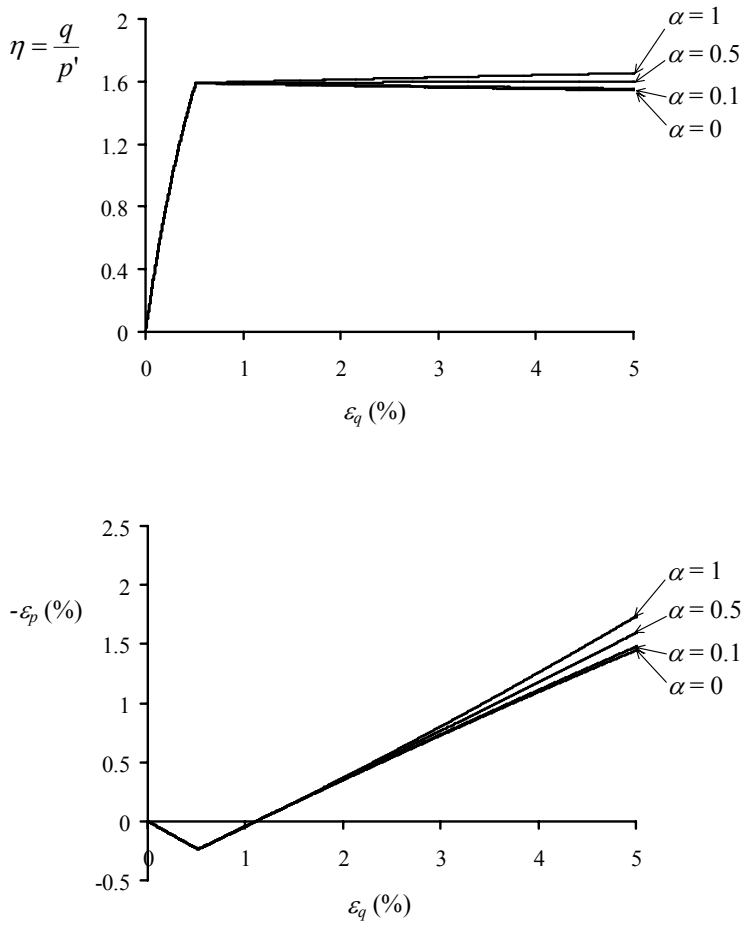

Figure 5.5. Test 5: Drained compression of a dense sample of Erksak 330/0.7 sand

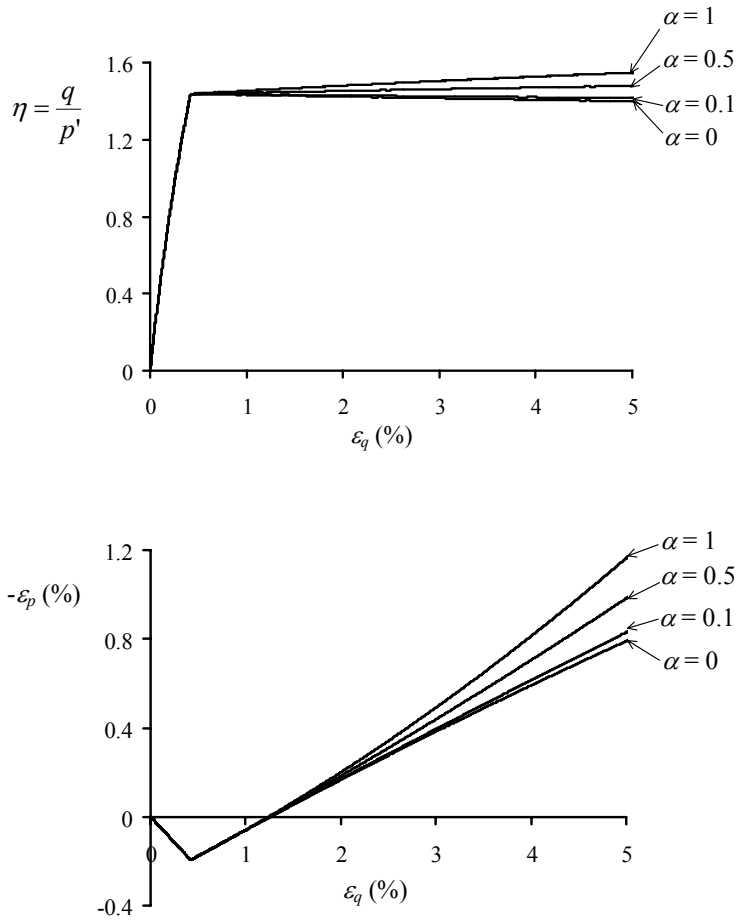

Figure 5.6. Test 6: Drained compression of a medium sample of Erksak 330/0.7 sand

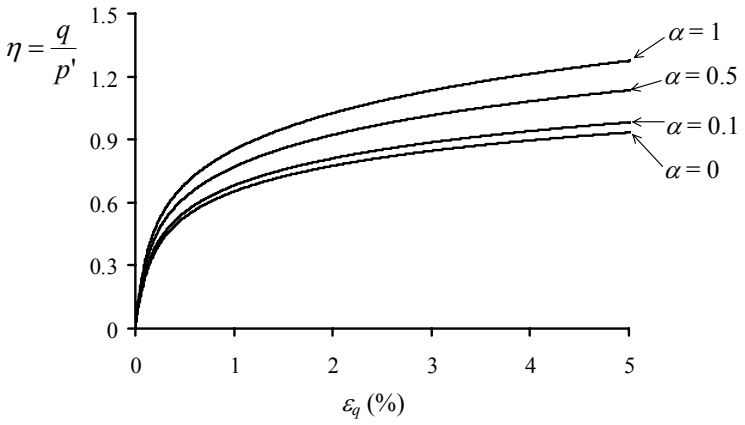

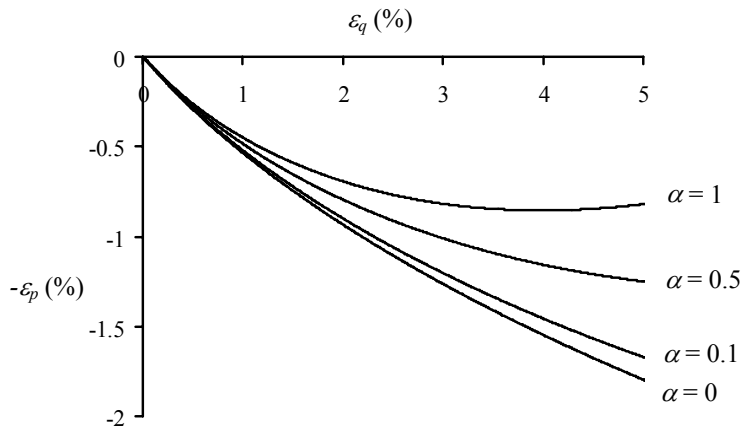

Figure 5.7. Test 7: Drained compression of a loose sample of Erksak 330/0.7 sand

5.3.3. Undrained behaviour of very loose sand (Tests 8-11)

M=1.19, λ=0.0168, κ=0.005, μ=0.3, Γ=2.06, n=3, $\xi_R=\xi_o$

Analyses of undrained loose Ottawa sand using CASM-d are shown in Figures 5.8-5.11. In these figures, the shear stress–axial strain curves (q,ε_1) and the stress paths (q,p') are plotted. In a similar fashion to the previous tests, the new model makes a big difference when predicting the behaviour of loose sands.

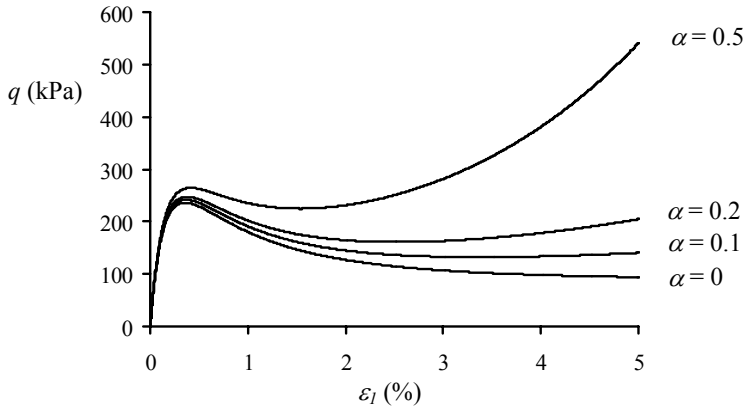

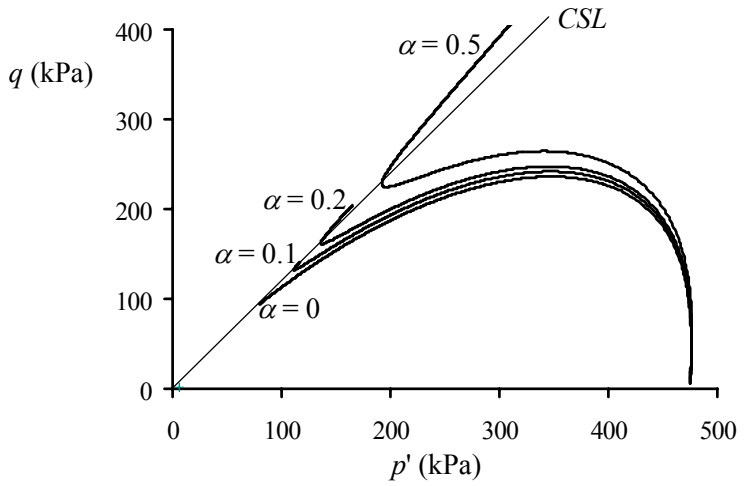

Figure 5.8. Test 8: Undrained compression of a very loose Ottawa sand (e_o=0.793, p'_o=475 kPa)

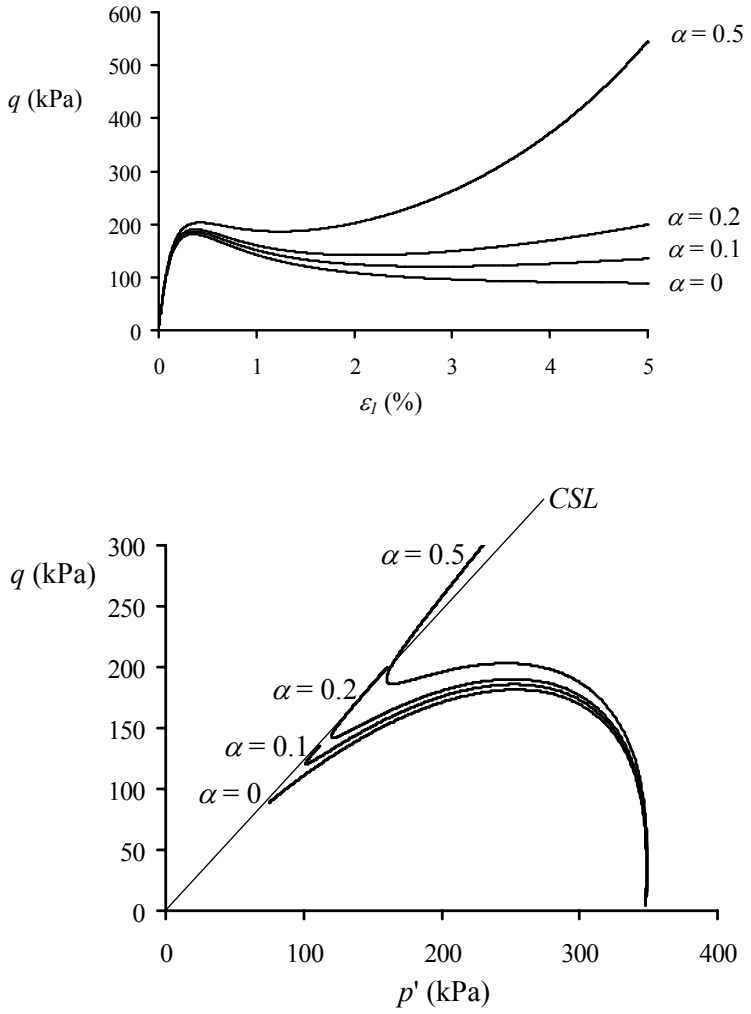

Figure 5.9. Test 9: Undrained compression of a very loose Ottawa sand (e_o=0.793, p'_o=350 kPa)

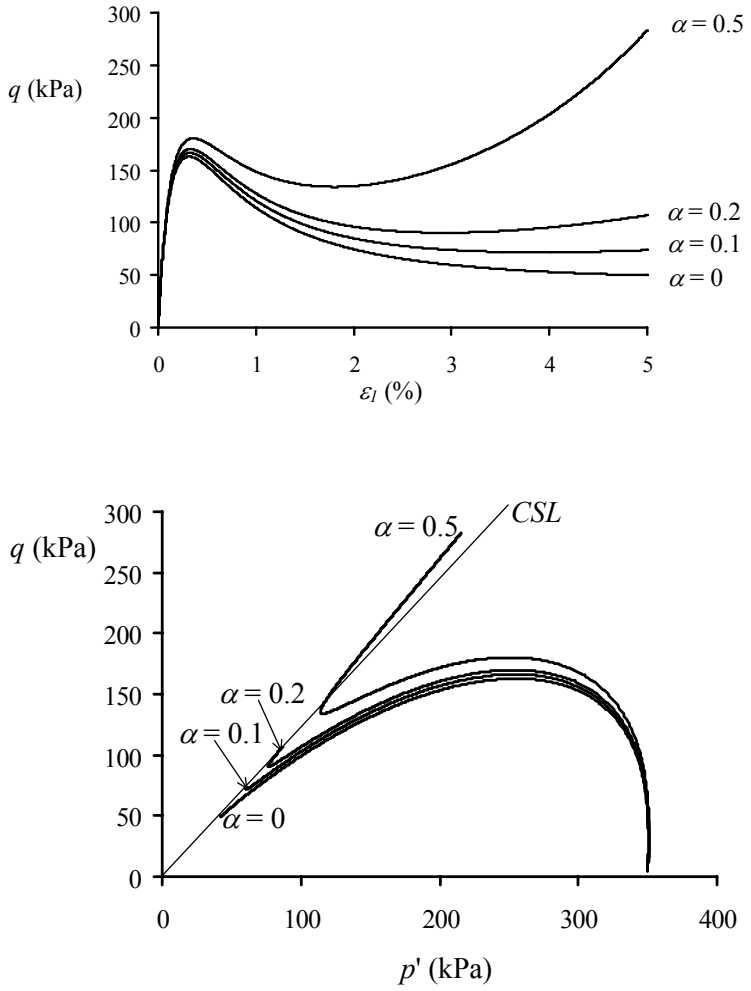

Figure 5.10. Test 10: Undrained compression of a very loose Ottawa sand (e_o=0.804, p'_o=350 kPa)

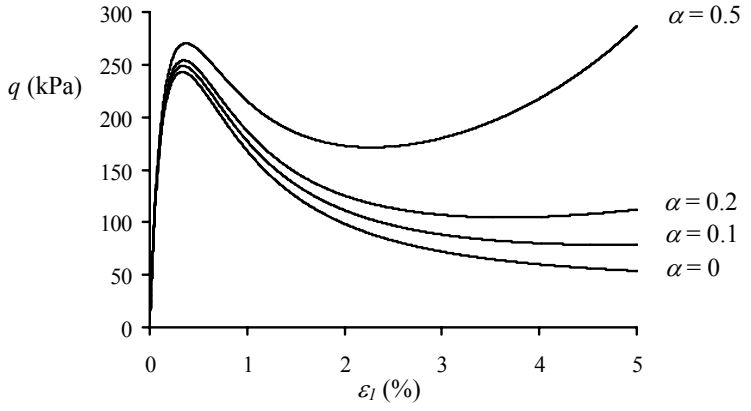

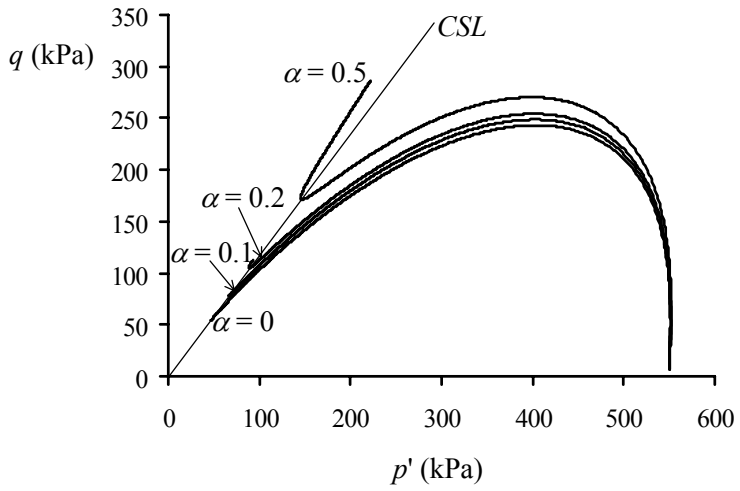

Figure 5.11. Test 11: Undrained compression of a very loose Ottawa sand (e_o=0.805, p'_o=550 kPa)

It can be seen in Figures 5.3 and 5.8-5.11 that when α is positive, undrained tests of normally overconsolidated clay and very loose sands exhibit a marked a peak in their (q,ε_1) curves. Thereafter, q decreases and finally it starts increasing again at the end of the test. This is a very important behaviour of undrained soils which was first reported by Bishop and Henkel (1957). Figure 5.12 shows the data produced by Bishop and Henkel (1957) and other authors (Hyodo et. al., 1994; Coop, 1990) who have also observed this behaviour in sands.

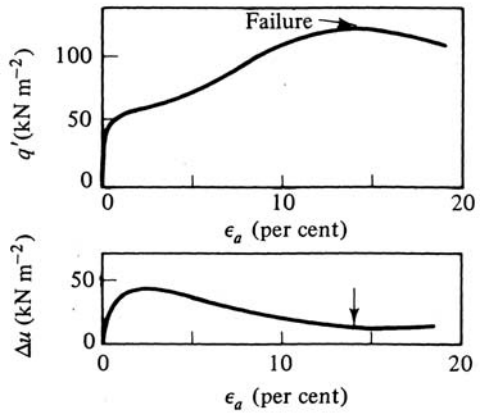

(a) Undrained test of loose Brasted sand (Bishop and Henkel, 1957)

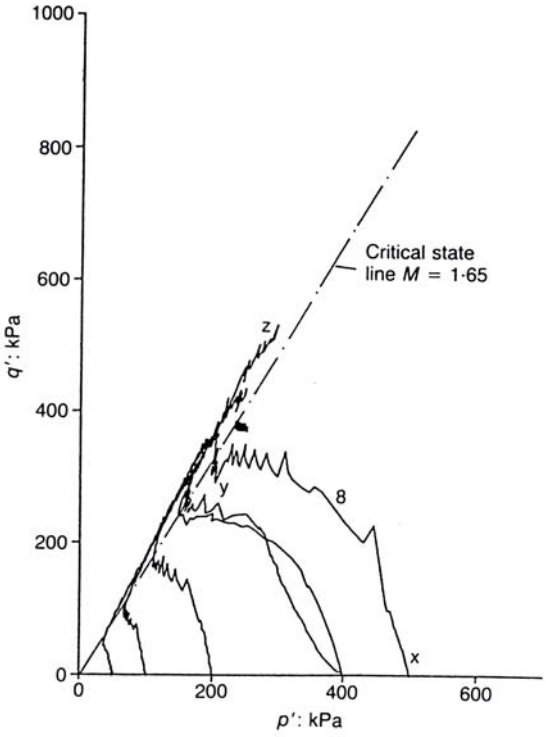

(b) Undrained stress paths of loose Dogs Bay sand (Coop, 1990)

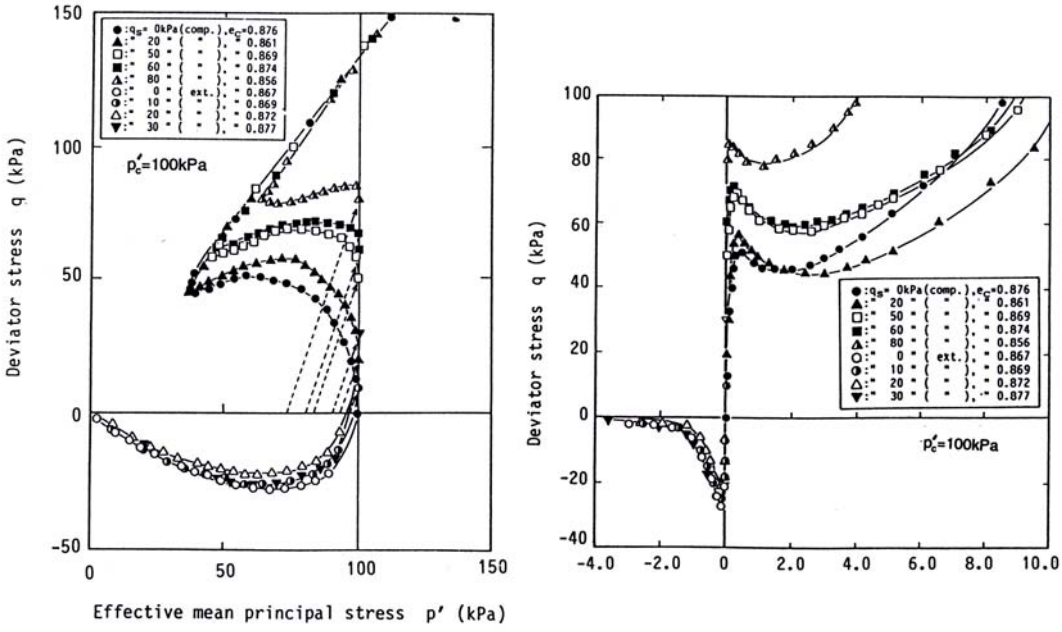

(c) Undrained stress paths and stress-strain curves of loose Toyoura sand (Hyodo et. al., 1994)

Figure 5.12. Data from undrained triaxial tests on loose sands

5.4. SUMMARY

In summary, an extension of CASM has been presented in this chapter by assuming that the work done by the deviatoric stresses also gives an additional contribution to hardening. Only one more parameter (α) is introduced. The new model, called CASM-d, can be reduced to the original model CASM by setting the new parameter equal to zero.

The new model has been generalised into the three-dimensional stress space and then successfully implemented into CRISP. The same set of classical triaxial tests used in Chapter 4 has been used to validate and assess the performance of CASM-d. It has been found that the deviatoric contribution to the soil hardening made a profound difference on the performance of the new model. In particular, one very important behavioural aspect of normally consolidated clays and loose sands can be predicted by CASM-d. This is the reappearance of hardening behaviour once the material has softened. Experimental data has been used to verify this feature of soil behaviour.

However, one drawback of the new model has been indicated. The critical state is not reached in this model even at a very high level of strain. This is because the size of the yield surface (p'_o) keeps increasing as the soil reaches its failure state. In this model, $\delta p'_o$ is also dependent upon the incremental plastic deviatoric strain $\left(\delta\varepsilon_q^p\right)$ and this quantity is not zero at critical state. Therefore, some modification should be done so that the value of α decays to zero as the critical state is reached.

CHAPTER 6

CASM-b: A NEW BOUNDING SURFACE MODEL

6.1. INTRODUCTION

The development of critical state soil mechanics was a major advance in the use of plasticity theory in geomechanics. Still however, some very important aspects of soil behaviour, mainly in relation to the cyclic response, cannot be adequately described. The principal reason is that the classical concept of a yield surface provides little flexibility when describing the change of the plastic modulus with loading direction and implies a purely elastic stress range within the yield surface. This results in overestimating the soil's stiffness and a lack of smooth transition from elastic to plastic behaviour of the soil (see Figures 4.9, 4.11, 4.12 and 4.13).

The need for new concepts in plasticity theory therefore became a necessity. There have been two major developments in this field over the last 35 years, namely the concept of multi-surface, kinematic hardening plasticity theory introduced by Mroz (1967) and Iwan (1967) and bounding surface plasticity theory introduced by Dafalias and Popov (1975) and Dafalias (1975).

The salient features of a bounding surface formulation are that plastic deformation may occur for stress states within the yield surface and it is possible to have a very flexible variation of the plastic modulus during a loading path.

In this chapter, CASM is extended into a bounding surface radial mapping plasticity model called CASM-b. The mathematical formulations of the model are presented first.

After which, the numerical implementation of CASM-b into CRISP is given. Finally, the new model is validated by analysing the same triaxial tests which were used in Chapters 4 and 5. A direct comparison is made between the results obtained using CASM-b and the original model CASM.

6.2. CASM-b, DESCRIPTION OF THE MODEL

6.2.1. Bounding surface

The bounding surface for CASM-b is the same as the yield surface of CASM and can be expressed in terms of the conventional triaxial variables as:

$$F = \left(\frac{q}{Mp'}\right)^n + \frac{\ln\left(\frac{p'}{p'_{oj}}\right)}{\ln r} \tag{6.1}$$

where p'_{oj} is the size of the bounding surface in the (p',q) plane.

6.2.2. Plastic potential

The plastic potential adopted in CASM-b is the same as that used in CASM and follows the stress-dilatancy relation of Rowe (1962):

$$G = 3M\left(\ln p' - \ln \beta\right) + \left(3 + 2M\right)\ln\left(\frac{2q + 3p'}{p'}\right) - \left(3 - M\right)\ln\left(\frac{3p' - q}{p'}\right) \tag{6.2}$$

6.2.3. Elastic parameters

The elastic part of this critical state model is the same as in CASM. Details of this can be found in Chapters 3 and 4.

6.2.4. Mapping rule

To define an image point on the bounding surface in a simple way, radial mapping is used. It is shown in Figure 6.1 that any stress state is associated with an image stress point. This is the intersection of the bounding surface with the straight line passing through the origin and the current stress state.

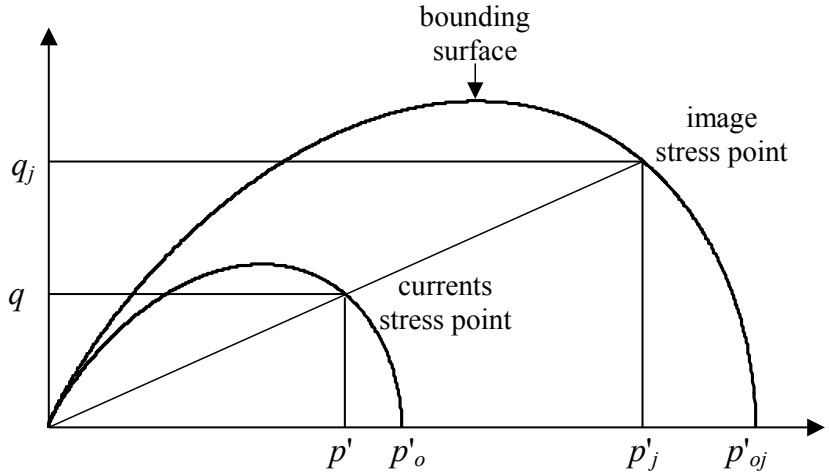

Figure 6.1. The mapping rule in CASM-b

It is assumed that the hardening modulus at the current stress point (H) is related to the hardening modulus at its corresponding image point (H_j) as well as to the ratio of distances from these two stress points to the origin.

6.2.5. Hardening modulus

The calculation of the hardening modulus (H) is the main new feature in CASM-b. Its derivation is presented in this section.

6.2.5.1. Hardening modulus at image point (H_j)

Assuming that the size of the bounding surface (p'_{oj}) is affected by the plastic volumetric strain $\left(\varepsilon_p^p\right)$ in the usual way:

$$\delta p'_{oj} = \frac{v p'_{oj}}{\lambda - \kappa} \delta \varepsilon_p^p \tag{6.3}$$

The consistency condition of the bounding surface requires

$$\frac{\partial F}{\partial p'} \delta p'_j + \frac{\partial F}{\partial q} \delta q_j + \frac{\partial F}{\partial p'_{oj}} \delta p'_{oj} = 0 \tag{6.4}$$

Since $\frac{\partial F}{\partial p'_{oj}} = \frac{-1}{p'_{oj} \ln r}$ we have:

$$\frac{\partial F}{\partial p'} \delta p'_j + \frac{\partial F}{\partial q} \delta q_j - \frac{1}{p'_{oj} \ln r} \frac{v p'_{oj}}{\lambda - \kappa} \delta \varepsilon_p^p = 0 \tag{6.5}$$

$$\frac{\partial F}{\partial p'} \delta p'_j + \frac{\partial F}{\partial q} \delta q_j - \frac{1}{\ln r} \frac{v}{\lambda - \kappa} \delta \varepsilon_p^p = 0 \tag{6.6}$$

The flow rule for CASM-b can be expressed as follows (Hill, 1950):

$$\delta \varepsilon_p^p = \frac{1}{H} dF \frac{\partial G}{\partial p'} = \frac{1}{H} \left(\frac{\partial F}{\partial p'} \delta p' + \frac{\partial F}{\partial q} \delta q \right) \frac{\partial G}{\partial p'} \tag{6.7}$$

It is assumed that the stress increments at the stress point ($\delta p'$,δq) and the image point ($\delta p'_j$,δq_j) give the same plastic strain increment. This assumption which was also used by Dafalias and Herrmann (1980) and Bardet (1986) is equivalent to:

$$\frac{1}{H} \left(\frac{\partial F}{\partial p'} \delta p' + \frac{\partial F}{\partial q} \delta q \right) \frac{\partial G}{\partial p'} = \frac{1}{H_j} \left(\frac{\partial F}{\partial p'} \delta p'_j + \frac{\partial F}{\partial q} \delta q_j \right) \left(\left. \frac{\partial G}{\partial p'} \right|_j \right) \tag{6.8}$$

$$\therefore \qquad \delta \varepsilon_p^p = \frac{1}{H_j} \left(\frac{\partial F}{\partial p'} \delta p'_j + \frac{\partial F}{\partial q} \delta q_j \right) \left(\left. \frac{\partial G}{\partial p'} \right|_j \right) \tag{6.9}$$

Substituting equation 6.9 into equation 6.6, we obtain:

$$\frac{\partial F}{\partial p'} \delta p'_j + \frac{\partial F}{\partial q} \delta q_j - \frac{v}{(\lambda - \kappa) \ln r} \frac{1}{H_j} \left(\frac{\partial F}{\partial p'} \delta p'_j + \frac{\partial F}{\partial q} \delta q_j \right) \left(\left. \frac{\partial G}{\partial p'} \right|_j \right) = 0 \tag{6.10}$$

$$\Leftrightarrow \qquad 1-\frac{\nu}{(\lambda-\kappa)\ln r}\frac{1}{H_j}\left(\left.\frac{\partial G}{\partial p'}\right|_j\right)=0 \tag{6.11}$$

$$\therefore \qquad H_j=\frac{\nu}{(\lambda-\kappa)\ln r}\left(\left.\frac{\partial G}{\partial p'}\right|_j\right) \tag{6.12}$$

Differentiating G with respect to p' gives

$$\left.\frac{\partial G}{\partial p'}\right|_j=3\left(\frac{3+2M}{2q_j+3p'_j}-\frac{3-M}{3p'_j-q_j}\right) \tag{6.13}$$

$$\therefore \qquad H_j=\frac{3\nu}{(\lambda-\kappa)\ln r}\left(\frac{3+2M}{2q_j+3p'_j}-\frac{3-M}{3p'_j-q_j}\right) \tag{6.14}$$

6.2.5.2. Hardening modulus at the stress point (H)

Due to the similarity in shape of the surfaces shown in Figure 6.1, the image stresses (p'_j,q_j) can be calculated from the current stresses (p',q) as follows:

$$\frac{p'}{p'_j}=\frac{q}{q_j}=\frac{p'_o}{p'_{oj}}=\gamma \text{ with } 0\le\gamma\le 1$$

$$p'_j=\frac{p'_{oj}}{p'_o}\times p'=\frac{p'}{\gamma}$$

$$q_j=\frac{p'_{oj}}{p'_o}\times q=\frac{q}{\gamma}$$

A specific feature of the bounding surface theory is that the hardening modulus (H) is not only dependent on the location of the image point but also is a function of the distance from the stress point to the bounding surface with the following requirements:

$$H=+\infty \text{ if } \gamma=0 \tag{6.15a}$$

$$H=H_j \text{ if } \gamma=1 \tag{6.15b}$$

The restrictions imposed by equation 6.15 ensure that the behaviour is almost elastic far from the bounding surface and that the stress point and bounding surface will move together when the current stress state lies on the bounding surface. The following form of calculating the hardening modulus has been proposed:

$$H = H_j + \frac{h}{p'}\frac{(1-\gamma)^m}{\gamma} \tag{6.16}$$

where h and m are two new material constants introduced in CASM-b. The term $\left(h/p'\right)$ represents the dependence of H on the current stress level and the material type, while the second term $\left[(1-\gamma)^m/\gamma\right]$ represents the mapping rule to satisfy the restrictions stated in equation 6.15.

It should be noted that equation 6.16 is only used to calculate the hardening modulus when the soil is being loaded; for unloading, purely elastic behaviour is still assumed.

A sensitivity study has been carried out to check the influences of the two new parameters (h and m) on the variation of the hardening modulus (H). Figures 6.2 and 6.3 show the results of this study. It can be seen that with the values of γ ($=p'_o/p'_{oj}$, see Figure 6.1) between 0.6 and 1, the values of h and m have no effect on H. This means the soil is assumed to behave as if the stress point is on the bounding surface ($H/H_j=1$). For values of γ smaller than 0.6, it is found that m has a much more influential role than h in terms of varying the value of H. Other forms of equation 6.16 should be investigated in future studies.

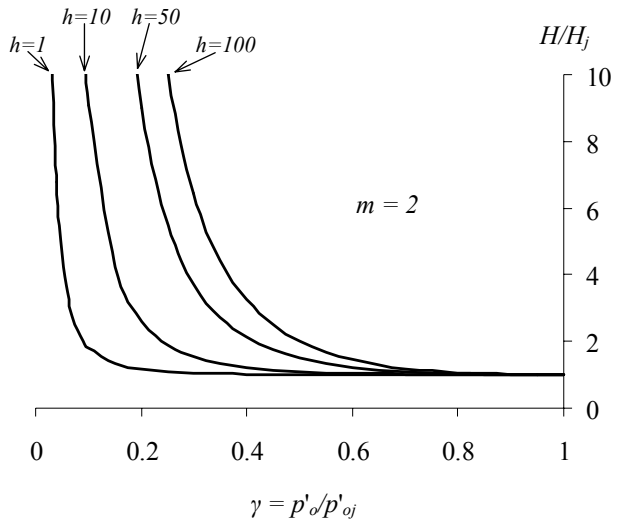

Figure 6.2. Variations of H with respect to h (m=2)

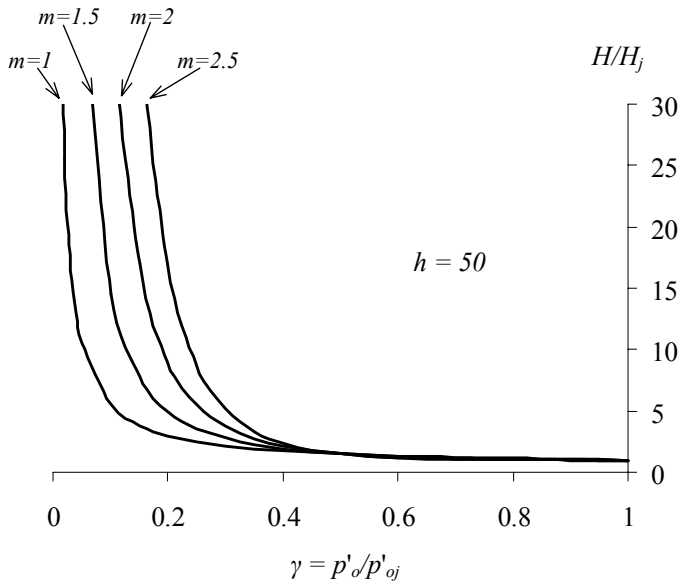

Figure 6.3. Variations of H with respect to m (h=50)

6.2.6. Incorporation of CASM-b into CRISP

Again CASM-b has been generalised into the three-dimensional stress space and then successfully implemented into CRISP. The procedures are similar to those described in Chapter 4. Similar to CASM-d which was in Chapter 5, the only part of the source code which needed to be modified was the calculation of the new hardening modulus where equations 6.14 and 6.16 were used instead of equation 4.13.

6.3. VALIDATION OF CASM-b

In this section, the performance of CASM-b is assessed by predicting the behaviour of clay and sand in the triaxial tests. These are the same tests which were used in Chapters 4 and 5. Only results for overconsolidated samples are presented here because CASM-b gives the same results as CASM if the soil is normally consolidated. As a result, only tests 2, 4, 5 and 6 were simulated by CASM-b.

6.3.1. Drained and undrained behaviour of heavily overconsolidated clays (Tests 2, 4)

M=0.9, λ=0.093, κ=0.025, μ=0.3, Γ=2.06, n=4.5, r=2.714, h=5.0, m=1.5

Figures 6.4 and 6.5 present the comparisons of CASM-b and CASM on heavily overconsolidated clays in which the deviatoric stress (q) and excess pore pressure (Δu) are plotted against the axial strain (ε_1). The experimental data is also shown (as dots) to compare the performance of both models.

It can be seen from Figures 6.4 and 6.5 that CASM-b can predict behaviour of clay under both drained and undrained loading conditions very well when compared to experimental data. Moreover, it gives more realistic predictions than those predicted by CASM and other traditional elastic-plastic models. This is achieved because the soil behaviour does not suddenly change from elastic to plastic when using CASM-b.

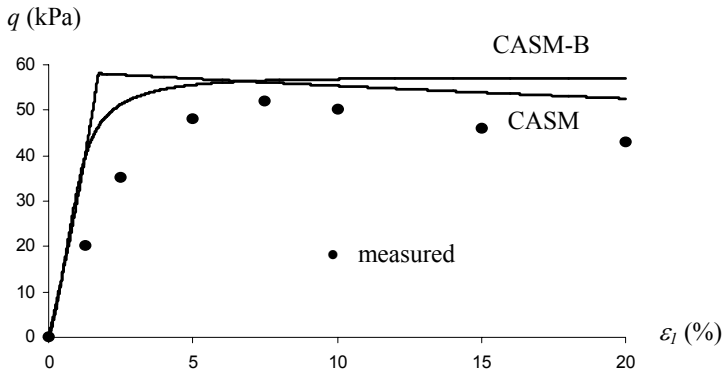

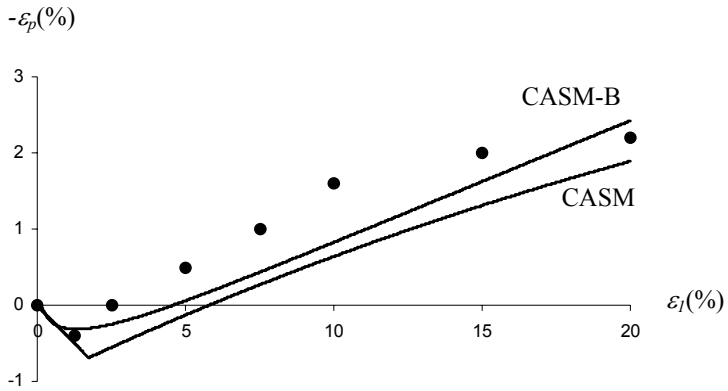

Figure 6.4. Test 2: Drained compression of a heavily overconsolidated sample of Weald clay

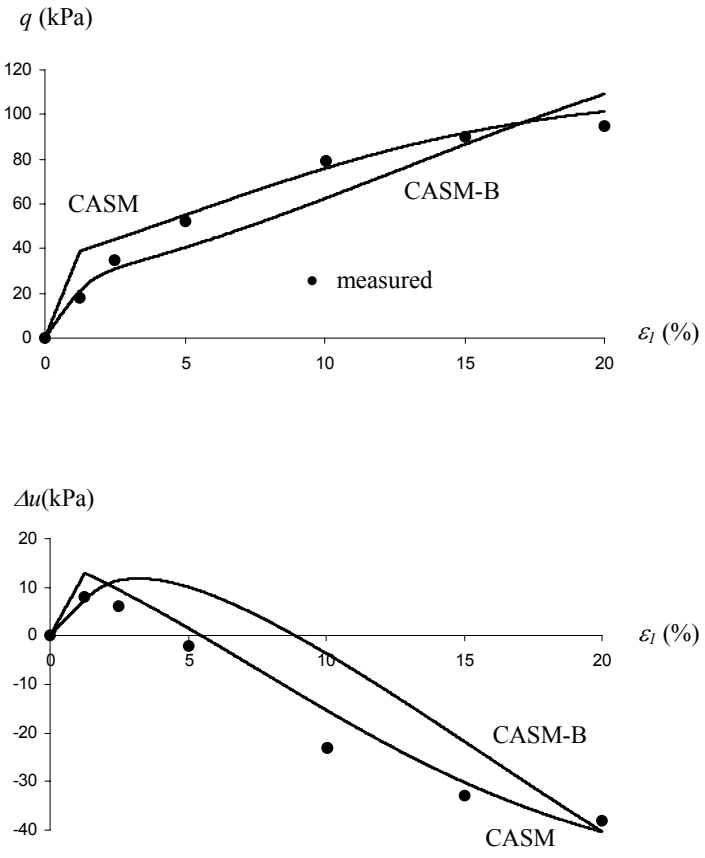

Figure 6.5. Test 4: Undrained compression of a heavily overconsolidated sample of Weald clay

6.3.2. Drained behaviour of medium and dense sands (Tests 5, 6)

M=1.2, λ=0.0135, κ=0.005, μ=0.3, Γ=1.8167, n=4.0, r=6792, h=10, m=2

Figures 6.6 and 6.7 present comparisons of the predictions and the measured behaviour for tests on the samples D667 and D662 respectively. The stress ratio (η=q/p') and volumetric strain (ε_p) are plotted against the deviatoric strain (ε_q). Again, the test data is presented as dots in these figures.

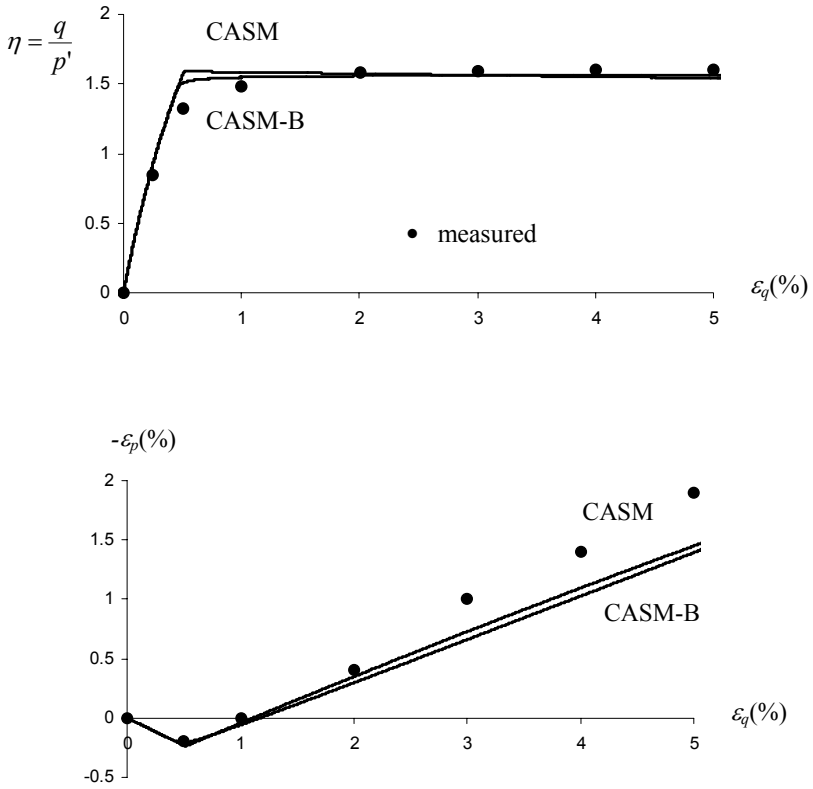

Figure 6.6. Test 5: Drained compression of a dense sample of Erksak 330/0.7 sand

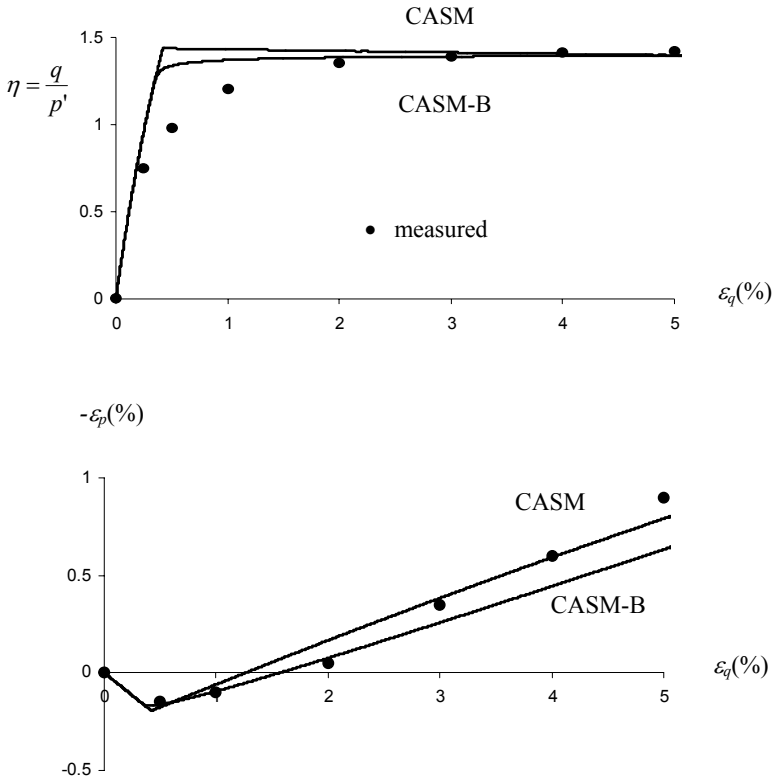

Figure 6.7. Test 6: Drained compression of a medium sample of Erksak 330/0.7 sand

It is shown in Figures 6.6 and 6.7 that CASM-b gives very similar results to CASM. Overall, both models are quite satisfactory for predicting the measured behaviour of sand.

6.4. SUMMARY

In summary, a new model called CASM-b which is based on the bounding surface plasticity theory has been developed from the original model CASM. Two new parameters (h and m) are introduced in the new model compared with CASM. These two parameters are used to provide a very flexible way of calculating the hardening modulus inside the bounding surface. A sensitivity study of the new parameters has been carried out to see the influence of these two parameters on the new model's performance. The new features of this model only apply when analysing overconsolidated materials. CASM-b will give the same results as CASM when the soil is normally consolidated.

The new model has been generalised into the three-dimensional stress space and successfully implemented into CRISP. Simulations of triaxial tests on overconsolidated clay and sand have been carried out to validate and assess the performance of the new model. It has been found that CASM-b gave better predictions than those predicted by CASM and other traditional elastic-plastic models. This is due to the fact that there is not a sudden change from elastic to plastic behaviour when modelling a soil using CASM-b. In other words, CASM-b can smooth the stress-strain curves to give more realistic predictions of soil behaviour.

It should be noted that the bounding surface formulation could also be used to distinguish between compacted and overconsolidated sands, such that at low stress levels, a compacted sand gives more volumetric strain. This can be done by choosing a suitable loading surface and by choosing a suitable value of m (see equation 6.16). This can then be used to generate the right sort of volumetric strain as a function of p' for a sand which is being isotropically normally consolidated from a low stress level to states on the linear normal consolidation line in the v-lnp' space.

CHAPTER 7

CASM-c: A NEW CYCLIC BOUNDING SURFACE MODEL

7.1. INTRODUCTION

The essential features of the Cam-clay models and CASM are that on a primary loading large plastic strains occur, but on subsequent unload-reload cycles within the yield surface only purely elastic strains are produced. This is not suitable for modelling the behaviour of soil under cyclic loading because in reality, all unload-reload cycles result in the gradual accumulation of permanent strain and pore pressure (if the soil is undrained) and hysteresis takes place.

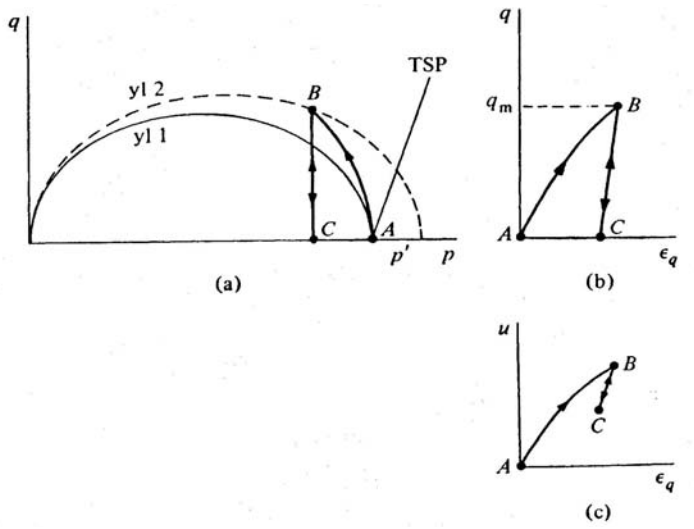

Figure 7.1. Response of clay to undrained cyclic loading according to conventional critical state models: (a) effective stress path, (b) stress:strain response and (c) pore pressure:strain response (Wood, 1990)

As an illustration, the response of soil to undrained cyclic loading, according to the conventional critical state models, is shown in Figure 7.1 (in page 97), whereas the observed typical response of real soil undergoing cyclic loading is shown in Figure 7.2.

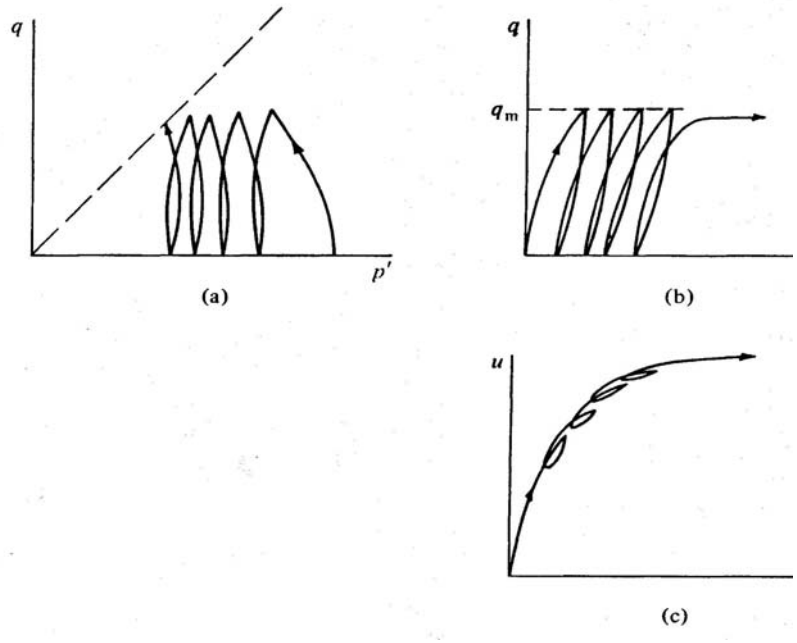

Figure 7.2. Typical response observed in undrained cyclic loading of clay: (a) effective stress path, (b) stress:strain response and (c) pore pressure:strain response (Wood, 1990)

Having models with cyclic loading prediction capability is very advantageous and essential for solving practical geotechnical problems for example, analysis of pavements or structures under earthquake, wind, snow or wave loading conditions. Various models such as the bounding surface model developed by Dafalias and Herrmann (1980), the 'Bubble' model by Al-Tabbaa (1987) and the three surface kinematic hardening (3SKH) model by Stallebrass (1990) can produce some of the essential features of soil under cyclic loading. The 'Bubble' and 3SKH models have been proven to model clay behaviour closely. Based on the bounding surface theory, McVay and Taesiri (1985) and Aboim and Roth (1982) proposed cyclic models which modelled the behaviour of sand closely.

In this chapter, the bounding surface model CASM-b which was developed in Chapter 6 is further extended. By having additional assumptions upon those in CASM-b for the calculations of the hardening modulus under different loading conditions, the new

model is able to produce some of the essential characteristics of soil under cyclic loading conditions. This new model is named CASM-c

Because it is developed from the original CASM and CASM-b models, all the superior features possessed by these models (described in previous chapters) are retained in CASM-c. These include the ability to predict the behaviour of clay and sand materials under both drained and undrained loading conditions. The ability to accurately predict the behaviour of heavily overconsolidated clay and sand remains a big advantage of this new unified cyclic model over existing models in the literature.

7.2. CASM-c, DESCRIPTION OF THE MODEL

7.2.1. Bounding surface, elastic parameters, plastic potential and mapping rule

All the assumptions about the bounding surface, elastic parameters, plastic potential and mapping rule presented in Chapter 6 for CASM-b are retained in CAM-c.

7.2.2. Hardening modulus

The assumptions made for calculating the hardening modulus are the new profound features of CASM-c. Loading is divided into three types, namely virgin loading, unloading and reloading. The first loading condition (virgin loading) is no different to that used in CASM-b. In a traditional elastic-plastic model, unloading and reloading are treated as one in terms of calculating the hardening modulus. However, in CASM-c they are considered as two different processes. This enables a gradual accumulation of permanent strain and/or pore pressure in unload-reload cycles and the hysteretic behaviour can be reproduced. The calculations of the hardening modulus are presented in the next three sections.

7.2.2.1. Hardening modulus for virgin loading

In a manner identical to that described in Chapter 6, the hardening modulus for the virgin (or first) loading is calculated based on the normal bounding surface plasticity theory. For completeness purposes, it is briefly presented here, see Chapter 6 for more detailed information.

$$H = H_j + \frac{h}{p'}\frac{(1-\gamma)^m}{\gamma} \tag{7.1}$$

where γ is a non-dimensional ratio between the current stress and the image stress and H_j is the hardening modulus calculated at the image stress point. They can be expressed as:

$$\frac{p'}{p'_j} = \frac{q}{q_j} = \frac{p'_o}{p'_{oj}} = \gamma \text{ with } 0 \le \gamma \le 1$$

$$H_j = \frac{3\nu}{(\lambda-\kappa)\ln r}\left(\frac{3+2M}{2q_j+3p'_j} - \frac{3-M}{3p'_j - q_j}\right)$$

It should be noted that all the stresses at the image stress point are denoted with a subscript *j* in the expressions above.

7.2.2.2. Hardening modulus for unloading

For unloading, the following expression for the hardening modulud used by McVay and Taesiri (1985) is adopted:

$$H = H_U \times \frac{1}{(1-\gamma)} \tag{7.2}$$

where γ is defined in 7.2.2.1 and H_U is a new unloading hardening parameter. Equation 7.2 ensures that:

$$\begin{cases} H = \infty & when \quad \gamma = 1 \\ H_U < H < \infty & when \quad 0 < \gamma < 1 \\ H = H_U & when \quad \gamma = 0 \end{cases}$$

The unloading behaviour can be summarised as follows:

- When the current stress point is on the bounding surface (γ=1), unloading starts, the behaviour is elastic and H=∞.
- As the stress point moves away from the bounding surface (0<γ<1), the soil becomes less stiff, the behaviour is elastic-plastic and H decreases.
- When the stress point is very far away from the bounding surface (γ reaches 0), H decreases toward its limit H_U.

7.2.2.3. Hardening modulus for reloading

For reloading, the hardening modulus is defined as:

$$H = H_j + H_R \times \left(\frac{1-\gamma}{\gamma}\right) \times \left(1+\varepsilon_q^p\right)^k \tag{7.3}$$

where again the definitions of γ and H_j are the same as in 7.2.2.1, ε_q^p is the plastic deviatoric strain, H_R is a new reloading hardening parameter and k is another new parameter which controls the rate at which shakedown occurs. We will see the effect each new parameter has on the performance of the model in section 7.3.1. Equation 7.3 ensures the following:

$$\begin{cases} H = \infty & when \quad \gamma = 0 \\ H_j < H < \infty & when \quad 0 < \gamma < 1 \\ H = H_j & when \quad \gamma = 1 \\ H > H_j + H_R\left(\frac{1-\gamma}{\gamma}\right) & when \quad k > 0 \\ H = H_j + H_R\left(\frac{1-\gamma}{\gamma}\right) & when \quad k = 0 \\ H < H_j + H_R\left(\frac{1-\gamma}{\gamma}\right) & when \quad k < 0 \end{cases}$$

The reloading process is the reverse of the unloading process and can be summarised as follows:

- When the stress point is very far away from the bounding surface ($\gamma \approx 0$), the behaviour is near elastic, $H=\infty$.
- As the stress point move toward the bounding surface ($0<\gamma<1$), the soil becomes less stiff, the behaviour is elastic-plastic and H decreases.
- When the stress point reaches the bounding surface ($\gamma=1$), the soil behaves exactly the same as the normal bounding surface model, $H=H_j$.

7.2.3. New parameters

There are three additional parameters introduced in CASM-c compared with the bounding surface model (CASM-b) in Chapter 6. They are H_U, H_R and k. The roles and units of each of the parameters are listed in Table 7.1 below:

Parameter	Role	Unit
H_U	controls unloading	$\left(1/_{stress}\right)$
H_R	controls reloading	$\left(1/_{stress}\right)$
k	controls the rate at which shakedown occurs	none

Table 7.1. New parameters introduced in CASM-c

The two parameters H_U and H_R are believed to be functions of the resilient hardening modulus ($H_{resilient}$) whose definition is shown in Figure 7.3.

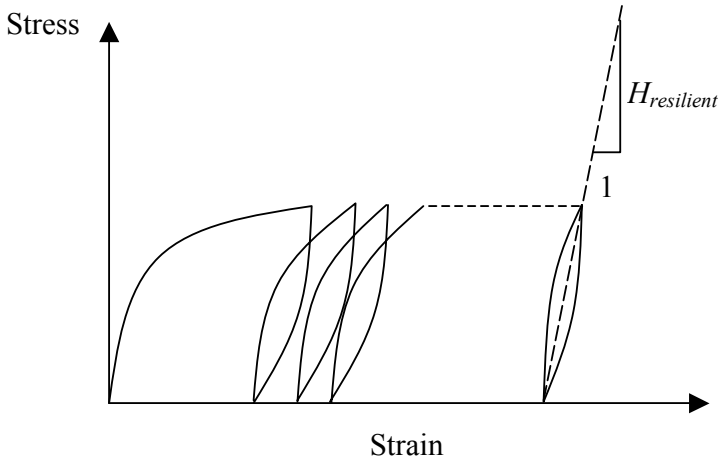

Figure 7.3. Typical stress-strain curve of soil under repeated loading

H_U and H_R control the slope of the stress-strain curve for unloading and reloading loading conditions respectively. The higher the values of these parameters, the stiffer the soil will be. In other words, the higher the values of H_U and H_R, the straighter the stress-strain curve will become. The effects of these parameters on the performance of the new model will be shown in sections 7.3.1 and 7.3.2 when parametric studies are carried out.

It is well known that shakedown is an intrinsic property of soil and is exhibited under repeated loading conditions. The basic assumption is that below a certain load (termed the 'shakedown load') the structure will eventually shakedown, i.e. the ultimate response will be purely elastic (reversible) or there is no more accumulation of plastic strain. If the applied load is higher than the shakedown load, the structure will fail in the sense that the structural response is always plastic (irreversible) however many times the load is applied. The new parameter k has the role of controlling the shakedown behaviour of the soil in this model.

It is believed that k is dependent upon a number of factors, they include the type of materials, the stress history as well as the current stress level of the soil. The manner of this parameter needs to be examined more carefully in future studies. Figure 7.4 shows the relationship between the permanent deformation (or strain level) and the number of cycles of loading for different values of k. The figure can be explained as follows:

- When $k>0$, the reloading hardening modulus (H) increases with the strain level. This means that the soil gets stiffer as the level of strain increases, shakedown behaviour occurs and the deformation gets to a flat maximum as the number of cycles increases.
- When $k=0$, H does not increase or decrease with the strain level, the soil does not shake down and deformation increases with the number of cycles.
- When $k<0$, H decreases with the strain level and the soil becomes softer as the strain level increases. As a result, the deformation increases with the number of cycles and the rate of increase grows with the strain.

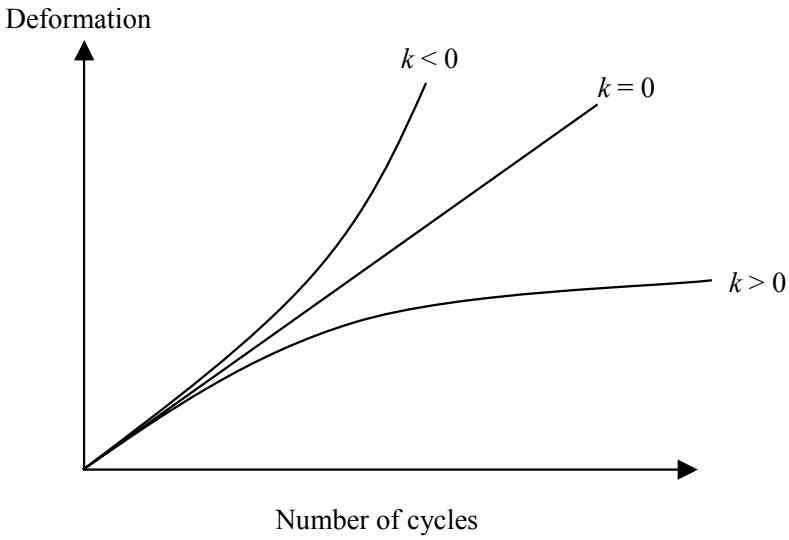

Figure 7.4. Effect of new parameter k on performance of CASM-c

7.2.4. Incorporation of CASM-c into CRISP

Again, CASM-c has been generalised into the three-dimensional stress space and then successfully implemented into CRISP. The procedures are similar to those described in Chapter 4. Similar to CASM-d (in Chapter 5) and CASM-b (in Chapter 6), the only part of the source code which needed to be modified was the calculation of the new hardening modulus where equations 7.1, 7.2 and 7.3 were used instead of equation 4.13. A new variable (flag variable) was also needed to distinguish between different loading conditions based on the state of the current stress point. In this study, the stress reversal convention was used to recognise a change in the loading direction.

7.3. APPLICATION OF CASM-c TO THE TRIAXIAL TEST

7.3.1. Effects of the three new parameters on the performance of CASM-c

To investigate the effect of the three new parameters (H_U, H_R and k) on the performance of the new model, a simple hypothetical drained cyclic triaxial test was analysed. The soil sample was assumed to be normally consolidated with an isotropic initial stress of

207 kPa (p'_i=p'_o=207 kPa). The cell pressure was kept constant at 207 kPa while a deviatoric stress of 200 kPa was loaded and then unloaded back to 0 kPa (one way cyclic loading). Four load cycles were applied.

The following soil parameters relevant to Weald clay were used:

M=0.9, λ=0.093, κ=0.025, μ=0.3, Γ=2.06, n=4.5, r=2.714

Two out of the three new parameters were kept constant in each of the following three sections. The third parameter was varied so that its effect on the model's performance could be seen. The ranges over which the new parameters vary were chosen so that they would clearly affect the performance of the model for this particular soil. Sections 7.3.1.1-7.3.1.3 show the results of this parametric analysis.

7.3.1.1. Effect of H_U (H_R=0.02, k=20)

Firstly, Figures 7.5-7.8 show the effect H_U has on the performance of the new model. This parameter is only used when the soil is being unloaded. The smaller the value of H_U, the more strain (both deviatoric and volumetric) the model will recover upon unloading. In other words, the bigger the value of H_U, the more permanent strains the model will produce. This can be explained as follows: a smaller value of H_U leads to the soil being softer during unloading and hence, larger amounts of strains are recovered.

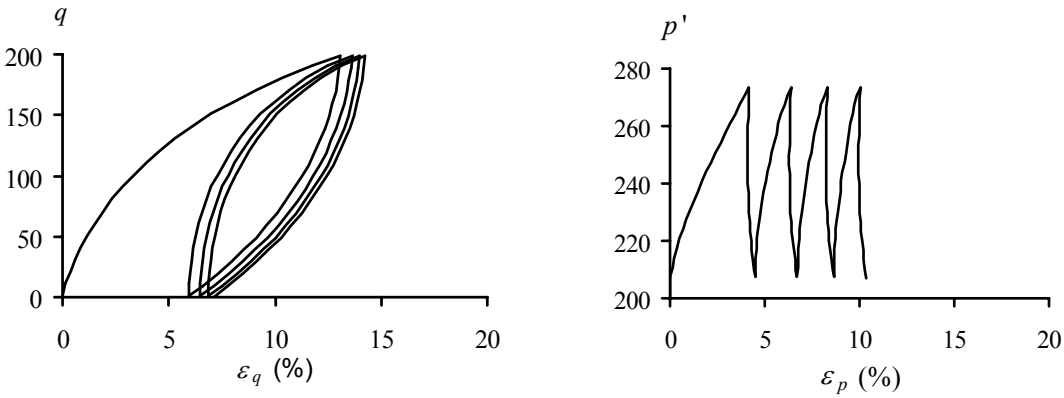

Figure 7.5. H_U=0.1

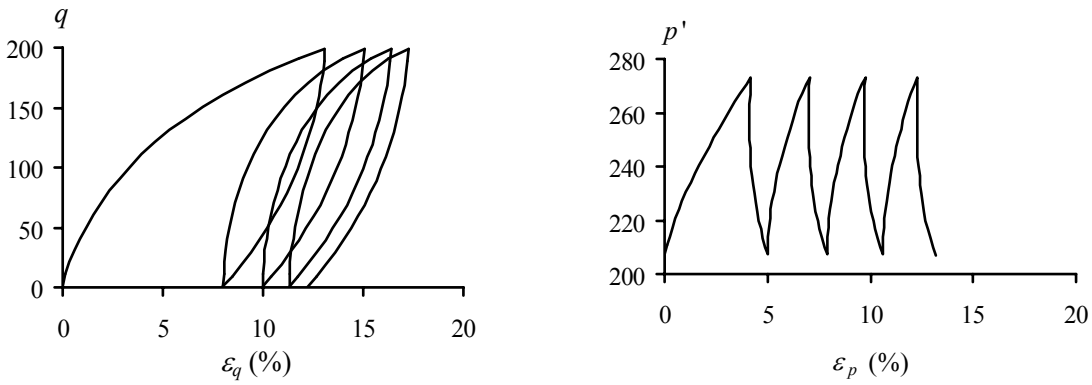

Figure 7.6. H_U=0.15

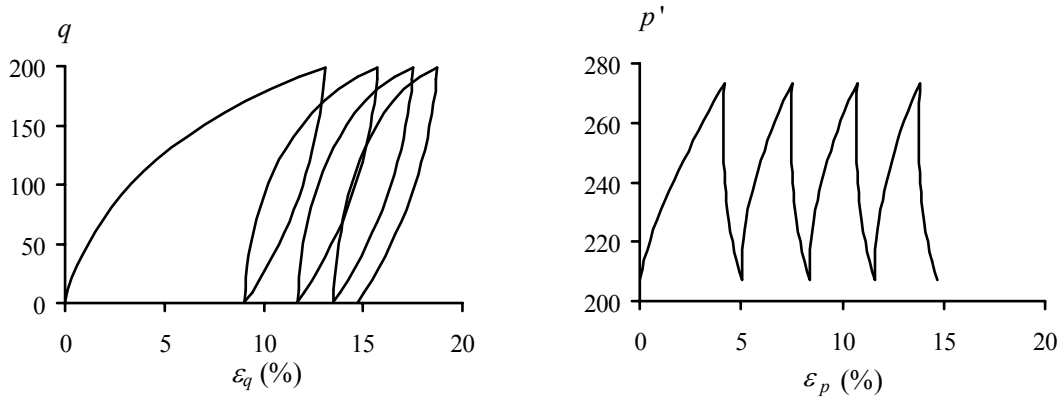

Figure 7.7. H_U=0.2

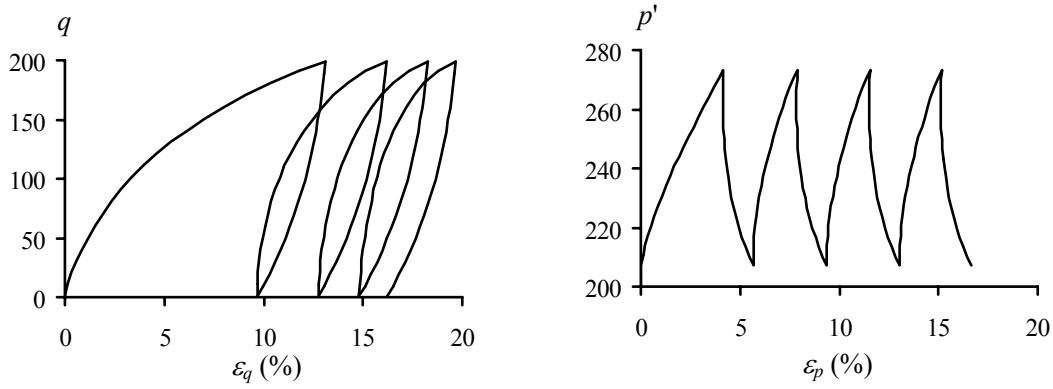

Figure 7.8. H_U=0.25

7.3.1.2. Effect of H_R (H_U=0.15, k=20)

Secondly, the effect of the new parameter H_R is investigated. Similar to H_U in the above section, H_R has the same effect but only when the soil is being reloaded. It can be seen in Figures 7.9-7.12 that permanent strains (both deviatoric and volumetric) increase as the value of H_R decreases. This is because a smaller value of H_R causes the soil to be softer during reloading and strains increase as a result.

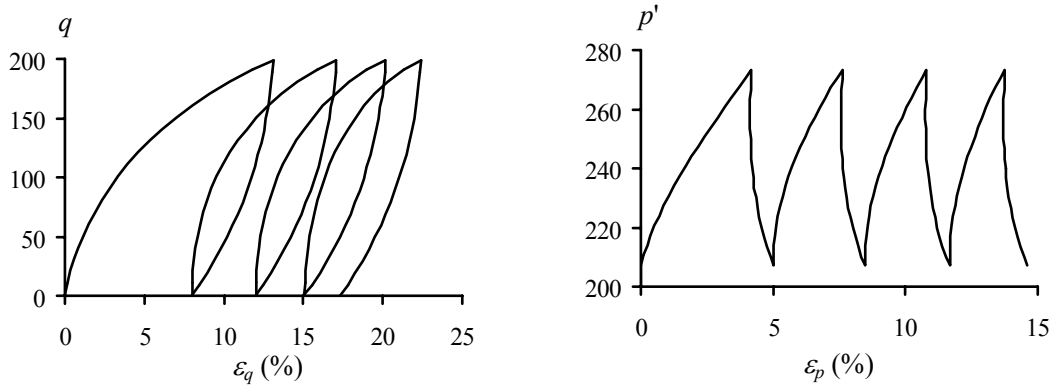

Figure 7.9. H_R=0.005

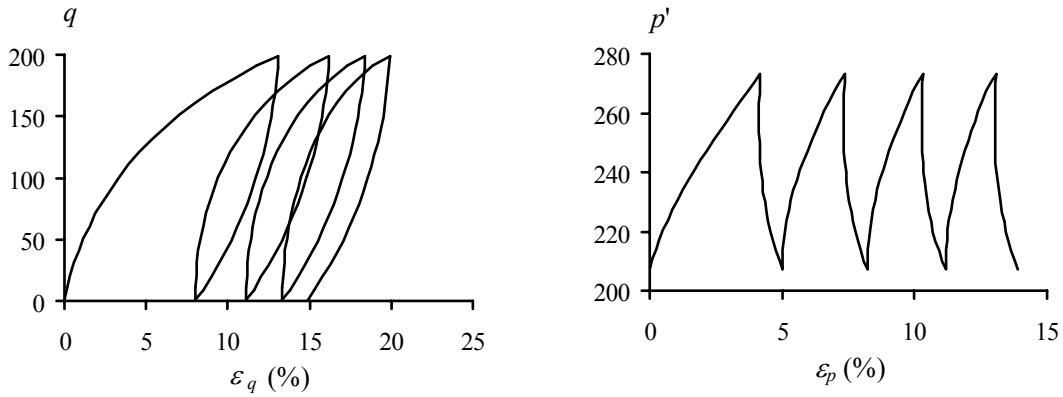

Figure 7.10. H_R=0.01

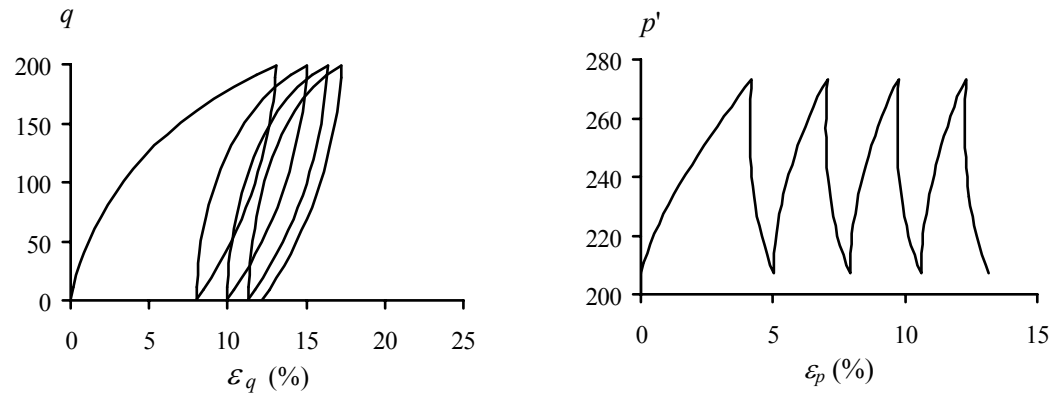

Figure 7.11. H_R=0.02

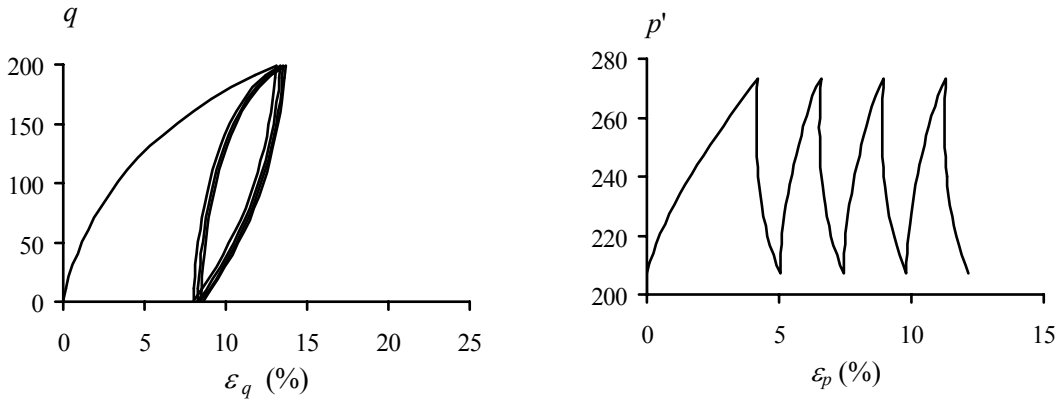

Figure 7.12. H_R=0.05

7.3.1.3. Effect of k (H_U=0.15, H_R=0.02)

Finally, k is the parameter that controls the rate at which shakedown behaviour of the soil occurs. Figures 7.13-7.15 show the results where positive values of k were assumed. It can be seen that a bigger value of k will make the soil shakedown faster. This can be easily explained by looking at equation 7.3: a bigger value of k will make the soil become harder during reloading. Also, the soil becomes harder faster if the plastic deviatoric strain is bigger. As a result of all of these, less strain and shakedown behaviour occurs.

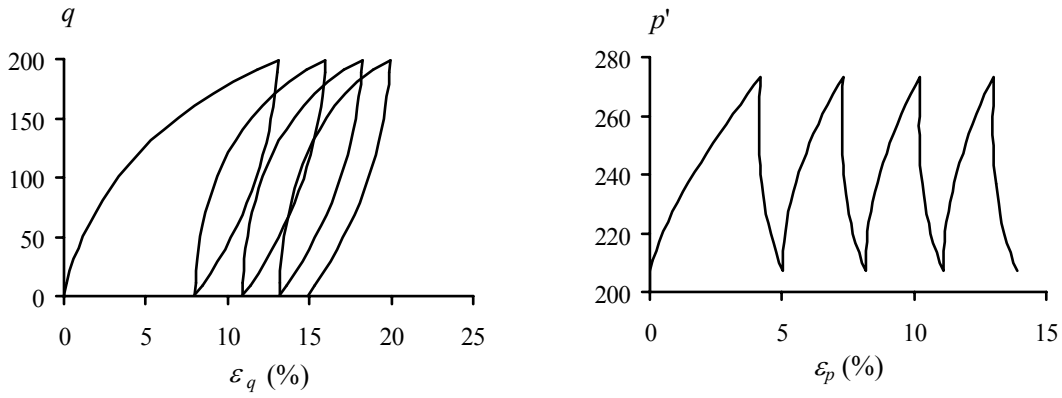

Figure 7.13. *k*=15

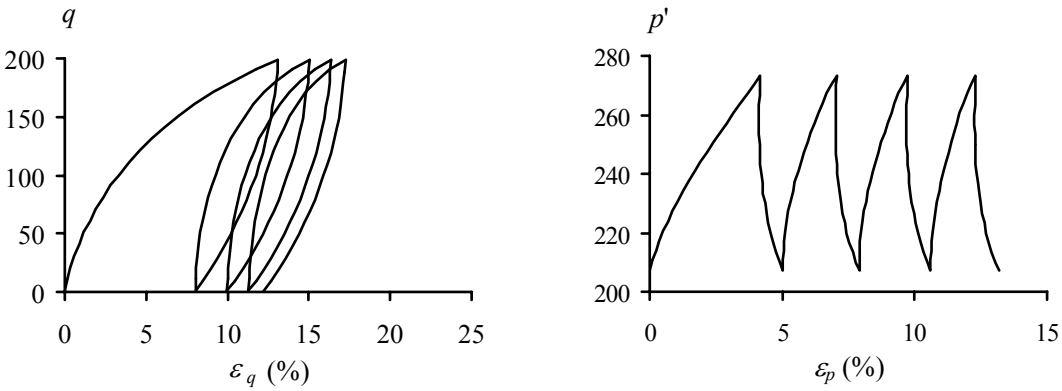

Figure 7.14. *k*=20

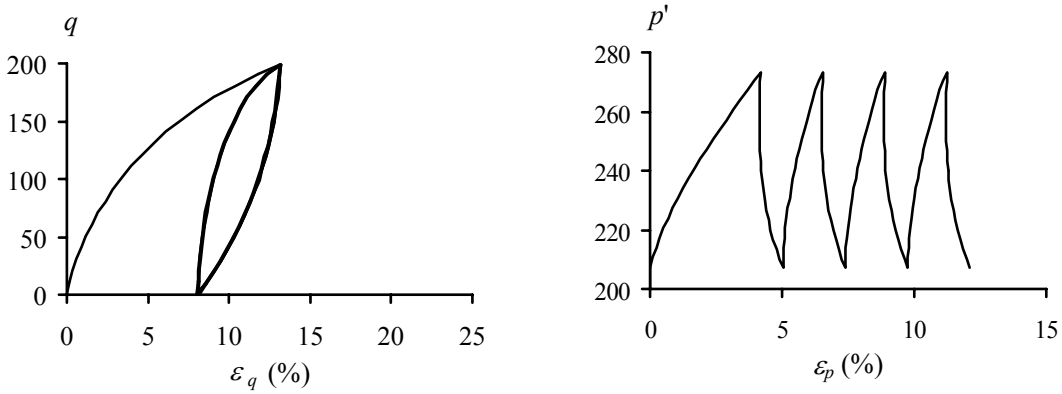

Figure 7.15. *k*=30

Figure 7.16 shows the results when k=-10. As expected, when a negative value of k is used the permanent strains accumulated in each cycle increase with the number of cycles. This behaviour often occurs when the applied load exceeds the 'shakedown load' of the material.

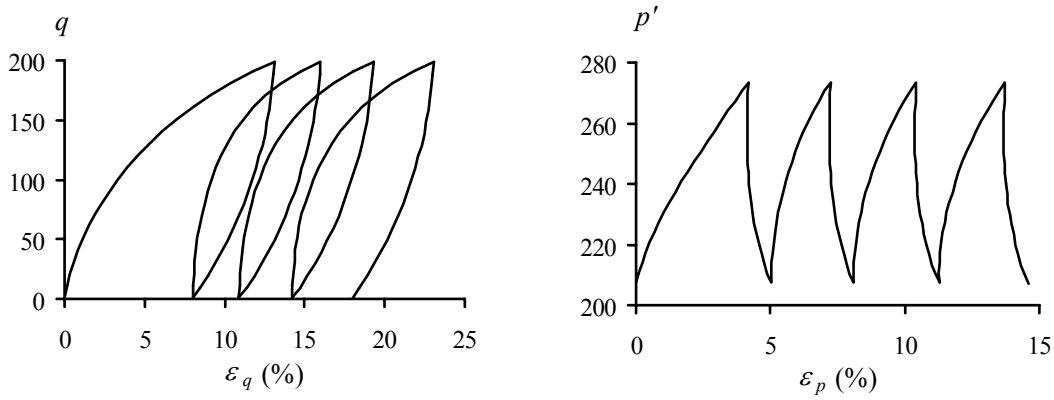

Figure 7.16. k=-10

It should be remembered that k depends upon many factors, its value is expected to be very much different from one soil to another as well as from one analysis to another. A more comprehensive investigation of this parameter is needed in future studies.

7.3.2. Comparison with experimental data

After examining the behaviour of the new model, the next logical step is to validate it by comparing the finite element results with some experimental data available in the literature. And it is carried out in this section.

Three sets of data are chosen to validate the model:

- Firstly, results from drained cyclic tests on Speswhite kaolin performed by Al Tabbaa (1987) are used.
- The second set of data is reported by Li and Meissner (2002) on testing of an undrained clay.
- Finally, tests conducted by Tasuoka (1972) and Tasuoka and Ishihara (1974) on loose drained Fuji river sand are compared with the results predicted by CASM-c.

7.3.2.1. Drained clay under one way cyclic loading

Figure 7.17a shows the results of cyclic tests on normally consolidated Speswhite kaolin conducted by Al Tabbaa (1987) where the stress ratio (η=q/p') is plotted against the deviatoric (ε_q) and volumetric (ε_p) strains. The soil was isotropically consolidated to p'=300 kPa and then loaded cyclically between a stress ratio (η) of 0 and 0.34 at a constant cell pressure. The critical state parameters for this soil were taken from Hau (2003). The value of κ for kaolin reported in the literature varies from one author to another, a typical value of κ=0.03 was chosen by the author in this study. Other parameters were also chosen by the author:

M=0.86, λ=0.19, κ=0.03, μ=0.3, Γ=3.056, n=2.0, r=2.718, h=5.0, m=1.0, H_U=0.15, H_R=0.5, k=30

The simulation of this test by CASM-c is shown in Figure 7.17b. It can be seen that CASM-c overestimates the deviatoric strain and yet underestimates the volumetric strain in this case. This is due to the flow rule used in CASM. It means that for this particular clay, the Rowe's stress-dilatancy relation is not applicable. Instead, a bigger ratio of incremental plastic volumetric strain to incremental plastic deviatoric strain $\left(\partial\varepsilon_p^p / \partial\varepsilon_q^p\right)$ should be used. However, it shows that the overall behaviour of the soil under cyclic loading can be reproduced by CASM-c.

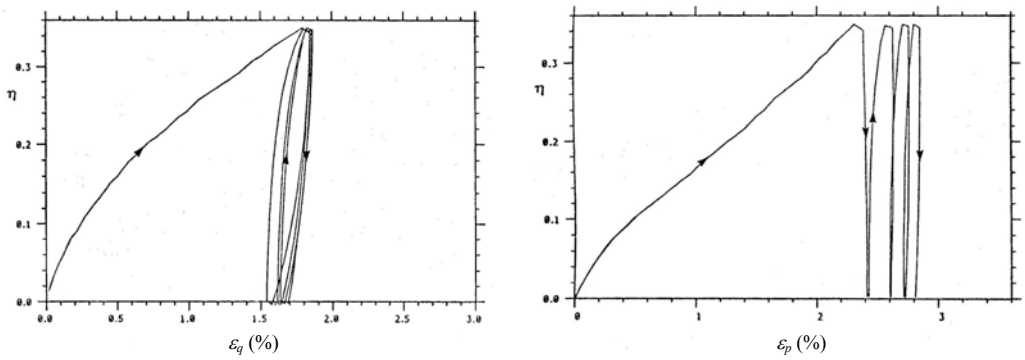

(a) Data (Al Tabbaa, 1987)

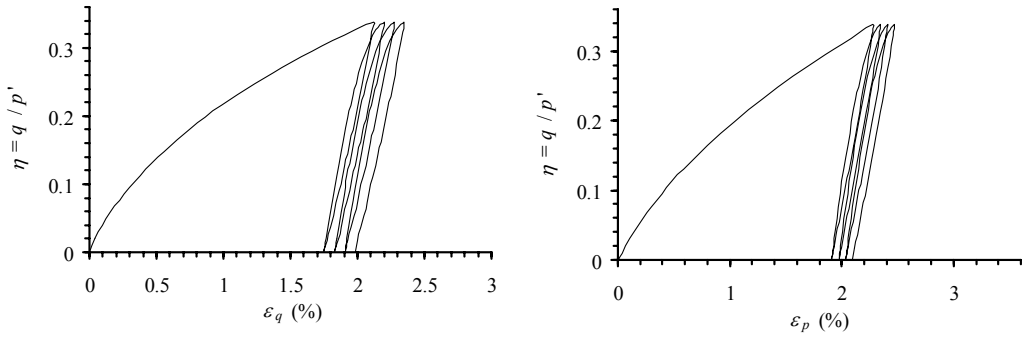

(b) Simulation by CASM-c

Figure 7.17. Drained one way cyclic loading of Speswhite kaolin

7.3.2.2. Undrained clay under one and two way cyclic loading

CASM-c was also used to simulate the test results of a commercially available clay. The tests were performed by Li and Meissner (2002). They reported the results of triaxial tests for soil samples under cyclic loading conditions which were isotropically reconsolidated with *OCR*=1 and 5.1. All tests were stress-controlled. Both one way and two way cyclic loading tests were carried out. The initial conditions can be found in the captions of Figures 7.18-7.21. The critical state parameters for this clay were also reported by Li and Meissner (2002), other parameters for the model were typical values chosen by the author. All the parameters are listed below:

M=0.772, λ=0.173, κ=0.034, μ=0.3, Γ=2.06, n=2.0, r=2.718, h=5.0, m=1.0, H_U=0.3, H_R=0.1, k varies

It should be noted that k is dependent upon many factors including the stress history. That is why the value of k varies from one analysis to another. For each of the analyses presented in this section, the value of the parameter k will be shown in the figure caption. This also applies in section 7.3.2.2.

Figures 7.18 and 7.19 show the experimental data (Figures 7.18a and 7.19a) and simulation results (Figures 7.18b and 7.19b) for the case of one way cyclic loading with *OCR*=1 and 5.1 respectively. In these figures, the excess pore water pressure (Δu) and deviatoric stress (q) are plotted against the number of cycles and deviatoric strain (ε_q)

respectively. These figures show that CASM-c can quantitatively predict the behaviour of undrained clay subjected to one way cyclic loading conditions.

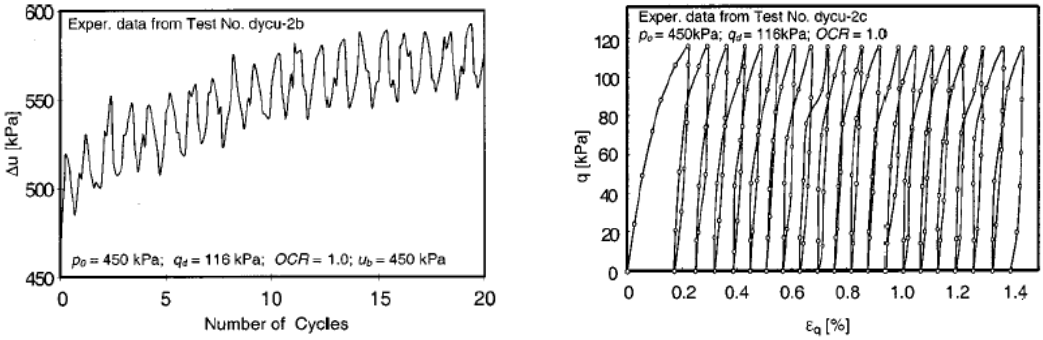

(a) Data (Li and Meissner, 2002)

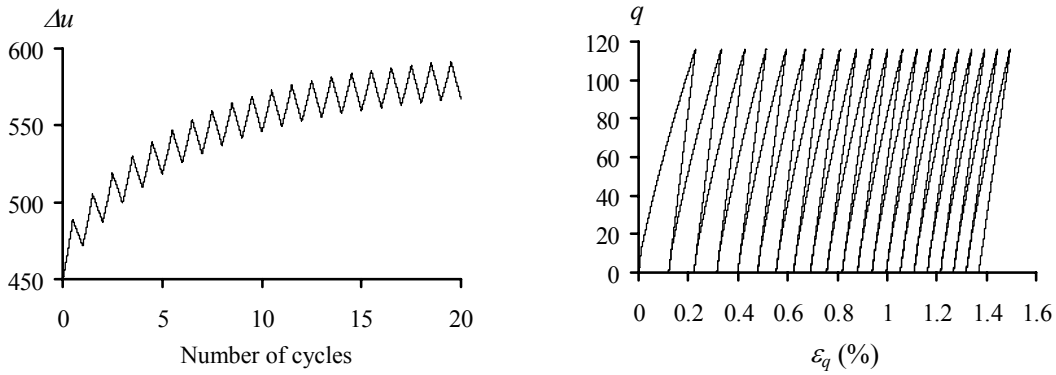

(b) Simulation by CASM-c

Figure 7.18. Undrained one way cyclic loading of normally consolidated clay, k=10

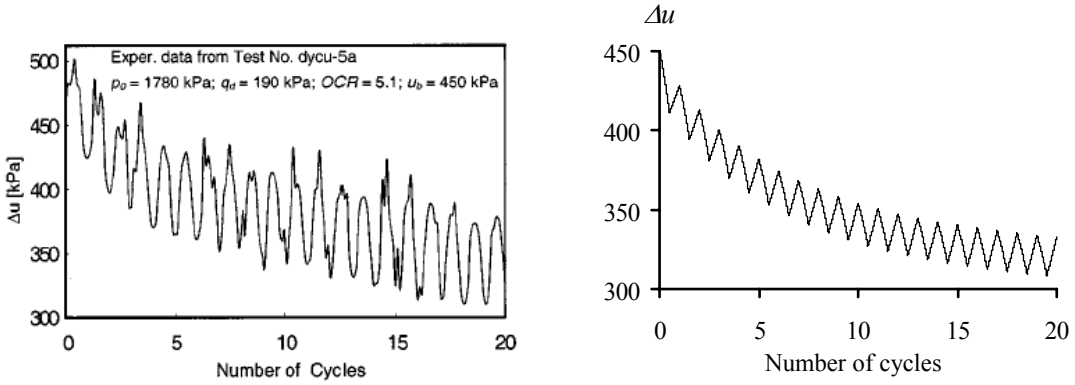

(a) Data (Li and Meissner, 2002) (b) Simulation by CASM-c

Figure 7.19. Undrained one way cyclic loading of overconsolidated clay, k=12

Figures 7.20 and 7.21 show the experimental data (Figures 7.20a and 7.21a) and the simulation results (Figures 7.20b and 7.21b) for the case of two way cyclic loading with *OCR*=1 and 5.1 respectively. Again it can be seen that CASM-c produces satisfactory results when compared with observational data.

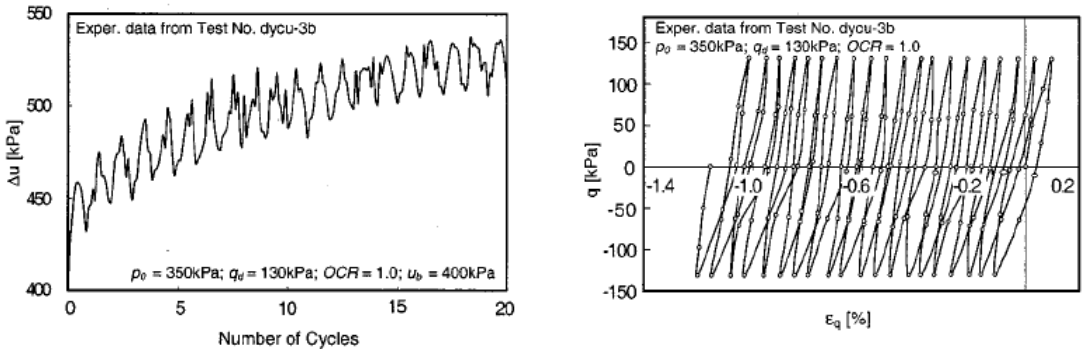

(a) Data (Li and Meissner, 2002)

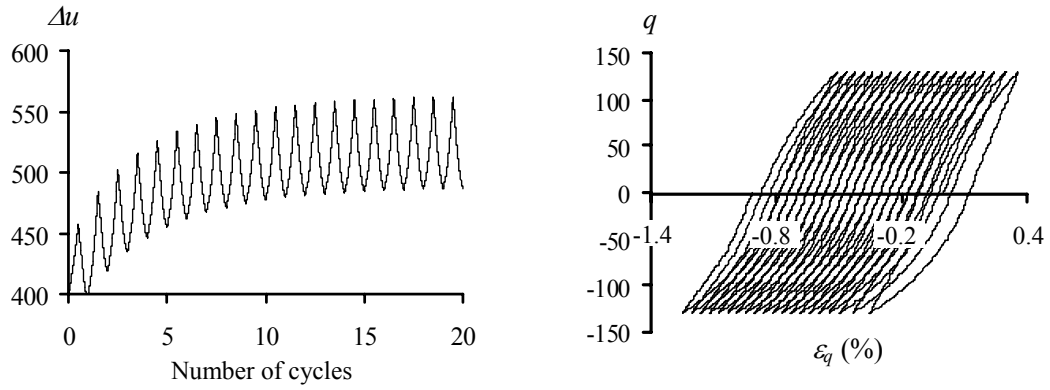

(b) Simulation by CASM-c

Figure 7.20. Undrained two way cyclic loading of normally consolidated clay, *k*=15

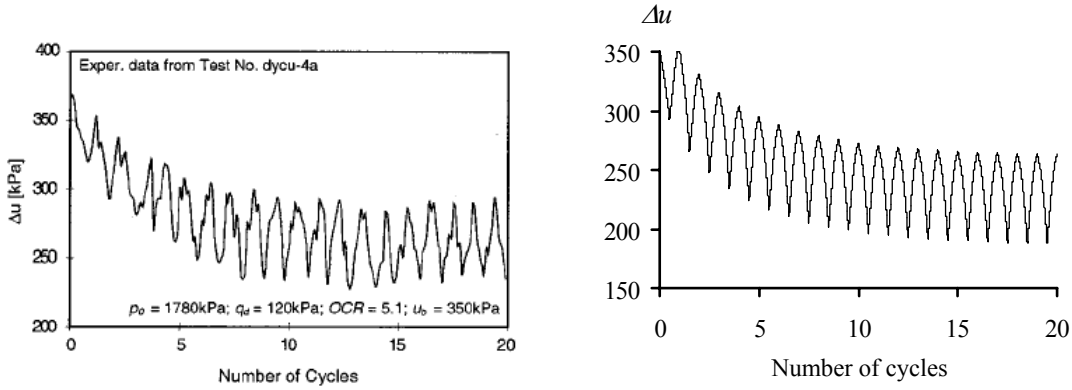

(a) Data (Li and Meissner, 2002) (b) Simulation by CASM-c

Figure 7.21. Undrained two way cyclic loading of overconsolidated clay, k=18

7.3.2.3. Drained sand under one and two way cyclic loading

In this section, CASM-c is used to simulate the triaxial tests on Fuji river sand conducted by Tasuoka (1972) and Tasuoka and Ishihara (1974). This set of classical tests has been used by many researchers (e.g. Ishihara et. al., 1975; Wood, 1982; Bardet, 1986) when making a research review or validating their constitutive models. Only results of tests on loose drained sand were used in this study.

The material tested was the sand secured from the Fuji river bed. All the tests were done by changing the axial load while keeping the cell pressure constant throughout. The initial conditions are shown in the captions of Figures 7.22 and 7.23. The critical state parameters for this sand were taken from Bardet (1986), other parameters for the model were typical values chosen by the author. All the parameters are listed below:

M=1.5, λ=0.12, κ=0.01, μ=0.3, Γ=1.467, n=4.5, r=10.0, h=5.0, m=1.0, H_U=0.4, H_R=0.3, k varies

Figure 7.22 shows the experimental data (Figure 7.22a) and simulation results (Figure 7.22b) of drained one way cyclic loading of loose Fuji river sand where volumetric and shear strains are plotted against the stress ratio (η=q/p'). The volumetric and shear strains in Figure 7.22 are defined as v=(ε_a+2ε_r) and ε=(ε_a–ε_r) respectively (ε_a and ε_r denote the axial and radial components of strain developed in the triaxial sample).

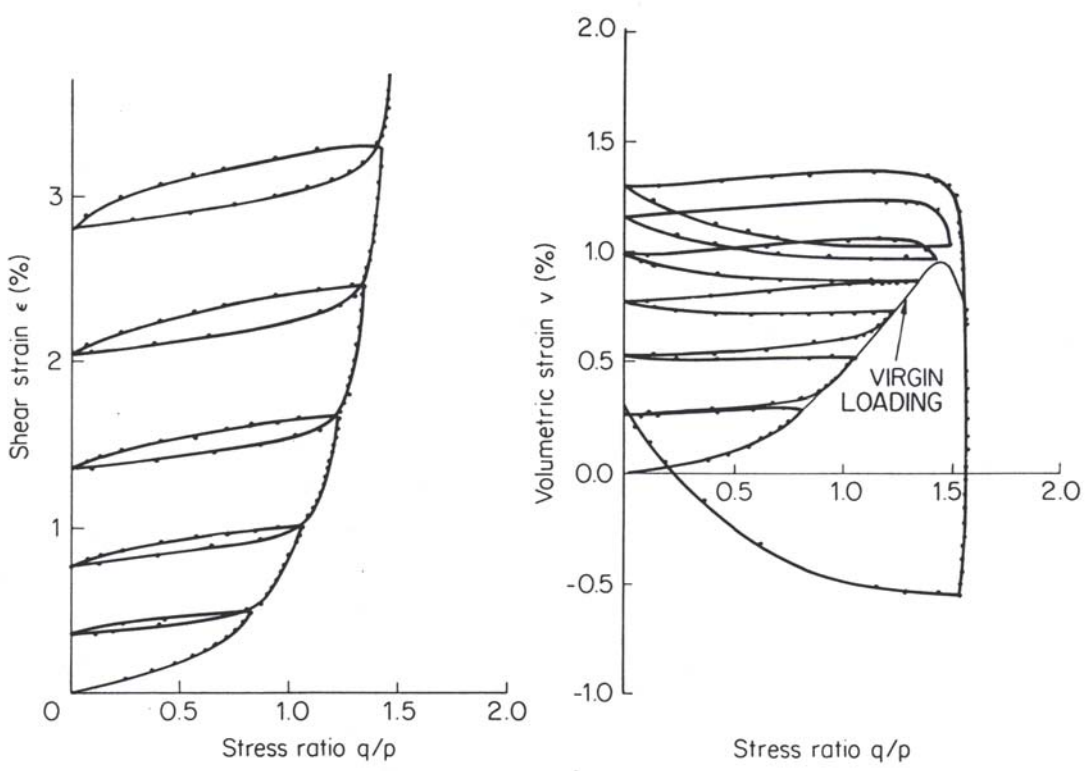

(a) Data (Wood, 1982; after Tasuoka, 1972)

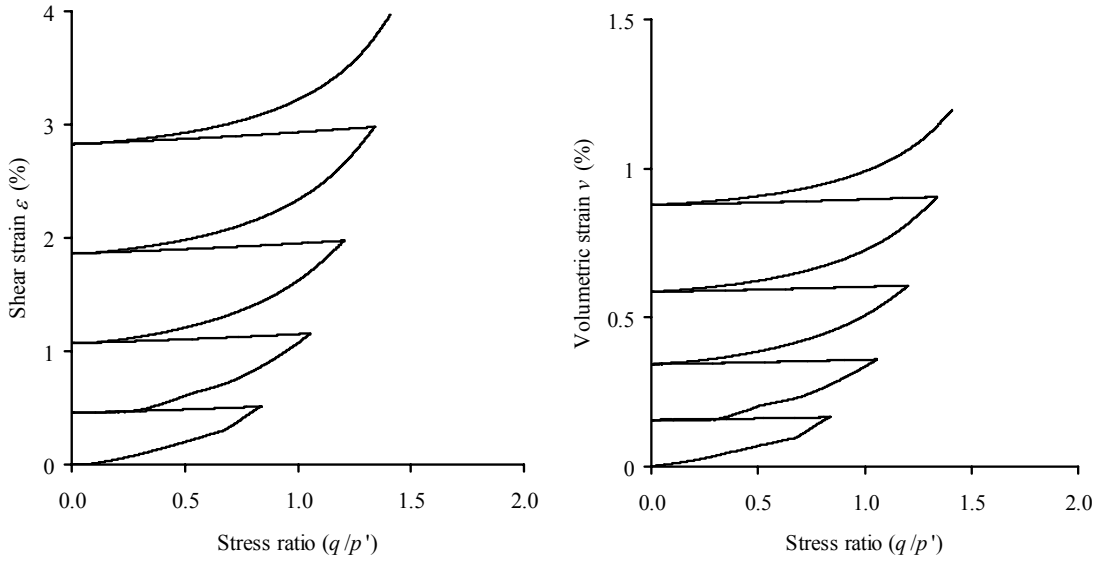

(b) Simulation by CASM-c

Figure 7.22. Drained one way cyclic loading of loose Fuji river sand, k=10 (e_o=0.723, σ'_r=0.5 kg/cm^2)

Figure 7.23 shows the experimental data (Figure 7.23a) and simulation results (Figure 7.23b) of the drained two way cyclic loading of loose Fuji river sand. Again, volumetric and deviatoric strains are plotted against the stress ratio (η=q/p'). The volumetric strain (ε_v) in this case is the same as v in Figure 7.22, while the deviatoric strain is defined as ε_q=2(ε_a−ε_r)/3. Figures 7.22 and 7.23 show that CASM-c can also satisfactorily predict the behaviour of sand under cyclic loading conditions.

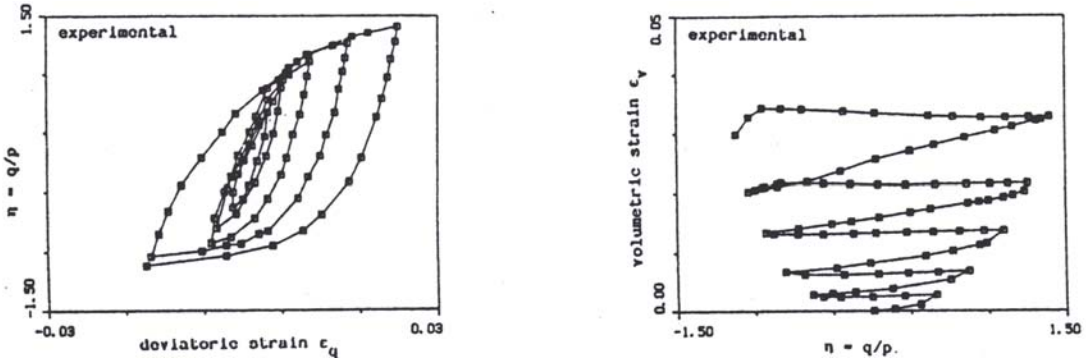

(a) Data (Bardet, 1986; after Tasuoka and Ishihara, 1974)

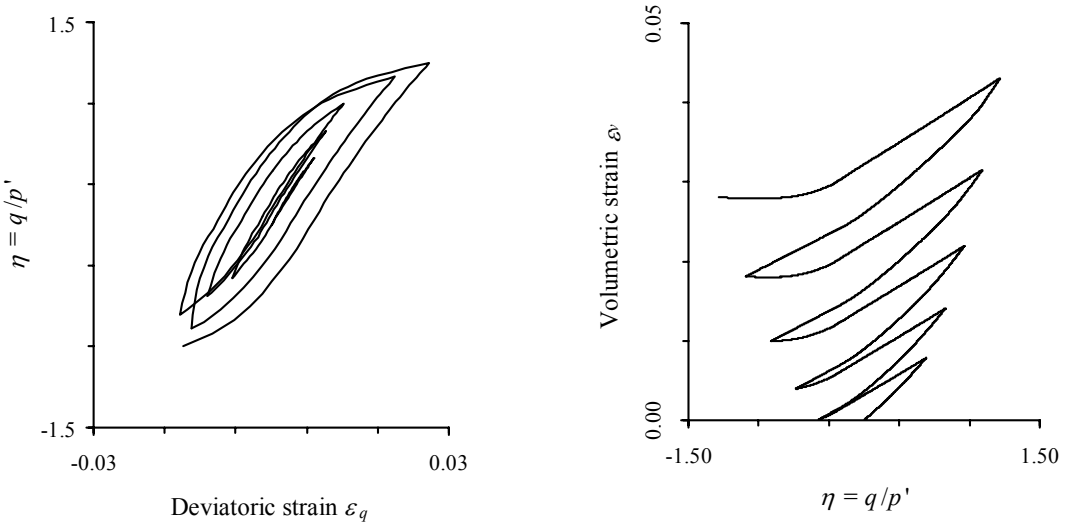

(b) Simulation by CASM-c

Figure 7.23. Drained two way cyclic loading of loose Fuji river sand, k=15 (e_o=0.74, σ'_r=2.0 kg/cm^2)

7.4. SUMMARY

In summary, an extension of the bounding surface model presented in Chapter 6 has been described in this chapter. The important new feature of this new model, called CASM-c, is its ability to model the behaviour of soil under cyclic loading conditions. For static loading conditions, CASM-c gives the same results as CASM-b. There are three new parameters (compared to CASM-b) introduced in the new model, they are used to control the unloading behaviour, the reloading behaviour and the shakedown behaviour of the soil. A parametric study of the three new parameters has been carried out. It has been found that CASM-c was very flexible in predicting soil behaviour.

The new model has been generalised into the three-dimensional stress space and then successfully implemented into CRISP. Three sets of cyclic triaxial tests have been used to compare the simulation results predicted by CASM-c. The tests have been chosen so that CASM-c could be validated and its performance could be assessed by a variety of materials under different cyclic loading conditions. In the first test, it has been found that CASM-c overestimated the deviatoric strain and underestimated the volumetric strain. This is believed to be caused by the flow rule used. A different stress-dilatancy relation for that particular clay would be more appropriate. In the other two tests, it has been found that CASM-c could satisfactorily predict the overall behaviour of both clay and sand under a variety of cyclic loading conditions.

CHAPTER 8

APPLICATIONS

8.1. INTRODUCTION

After describing and validating CASM and its extensions in Chapters 3, 4, 5 ,6 and 7, some of their applications are presented in this chapter. However, only CASM, CASM-b and CASM-c are used in the analyses. CASM-d is not used in this chapter because it is the author's opinion that this model needs further modifications (i.e. the conditions for the critical state to be reached) before it can be used to solve practical problems.

A number of typical geotechnical engineering problems are examined. The first problem is the analysis of a pressuremeter test in undrained clay where the effects of both the stress history and the pressuremeter's two-dimensional geometry are investigated. The behaviour of surface rigid strip and circular footings in undrained clay and drained sand are simulated next. After the footings, analyses on behaviour of horizontal strip anchors in undrained clay and drained sand are presented. The effect of the stress history on the behaviour of both the footings and anchors is closely examined. Finally, CASM-c is used to model the behaviour of a hypothetical pavement. The pavement consists of a layer of drained sand on top of a layer of drained clay. This is used to illustrate the ability of CASM-c to predict the behaviour of both clay and sand under cyclic loading conditions. All the results are presented as design charts whenever possible to enable the direct hand calculation of the soil's bearing capacity in these problems.

In order to achieve equilibrium, CRISP requires that all the free surfaces in the mesh are applied with surcharges which are equal to the isotropic initial stress (p'_i). This condition was satisfied for all the analyses in this thesis.

Some assumptions have been made in this chapter. The soils used are assumed to be homogeneous, isotropic and weightless (γ=0). The overconsolidation ratio (OCR) in this thesis is defined in terms of the mean effective stresses, i.e. if the soil is isotropically normally consolidated to a mean effective stress of $p'=p'_o$ and then isotropically unloaded and allowed to swell to $p'=p'_i$, the OCR is defined as the ratio of these two mean effective stresses:

$$OCR = \frac{p'_o}{p'_i} \tag{8.1}$$

It should be reminded that this is not the conventional definition of the overconsolidation ratio ($OCR_{\text{conventional}}$) which is defined as the maximum previous vertical effective stress divided by the current vertical effective stress.

To start a simulation with an overconsolidated sample of clay, CRISP only requires the input of an initial isotropic stress (p'_i) and a preconsolidation pressure (p'_o). Hence, an initial specific volume (v_o) was assumed for the clay, after that p'_i and p'_o were calculated from equation 8.1 together with the following expression (which can be easily obtained using the critical state soil mechanics theory):

$$v_o = \Gamma - \kappa \ln p'_i - (\lambda - \kappa) \ln\left(\frac{p'_o}{r}\right) \tag{8.2}$$

A similar procedure was used to obtain the initial stresses of a sample of sand with an initial state parameter ξ_o. But in this case, p'_i and p'_o are linked with ξ_o by the following expressions (this can also be easily obtained using critical state soil mechanics):

$$p'_i = e^{\left[\ln\left(\frac{\Gamma - v_o}{\lambda}\right) + \frac{\xi_o}{\lambda}\right]} \tag{8.3}$$

$$p'_o = e^{\left[\frac{\Gamma + (\lambda - \kappa)\ln r - v_o - \kappa \ln p'_i}{\lambda - \kappa}\right]} \tag{8.4}$$

For analyses involving undrained clays, an important quantity which is assumed to be constant is the theoretical undrained shear strength and it is named S_u in this thesis. This quantity is often used to normalise with the bearing capacity so that the effect of the stress history on the behaviour of the clays can be seen. The calculation of S_u using the soil's parameters and initial conditions is presented next in this section.

A soil with a specific volume v will end on the critical state line at a mean effective stress p'_f and deviatoric stress q_f when tested under undrained triaxial compression. From the Mohr circle of effective stresses at failure, S_u is calculated as:

$$S_u = \frac{q_f}{2} = \frac{Mp'_f}{2} = \frac{M}{2}\exp\left(\frac{\Gamma - v}{\lambda}\right) \tag{8.5}$$

Under triaxial loading conditions, by calculating v as a function of p'_o and OCR, the theoretical undrained shear strength of the soil (S_u) can be linked to the consolidation history by the following expression:

$$S_u = \frac{M}{2}\exp\left[\frac{(\Gamma - N)}{\lambda} + \ln(p'_o) - \left(\frac{\kappa}{\lambda}\right)\ln(OCR)\right] \tag{8.6}$$

Again, the Tangent Stiffness Technique is used as the non-linear solution scheme throughout Chapter 8. The number of increments for each analysis in this chapter varies depending on the problems. For each problem, a sensitivity study of the number of increments was carried out. After deciding the size and the density of the finite element mesh, a small number of increments was chosen to simulate the problem, the number of increments was then increased until stable results were obtained.

For simplicity, only two soils were used in all the analyses presented in this chapter. They are London clay and Ticino sand. The critical state constants for these materials were taken from Yu (1998) and Been and Jefferies (1985) respectively. Other model constants were chosen by the author and they are shown in Table 8.1.

	M	λ	κ	μ	Γ	n	r	h	m	H_U	H_R	k
London clay	0.89	0.161	0.062	0.3	2.759	2.0	2.718	5.0	1, 2	0.15	0.05	5.0
Ticino sand	1.3	0.04	0.01	0.3	1.986	2.0	4.0	30.0	3.0	0.5	0.1	20.0

Table 8.1. Model constants for soils used in Chapter 8

8.2. ANALYSES OF THE PRESSUREMETER TEST USING CASM

In this section, simulations of the pressuremeter test (see Figure 8.1) are carried out using the finite element method. Two problems are analysed. The first one investigates the effect of the stress history on the undrained shear strength of London clay assuming that the pressuremeter has a length to diameter ratio (L/D) of infinity. Two methods of interpretation are used to obtain the undrained shear strength. The second problem looks at the two-dimensional geometry effects on self-boring pressuremeter tests in undrained clay. Both CASM and the modified Cam-clay model are employed in this problem.

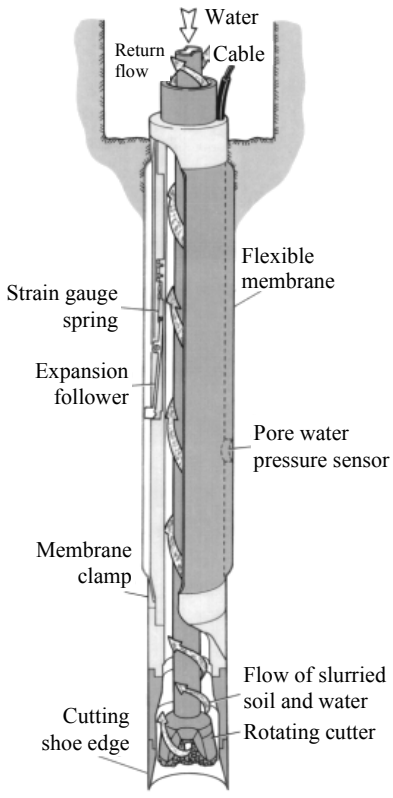

Figure 8.1. Self-boring pressuremeter

8.2.1. OCR effect in pressuremeter test

8.2.1.1. Introduction to the problem

Since their development, self-boring pressuremeters have gained wide acceptance as a valuable site investigation tool (Wroth, 1984; Mair and Wood, 1987; Clarke, 1995; Yu, 2000). The ability of the self-boring pressuremeter to be inserted into the soil with only minor disturbance makes it a very useful in-situ testing device. Once inserted into the soil, the cylindrical membrane of the pressuremeter is inflated and the pressure/displacement response is measured. In order to derive the soil properties, the measured pressure-displacement response of the soil has to be analysed.

Gibson and Anderson (1961) were able to derive the following simple equation for determining the undrained shear strength:

$$\psi = \psi_{\lim} + S_u \ln\left(\frac{\Delta V}{V}\right) \tag{8.7}$$

where ψ is the pressuremeter pressure, $\psi_{\lim}$ is the pressuremeter limit pressure, S_u is the undrained shear strength of the clay and $\left(\Delta V / V\right)$ is the volumetric strain which for small strains is equal to two times the cavity strain (ε).

From this expression, the plastic part of the pressuremeter loading curve is a straight line when the test results are plotted in a log scale as the total cavity pressure ψ against the volumetric strain $\left(\Delta V / V\right)$ (see Figure 8.2). Their cavity expansion solution shows that the slope of this straight line is equal to the undrained shear strength of the soil.

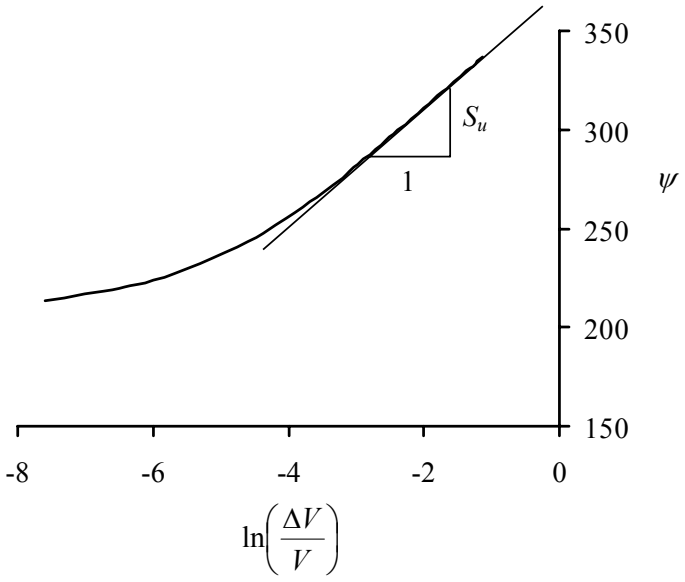

Figure 8.2. Pressuremeter loading curve in a perfectly plastic Tresca soil

Using cavity expansion theory, Houlsby and Withers (1988) developed a theoretical interpretation method for deriving soil properties from a cone pressuremeter test in undrained clays. For the case of a cylindrical cavity, the unloading pressure-displacement curve is defined as:

$$\psi = \psi_{\lim} - 2S_u\left[1 + \ln\left[(\varepsilon)_{\max} - \varepsilon\right] - \ln\left(\frac{S_u}{G}\right)\right] \tag{8.8}$$

where ψ is the pressuremeter pressure, $\psi_{\lim}$ is the expansion limit pressure, ε is the cavity strain, $(\varepsilon)_{\max}$ is the maximum cavity strain at the start of the unloading phase, S_u is the undrained shear strength of the soil and G is the shear modulus.

The large strain unloading solution of Houlsby and Withers (1988) defined by equation 8.8 is summarised in Figure 8.3. This shows that the plastic unloading slope in the plot of ψ against $-\ln[(\varepsilon)_{\max}-\varepsilon]$ is controlled by the soil strength. The slope of the pressuremeter unloading curve in such a plot is in fact twice the undrained shear strength of the soil (S_u). From this figure, it is also possible to estimate the shear modulus and the initial horizontal stress.

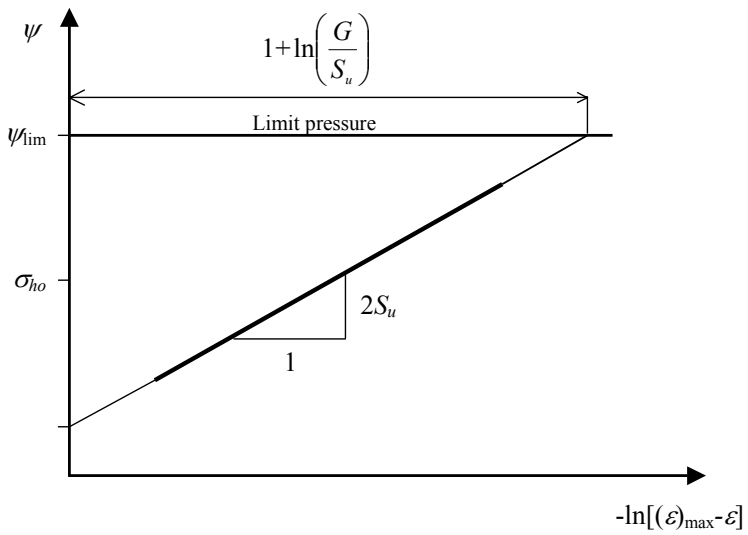

Figure 8.3. Graphical method using unloading curve (Houlsby and Withers, 1988)

CASM was used to analyse the pressuremeter test in undrained London clay with different initial state conditions. Both methods mentioned above were used to obtained the undrained shear strength of the clay.

The finite element mesh used for the pressuremeter analysis is shown in Figure 8.4. Fifteen-noded cubic strain triangle elements were used. In the analyses, a finite outer radius was set to be 100 times the radius of the cavity. A sensitivity study suggested that this outer radius was sufficiently large for simulating the behaviour of a cavity expansion in an infinite clay soil for the soil constants used in the calculations. In the next sections, finite element analyses of the pressuremeter test using both loading and unloading methods mentioned above are presented.

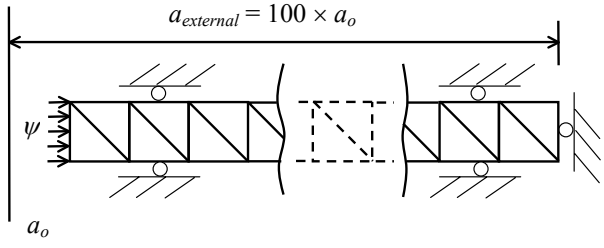

Figure 8.4. Finite element mesh for pressuremeter analysis

8.2.1.2. Pressuremeter analysis using Gibson and Anderson's method

Analyses of the pressuremeter test were carried out to find the undrained shear strength of London clay with different consolidation histories using Gibson and Anderson's method. All the tests in this section and in 8.2.1.3 were stress-controlled.

Figure 8.5 shows the computed pressuremeter curves for different stress histories in the range of cavity expansion from 0% to 15% of the initial inner radius (a_o). It should be noted that the analyses were conducted at different initial stresses and void ratios for different stress histories. This is due to the fact that the preconsolidation pressure (p'_o) was assumed to be the same for all the tests.

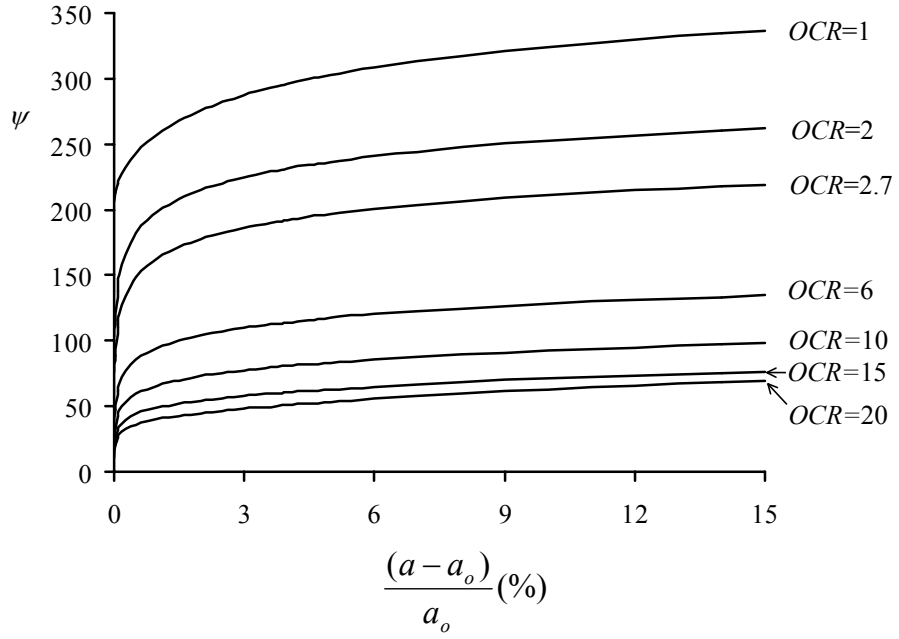

Figure 8.5. Load displacement curves with different stress histories

The interpretation procedure of Gibson and Anderson (1961) was used to derive the undrained shear strength (S_G) from pressuremeter curves in the cavity strain range between 5% and 15% (Figure 8.6). It is noted that only the plastic part of the pressuremeter curve is presented in Figure 8.6. The pressuremeter pressure (i.e. cavity pressure) has been normalised by the theoretical triaxial undrained shear strength (S_u) of the soil so that all the curves can fit into one single figure. For the calculation of undrained shear strength, the non-normalised pressuremeter pressure versus volumetric strain curve was used.

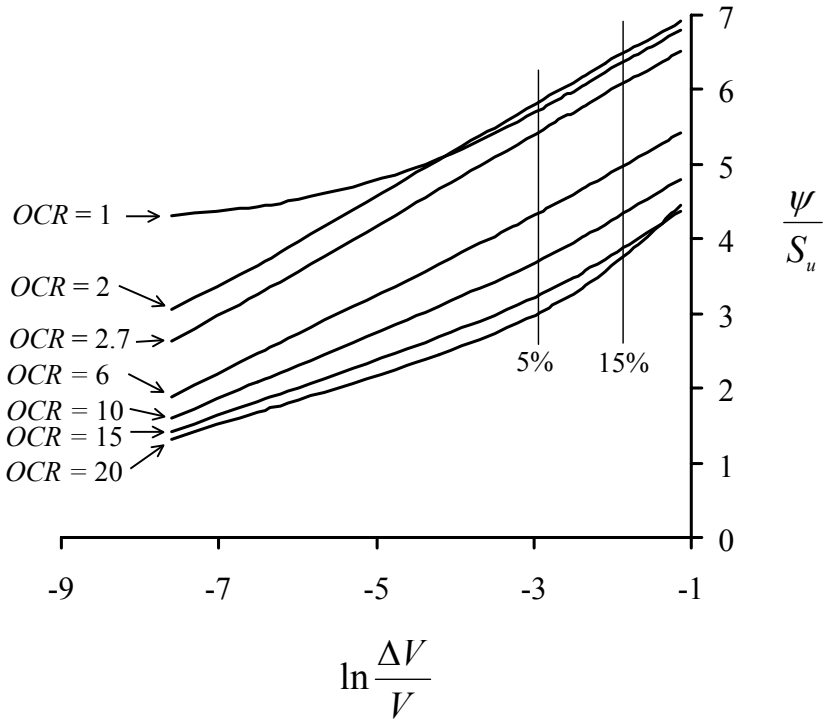

Figure 8.6. Plastic portion of loading curves for different stress histories

The variation of the ratio of S_G to the theoretical triaxial undrained shear strengths (S_u) with the value of overconsolidation ratio is presented in Figure 8.7. It can be seen from Figure 8.7 that for normally consolidated and lightly overconsolidated clays the derived pressuremeter undrained shear strength (S_G) is very close to the theoretical undrained shear strength (S_u). However, for heavily overconsolidated clays, the shear strength derived from the pressuremeter curves is significantly less than the triaxial value with the difference increasing with the value of overconsolidation ratio (*OCR*).

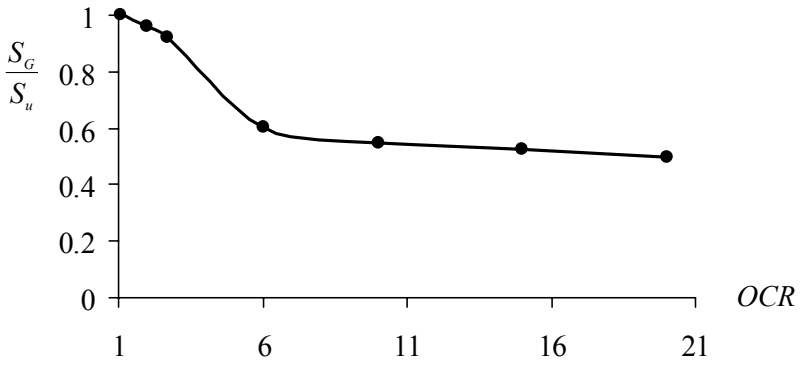

Figure 8.7. Ratio of pressuremeter strength (obtained from Gibson and Anderson's method) to triaxial strength versus *OCR*

8.2.1.3. Pressuremeter analysis using Houlsby and Withers's method

Analyses were also carried out to estimate the undrained shear strength of London clay using the method of interpretation proposed by Houlsby and Withers (1988). The expansion and contraction phases of the test were modelled as the expansion and contraction of a cylindrical cavity with initial radius of a_o. Different strain levels were tried for the expansion phase and it was found that as long as the cavity strain is large enough (ε>30%), the results obtained were not significantly different. In this study, the cylindrical cavity was expanded to a logarithmic strain (ε) of approximately 55% before unloading.

Undrained London clay with different consolidation histories (*OCR*=1 to 20) was again tested. The results for the case with *OCR*=1 are shown in Figures 8.8 and 8.9.

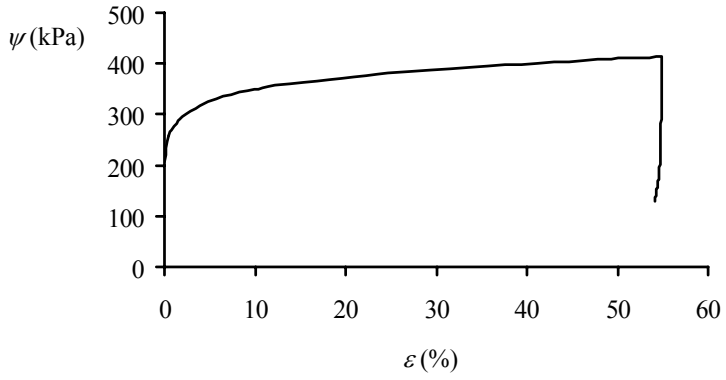

Figure 8.8. Pressuremeter expansion-contraction curve (*OCR*=1)

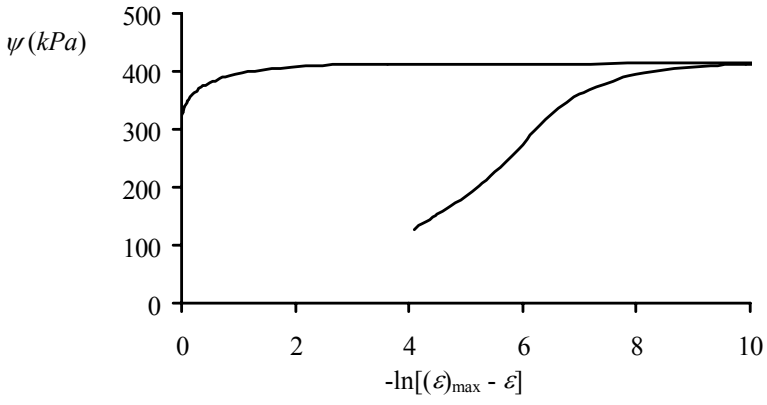

Figure 8.9. Pressuremeter expansion-contraction curve on logarithmic plot (*OCR*=1)

The undrained shear strength of London clay was derived by interpreting the procedure of Houlsby and Withers's (1988). The variation of the ratio of the pressuremeter undrained shear strength obtained from this method (S_H) to the theoretical triaxial undrained shear strength (S_u) with the value of overconsolidation ratio is presented in Figure 8.10. It can be seen that the results are very similar to those given by Gibson and Anderson's interpretation procedure. For normally consolidated and lightly overconsolidated clays, S_H is slightly higher than S_u. However, for heavily overconsolidated clays, S_H is significantly less than S_u with the differences increasing with the value of the overconsolidation ratio.

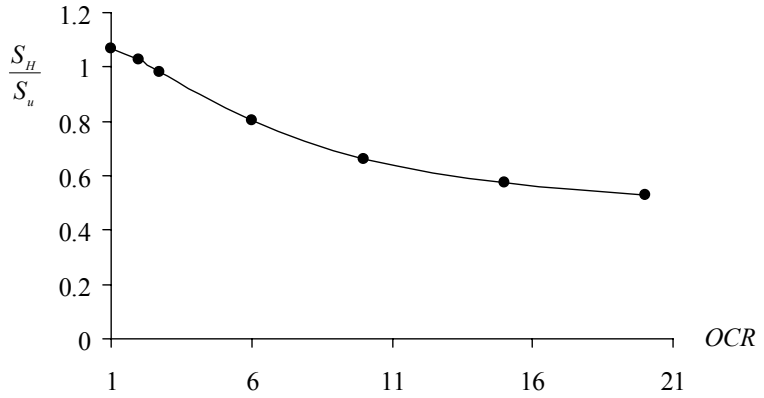

Figure 8.10. Ratio of pressuremeter strength (obtained from Houlsby and Withers's method) to triaxial strength versus *OCR*

8.2.1.4. Comments on the two methods

A comparison of the results obtained from the two different methods is plotted in Figure 8.11. Even though the undrained shear strength was obtained by two totally different methods (by the means of the expansion curve in Gibson and Anderson (1961) and the expansion-contraction curve in Houlsby and Withers (1988)), the trends are very similar. They also closely agree with the analytical results obtained by Yu and Collins (1998) who used a slightly different critical state model.

In general, the undrained shear strength S_G predicted by Gibson and Anderson's procedure is slightly lower than the strength S_H obtained from Houlsby and Withers's procedure. The ratio S_G/S_u does not change significantly with *OCR* values greater than 6, whereas S_H/S_u decreases gradually with increasing values of *OCR*.

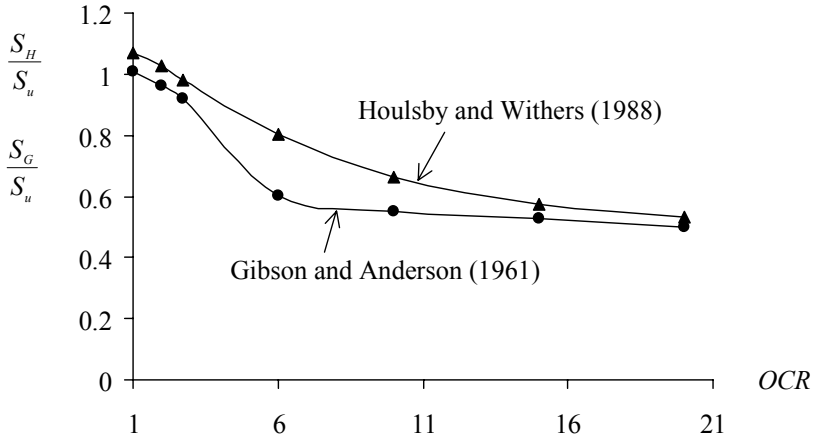

Figure 8.11. Comparison of Gibson and Anderson and Houlsby and Withers's methods

The one factor which is clear from these results is that the undrained shear strength is very much dependent upon the consolidation history of the soil. The strength obtained from these methods can be up to 50% less than the theoretical triaxial undrained shear strength for clay with the overconsolidation ratio of 20.

8.2.2. Analysis of pressuremeter geometry effects

8.2.2.1. Introduction to the problem

It was described earlier that one of the usual interpretation methods for the pressuremeter test is based on the analysis proposed by Gibson and Anderson (1961) for undrained clays. Gibson and Anderson assumed (in effect) that the expansion of pressuremeters of a finite length can be simulated as that of an infinitely long pressuremeter (i.e. infinitely long cylindrical cavity expansion). This assumption enabled them to bypass the complexities involved in the two-dimensional expansion of a finite cylindrical cavity.

The work of Gibson and Anderson was a significant advance in the analysis of pressuremeter tests. It allowed the pressuremeter to be used to obtain fundamental soil properties rather than purely serve as a basis for developing empirical design methods for various soil foundations.

For pressuremeters with a large length to diameter ratio (*L/D*), the expansion will take place under conditions approximating axial symmetry and plane strain in the vertical direction. Under such circumstances, the expansion curve would closely match that for the expansion of an infinitely long pressuremeter. In this case the analysis of Gibson and Anderson (1961) would lead to an accurate estimation of undrained shear strength.

However, values of the undrained shear strength calculated using the Gibson and Anderson method have often been found to be considerably higher than those measured from other in-situ or laboratory tests (Wroth, 1984; Mair and Wood 1987). The influence of the two-dimensional pressuremeter geometry has been widely established as a possible explanation for these discrepancies. Some commercial pressuremeters have an *L/D* value of about 4 or 6 and therefore the pressuremeter geometry effects could be very significant.

An ideal way of studying the effect of two-dimensional pressuremeter geometry is to perform finite element analyses. Using the finite element analysis, the pressuremeter tests can be simulated as the expansion of a finite length pressuremeter membrane. A two-dimensional finite element mesh can be used to perform such calculations and the results can then be compared with those for an one-dimensional cylindrical cavity expansion (which would simulate the expansion of an infinitely long pressuremeter). In this way, a numerical simulation of finite length pressuremeter tests can be compared to a simulation of infinitely long pressuremeter tests for which the analysis of Gibson and Anderson (1961) strictly applies.

Studies of pressuremeter geometry effects in clay using axis-symmetric finite element formulations have been carried out by Yu (1990), Yeung and Carter (1990), and Houlsby and Carter (1993) among others. In the study conducted by Yu (1990), the soil was idealised as elastic-perfectly plastic deforming under constant volume conditions and obeying the Von Mises criterion. The initial stress state for each test was isotropic. The study considered three length to diameter ratios of 4, 6 and 8. The undrained shear strength was determined from strain ranges of 2-5% and 2-10% using the least squares method. Calibration calculations were also conducted using an infinitely long pressuremeter to account for possible numerical errors. The comparison between the calculated undrained shear strengths and the value obtained with an infinite *L/D* showed

a significant overestimation of the undrained shear strength due to the finite values of *L/D*. Yu also found that the finite length effects increased with the soil rigidity index (defined as the ratio of the shear modulus to the undrained shear strength, G/S_u). For the study by Houlsby and Carter (1993), the soil was idealised as elastic-perfectly plastic and adopted the Tresca criterion. The study considered *L/D* values of 4, 6 and 10 and the results were also standardised using an equivalent test with an infinite *L/D*. The undrained shear strength was estimated from the strain range of 2-5% using a line of best fit. Houlsby and Carter found that for a length to diameter ratio of 6 and rigidity indices between 200 and 500, the derived strengths were about 25-43% higher than the actual shear strength of the soil.

In almost all the existing numerical studies of pressuremeter geometry effects, the soil has been modelled as an elastic-perfectly plastic material. This theory assumes that after the soil in a region around the pressuremeter reaches the yield point, it behaves plastically and has a constant shear strength value. Soils do not behave exactly as elastic-perfectly plastic materials but can undergo strain hardening or softening. Strain hardening or softening of the soil after yield could influence the response of the soil to pressuremeter geometry effects. Critical state soil models are capable of taking into account strain hardening/softening and the variable soil shear resistance. This means that critical state models are capable of accounting for the stress history effects and are therefore more accurate for use in modelling overconsolidated soils. For this reason, such models would be more appropriate for studying the pressuremeter geometry effects than elastic-perfectly plastic soil models, especially for clays with a high *OCR*.

In this section, results of a comprehensive numerical study into pressuremeter geometry effects using critical state soil models are presented. Finite element analysis has been used to obtain finite length corrections for self-boring pressuremeter tests in undrained London clay. An effective stress formulation was employed because it is appropriate with critical state soil models. The usual total stress analysis was not used because it is not suitable when the strength of the soil is variable, nor is it appropriate for highly overconsolidated soils (Yu and Collins, 1998).

8.2.2.2. Finite element analysis of pressuremeter geometry effects

The finite element method was used to simulate the self-boring pressuremeter tests in clay. This is to simulate the axis-symmetric expansion of a finite length pressuremeter membrane in an undrained clay. The analysis was based on an effective stress formulation and was conducted for soils with several different overconsolidation ratios (*OCR*). Two critical state soil models were used to describe soil behaviour. All the analyses in this section were stress-controlled.

The finite element mesh was made up of fifteen-noded triangular elements. Due to symmetry, only half of the soil mass needed to be modelled. The radius of the pressuremeter was set to one unit and the length of the mesh in both the radial and axial (i.e. vertical) directions was 200 units. The size of the mesh domain (in both radial and vertical directions) was set to be sufficiently large so that the outside boundaries would have little influence on the numerical results. The mesh was designed so that the density of the elements was greatest in regions where high stresses were expected. This allows for the greater accuracy of a fine mesh where it is needed, whilst keeping the number of elements to a manageable size. Figure 8.12 shows a schematic diagram of a typical mesh to illustrate this. Following the work of Yu (1990) and Houlsby and Carter (1993), the pressuremeter was modelled as rigid and extending to infinity above and below the membrane. This achieves the desired effect of preventing inward movement at the pressuremeter boundary. The centre of the pressuremeter membrane was situated at the left hand corner of the mesh. At the inner radius of the mesh, the eight elements at the centre were all of the same size. This allowed the same mesh to be used to obtain the four different length to diameter ratios. The four length to diameter ratios of 20, 15, 10 and 5 were achieved by using 8, 6, 4 and 2 elements to model the soil adjacent to the pressuremeter membrane respectively. One-dimensional cylindrical cavity expansions were used to model pressuremeter tests with an infinite length to diameter ratio.

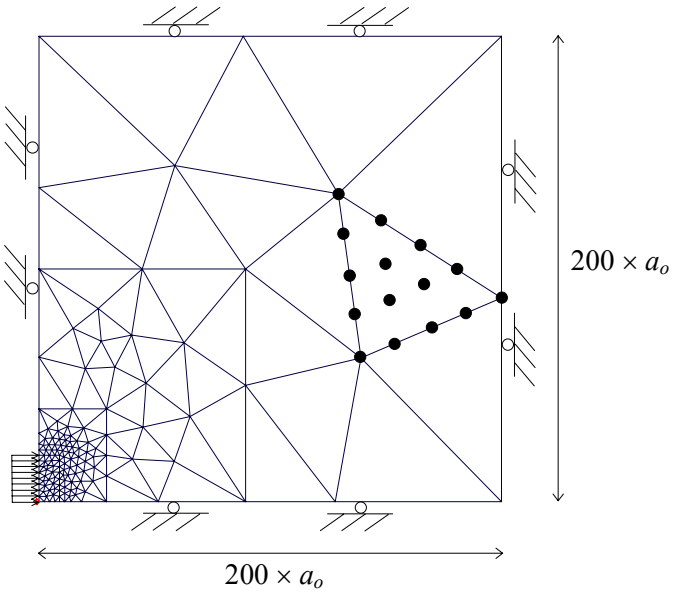

Figure 8.12. Schematic diagram of the finite element mesh (*L/D*=20)

The two critical state models used in the study were modified Cam-clay and CASM with n=2.0 and r=2.718.

All the pressuremeter analyses were performed in two steps, the first step set up an initial stress state and the second performed the loading analysis. For each model, a constant preconsolidation pressure was used. Different overconsolidation ratios were achieved by starting the test at different initial stresses. During the loading stage, the pressure was applied uniformly to the elements representing the soil adjacent to the membrane. The maximum value of the applied pressure was chosen so that the final cavity strain at the centre of the membrane was always greater than 10%. The values of the *OCR* used were 1.0, 2.0, 2.718, 5.0, 10.0, 15.0 and 20.0.

8.2.2.3. Results and discussion

Because the soil is modelled by the critical state theory, the section of the pressuremeter curve after yield is, in general, not necessarily linear (Yu and Collins, 1998). For this reason it is usual to determine the slope from a fixed section of the curve using least squares or a line of best fit. Yu (1990) for instance used the section of the curve corresponding to the strain ranges of 2-5% and 2-10%. For this study three different strain ranges of 2-5%, 3-10% and 5-10% were used to determine the undrained shear

strength of the clay. This would demonstrate any possible effect on the results the strain range (over which the pressure-expansion curve is fitted) had (Yu, 1990; Houlsby and Carter, 1993). It is noted that all the strains mentioned in this section are volumetric strains.

For each soil model used, 35 sets of analyses were performed. Figure 8.13 shows a comparison of the pressuremeter results obtained for different length to diameter ratios where the strain range is taken as 2-5%. As expected, the pressuremeter curves, which are plotted in terms of the pressuremeter pressure (ψ) against the cavity strain (ε), show an increase in stiffness with a decrease in the length to diameter ratio.

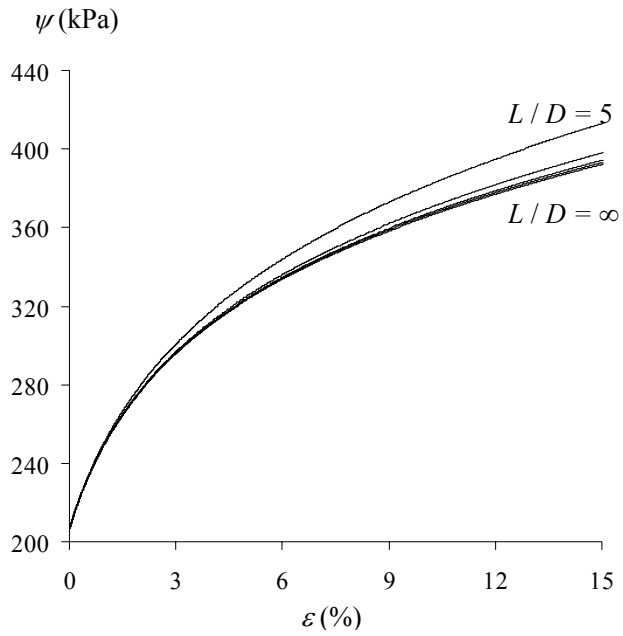

Figure 8.13. Pressuremeter curves with different *L/D* ratios, *OCR*=1, CASM

Figure 8.14 shows another comparison of the same analyses, this time with the pressuremeter curves plotted on a semi-log scale.

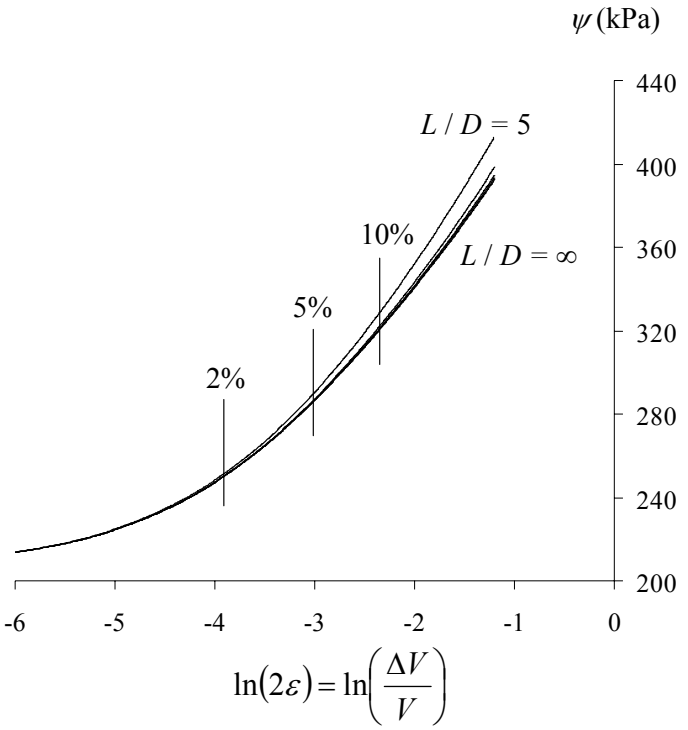

Figure 8.14. Pressuremeter curves (semi-log scale) with different *L/D* ratios, *OCR*=1, CASM

The results of the analyses for the cases which use strain range of 2-5% are shown in Tables 8.2 and 8.3. The values listed in these tables are the slopes from the graphs of pressure against ln(2ε). Following the analysis of Gibson and Anderson (1961), this is the value generally taken as the undrained shear strength.

OCR	*L/D*=5	*L/D*=10	*L/D*=15	*L/D*=20	*L/D*=∞
1	57.2	52.5	51.6	51.3	49
2	45.9	43.4	42.8	42.5	41
2.718	40.2	38.3	37.85	37.6	36.7
5	29.6	28.55	28.2	28	27.6
10	19.3	18.85	18.63	18.5	18.3
15	15	14.8	14.65	14.5	14.45
20	12.8	12.7	12.6	12.5	12.5

Table 8.2. Undrained shear strength (kPa) deduced from numerical results using CASM (2-5%)

OCR	*L/D*=5	*L/D*=10	*L/D*=15	*L/D*=20	*L/D*=∞
1	74.6	70.1	69.2	66.7	62
2	60	57.3	56.5	55.8	53
2.718	57.1	55.3	54.7	54.2	52
5	44	43.2	42.9	42.6	41.5
10	26.5	26.2	25.9	25.8	25.5
15	18.4	18.1	18	17.9	17.8
20	15.2	15.03	14.98	14.9	14.9

Table 8.3. Undrained shear strength (kPa) deduced from numerical result using modified Cam-clay (2-5%)

To account for the pressuremeter geometry effects, correction factors were calculated for each of the finite length pressuremeter results. The correction factors were calculated as the ratio of the slope derived from infinitely long pressuremeters to that from finite length pressuremeters with various *L/D* values (e.g. $S_{um}^{\infty} / S_{um}^{5}$ for *L/D* of 5). The correction factors can then be used to correct for pressuremeter geometry effects in field tests. The slope calculated from a field test can be multiplied by the appropriate correction factor to give the slope that would have been measured if the pressuremeter were infinitely long. The analysis of Gibson and Anderson (1961) applies for an infinite *L/D*, the slope being equal to the undrained shear strength. The correction factors for the 2-5% case are shown in Tables 8.4 and 8.5.

OCR	$S_{um}^{\infty} / S_{um}^{5}$	$S_{um}^{\infty} / S_{um}^{10}$	$S_{um}^{\infty} / S_{um}^{15}$	$S_{um}^{\infty} / S_{um}^{20}$
1	0.8567	0.9333	0.9496	0.9552
2	0.8932	0.9447	0.958	0.9647
2.718	0.913	0.9582	0.9696	0.9761
5	0.9324	0.9667	0.9787	0.9857
10	0.9482	0.9708	0.9823	0.9892
15	0.9633	0.9764	0.9863	0.9966
20	0.9766	0.9843	0.9921	1

Table 8.4. $S_{um}^{\infty} / S_{um}^{L/D}$ for CASM (2-5%)

OCR	$S_{um}^{\infty} / S_{um}^{5}$	$S_{um}^{\infty} / S_{um}^{10}$	$S_{um}^{\infty} / S_{um}^{15}$	$S_{um}^{\infty} / S_{um}^{20}$
1	0.8311	0.8845	0.896	0.9295
2	0.8833	0.925	0.9381	0.9498
2.718	0.9107	0.9403	0.9506	0.9594
5	0.9432	0.9606	0.968	0.9742
10	0.9623	0.975	0.9838	0.9884
15	0.9674	0.984	0.988	0.992
20	0.9803	0.9914	0.9947	1

Table 8.5. $S_{um}^{\infty} / S_{um}^{L/D}$ for modified Cam-clay (2-5%)

All the results are also shown graphically in Figures 8.15-8.26 where the correction factors are plotted against the diameter to length ratio (i.e. *D*/*L*) and the *OCR* value. The results show that the overestimation of the soil strength due to the pressuremeter geometry effect is most significant when the *L/D* ratio is small. The results also indicate that the overestimation of strength decreases when the soil becomes more overconsolidated. The largest overestimation of strength in this study was for an *L/D* ratio of 5 and an overconsolidation ratio of 1 (using the modified Cam-clay model). In this case, the overestimation of the strength was roughly 17%. The effect of the overconsolidation ratio on the results decreased significantly as *L/D* increased and eventually the overestimation of strength became negligible. For an *L/D*=20, the greatest overestimation of strength was less than 7% (for the case of the modified Cam-clay model).

From Figures 8.15-8.26, it can be seen that the strain range over which the pressuremeter curve is fitted has an influence on the derivation of undrained shear strength. The overestimation of undrained shear strength is smallest when the strain range is 5-10% and largest when the strain range is 2-5%.

A comparison with earlier studies using elastic-perfectly plastic soil models shows that the effective stress analysis with critical state models predicts smaller geometry effects. This indicates that the effects of variable soil shear resistance and effective stress analysis are significant when we consider pressuremeter geometry effects in clay.

Even though the undrained shear strengths obtained with modified Cam-clay are higher than those obtained with CASM (Tables 8.2 and 8.3), no significant difference in the correction factors was found between the two critical state soil models. This suggests that the *L*/*D* effects are not very sensitive to the choice of critical state models. However, as shown clearly by Yu and Collins (1998), the actual value of the undrained shear strength deduced from the pressuremeter curve was very sensitive to the choice of plasticity models used to represent the soil behaviour.

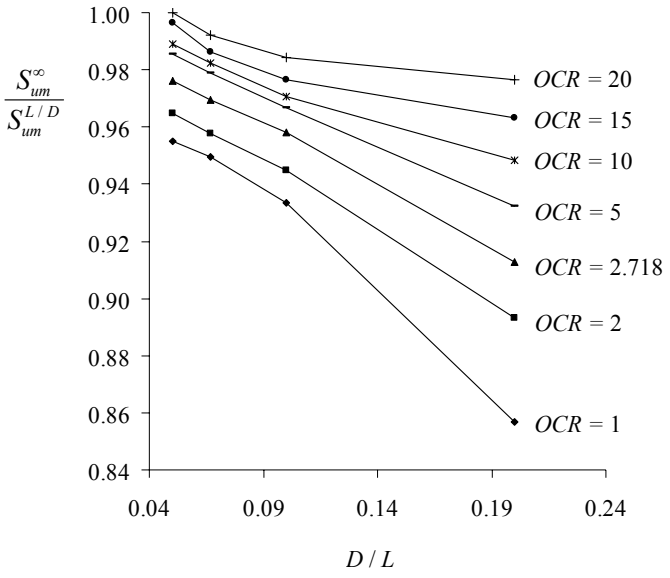

Figure 8.15. Plot of $S_{um}^{\infty} / S_{um}^{L/D}$ vs. *D*/*L* ratio for CASM (2-5%)

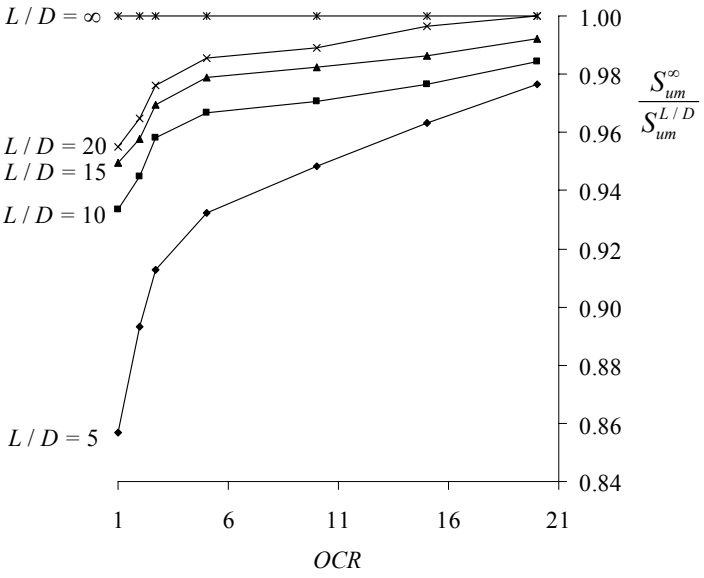

Figure 8.16. Plot of $S_{um}^{\infty} / S_{um}^{L/D}$ vs. *OCR* value for CASM (2-5%)

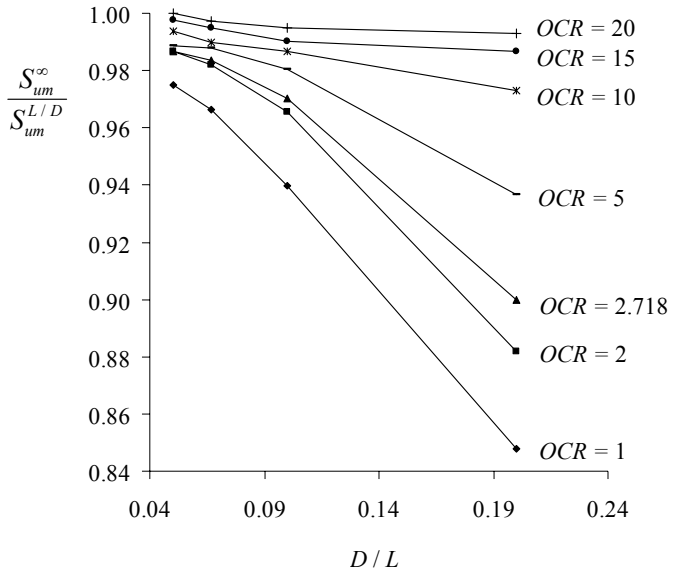

Figure 8.17. Plot of $S_{um}^{\infty} / S_{um}^{L/D}$ vs. *D*/*L* ratio for CASM (3-10%)

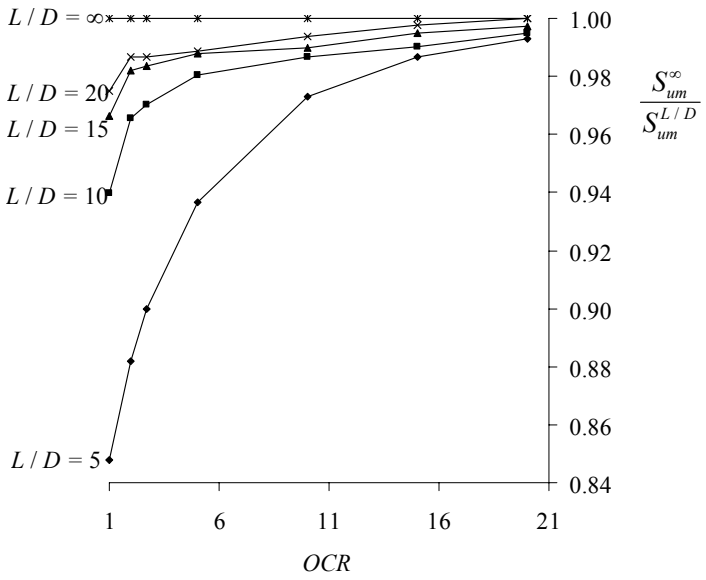

Figure 8.18. Plot of $S_{um}^{\infty} / S_{um}^{L/D}$ vs. *OCR* value for CASM (3-10%)

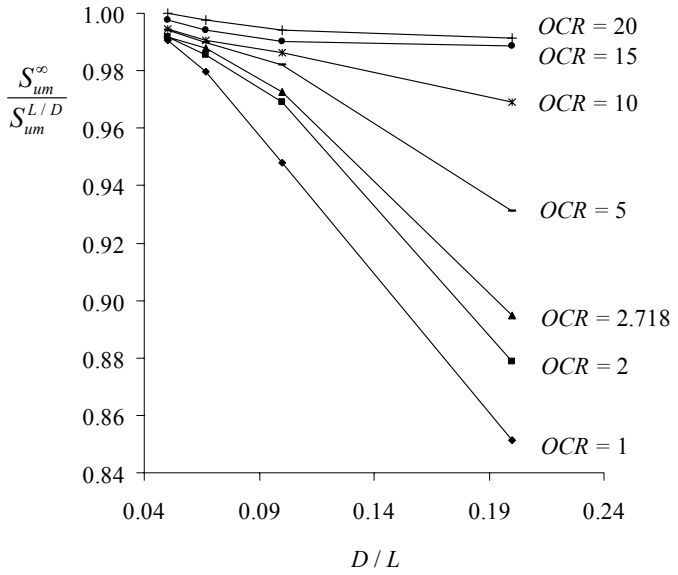

Figure 8.19. Plot of $S_{um}^{\infty} / S_{um}^{L/D}$ vs. *D*/*L* ratio for CASM (5-10%)

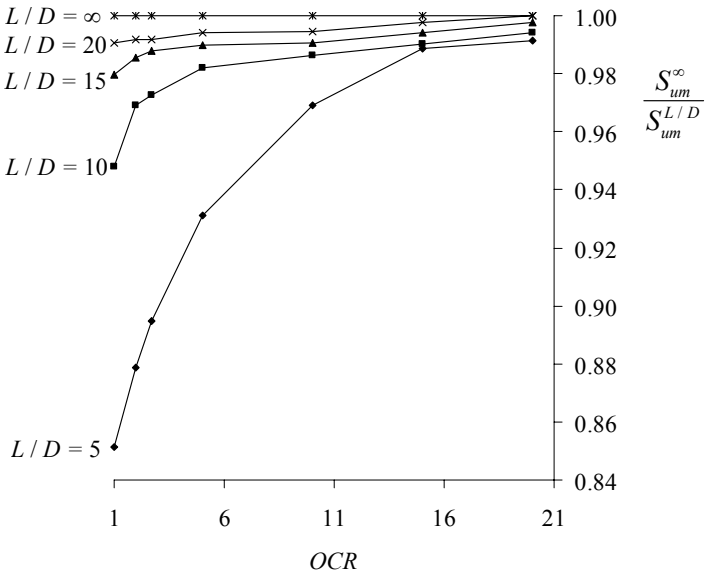

Figure 8.20. Plot of $S_{um}^{\infty} / S_{um}^{L/D}$ vs. *OCR* value for CASM (5-10%)

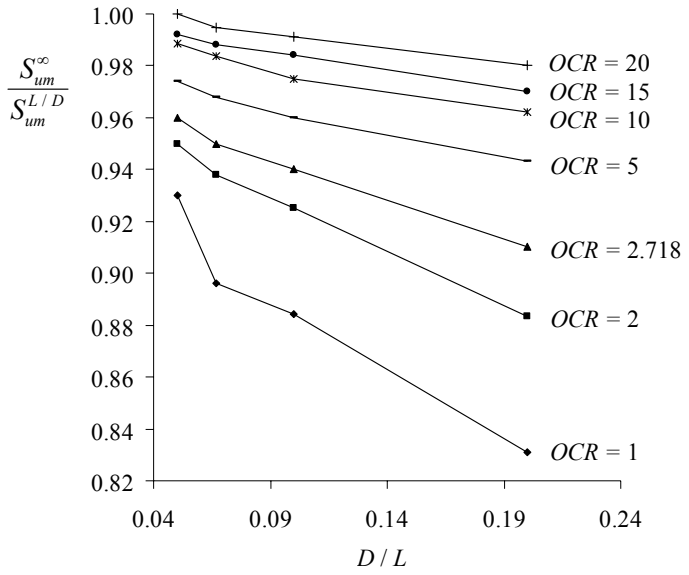

Figure 8.21. Plot of $S_{um}^{\infty} / S_{um}^{L/D}$ vs. D/L ratio for modified Cam-clay (2-5%)

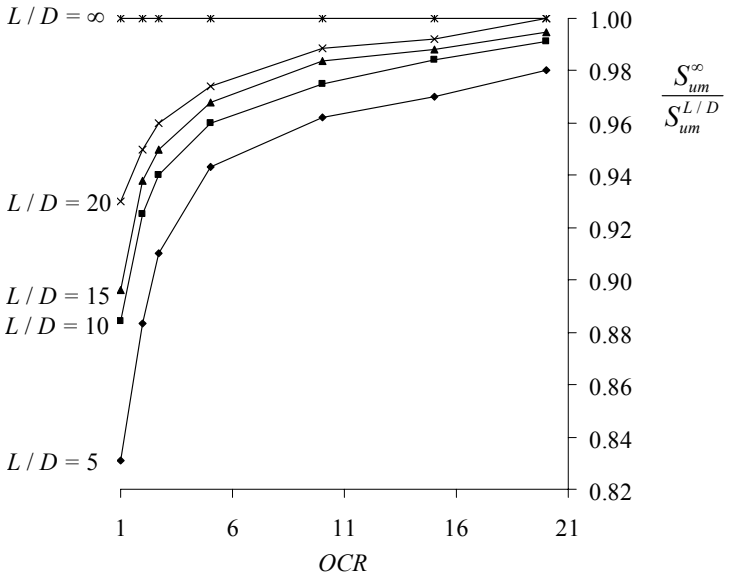

Figure 8.22. Plot of $S_{um}^{\infty} / S_{um}^{L/D}$ vs. *OCR* value for modified Cam-clay (2-5%)

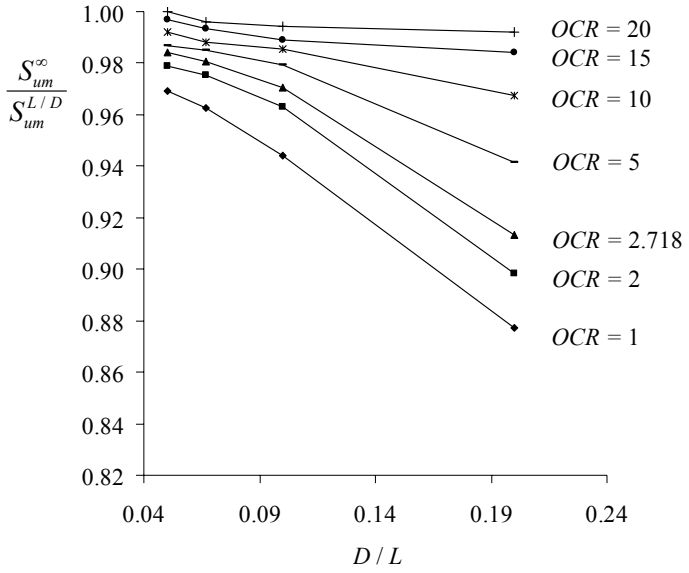

Figure 8.23. Plot of $S_{um}^{\infty} / S_{um}^{L/D}$ vs. D/L ratio for modified Cam-clay (3-10%)

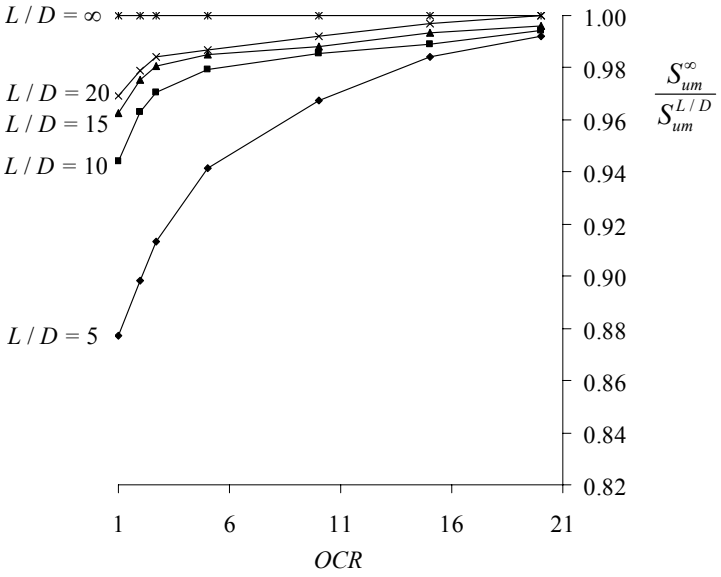

Figure 8.24. Plot of $S_{um}^{\infty} / S_{um}^{L/D}$ vs. OCR value for modified Cam-clay (3-10%)

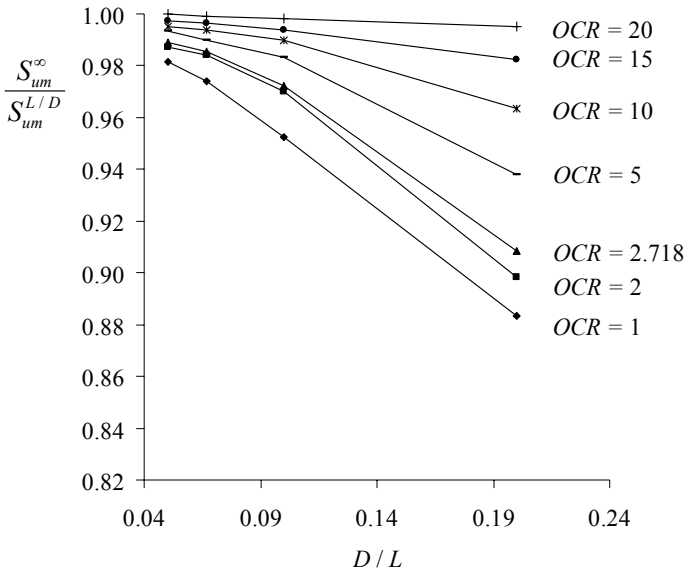

Figure 8.25. Plot of $S_{um}^{\infty} / S_{um}^{L/D}$ vs. D/L ratio for modified Cam-clay (5-10%)

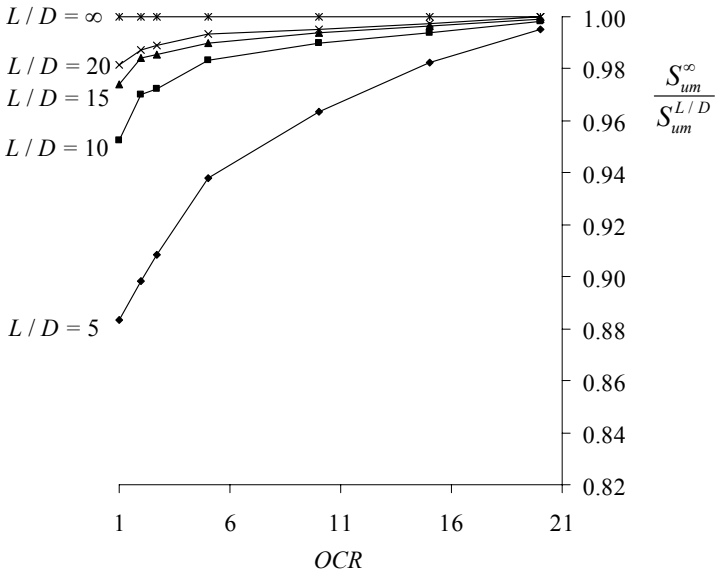

Figure 8.26. Plot of $S_{um}^{\infty} / S_{um}^{L/D}$ vs. *OCR* value for modified Cam-clay (5-10%)

8.3. ANALYSIS OF RIGID SURFACE STRIP FOOTINGS USING CASM AND CASM-b

8.3.1. Introduction to the problem

Strip or continuous footing has a length significantly greater than its width. It is generally used to support a series of columns or a wall. This is a typical plane strain problem and one of two special cases of a general three-dimensional state of strain which has a practical importance in soil mechanics (the other type is the axis-symmetric problem). In plane strain problem, the deformation in the longitudinal direction is considered to be zero.

The strip footing problem is analysed in this section. The behaviour of the strip footing on undrained London clay and on drained Ticino sand was investigated using CASM. Soils with different overconsolidation ratios (London clay) and initial state parameters (Ticino sand) were modelled to see the effect stress history had upon the behaviour of a strip footing. CASM-b was also used to analyse the strip footing on undrained London clay. The analyses were displacement-controlled, the applied vertical load was calculated from the nodal reaction forces.

8.3.2. Strip footing on undrained London clay using CASM

Analyses were carried out with an *OCR* equal to 1, 2, 2.7, 4, 6, 8, 10, 15 and 20. The finite element mesh used consisted of six-noded linear strain triangle elements. This is shown in Figure 8.27. There is a vertical plane of symmetry through the centre of the footing hence, the finite element analysis only needs to consider half of the problem.

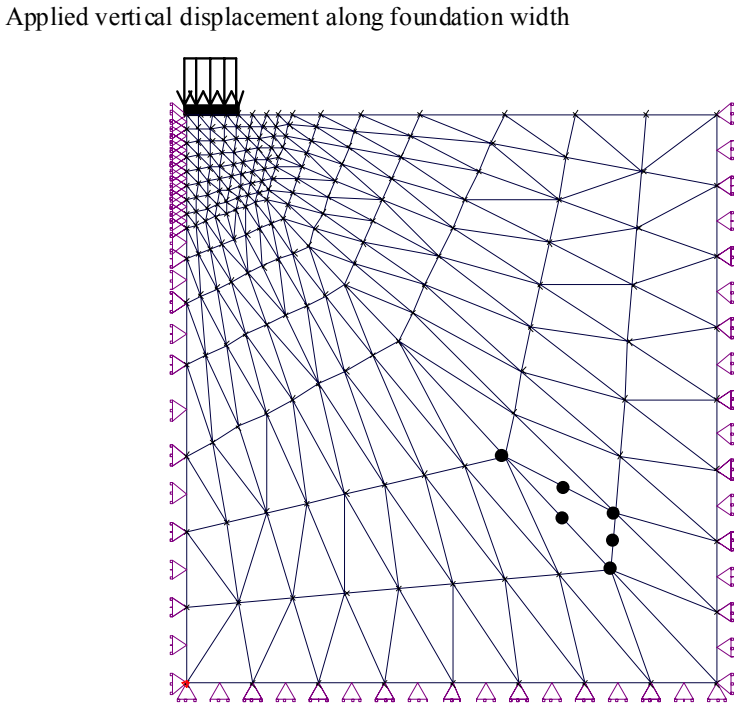

Figure 8.27. Finite element mesh for the strip footing analysis

The bearing capacity of a vertically loaded footing on undrained clay can be expressed as:

$$\frac{Q_u}{A} = q_u = N_c S_u + \sigma_o \tag{8.9}$$

where Q_u is the maximum vertical load that can be applied to the footing, A is its area, N_c is the bearing capacity factor, S_u is the undrained shear strength of the soil under triaxial loading conditions and σ_o is the initial stress.

Firstly, the finite element results obtained from CASM were compared with results obtained from the Tresca model. The initial stresses were chosen so that the soil was overconsolidated with an *OCR* of 2.718 at the beginning of the test. The stress path is shown in Figure 8.28. By starting the test at this point, the soil will fail as soon as it reaches the yield surface because that is the point where it meets the critical state condition (stress path meets the critical state line). This means that with this initial stress condition, CASM will basically behave like an elastic perfectly plastic model.

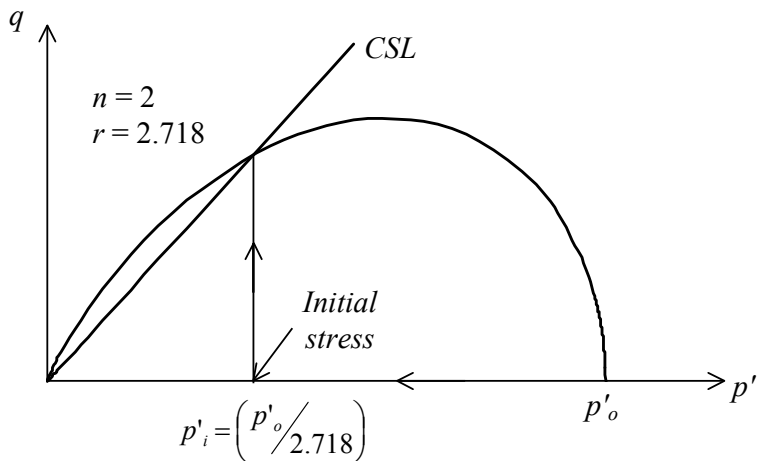

Figure 8.28. Stress path for loading of a strip footing (*OCR*=2.718)

The results for these analyses are shown in Figure 8.29 where q_v is the average applied vertical pressure. It can be seen from Figure 8.29 that the solutions from CASM and the Tresca model agree very well with each other. Plasticity theory indicates that, for a strip footing resting on an undrained clay with a constant strength, the bearing capacity factor should be $N_c=2+\pi=5.14$. This is shown as the analytical solution in Figure 8.29. As expected, the finite element solutions for both CASM and the Tresca model slightly overestimate the analytical results by giving the limit load factors of 5.21 and 5.31 respectively. This overestimation is known to be caused by the excessive kinematical constraints on the finite element mesh imposed by the incompressibility condition in an undrained analysis (Sloan and Randolph, 1982).

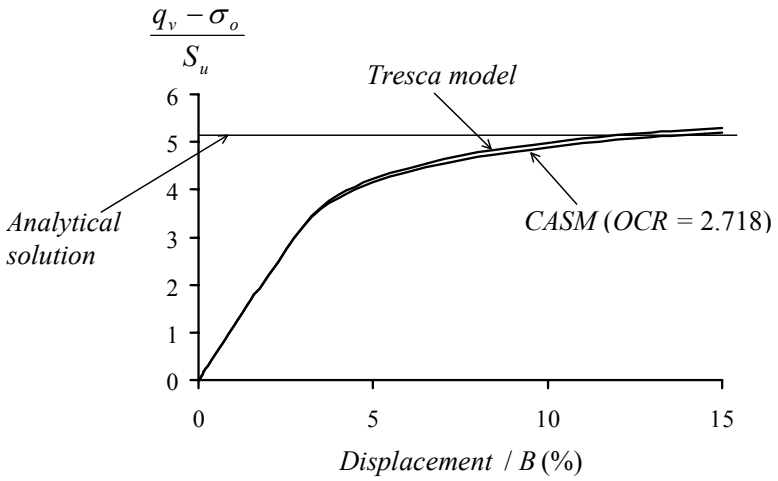

Figure 8.29. Comparison of CASM with the Tresca model for a strip footing

The load displacement curves for two cases (*OCR*=2 and *OCR*=20) are shown in Figure 8.30. It was found that the collapse load was far from being mobilised for heavily overconsolidated clay when the displacement was at 15% of the footing width.

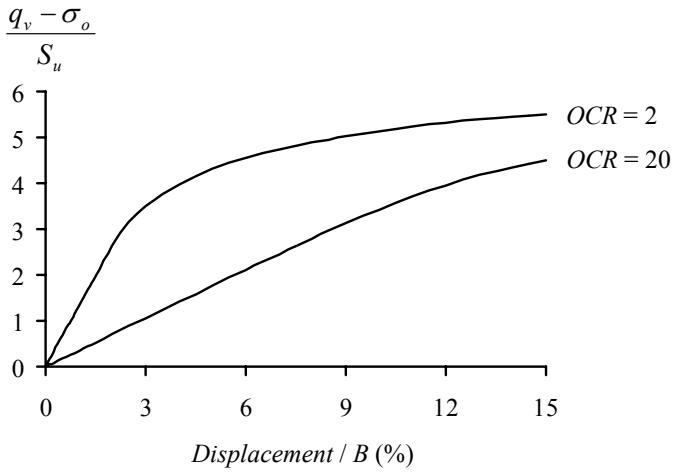

Figure 8.30. Load displacement curves for a strip footing (*OCR*=2 and *OCR*=20)

Figure 8.31 presents the summary of the analyses where the mobilised bearing capacity factor $N_c^{mob}\left[=\left(q_u-\sigma_o\right)\Big/ S_u\right]$ is plotted against the overconsolidation ratio. It should be noted that the values of N_c^{mob} shown in Figure 8.31 were the values taken when the vertical displacement was 15% of the footing width. For very high *OCR* values, N_c^{mob} may not yet have reached its maximum (i.e. reached a constant value). The value of 15% was chosen just for the comparison of N_c^{mob} at various *OCR* values. It is clear from Figure 8.31 that the behaviour of a strip footing is dependent upon the stress history (i.e. *OCR* value) of the soil.

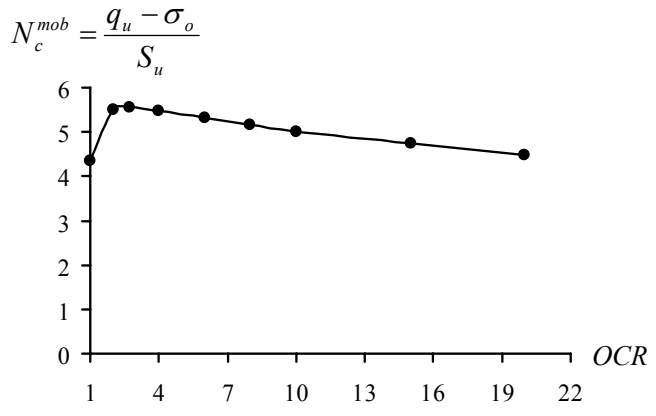

Figure 8.31. Dependence of mobilised N_c^{mob} on *OCR* value for a strip footing

8.3.3. Strip footing on undrained London clay using CASM-b

The bounding surface model CASM-b has also been used to simulate the behaviour of the strip footing on undrained London clay. The new parameter h was set equal to 5 while two values of m (m=1 and m=2) have been used to see the effect of this new parameter on the numerical results. The results obtained from CASM are also shown for comparison purposes.

Figure 8.32 shows the relationship between the overconsolidation ratio and the normalised bearing capacity factor (N_c^{mob}). For normally consolidated soil (OCR=1), CASM-b gave exactly the same results as CASM because no modification has been made in CASM-b that alters the behaviour once the stress point lies on the bounding surface. For overconsolidated clay, it can be seen that CASM-b gave a more conservative bearing capacity than CASM. This is expected because the stiffness of the soil before reaching the bounding surface used by CASM-b is lower than that predicted by CASM. Figure 8.32 can be used as a design chart for the hand calculation of the bearing capacity of a strip footing on undrained London clay having different stress histories.

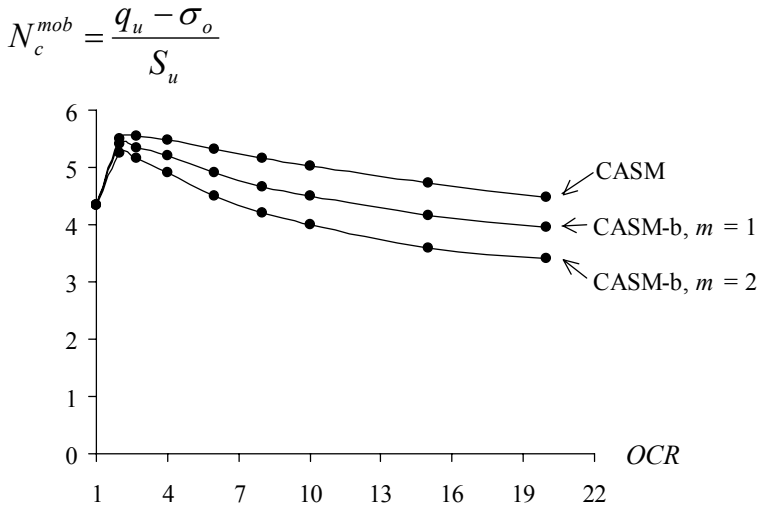

Figure 8.32. Dependence of mobilised N_c^{mob} on OCR value for a strip footing using CASM-b

8.3.4. Strip footing on drained Ticino sand using CASM

Yu (1998) stated that the state parameter could be regarded as a better quantity than the *OCR* for describing soil response under various loading conditions, especially for sand. Work on dense and loose sands by Been and Jefferies (1985) and Sladen et al. (1985) also suggested that the state parameter could be confidently used to describe much of the behaviour of granular materials over a wide range of stresses and densities. Therefore, it is expected that the state parameter for sand will play a similar role as the overconsolidation ratio for clay. Analyses have been carried out with Ticino sand having initial state parameters (ξ_o) of 0.02, 0.0, -0.02, -0.04, -0.06 and -0.08.

The load displacement curves for different initial state parameters are plotted in Figure 8.33 where the pressure is normalised by the initial stress. Again the analyses were carried out until the vertical displacement reached 15% of the footing width. It can be seen that limit pressures are not mobilised for very dense sands (ξ=-0.06 and ξ=-0.08 in Figure 8.33).

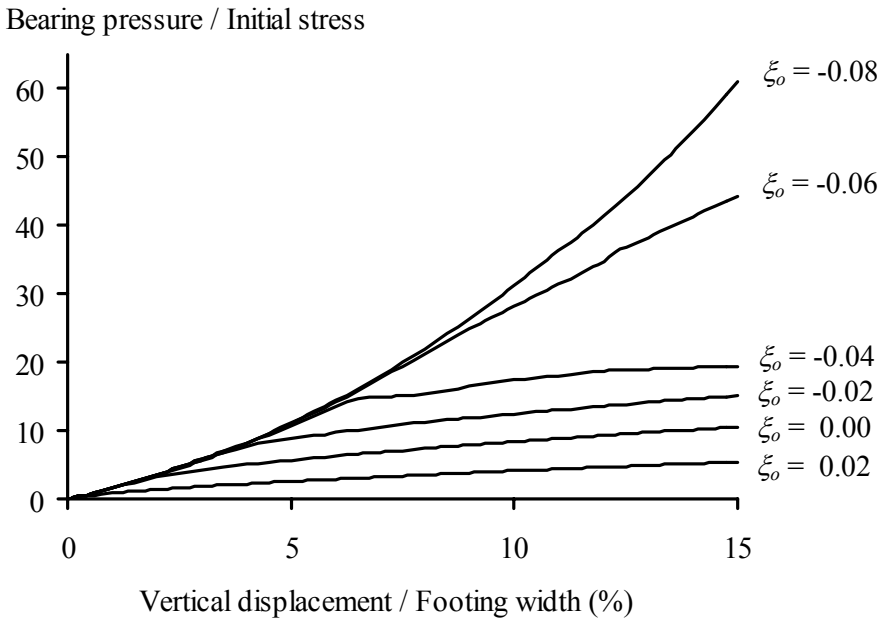

Figure 8.33. Load displacement curves of a strip footing on sand

8.4. ANALYSIS OF RIGID SURFACE CIRCULAR FOOTINGS USING CASM

8.4.1. Introduction to the problem

A circular footing is generally an individual foundation designed to carry a single column load although there are occasions when it supports two or three columns. This is a typical axis-symmetric problem (i.e. the strain in the circumferential direction is zero).

In this section, CASM is again used to investigate the behaviour of a circular footing on undrained London clay and drained Ticino sand. Soils with different overconsolidation ratios (London clay) and initial state parameters (Ticino sand) were modelled to see the effect stress history has upon the behaviour of circular footings. Again, the analyses were displacement-controlled with the applied vertical load obtained from the nodal reaction forces.

8.4.2. Circular footing on undrained London clay using CASM

The same analysis was repeated for a surface circular footing. The mesh shown in Figure 8.27 was used again however, the previous elements were replaced with fifteen-noded cubic strain triangle elements. The results are shown in Figures 8.34-8.36. The behaviour of a circular footing is very similar to that of a strip footing. As expected, the mobilised bearing capacity factor of a circular footing was slightly higher than that of a strip footing.

As shown in Figure 8.34, the comparison between CASM and Tresca results shows a very good agreement. Once again, the finite element results slightly overestimate the analytical solution (N_c=5.69) by calculating the mobilised bearing capacities of 5.83 and 5.92 respectively.

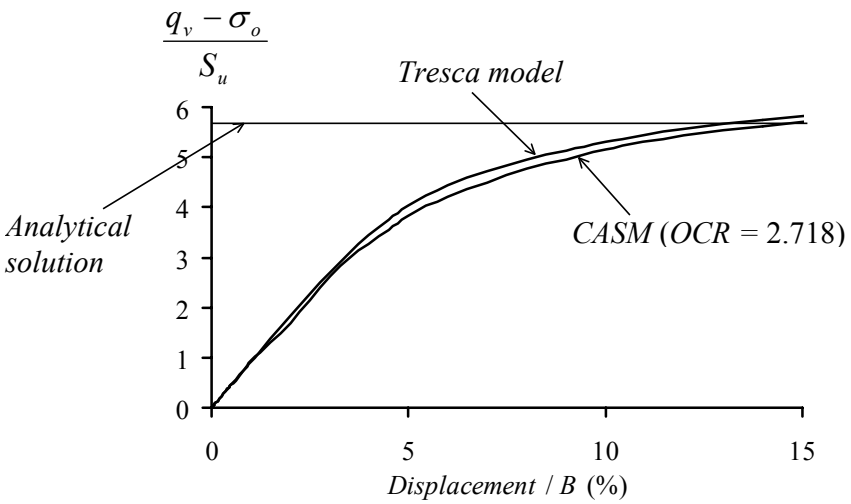

Figure 8.34. Comparison of CASM with the Tresca model for a circular footing

The load displacement curves for two specific cases (*OCR*=2 and *OCR*=20) are shown in Figure 8.35. Again, it was found that the collapse load was far from being mobilised for heavily overconsolidated clay when the displacement was equal to 15% of the footing width.

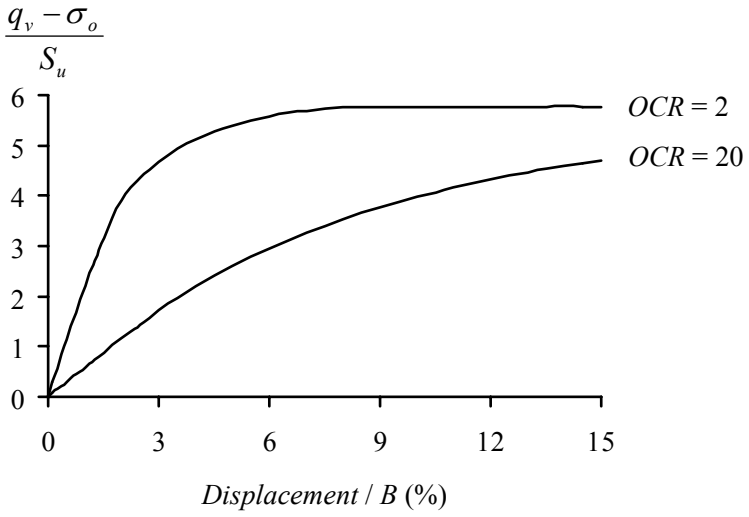

Figure 8.35. Load displacement curves for a circular footing (*OCR*=2 and *OCR*=20)

Figure 8.36 presents the summary of the analyses for a circular footing. It is evident from Figure 8.36 that the bearing capacity of a circular footing is also dependent upon the stress history of the soil.

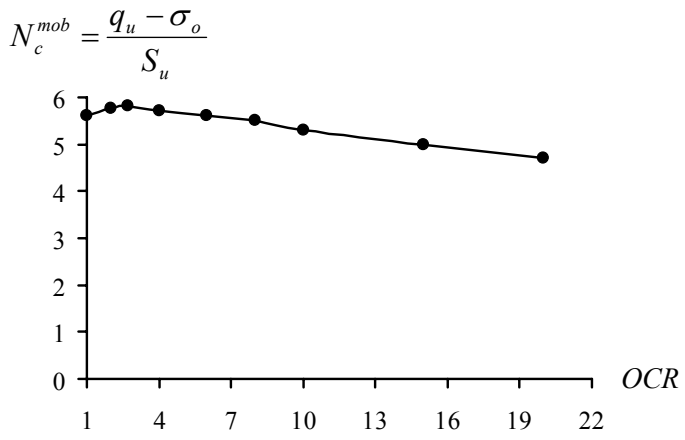

Figure 8.36. Dependence of mobilised N_c on *OCR* value for a circular footing

8.4.3. Circular footing on drained Ticino sand using CASM

Analyses have also been carried out using Ticino sand having initial state parameters of 0.02, 0.0, -0.02, -0.04, -0.06 and -0.08. The load displacement curves for different initial state parameters are plotted in Figure 8.37 where the pressure is normalised by the initial stress. Again the analyses were carried out until the vertical displacement reached 15% of the footing width and it can be seen that limit pressures were not mobilised for very dense sands at this displacement (ξ=-0.04, ξ=-0.06 and ξ=-0.08 in Figure 8.37). The behaviour of a circular footing in sand is very similar to that of a strip footing.

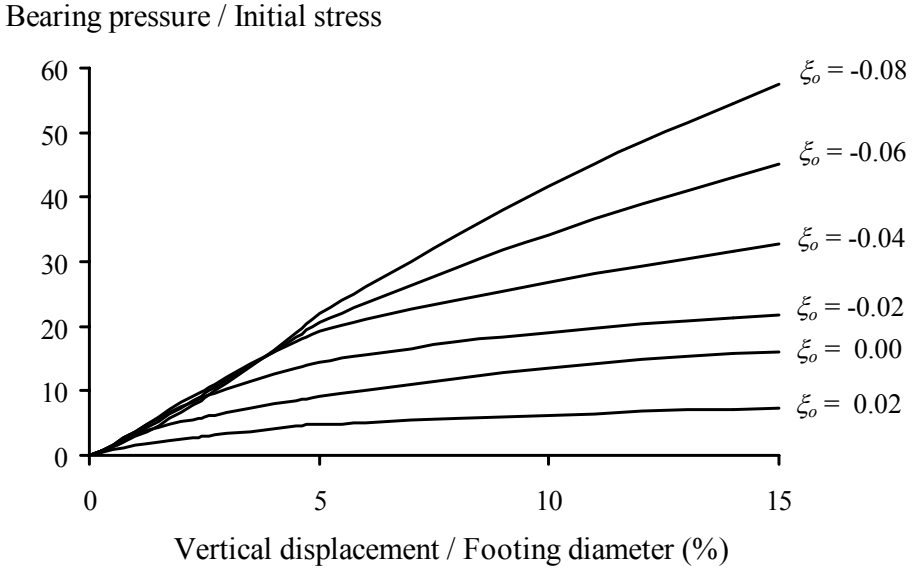

Figure 8.37. Load displacement curves of a circular footing on sand

8.5. ANALYSIS OF HORIZONTAL STRIP ANCHORS USING CASM

8.5.1. Introduction to the problem

Anchor plates are generally used in the design and construction of structures requiring uplift resistance. These include transmission towers, bridges, tension roofs and submerged pipelines. During the last 30 years, much experimental and theoretical work on the ultimate pullout capacity of anchor plates has been published. An overview of the topic can be found in Das (1990).

The prediction of anchor plate behaviour is usually restricted to either the limiting conditions of elastic displacement (e.g. Fox, 1948; Rowe and Booker, 1979) or the ultimate capacity (e.g. Meyerhof and Adams, 1968; Vesic, 1971). Rowe and Davis (1982a, 1982b) presented a rigorous numerical study to determine the pullout capacity of anchors in both clay and sand. These were obtained by assuming that the soil can be modelled by the Mohr-Coulomb failure criterion. A study of the lower and upper bound limit analysis of strip anchors in both homogeneous and inhomogeneous clays has also been presented by Merifield et al (2001).This study utilised a rigid perfectly-plastic soil model obeying the Tresca yield criterion.

In this section, a finite element study of horizontal anchors subject to uplift forces is presented. This study makes use of CASM. The effects of the depth to width ratio of the anchor and the stress history of the soil are considered. In the drained analysis with Ticino sand, the finite element calculations of the anchor behaviour using the Mohr-Coulomb plasticity model were also carried out for comparison purposes. All analyses were displacement-controlled and the applied vertical load was calculated from the nodal reaction forces.

A general layout of the anchor problem is shown in Figure 8.38. The ultimate pullout capacity (Q_u) of an anchor can be expressed as a function of the following factors:

$$Q_u = f(H/B, S_u, OCR, \sigma_o) \tag{8.10}$$

where H is the depth of embedment measured from the surface of the ground to the bottom of the anchor plate, B is the width of the anchor plate, S_u is the undrained shear strength of the soil (in the case of undrained analysis), OCR represents the stress history of the soil and σ_o is the isotropic initial stresses.

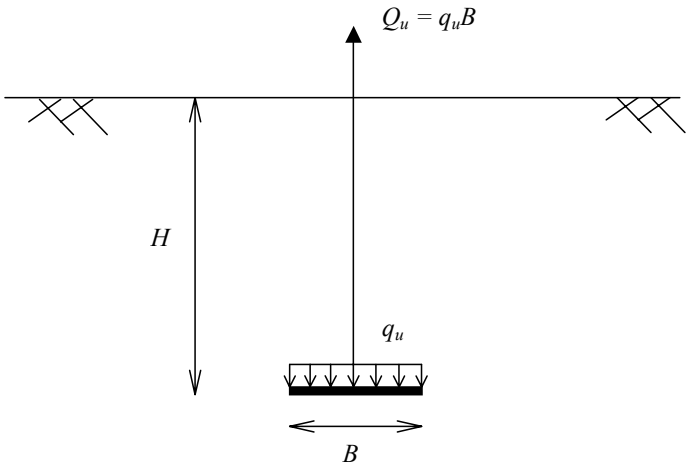

Figure 8.38. Layout of horizontal strip anchor

For simplicity, the anchor was assumed to be thin and perfectly rigid. The analysis assumed a plane strain condition (i.e. the anchor was considered to be an infinite strip). The finite element mesh (which consists of six-noded linear strain triangle elements) and its associated boundary conditions are shown in Figure 8.39.

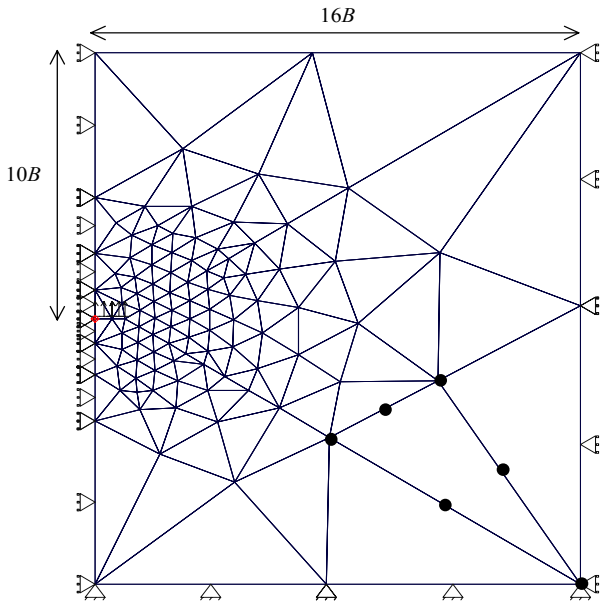

Figure 8.39. Finite element mesh for the horizontal anchor problem (H/B=10)

8.5.2. Horizontal strip anchors in undrained London clay using CASM

The average applied pressure (q_u) required to cause undrained failure of an anchor in a saturated clay can be expressed in the following form:

$$q_u = N_c S_u + \sigma_o \tag{8.11}$$

where S_u is the undrained shear strength of the clay, σ_o is the initial stress and N_c is the breakout factor which should depend on the embedment ratio and *OCR*.

Finite element analyses were carried out to solve the anchor problem with different embedment ratios (*H/B*=1 to 12) and stress histories (*OCR*=1 to 20). Figures 8.40 and 8.41 present the finite element results obtained from these analyses.

Figure 8.40 shows the load displacement curves for the cases with *H/B*=6 and *OCR*=2 (q_v is the applied average vertical pressure). It is clear that with a vertical displacement of 30% of the anchor width, the limit load is not reached in some cases such as those with heavily overconsolidated soils (Figure 8.40a) and those with deeper anchors (Figure 8.40b).

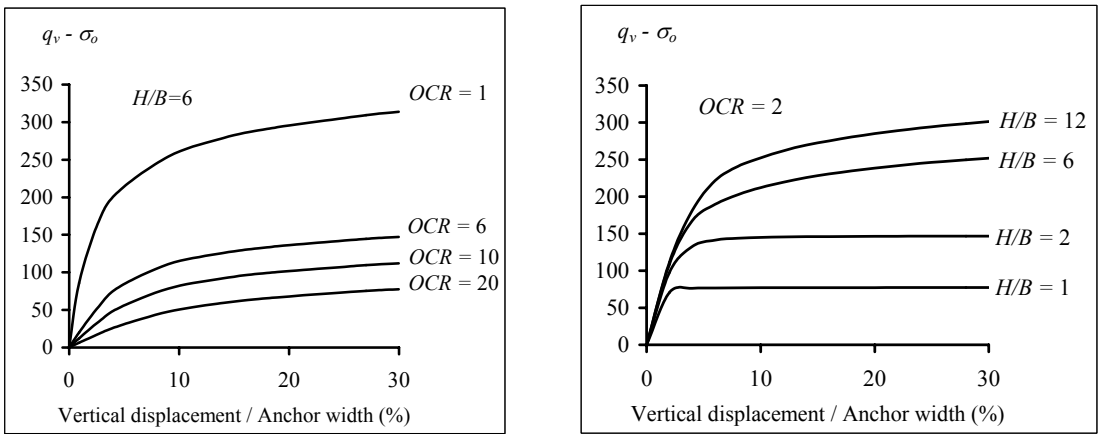

(a) (b)

Figure 8.40. Load displacement curves for strip anchors

Figure 8.41 summarises the breakout factor (N_c) as a function of the embedment ratios and *OCR* values. It should be noted that the value of N_c in this figure is calculated when the vertical displacement is 30% of the anchor width. Again, it can be seen that for

heavily overconsolidated clays (Figure 8.41a) and deeper anchors (Figure 8.41b) critical states are reached after larger displacements. The results are presented in charts so that they may be used directly in hand calculations for estimating the failure load of undrained strip anchors.

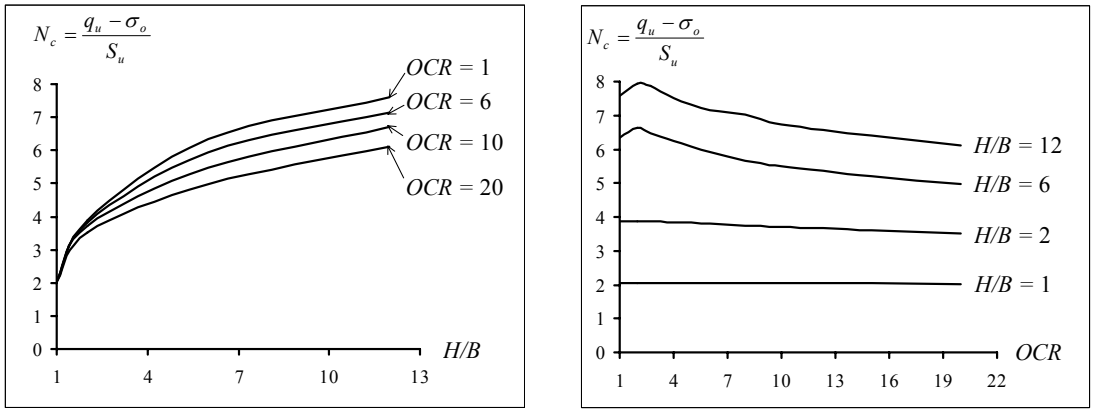

(a) (b)

Figure 8.41. Dependence of breakout factor on embedment ratio (a) and *OCR* (b)

It is evident from Figure 8.41 that the limit load of horizontal strip anchors is not only dependent on the embedment ratio but also on the stress history of the soil (i.e. the *OCR*).

8.5.3. Horizontal strip anchors in drained Ticino sand using CASM

The procedure described in the previous section is repeated here for sand. However, the initial state parameter (ξ_o) was used instead of the overconsolidation ratio (*OCR*).

It has been mentioned earlier that the state parameter can be regarded as a better quantity than the overconsolidation ratio for describing soil response under various loading conditions, especially for sands. Analyses have been carried out with Ticino sand having initial state parameters (ξ_o) of 0.02, 0.0, -0.02, -0.04, -0.06 and -0.08.

Firstly, the anchor behaviour was analysed using the Mohr-Coulomb model. A sensitivity study has shown that varying the value of the dilation angle did not affect the anchor collapse load. Hence, only the results obtained using a fully associated flow rule

are presented here (where the angle of friction ϕ = angle of dilation ψ = 30°). The anchor capacity factor as a function of the embedment ratio is plotted in Figure 8.42. The cavity expansion solution by Yu (2000) is also shown for comparison. It can be seen that the finite element results are slightly lower than the results obtained from cavity expansion theory, this is as expected because the cavity expansion results are known to be very similar to the upper bound solutions (Yu, 2000).

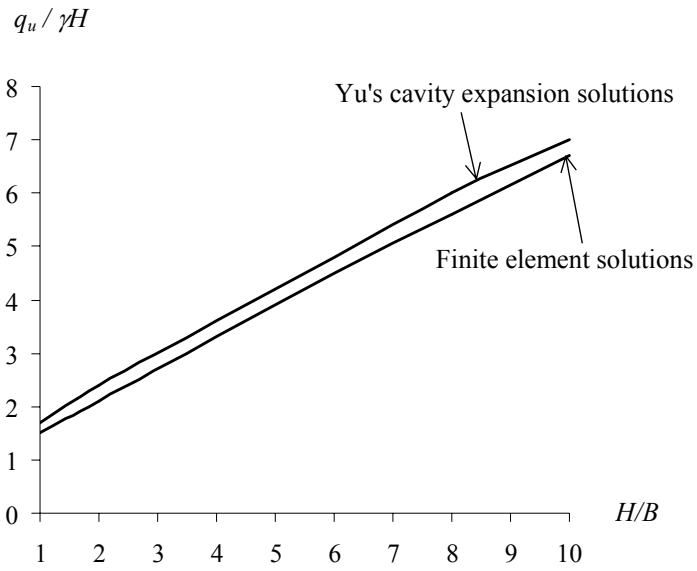

Figure 8.42. Capacity factor vs. embedment ratio, Mohr-Coulomb model

Finite element analysis of behaviour of anchors in Ticino sand using CASM was also carried out. The results are shown in Figures 8.43 and 8.44.

Figure 8.43 presents the load displacement curves for the cases with H/B=1 (Figure 8.43a) and ξ_o=-0.02 (Figure 8.43b) respectively. It should be noted that the results shown in Figure 8.43a were obtained by assuming that the soil samples had different initial stresses due to different initial state parameters. Unlike clay, anchors buried in sand collapse at smaller deformations. However, the results still show that for deep anchors and dense sands, it would require a relatively larger deformation to reach the collapse loads than that required for shallow anchors and loose sands.

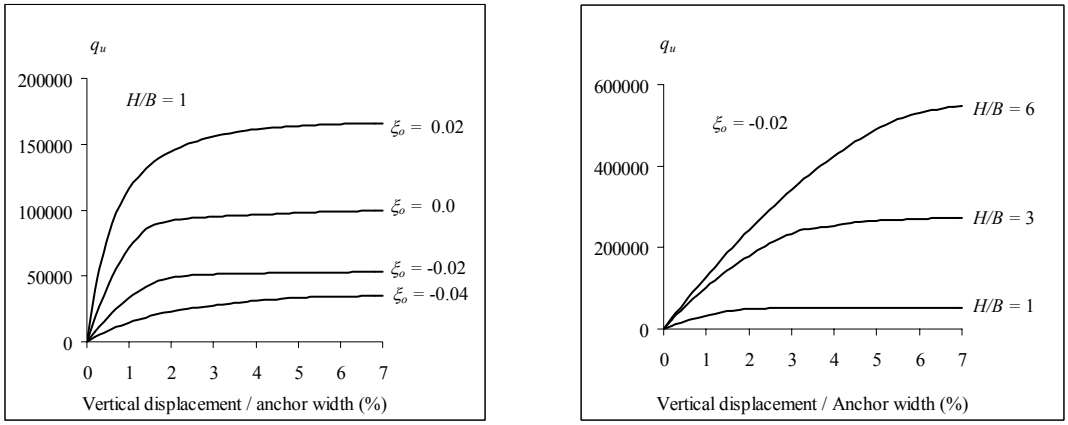

(a) (b)

Figure 8.43. Load displacement curves for sands, CASM

A summary of all the results for anchors in sand is shown in Figure 8.44. The limit load is plotted as a function of the embedment ratio (Figure 8.44a) and the initial state parameter (Figure 8.44b). The limit load (q_u) is normalised by the initial stress (p_i). For a given value of ξ_o, the capacity factor (N_q=q_u/p_i) increases linearly with the embedment ratio (H/B) and N_q also increases as the sand increases in density. Again, Figure 8.44 can be used directly in hand calculations to estimate the failure load of horizontal anchors in sand.

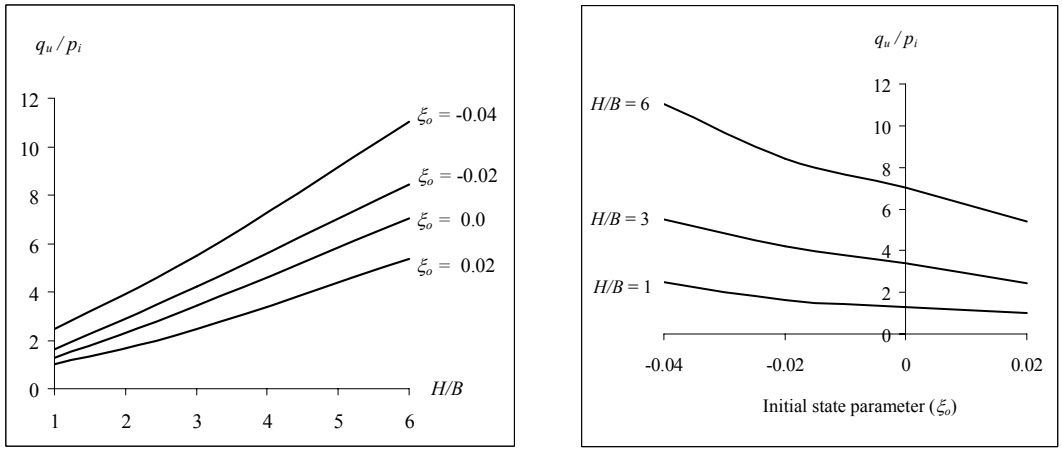

(a) (b)

Figure 8.44. Capacity factor vs. embedment ratio and initial state parameter using CASM

8.6. PAVEMENT ANALYSIS USING CASM-c

8.6.1. Introduction to the problem

The purpose of a pavement is to support loads induced by traffic and to distribute these loads safely to the foundation. In this section, CASM-c is used to model the behaviour of an unpaved pavement. This hypothetical pavement has two different layers of material: a layer of drained Ticino sand on top of a 1200 mm layer of drained London clay. This is another typical geotechnical engineering problem, analysing this problem demonstrates the ability of CASM-c to model the behaviour of both clay and sand under cyclic loading conditions.

Consider a wheel with a load of 600 kPa and a width of 150 mm was cyclically loaded 500 times. The sand was assumed to be dense with the initial state parameter ξ_o=-0.02, while the clay was assumed to be heavily overconsolidated with an *OCR*=10.

Three different sand layer thicknesses of 300 mm, 400 mm and 500 mm were modelled. The layout of the problem and the finite element mesh for the 300 mm case are shown in Figures 8.45 and 8.46 respectively. The mesh consisted of fifteen-noded cubic strain triangle elements and this problem was considered to be axis-symmetric. A sensitivity study of the size of the finite element mesh was carried out and it was found that the dimensions shown in Figure 8.46 kept the number of elements to a manageable size whilst also giving stable results.

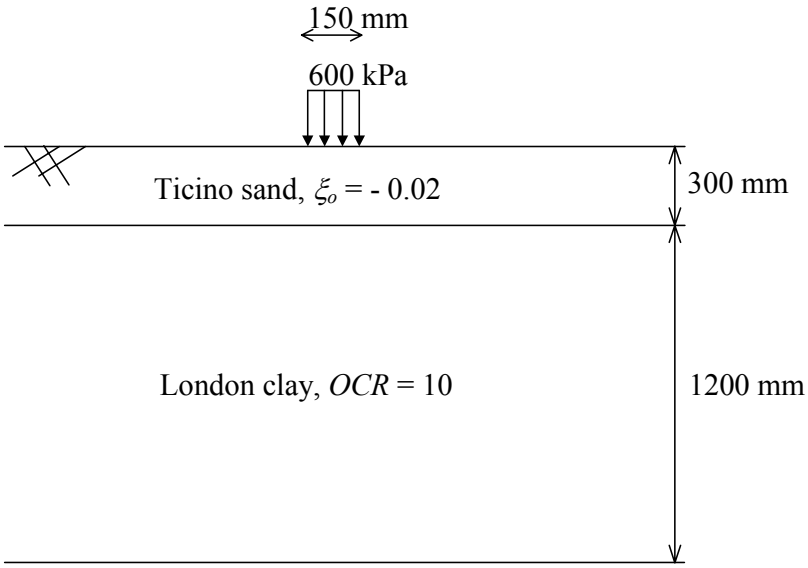

Figure 8.45. Layout of the pavement problem with 300 mm of sand

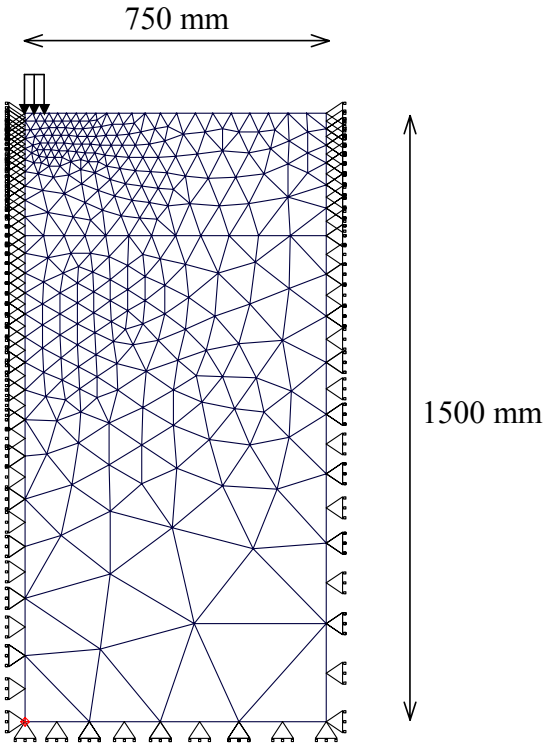

Figure 8.46. Finite element mesh for the pavement problem with 300 mm of sand

It is noted that the new parameter m was set equal to 2.0 for London clay in these analyses. The values of all other parameters are shown in Table 8.1. The three analyses carried out were stress-controlled.

8.6.2. Analysis of two layers pavement using CASM-c

Figure 8.47 summarises all the results of the analysis of the two layered pavement problem where the vertical permanent deformation is plotted against the number of cycles of loading. It can be seen that the permanent deformation is a function of the thickness of the granular layer. The thicker the layer of sand is, the less deformation will occur.

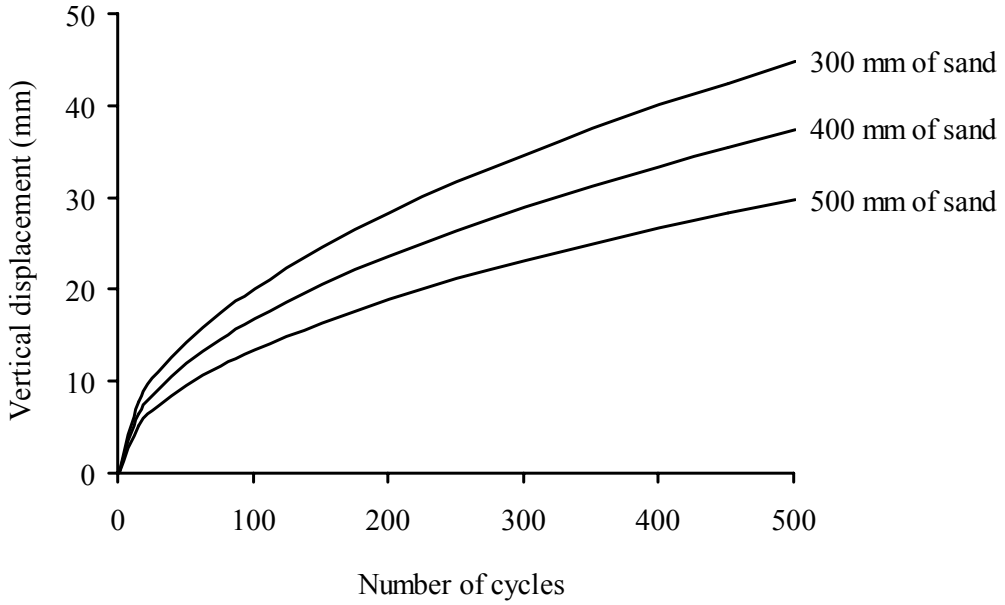

Figure 8.47. Vertical deformation versus number of cycles for two layers pavement

8.7. SUMMARY

Some applications of CASM, CASM-b and CASM-c have been presented in this chapter. A variety of typical boundary value problems have been analysed and it has been shown that CASM and its extensions can satisfactorily model all the problems encountered. They have proven themselves to be very robust and useful tools for solving a wide range of practical geotechnical problems under different loading conditions. The following conclusions can be made:

The analysis of the infinite length to diameter ratio ($L/D=\infty$) pressuremeter has been carried out using CASM. The results have shown that the conventional total stress

analysis, which uses elastic perfectly plastic models, tends to overestimate the mobilised undrained shear strength of overconsolidated clays. The overestimation increases with the value of the overconsolidation ratio (*OCR*). It is therefore essential to adopt an effective stress analysis with a realistic soil model for solving undrained problems involving overconsolidated clays.

The effect of the geometry on the interpretation of the pressuremeter test has been investigated using CASM. The conventional methods of pressuremeter analysis do not take into account the effect of the two-dimensional pressuremeter geometry and as a result, the undrained shear strength values derived from field tests can be significantly higher than the true value. The results have been presented as correction factors so that they may be directly applied to field test results to account for the geometry effects. It has been shown that the overconsolidation ratio has a significant effect on the overestimation of shear strength caused by neglecting the actual pressuremeter geometry. The strain range over which the shear strength is deduced also has some effects on the correction factors. A comparison of the results of this study with those of earlier studies using total stress analysis with perfectly plastic models has suggested that the overestimation predicted by critical state models was generally not as large as that predicted by elastic-perfectly plastic soil models. This is particularly true for heavily overconsolidated clays where *OCR* values are high.

The analyses of surface rigid strip and circular footings resting upon undrained London clay and drained Ticino sand with different stress histories have been carried out using CASM and CASM-b. The results obtained from using an elastic perfectly plastic model for undrained clay have been shown to be only a special case of the results obtained from critical state models which use an effective stress approach. Strip and circular footings have been found to behave very similarly. However, the bearing capacity of a circular footing is slightly higher than that of a strip footing. The load displacement curves show that at a vertical displacement of 15% of the footing width (or diameter), the ultimate strength of the soil has not mobilised for heavily overconsolidated clays and dense sands. It has been also found that the bearing capacity of the footings was markedly dependent upon the stress history of the soil. CASM-b has given a more conservative bearing capacity for the strip footing because the soil is assumed to be softer inside the bounding surface in this model.

The problem of horizontal strip anchors in undrained London clay and drained Ticino sand has been analysed. It has been found that deep anchors and heavily overconsolidated soils required a relatively larger deformation in order to reach the collapse loads when compared to shallow anchors and lightly overconsolidated soils. It has also been found that the limit load of anchors was a function of both the stress history of the soil as well as the embedment ratio (H/D).

CASM-c has been used to model the behaviour of a hypothetical pavement. The pavement consists of a layer of drained Ticino sand on top of a layer of drained London clay. The ability of CASM-c to predict the behaviour of both clay and sand under cyclic loading conditions has been illustrated. Three different thicknesses of the sand layer have been simulated. Permanent deformation of the pavement has been found to be a function of the thickness of the sand layer. The thicker the sand layer is, the less permanent deformation will occur.

All the results in this chapter have been presented as design charts whenever possible so that they can be used in hand calculation designs. However, it should be noted that the main purpose of the analyses in this chapter is to illustrate the prediction capabilities of CASM and its extensions. Hence, more rigorous numerical analyses and comparisons with experimental data are needed before the results can be incorporated into any design guide.

CHAPTER 9

CONCLUSIONS AND RECOMMENDATIONS

9.1. SUMMARY AND CONCLUSIONS

The work described in this thesis has three objectives:

1. *To incorporate a unified critical state model (CASM) into a finite element code.*
2. *To extend CASM by incorporating a new non-linear elasticity rule, the combined hardening concept and the bounding surface plasticity theory.*
3. *To evaluate and apply CASM and its extensions to analyse a variety of typical boundary value problems in geotechnical engineering.*

In the following sections, the conclusions that can be drawn from this research are summarised to demonstrate how these objectives were achieved.

9.1.1. Finite element implementation of CASM into CRISP

To evaluate its adequacy, CASM had to be implemented into a finite element code. A finite element package called CRISP (CRitical State soil mechanics Program) was chosen. This program was introduced mainly to incorporate the critical state type of constitutive models.

In Chapter 4, the process of incorporating CASM into CRISP was described. This included the formulation of the model in the three-dimensional stress space, computer implementation and verification of the model. The shapes of the yield and plastic potential surfaces in the deviatoric plane were chosen and justified using experimental and numerical evidence.

CASM was validated by comparing its finite element results with a series of classical triaxial test results and also the finite element results obtained from the original Cam-clay model. It was found that the predictions by CASM were consistently better than those from Cam-clay for normally and overconsolidated clays under both drained and undrained loading conditions. In particular, CASM has been found to be able to capture reasonably well the overall behaviour of overconsolidated clay and sand observed in the laboratory.

9.1.2. New non-linear elasticity rule

Also in Chapter 4, a new non-linear elastic rule used for clay materials proposed by Houlsby and Wroth (1991) was adopted for CASM and its extensions. This new rule provides a realistic variation of the shear modulus with pressure and the overconsolidation ratio. A second advantage is that the rigidity index (G/S_u), which plays an important role in many geotechnical engineering analyses, can be expressed as a power function of the overconsolidation ratio.

9.1.3. New combined volumetric-deviatoric hardening model, CASM-d

In Chapter 5, a new combined volumetric-deviatoric hardening model called CASM-d was proposed. The new model assumes that the work of the deviatoric stresses also gives an additional contribution to hardening. A new parameter (α) was introduced and the new model can be reduced to the original CASM by setting α equal to zero.

CASM-d was generalised into the three-dimensional stress space and then successfully implemented into CRISP. Its performance when analysing the triaxial tests was shown by its comparisons with results obtained from the original model CASM and

observational data. It was found that the deviatoric contribution from hardening made a profound difference on the performance of the new model. In particular, one very important behaviour of normally consolidated clays and loose sands can be predicted by CASM-d. This is the reappearance of the hardening behaviour once the material has softened. Experimental data was used to confirm this feature of soil behaviour.

9.1.4. New bounding surface model, CASM-b

In Chapter 6, a new model called CASM-b was proposed. It is formulated based on the bounding surface plasticity theory. Two new parameters (h and m) are introduced in the new model. A sensitivity study of the new parameters was carried out. The new features of this model only apply when analysing overconsolidated materials, CASM-b will give the same results as CASM when the soil is normally consolidated.

The generalisation into the three-dimensional stress space and the implementation of CASM-b into CRISP were presented. The derivation of the hardening modulus was described in detail because this is the most important new feature of CASM-b. Simulations of the triaxial tests on overconsolidated clays and sands were carried out to validate and assess the performance of CASM-b. It was found that CASM-b gave better predictions than those predicted by CASM and other traditional elastic-plastic models when the stress state of the soil is inside the bounding surface. This was achieved due to the fact that there was not a sudden change from the elastic to plastic behaviour of the soil in CASM-b. In other words, CASM-b could smooth the stress-strain curves to give more realistic predictions of soil behaviour.

9.1.5. New cyclic bounding surface model, CASM-c

In Chapter 7, a new cyclic bounding surface model called CASM-c was proposed. The bounding surface model in Chapter 6 was extended further to give CASM-c. The new important feature of CASM-c is its ability to model soil behaviour under cyclic loading conditions. For static loading conditions, CASM-c gives the same results as CASM-b. When compared to CASM-b, there are three extra parameters (H_U, H_U and k) introduced in this new model, these are used to control the unloading behaviour, the reloading

behaviour and the shakedown behaviour of the soil. A parametric study of the three new parameters was carried out. It was found that CASM-b was very flexible in predicting the behaviour of soil.

The new model was generalised into the three-dimensional stress space and then successfully implemented into CRISP. Three sets of cyclic triaxial tests were used to compare with the simulation results predicted by CASM-c. The tests were chosen so that CASM-c could be validated and its performance could be assessed by a variety of materials under different cyclic loading conditions. It was found that CASM-c could satisfactorily predict the overall behaviour of both clay and sand under different cyclic loading conditions.

9.1.6. Applications of CASM, CASM-b and CASM-c to boundary value problems

In Chapter 8, some applications of CASM, CASM-b and CASM-c were presented. A variety of problems were analysed, namely the analysis of the pressuremeter test, surface rigid strip and circular footings, horizontal strip anchors and a pavement under cyclic loading. It was shown that CASM and its extensions can satisfactorily model all the practical problems encountered. They proved themselves to be very robust and useful tools for solving a wide range of practical geotechnical problems under different loading conditions.

By using the effective stress analysis approach, the effect of stress history on the behaviour of soils under both drained and undrained loading conditions was investigated with deep interest. It was found that the stress history of the soil had a significant effect on the computed solutions of all the problems analysed. Such an effect cannot be easily taken into account using a total stress formulation analysis.

9.2. RECOMMENDATIONS FOR FUTURE WORK

The numerical examples presented in this study have demonstrated the very good predictive capabilities of CASM and its extensions for various aspects of soil behaviour. However, detailed parametric, laboratory and field studies are still required before the general validity of these models can be fully established.

9.2.1. Further modifications

CASM-d in Chapter 5 needs to be modified so that the critical state can be reached. One way of doing this is to make an assumption about the dependence of the new parameter α upon the state of the soil. By assuming that α decays towards zero as the stress ratio approaches the M value, the size of the yield surface will stop increasing at failure and therefore a critical state for the soil could be reached. The following expression of the hardening law could be used to overcome this problem (Liu, 2004):

$$\delta p'_o = \frac{v p'_o}{(\lambda - \kappa)} \left[\delta \varepsilon_p^p + \alpha \left| \frac{M - \eta}{M} \right| \delta \varepsilon_q^p \right] \tag{9.1}$$

In Chapter 6, new relationships between the hardening modulus at the current stress point inside the bounding surface (H) and the hardening modulus at its image stress point on the bounding surface (H_j) should be studied more carefully. The currently used relationship needs two new parameters in order to function, this could be reduced to one. A new good relationship will help the predictive capability of the model inside the bounding surface significantly.

A few modifications could be done to improve the cyclic model (CASM-c) in Chapter 7. The model currently needs three new parameters (H_U, H_R and k). Future studies should be focused on reducing this to two or one parameter. The theoretical derivations of these new parameters should be also obtained. At the moment, the new parameters are chosen arbitrarily to fit the triaxial observational data and then the chosen parameters are implemented into the finite element program to solve boundary value problems. Efforts should be made to understand the nature of these parameters so that they may be directly measured in the laboratory or correlated to other measurable

parameters. Finally, other improved definitions of the hardening modulus for different load cases could be studied based on the constraints set out by the bounding surface plasticity theory.

9.2.2. New flow rules

It is shown in section 7.3.2.1 that the current flow rule which follows the stress-dilatancy relation by Rowe (1962) does not accurately predict the behaviour of all types of materials (Speswhite kaolin in this case). Hence, it is felt that for CASM, new more flexible flow rules are needed. Yu (2003) has proposed a new simple stress-dilatancy relation:

$$\frac{\delta\varepsilon_p^p}{\delta\varepsilon_q^p} = \frac{M^n - \eta^n}{c\,\eta^{n-1}} \tag{9.2}$$

where n is the familiar CASM parameter and c is a quantity which can be analytically derived from other basic parameters.

It is interesting to note that the original Cam-clay flow rule can be reduced from this new flow rule by having n=1 and c=1 and also the modified Cam-clay flow rule can be obtained by substituting n=2 and c=2 into equation 9.2. By integrating equation 9.2 we will obtain the following new expression for the plastic potential:

$$G = c\ln\left[1-(1-c)\left(\frac{\eta}{M}\right)^n\right] - n(1-c)\ln\left(\frac{p'}{p'_o}\right) \tag{9.3}$$

The next steps are to generalise equation 9.3 into the three-dimensional stress space and then implement it into a finite element program. It is believed that these new flow rules will significantly improve the performance of CASM due to its generality and flexibility.

9.2.3. Incorporation of the kinematic hardening plasticity theory into CASM

It was mentioned in the literature review that bounding surface theory is only one of two major developments in the field of constitutive modelling over the last 35 years. The other is the kinematic hardening plasticity theory or multi-surface theory which was first introduced by Mroz (1967) and Iwan (1967). This concept is much more complicated than the bounding surface concept both mathematically and numerically. However, some very important behaviours of soils can only be reproduced by this type of models; for example, the capability to model both anisotropy and the effect of the stress history of the soil.

Some initial work has been done to incorporate the kinematic hardening concept into CASM. The new model, called CASM-k, has been proposed and generalised into the three-dimensional stress space. The formulations for this new model can be found in Appendix B. However, due to the constraint of time and some numerical difficulties encountered, CASM-k has not been validated. Therefore, work on this model should be carried out in future studies.

APPENDIX A. MATERIAL CONSTANTS

The following table lists the model constants of all the soils used for analyses in this thesis. The soils are very common and their properties and behaviour are readily available in the literature. Critical state constants for these soils are adopted from the literature. Other constants for use in CASM and its extensions are typical values chosen by the author.

	M	λ	κ	μ	Γ	n	r	h	m	H_U	H_R	k
London clay	0.89	0.161	0.062	0.3	2.759	2.0	2.718	5.0	varies	0.15	0.05	5.0
Weald clay	0.9	0.093	0.025	0.3	2.06	4.5	2.718	5.0	1.5	N/A	N/A	N/A
Speswhite kaolin clay	0.86	0.19	0.03	0.3	3.056	2.0	2.718	5.0	1.0	0.15	0.5	30
Li&Meissner clay	0.772	0.173	0.034	0.3	2.06	2.0	2.718	5.0	1.0	0.3	0.1	varies
Ticino sand	1.3	0.04	0.01	0.3	1.986	2.0	4.0	30.0	3.0	0.5	0.1	20.0
Erksak sand	1.2	0.0135	0.005	0.3	1.8167	4.0	6792	10.0	2.0	N/A	N/A	N/A
Ottawa sand	1.19	0.0168	0.005	0.3	2.06	3.0	varies	N/A	N/A	N/A	N/A	N/A
Fuji river sand	1.5	0.12	0.01	0.3	1.467	4.5	10.0	5.0	1.0	0.4	0.3	varies

Table A.1. Material constants

APPENDIX B. PROPOSED TRIAXIAL FORMULATIONS FOR CASM-k

B.1. Bounding surface

$$F = \left(\frac{q}{Mp'} \right)^n + \frac{\ln\left(\frac{p'}{p'_o} \right)}{\ln r} \tag{B.1}$$

B.2. Yield surfaces

$$f_1 = \left(\frac{q - q_\alpha}{M(p' - p'_\alpha)} \right)^n + \frac{\ln\left(\frac{p' - p'_\alpha}{S \times p'_o} \right)}{\ln r} \tag{B.2}$$

$$f_2 = \left(\frac{q - q'_\alpha}{-M(p' - p'_\alpha)} \right)^n + \frac{\ln\left(\frac{p' - p'_\alpha}{S \times p'_o} \right)}{\ln r} \tag{B.3}$$

where:

$S\ (\leq 1)$ Size ratio between the yield surface and the bounding surface at initial stress. When S is equal to 1, CASM is recovered.

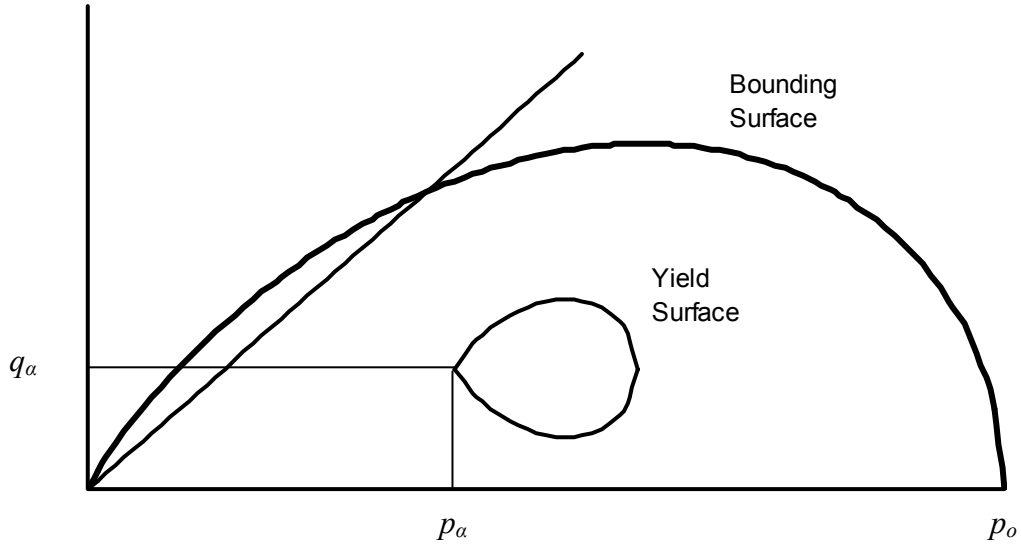

Figure B.1. Bounding surface and yield surface of CASM-k

B.3. Plastic potential

$$G(\sigma,\beta)=3M\left(\ln p'-\ln\beta\right)+\left(3+2M\right)\ln\left(\frac{2q+3p'}{p'}\right)-\left(3-M\right)\ln\left(\frac{3p'-q}{p'}\right) \qquad \text{(B.4)}$$

B.4. Elastic properties

Inside the yield surface, the material is assumed to be the same as the standard Cam-clay models.

B.5. Translation rules

The translation of the yield surface is assumed to be separated into two components. The first part is associated with change in stress state which necessitates an alteration in the position of the yield surface in order to ensure that the stress point still lies on the yield surface. The second is associated with the simultaneous change in geometry of the yield and bounding surfaces.

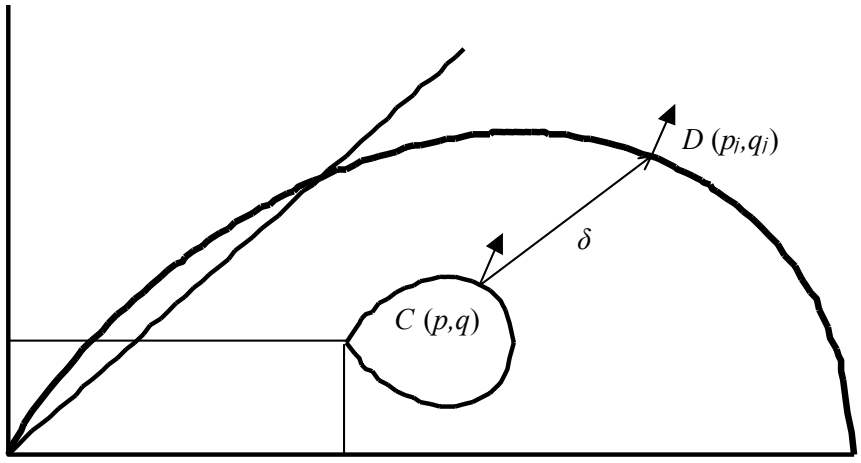

Figure B.2. Translation rules of CASM-k

The yield surface moves such that it translates within the bounding surface, following the rule that guarantees the yield and bounding surface can touch at a common tangent, but never intersect. This rule states the yield surface should move along a vector β,

which joins the current stress state, $C(p,q)$ to its conjugate point on the bounding surface, $D(p_j,q_j)$. Both points C and D have the same direction of the outward normal.

$$\begin{bmatrix} \delta p'_{\alpha} \\ \delta q_{\alpha} \end{bmatrix} = A \times \beta \tag{B.5}$$

where A is a scalar quantity to be determined once the full expression for the translation rule is obtained.

We have

$$\beta = \left(p'_{j}, q_{j}\right) - \left(p', q\right) \tag{B.6}$$

Because the points C and D have the same outward normal, the lines from these points to the origins (0,0) and (p'_{α},q_{α}), respectively, have the same slopes. Hence, from geometry:

$$\left(p', q\right) - \left(p'_{\alpha}, q_{\alpha}\right) = S\left\{\left(p'_{j}, q_{j}\right) - \left(0,0\right)\right\} \tag{B.7}$$

Combine (5) and (6), we have:

$$\beta = \begin{bmatrix} \dfrac{p' - p'_{\alpha}}{S} - p' \\ \dfrac{q - q_{\alpha}}{S} - q \end{bmatrix} \tag{B.8}$$

Hence,

$$\begin{bmatrix} \delta p'_{\alpha} \\ \delta q_{\alpha} \end{bmatrix} = A \times \begin{bmatrix} \dfrac{p' - p'_{\alpha}}{S} - p' \\ \dfrac{q - q_{\alpha}}{S} - q \end{bmatrix} \tag{B.9}$$

The second part of the translation of the yield surface represents the entire translation when the yield and bounding surfaces are in contact at the current stress point. In this case vector β is equal to zero. The translation of (p'_{α},q_{α}) by an amount $(\delta p'_{\alpha},\delta q_{\alpha})$ is related to the expansion of the bounding surface δq_o as the following expression:

$$\begin{bmatrix} \delta p'_{\alpha} \\ \delta q_{\alpha} \end{bmatrix} = \frac{\delta p'_{o}}{p_{o}} \begin{bmatrix} p'_{\alpha} \\ q_{\alpha} \end{bmatrix} \tag{B.10}$$

Hence, the full expression for the translation rule become:

$$\begin{bmatrix} \delta p'_{\alpha} \\ \delta q_{\alpha} \end{bmatrix} = \frac{\delta p'_{o}}{p'_{o}} \begin{bmatrix} p'_{\alpha} \\ q_{\alpha} \end{bmatrix} + A \times \begin{bmatrix} \frac{p'-p'_{\alpha}}{S} - p' \\ \frac{q-q_{\alpha}}{S} - q \end{bmatrix} \tag{B.11}$$

Consistency condition states that:

$$df = \frac{\delta f}{\delta p'}\delta p' + \frac{\delta f}{\delta q}\delta q + \frac{\delta f}{\delta p'_{\alpha}}\delta p'_{\alpha} + \frac{\delta f}{\delta q_{\alpha}}\delta q_{\alpha} + \frac{\delta f}{\delta p'_{o}}\delta p'_{o} = 0 \tag{B.12}$$

where:

$$\frac{\delta f_1}{\delta p'} = \frac{-n}{(p'-p'_{\alpha})^{n+1}}\left(\frac{q-q_{\alpha}}{M}\right)^{n} + \frac{1}{(p'-p'_{\alpha})\ln r}$$

$$\frac{\delta f_1}{\delta q} = n(q-q_{\alpha})^{n-1}\left(\frac{1}{M(p'-p'_{\alpha})}\right)^{n}$$

$$\frac{\delta f_1}{\delta p'_{\alpha}} = \frac{n}{(p-p_{\alpha})^{n+1}}\left(\frac{q-q_{\alpha}}{M}\right)^{n} - \frac{1}{(p'-p'_{\alpha})\ln r} = -\frac{\delta f_1}{\delta p'}$$

$$\frac{\delta f_1}{\delta q_{\alpha}} = -n(q-q_{\alpha})^{n-1}\left(\frac{1}{M(p'-p'_{\alpha})}\right)^{n} = -\frac{\delta f_1}{\delta q}$$

$$\frac{\delta f_1}{\delta p'_{o}} = -\frac{1}{p'_{o}\ln r}$$

So,

$$\left[\frac{-n}{(p'-p'_\alpha)}\left(\frac{q-q_\alpha}{M(p'-p'_\alpha)}\right)^n+\frac{1}{(p'-p'_\alpha)\ln r}\right](\delta p'-\delta p'_\alpha)+\left(\frac{q-q_\alpha}{M(p'-p'_\alpha)}\right)^n\frac{n}{(q-q_\alpha)}(\delta q-\delta q_\alpha)$$
$$-\frac{\delta p'_o}{p'_o\ln r}=0$$

Substituting value of δp_α and δp_α into the above we have:

$$X_1\left[\delta p'-\frac{\delta p'_o}{p'_o}p'_\alpha-A_2\left(\frac{p'-p'_\alpha}{S}-p'\right)\right]+Y_1\left[\delta q-\frac{\delta p'_o}{p'_o}q_\alpha-A_2\left(\frac{q-q_\alpha}{S}-q\right)\right]-\frac{\delta p'_o}{p'_o\ln r}=0$$

where:

$$X_1=\left[\frac{-n}{(p'-p'_\alpha)}\left(\frac{q-q_\alpha}{M(p'-p'_\alpha)}\right)^n+\frac{1}{(p'-p'_\alpha)\ln r}\right]$$

$$Y_1=\left(\frac{q-q_\alpha}{M(p'-p'_\alpha)}\right)^n\frac{n}{(q-q_\alpha)}$$

So,

$$A_1=\frac{-\frac{\delta p'_o}{p'_o\ln r}+X_1\left(\delta p'-\frac{\delta p'_o}{p'_o}p'_\alpha\right)+Y_1\left(\delta q-\frac{\delta p'_o}{p'_o}q_\alpha\right)}{X_1\left(\frac{p'-p'_\alpha}{S}-p'\right)+Y_1\left(\frac{q-q_\alpha}{S}-q\right)} \qquad \text{(B.13)}$$

where:

$$\frac{\delta f_2}{\delta p'}=\frac{-n}{(p'-p'_\alpha)^{n+1}}\left(\frac{q-q_\alpha}{-M}\right)^n+\frac{1}{(p'-p'_\alpha)\ln r}$$

$$\frac{\delta f_2}{\delta q}=n(q-q_\alpha)^{n-1}\left(\frac{1}{-M(p'-p'_\alpha)}\right)^n$$

$$\frac{\delta f_2}{\delta p'_\alpha}=\frac{n}{(p'-p'_\alpha)^{n+1}}\left(\frac{q-q_\alpha}{-M}\right)^n-\frac{1}{(p'-p'_\alpha)\ln r}=-\frac{\delta f_2}{\delta p'}$$

$$\frac{\delta f_2}{\delta q'_\alpha} = -n(q-q_\alpha)^{n-1}\left(\frac{1}{-M(p'-p'_\alpha)}\right)^n = -\frac{\delta f_2}{\delta q}$$

$$\frac{\delta f_2}{\delta p'_o} = -\frac{1}{p'_o \ln r}$$

So,

$$\left[\frac{-n}{(p'-p'_\alpha)}\left(\frac{q-q_\alpha}{M(p'-p'_\alpha)}\right)^n + \frac{1}{(p'-p'_\alpha)\ln r}\right](\delta p'-\delta p'_\alpha) + \left(\frac{q-q_\alpha}{M(p'-p'_\alpha)}\right)^n \frac{n}{(q-q_\alpha)}(\delta q-\delta q_\alpha)$$
$$-\frac{\delta p'_o}{p'_o \ln r} = 0$$

Substituting value of $\delta p'_\alpha$ and $\delta p'_\alpha$ into the above we have:

$$X_2\left[\delta p'-\frac{\delta p'_o}{p'_o}p'_\alpha - A_2\left(\frac{p'-p'_\alpha}{S}-p'\right)\right] + Y_2\left[\delta q-\frac{\delta p'_o}{p'_o}q_\alpha - A_2\left(\frac{q-q_\alpha}{S}-q\right)\right] - \frac{\delta p'_o}{p'_o \ln r} = 0$$

where:

$$X_2 = \left[\frac{-n}{(p'-p'_\alpha)}\left(\frac{q-q_\alpha}{-M(p'-p'_\alpha)}\right)^n + \frac{1}{(p'-p'_\alpha)\ln r}\right]$$

$$Y_2 = \left(\frac{q-q_\alpha}{-M(p'-p'_\alpha)}\right)^n \frac{n}{(q-q_\alpha)}$$

So,

$$A_2 = \frac{-\frac{\delta p'_o}{p'_o \ln r} + X_2\left(\delta p'-\frac{\delta p'_o}{p'_o}p'_\alpha\right) + Y_2\left(\delta q-\frac{\delta p'_o}{p'_o}q_\alpha\right)}{X_2\left(\frac{p'-p'_\alpha}{S}-p'\right) + Y_2\left(\frac{q-q_\alpha}{S}-q\right)} \qquad \text{(B.14)}$$

B.6. Hardening rules

$$\Delta\sigma = D^{ep}\Delta\varepsilon$$

$$D^{ep} = D^e - \frac{D^e \frac{\partial G}{\partial \sigma}\left[\frac{\partial F}{\partial \sigma}\right]^T D^e}{\left[\frac{\partial F}{\partial \sigma}\right]^T D^e \frac{\partial G}{\partial \sigma} + H}$$

$$H_D = \frac{\mu}{(\lambda - \kappa)\ln r}\left(\frac{9 + 6M}{3p'_j + 2q_j} - \frac{9 - 3M}{3p'_j - q_j}\right)$$

$$H = H_D + \frac{h}{p'}(\delta)^m$$

where:

h	The new material constant (similar to CASM-b)
δ	The distance between the current stress point and the conjugate point ($\|CD\|$ in Figure B.2).
m	A new material constant for CASM-k

B.7. First derivatives of yield surfaces

$$\frac{\partial f_1}{\partial \sigma} = \frac{\partial f_1}{\partial p'}\frac{\partial p'}{\partial \sigma} + \frac{\partial f_1}{\partial q}\frac{\partial q}{\partial \sigma}$$

$$\frac{\delta f_1}{\delta p'} = \frac{-n}{(p' - p'_\alpha)^{n+1}}\left(\frac{q - q_\alpha}{M}\right)^n + \frac{1}{(p' - p'_\alpha)\ln r}$$

$$\frac{\delta f_1}{\delta q} = n(q - q_\alpha)^{n-1}\left(\frac{1}{M(p' - p'_\alpha)}\right)^n$$

$$\frac{\partial p'}{\partial \sigma} = \frac{1}{3}\begin{bmatrix}1 & 1 & 1 & 0 & 0 & 0\end{bmatrix}$$

$$\frac{\partial q}{\partial \sigma} = \frac{3}{2q}\begin{bmatrix}(\sigma_x - p') & (\sigma_y - p') & (\sigma_z - p') & 2\tau_{xy} & 2\tau_{zx} & 2\tau_{yz}\end{bmatrix}$$

Hence,

$$\frac{\delta f_1}{\delta \sigma_x} = \frac{1}{3}\left[\frac{-n}{(p'-p'_\alpha)^{n+1}}\left(\frac{q-q_\alpha}{M}\right)^n + \frac{1}{(p'-p'_\alpha)\ln r}\right] + \frac{3}{2q}n(q-q_\alpha)^{n-1}\left(\frac{1}{M(p'-p'_\alpha)}\right)^n(\sigma_x - p')$$

$$\frac{\delta f_1}{\delta \sigma_y} = \frac{1}{3}\left[\frac{-n}{(p'-p'_\alpha)^{n+1}}\left(\frac{q-q_\alpha}{M}\right)^n + \frac{1}{(p'-p'_\alpha)\ln r}\right] + \frac{3}{2q}n(q-q_\alpha)^{n-1}\left(\frac{1}{M(p'-p'_\alpha)}\right)^n(\sigma_y - p')$$

$$\frac{\delta f_1}{\delta \sigma_z} = \frac{1}{3}\left[\frac{-n}{(p'-p'_\alpha)^{n+1}}\left(\frac{q-q_\alpha}{M}\right)^n + \frac{1}{(p'-p'_\alpha)\ln r}\right] + \frac{3}{2q}n(q-q_\alpha)^{n-1}\left(\frac{1}{M(p'-p'_\alpha)}\right)^n(\sigma_z - p')$$

$$\frac{\delta f_1}{\delta \tau_{xy}} = \frac{3}{q}n(q-q_\alpha)^{n-1}\left(\frac{1}{M(p'-p'_\alpha)}\right)^n \tau_{xy}$$

$$\frac{\delta f_1}{\delta \tau_{yz}} = \frac{3}{q}n(q-q_\alpha)^{n-1}\left(\frac{1}{M(p'-p'_\alpha)}\right)^n \tau_{yz}$$

$$\frac{\delta f_1}{\delta \tau_{zx}} = \frac{3}{q}n(q-q_\alpha)^{n-1}\left(\frac{1}{M(p'-p'_\alpha)}\right)^n \tau_{zx}$$

$$\frac{\partial f_2}{\partial \sigma} = \frac{\partial f_2}{\partial p'}\frac{\partial p'}{\partial \sigma} + \frac{\partial f_2}{\partial q}\frac{\partial q}{\partial \sigma}$$

$$\frac{\delta f_2}{\delta p} = \frac{-n}{(p'-p'_\alpha)^{n+1}}\left(\frac{q-q_\alpha}{-M}\right)^n + \frac{1}{(p'-p'_\alpha)\ln r}$$

$$\frac{\delta f_2}{\delta q} = n(q-q_\alpha)^{n-1}\left(\frac{1}{-M(p'-p'_\alpha)}\right)^n$$

$$\frac{\partial p'}{\partial \sigma} = \frac{1}{3}\begin{bmatrix}1 & 1 & 1 & 0 & 0 & 0\end{bmatrix}$$

$$\frac{\partial q}{\partial \sigma} = \frac{3}{2q}\begin{bmatrix}(\sigma_x - p') & (\sigma_y - p') & (\sigma_z - p') & 2\tau_{xy} & 2\tau_{zx} & 2\tau_{yz}\end{bmatrix}$$

Hence,

$$\frac{\delta f_2}{\delta \sigma_x} = \frac{1}{3}\left[\frac{-n}{(p'-p'_\alpha)^{n+1}}\left(\frac{q-q_\alpha}{-M}\right)^n + \frac{1}{(p'-p'_\alpha)\ln r}\right] + \frac{3}{2q}n(q-q_\alpha)^{n-1}\left(\frac{1}{-M(p'-p'_\alpha)}\right)^n(\sigma_x - p')$$

$$\frac{\delta f_2}{\delta \sigma_y} = \frac{1}{3}\left[\frac{-n}{(p'-p'_\alpha)^{n+1}}\left(\frac{q-q_\alpha}{-M}\right)^n + \frac{1}{(p'-p'_\alpha)\ln r}\right] + \frac{3}{2q}n(q-q_\alpha)^{n-1}\left(\frac{1}{-M(p'-p'_\alpha)}\right)^n(\sigma_y - p')$$

$$\frac{\delta f_2}{\delta \sigma_z} = \frac{1}{3}\left[\frac{-n}{(p'-p'_\alpha)^{n+1}}\left(\frac{q-q_\alpha}{-M}\right)^n + \frac{1}{(p'-p'_\alpha)\ln r}\right] + \frac{3}{2q}n(q-q_\alpha)^{n-1}\left(\frac{1}{-M(p'-p'_\alpha)}\right)^n(\sigma_z - p')$$

$$\frac{\delta f_2}{\delta \tau_{xy}} = \frac{3}{q}n(q-q_\alpha)^{n-1}\left(\frac{1}{-M(p'-p'_\alpha)}\right)^n \tau_{xy}$$

$$\frac{\delta f_2}{\delta \tau_{yz}} = \frac{3}{q}n(q-q_\alpha)^{n-1}\left(\frac{1}{-M(p'-p'_\alpha)}\right)^n \tau_{yz}$$

$$\frac{\delta f_2}{\delta \tau_{zx}} = \frac{3}{q}n(q-q_\alpha)^{n-1}\left(\frac{1}{-M(p'-p'_\alpha)}\right)^n \tau_{zx}$$

REFERENCES

Aboim, C.R., Roth, W.N. (1982) Bounding surface plasticity theory applied to cyclic loading of sand. *International Symposium on Numerical Models in Geomechanics*, Zurich, *pp. 65-72*.

Adachi, T., Oka, F. (1982) Constitutive equations for normally consolidated clay based on Elasto-Viscoplasticity, *Soils and Foundations, 22(4), pp. 57-70*.

Adachi, T., Okano, M. (1974) A constitutive equation for normally consolidated clay, *Soils and Foundations, 14(4), pp. 55-73.*

Al-Tabbaa, A. (1987) Permeability and stress-strain response of Speswhite Kaolin, *PhD Thesis,* University of Cambridge.

Atkinson, J.H. (2000) Non-linear soil stiffness in routine design, *Géotechnique, 50(5), pp. 487-508.*

Bardet, J. F. (1986) Bounding surface plasticity model for sands, *Journal of Engineering Mechanics, ASCE*, *112(11), pp. 1198-1217*.

Been, K., Jefferies, M.G. (1985) A state parameter for sands. *Géotechnique, 35(2), pp. 99-112.*

Been, K., Jefferies, M.G., Hachy, J.E. (1991) The critical state of sands. *Géotechnique, 41(3), pp. 365-381.*

Bishop, A.W., Henkel, D.J. (1957) *The Measurement of Soil Properties in the Triaxial Test*, Edward Arnold Ltd, London.

Bolton, M.D. (1991) *A Guide to Soil Mechanics,* Chung Hwa Book Co, Hong Kong.

Britto, A.M. (1987), Gunn, M.J. (1987) *Critical State Soil Mechanics via Finite Elements*, John Wiley & Sons.

Clarke, B.G. (1995). *Pressuremeters in Geotechnical Design*. Blackie, London.

Collins, I.F., Kelly, P.A. (2002) A thermomechanical analysis of a family of soil models. *Géotechnique. 52(7), pp. 507-518.*

Collins, I.F., Houlsby, G.T., (1997). Application of thermomechanical principles to the modelling of geotechnical materials. *Proceedings of Royal Society Ser. A53*, *pp. 1975-2001*.

Coop, M., The mechanics of uncemented carbonate sands. (1990) *Géotechnique, 40(4), pp. 607-626.*

Coop, M.R., Lee, I.K. (1993) The behaviour of granular soils at elevated stresses, *Predictive Soil Mechanics, Wroth Memorial Symposium*, Thomas Telford, London, *pp. 186–198.*

Crouch, R.S., Wolf, J.P., Dafalias, Y.F. (1994) Unified critical state bounding surface plasticity model for soil, *Journal of Engineering mechanics, ASCE, 120(11), pp. 2251–2270.*

Dafalias, Y.F. (1975) On cyclic and anisotropy plasticity, *PhD Thesis*, University of California at Berkeley.

Dafalias, Y.F. (1982) Bounding surface elastoplasticity viscoplasticity for particulate cohesive media, *Proc. IUTAM Symposium on Deformation and Failure of Granular Materials*, A.A. Balkema, Rotterdam.

Dafalias, Y.F., Herrmann, L.R. (1980) Bounding surface formulation of soil plasticity, *Soil Mechanics-Transient and Cyclic Loads,* Wiley, New York., *pp. 253-282.*

Dafalias, Y.F., Herrmann, L.R. (1987a) Bounding surface plasticity. I: Mathematical foundation and hypoplasticity, *Journal of Engineering Mechanics, ASCE, 112(9), pp. 966-987.*

Dafalias, Y.F., Herrmann, L.R. (1987b) Bounding surface plasticity. II: Application to isotropic cohesive soils, *Journal of Engineering Mechanics, ASCE, 112(12), pp. 1263-1291.*

Dafalias, Y.F., Popov, E.P. (1975) A model of non-linearly hardening materials for Complex Loading, *Acta Mechanica, 21, pp. 173-192.*

Das, B.M. (1990) *Earth Anchors,* Elsevier, Amsterdam.

Desai, C.S. (1979) *Elementary Finite Element Method,* Prentice Hall, USA.

Fox E.N. (1948) The mean elastic settlement of a uniformly loaded area at a depth below the ground surface. *Proceedings of the 2nd International Conference on Soil Mechanics and Foundation Engineering,* Rotterdam*, 1, pp. 129-132.*

Gens, A., Potts, D.M. (1988) Critical state models in computational mechanics. *Engineering Computation, 5, pp. 178-197*.

Gibson, R.E., Anderson, W.F. (1961) In-situ measurement of soil properties with the pressuremeter, *Civil Engineering Public Works Review*, *56, pp. 615-618*.

Hashiguchi, K. (1985). Two- and three-surface models of plasticity. *Proceedings of the 5th International Conference on Numerical Methods in Geomechanics*, Nagoya, *pp. 125-134.*

Hau, K.W. (2003) Application of e three-surface kinematic hardening model to the repeated loading of thinly surfaced pavements. *PhD thesis*, The University of Nottingham, UK.

Hill, R. (1950) *The mathematical theory of plasticity*, Oxford University Press, London.

Houlsby, G.T. (1981) A study of plasticity theories and their applicability to soils, *Ph.D. Thesis*, University of Cambridge

Houlsby, G.T. (1985) The use of a variable shear modulus in elastic-plastic models for clays, *Computers and Geotechnics, 1(1), pp. 3-21.*

Houlsby, G.T., Carter, J.P. (1993). The effects of pressuremeter geometry on the results of tests in clay. *Géotechnique, 43(4), pp. 567-576*.

Houlsby, G.T., Purzin, A.M. (2000) A thermomechanical framework for constitutive models for rate-independent dissipative materials. *International Journal of Plasticity*, *16(9), pp. 1017-1047*.

Houlsby, G.T., Withers, N.J. (1988) Analysis of the cone pressuremeter test in clay, *Géotechnique*, *38(4), pp. 575-587*.

Houlsby, G.T., Wroth, C.P. (1991) The variation of the shear modulus of a clay with pressure and overconsolidation ratio, *Soils and foundations, 31(3), pp 138-143.*

Hyodo, M., Tanimizu, H., Yasufuku, N., Murata, H. (1994) Undrained cyclic and monotonic triaxial behaviour of saturated sand. *Soils and foundations, 34(1), pp. 19-32.*

Ishihara, K., Tasuoka, F., Yasuda, F., Yasuda, S. (1975) Undrained deformation and liquefaction of sand under cyclic stresses, *Soils and foundations*, *15(1), pp 29-44*.

Iwan, D.W. (1967) On a class of models for the yielding behaviour of continuous and composite systems, *Journal of Applied Mechanics, ASME, 34, pp. 612-617.*

Jardine, R.J., Symes, M.J., Burland, J.B. (1984) The measurement of soil stiffness in the triaxial apparatus, *Géotechnique, 34(3), pp. 323-340.*

Jefferies, M.G. (1993) Non-sand: a simple critical state model for sand. *Géotechnique, 43(1), pp. 91-103.*

Katona, M.G. (1984) Evaluation of viscoplastic cap model, *Journal of Geotechnical Engineering, ASCE, 110(8), pp. 1106-1125.*

Katona, M.G., Mulert, M.A. (1984) A viscoplastic cap model for soils and rock, *Mechanics of Engineering Materials,* John Wiley and Sons, New York.

Liu, M.D. (2004) Personal communication.

Khong, C.D., Yu, H.S. (2002) Computational aspects of a unified critical state model for clay and sand, *Proceedings of the 8th International Symposium on Numerical Models in Geomechanics,* Rome, *pp 271-277*.

Khong, C.D., Yu, H.S. (2003) Stress history effects of undrained analysis using critical state models, Submitted to *International Journal of Geomechanics*.

Kolymbas, D., Wu, W. (1993) Introduction to hypoplasticity, *Modern Approaches to Plasticity,* edited by Kolymbas, *pp. 213-233.*

Kolymbas, D. (1991) Computer aided design of constitutive laws, *International Journal of Numerical and Analytical Methods in Geomechanics*, *15, pp. 593-604.*

Krenk, S. (2000) Characteristic state plasticity for granular materials. Part I: Basic theory. *International Journal of Solids and Structures, 37, pp. 6343-6360.*

Kutter, B.L., Sathialingam, N. (1992) Elastic-viscoplastic modeling of rate-dependent behaviour of clays, *Géotechnique, 42(3), pp. 427-441.*

Lade, P.V. (1984) Failure criterion for frictional materials, Chapter 20 in *Mechanics of Engineering Materials*, Edited by Desai, C.S. and Gallagher, R.H. Wiley, *pp. 385-402.*

Li, T., Meissner, H. (2002) Two-surface plasticity model for cyclic undrained behaviour of clay, *Journal of Geotechnical and Geoenvironmental Engineering, ASCE, 128(7), pp. 613-626.*

Love, A.E.H (1927) *A Treatise on the Mathematical Theory of Elasticity.* Dover Publications, New York.

Mair, R.J., Wood, D.M. (1987). Pressuremeter testing: Methods and interpretation. *CIRIA Ground Engineering Report: in-situ testing*. Butterworths, London.

McDowell, G.R., Hau, K.W. (2003) A simple non-associated three surface kinematic hardening model, *Géotechnique, 53(3), pp. 433-437.*

McVay, M., Taesiri, Y. (1985) Cyclic behaviour of pavement base materials. *Journal of Geotechnical Engineering, ASCE, 111(1), pp. 1-17.*

Merifield, R.S., Sloan S.W., Yu H.S. (2001) Stability of plate anchors in undrained clay. *Géotechnique, 51(2), pp. 141-153.*

Meyerhoff, G.G., Adams J.I. (1968) The ultimate uplift capacity of foundations. *Canadian Geotechnical Journal, 5(4), pp. 225-244.*

Mroz, Z. (1966) On forms of constitutive laws for elastic-plastic solids, *Arch. Mech. Stos., 18, pp. 3-35.*

Mroz, Z. (1967) On the description of anisotropic workhardening, *Journal of the Mechanics and Physics of Solids, 15, pp. 163-175.*

Mroz, Z., Norris, V.A., Zienkiewicz, O.C. (1978) An anisotropic hardening model for soils and its application to cyclic loading, *International Journal of Numerical and Analytical Methods in Geomechanics, 2, pp. 203-221.*

Mroz, Z., Norris, V.A., Zienkiewicz, O.C. (1979) Application of an anisotropic hardening model in the analysis of elastoplastic deformation of soils, *Géotechnique, 29(1), pp. 1-34*.

Mroz, Z., Pietruszczak, S. (1983) On hardening anisotropy of K_o- consolidated clays, *International Journal of Numerical and Analytical Methods in Geomechanics, 7(1), pp. 19-38.*

Nova, R. (1982) A viscoplastic constitutive model for normally consolidated clay, *Proc. IUTAM Symposium on Deformation and Failure of Granular Materials*, A.A. Balkema, Rotterdam.

Nova, R., Wood, D.M. (1978) An experimental program to define yield function for sand, *Soils and Foundations, 18(4), pp. 77-86.*

Nova, R., Wood, D.M. (1979) A constitutive model for sand in triaxial compression. *International Journal of Numerical and Analytical Methods in Geomechanics, 3, pp. 255-278.*

Ohta, H., Wroth, C.P. (1976) Anisotropy and stress reorientation in clay under load, *Proceedings of the 2nd International Conference on Numerical Methods in Geomechanics*, Blacksburg, *1, pp. 319-328.*

Parry, R.H.G. (1956) Strength and deformation of clay, *PhD Thesis,* University of London.

Pastor, M., Zienkiewicz, O.C., Leung, K.H. (1985) Simple model for transient soil loading an earthquake analysis. Part 2: Non-associative models for sands, *International Journal of Numerical and Analytical Methods in Geomechanics, 9, pp. 477-498.*

Pender, M.J. (1978) A model for the behaviour of overconsolidated soil, *Géotechnique, 28(1), pp. 1-25.*

Poorooshasb, H.B., Roscoe, K. H. (1961) The correlation of the results of shear tests with varying degrees of dilatation, *Proceedings of the 5th International Conference on Soil Mechanics, 1, pp. 297-304.*

Potts, D.M., Zdravkovic, L. (1999) *Finite Element Analysis in Geotechnical Engineering: Theory*, Thomas Telford, London.

Potts, D.M., Zdravkovic, L. (2001) *Finite Element Analysis in Geotechnical Engineering: Application*, Thomas Telford, London.

Potts, D.M., Gens, A. (1984) The effect of the plastic potential in boundary value problems involving plane strain deformation, *International Journal of Numerical and Analytical Methods in Geomechanics*, *8, pp. 341-354*.

Prevost, J.H. (1978) Plasticity theory for soil stress-strain behaviour, *Journal of the Engineering Mechanics, ASCE, 104(5), pp. 1177-1194.*

Puzrin, A.M., Houlsby, G.T. (2001) A thermomechanical framework for rate-independent dissipative materials with internal functions, *International Journal of Plasticity*, *17, pp. 1147-1165*.

Roscoe, K.H., Burland, J.B. (1968) On the Generalised Stress-Strain Behaviour of Wet Clay, *Engineering Plasticity*, Cambridge University Press, *pp. 535-609*.

Roscoe, K.H., Poorooshasb, H.B. (1963) A theoretical and experimental study of strains in triaxial tests on normally consolidated clays, *Géotechnique, 13(1), pp. 12-38.*

Roscoe, K.H., Schofield, A.N, Thurairajah, A. (1963) Yielding of clays in states wetter than critical, *Géotechnique, 13(3), pp. 211-240.*

Roscoe, K.H., Schofield, A.N, Wroth, C.P. (1958) On the yielding of soils, *Géotechnique, 8(1), pp. 22-53.*

Roscoe, K.H., Schofield, A.N, Wroth, C.P. (1959) Correspondence 'On the yielding of soils', *Géotechnique, 9(2), pp. 72-83.*

Roscoe, K.H., Schofield, A.N. (1963) Mechanical behaviour of an idealised wet clay. *Proceedings of the European Conference on Soil Mechanics and Foundation Engineering*, *1, pp. 47-54.*

Rowe, R.K., Booker, J.R. (1979) A method of analysis for horizontally embedded anchors in an elastic soil. *International Journal of Numerical and Analytical Methods in Geomechanics, 3(2), pp. 187-203.*

Rowe, R.K., Davis, E.H. (1982a) The behaviour of anchor plates in clay. *Géotechnique, 32(1), pp. 9-23.*

Rowe, R.K., Davis, E.H. (1982b) The behaviour of anchor plates in sand. *Géotechnique, 32(1), pp. 25-41.*

Rowe, P.W. (1962) The stress-dilatancy relation for static equilibrium of an assembly of particles in contact. *Proceedings of Royal Society A269: pp. 500-527*

Sasitharan, S., Robertson, P.K., Sego, D.C., Morgenstern, N.R. (1994) State boundary surface for very loose sand and its practical applications, *Canadian Geotechnical Journal, 31, pp. 321-334.*

Sathialingam, N. (1991) Elastic-viscoplastic modeling of rate dependent behaviour of clays, *PhD Thesis,* University of California at Davis.

Schofield, A.N., Wroth, C.P. (1968) *Critical State Soil Mechanics*, McGraw-Hill, New York.

Sekiguchi, H. (1984) Theory of undrained creep rupture of normally consolidated clays based on elasto-viscoplasticity, *Soils and Foundations, 24(1), pp. 129-147.*

Sheng, D., Sloan, S.W., Yu, H.S. (2000) Aspects of finite element implementation of critical state models. *Computational Mechanics, 26, pp. 185-196.*

Shibata, T., Karube, D. (1965) Influence of the variation of the intermediate principal stress on the mechanical properties of normally consolidated clays, *Proceedings of the 6th International Conference on Soil Mechanics and Foundation Engineering,* Montreal, *pp. 359 – 363.*

Sladen, J.A., D'Hollander, R.D.D., Krahn, J. (1985) The liquefaction of sands, a collapse surface approach, *Canadian Geotechnical Journal, 22(4), pp. 564–578.*

Stallebrass, S.E. (1990) The effect of recent stress history on the deformation of overconsolidated soils, *PhD Thesis*, City University, UK.

Stallebrass, S.E., Taylor, R.N. (1997) The development and evaluation of a constitutive model for the prediction of ground movements in overconsolidated clay. *Géotechnique, 47(2), pp. 235-253*.

Tasuoka, F., (1972) Shear tests in a triaxial apparatus – A fundamental study of the deformation of sand (in Japanese). *PhD Thesis*, Tokyo University

Tasuoka, F., Ishihara, K., (1974) Drained deformation of sand under cyclic stresses reversing direction, *Soils and foundations*, *14(3), pp. 51-65.*

Taylor, D.W. (1948) *Fundamentals of Soil Mechanics,* John Wiley, New York.

Vesic A. S. (1971) Breakout resistance of objects embedded in ocean bottom. *Journal of Soil Mechanics and Foundations, ASCE, 97(9), pp. 1185-1205.*

Whittle, A.J. (1993) Evaluation of a constitutive model for overconsolidated clays, *Géotechnique, 43(2), pp 289-313.*

Wood, D.M. (1990) *Soil Behaviour and Critical State Soil Mechanics*. Cambridge University Press.

Wood, D.M., (1982) Laboratory investigation of the behaviour of soils under cyclic loading: A review, *Soil Mechanics – Transient and Cyclic Loads*, edited by Pande, G.N. and Zienkiewicz, O.C., *pp. 513 – 582.*

Wroth, C.P. (1984). The interpretation of in-situ soil tests, *Géotechnique*, *34(4), pp. 449-489.*

Wroth, C.P., Houlsby, G.T. (1985) Soil mechanics – Property characterisation and analysis procedures, *Proceedings of the 11th International Conference on Soil Mechanics and Foundation Engineering*, San Francisco, *1, pp. 1-55*.

Wu, W., Kolymbas, D. (1990) Numerical testing of the stability criterion for hypoplastic constitutive equations. *Mech. Matter*. *9, pp. 245-253.*

Yeung, S.K., Carter, J.P. (1990). Interpretation of the pressuremeter test in clay allowing for membrane end effects and material non-homogeneity. *Proceedings of the 3rd International Symposium on Pressuremeters*, Oxford, *pp. 199-208*.

Yu, H.S. (1990). Cavity expansion theory and its application to the analysis of pressuremeters. *PhD Thesis,* The University of Oxford.

Yu, H.S. (1995) A unified critical state model for clay and sand. *Civil Engineering Research Report No 112.08.1995.* University of Newcastle, NSW 2308, Australia.

Yu, H.S. (1998) CASM: A unified state parameter model for clay and sand, *International Journal of Numerical and Analytical Methods in Geomechanics*, *22, pp. 621-653*.

Yu, H.S. (2000). *Cavity Expansion Methods in Geomechanics*, Kluwer Academic Publishers, The Netherlands.

Yu, H.S. (2003) Personal communication.

Yu, H.S., Collins, I.F. (1998) Analysis of self-boring pressuremeter tests in overconsolidated clays, *Géotechnique, 48(5), pp. 689-693*.

Yu, H.S., Khong, C.D. (2002a) Application of a unified plasticity model in finite element analysis, *Proceedings of the 3rd International Symposium on 3D Finite Element for Pavement Analysis, Design and Research,* Amsterdam, *pp. 253-267*.

Yu, H.S., Khong, C.D. (2002b) Computation of anchor behaviour using critical state models, *Proceedings of the 5th European Conference on Numerical Methods in Geotechnical Engineering,* Paris, *pp. 661-668*.

Yu, H.S., Khong, C.D. (2003) Bounding surface formulation of a unified critical state model for clay and sand, *Proceeding of the 3rd International Symposium on Deformation Characteristics of Geomaterials,* Lyon, *pp 1111-1118.*

Yu, H.S., Khong, C.D. (2003) Effects of hardening laws on performance of plasticity models, to be submitted to *Géotechnique*.

Ziegler, H. (1977) *An Introduction to Thermodynamics*, First ed., North Holland, Amsterdam.

Ziegler, H. (1983) *An Introduction to Thermodynamics*, Second ed., North Holland, Amsterdam.

Zienkiewicz, O.C., Humpheson, C. Lewis, R.W. (1975) Associated and non-associated viscoplasticity and plasticity in soil mechanics, *Géotechnique, 25(4), pp. 671-689.*

Zienkiewicz, O.C., Humpheson, C., (1977) Viscoplasticity: A generalised model for description of soil behaviour, *Numerical Methods in Geotechnical Engineering,* McGraw-Hill, New York.

Zienkiewicz, O.C., Naylor, D.J. (1973) Finite element studies of soils and porous media, *Lectures on Finite Elements in Continuum Mechanics,* UAH Press.

Zienkiewicz, O.C., Pande, G.N. (1977) Some useful forms of isotropic yield surfaces for soil and rock mechanics, *Finite Elements in Geomechanics, pp 179-198,* Wiley.

Zytynski, M., Randolph, M.F., Nova, R., Wroth, C.P. (1978) On modelling the unloading-reloading behaviour of soils, *International Journal of Numerical and Analytical Methods in Geomechanics, 2, pp. 87-93.*

HẾT